DEVELOPMENT OF HIGH-SPEED FIBRE-OPTICAL LASER SCANNING SYSTEM FOR DEFECT RECOGNITION

ABDULBASET ABUAZZA

Dublin City University

Ph.D. **2002**

DEVELOPMENT OF HIGH-SPEED FIBRE-OPTICAL LASER SCANNING SYSTEM FOR DEFECT RECOGNITION

By

ABDULBASET ABUAZZA

This thesis is submitted as the fulfilment of the Requirement for the award of degree of Doctor of Engineering (PhD)

By research form

Dublin City University

Faculty of Engineering and Design

School of Mechanical & Manufacturing Engineering

June 2002

Prof. M. A. El Baradie

Dr. D. Brabazon

Project Supervisors

In the Name of God, the Compassion
ate,
the Merciful

Dedicated

To

My Family

DECLARATION

I hereby certify that this material, which I now submit for assessment on the programme of my study leading to the award of Doctor of Philosophy is entirely my on work and has not been taken from the work of others save and to the extent that such work has been cited and acknowledged within the text of my work.

Signed: ___*Abuazza*_____ ID No: 96971801

Date: __14-06-2002_____

ACKNOWLEDGEMENTS

The author is indebted to his supervisors, Professor M. A. El-Baradie and Dr. Dermot Brabazon for their valuable advice, wholehearted aid and encouragement at all stages of the work.

I would like to express my sincere thanks and gratitude to Professor M. S. J. Hashmi, Head of the Department of Mechanical Engineering, DCU, for giving me the opportunity and facilities to carry out this work

Sincerest thanks to all the technical staff of the School of Mechanical and manufacturing Engineering, especially Mr. Martin Johnson, Mr. Keith Hickey and Mr. Jim Barry, for providing great help at different stages of the project also a special thanks to Mr. Michael May. I would like also to thank Mr. Pat Wagon the electronic technician of school of physics for his help in early stage of the work.

I would like to thank all my engineering colleagues and friends especially Hussam El-Sheikh for his help.

A special thanks also to my brother in-law Yusef Elbadri for his support and encouragement during my stay in Ireland.

Finally, I would like to thank to all of my family, especially my mother, father and wife for keeping me in their prayers and for their continual support.

AUTHOR

The author received his B.Sc. in Physics, and Diploma of Education from University of Al-Fatah physics department, in 1983. After graduation, joined a high school of education in Tripoli, Libya. Duties: Teaching responsibilities include laboratory demonstration 1984-1994. He was a part time working as researcher assistant in Postgraduate Center for Electro-Optic, Tripoli, 1992-1994. Master of Science (M.Sc.) Physics, in 1994. He was joined physics department University of Al-Fatah, Faculty of science department of physics Duties include Lucturer assistant Teaching different first year phisics courses. Part time job in the university of Al-Fatah Medical sciences, Tripoli, Libya.Duties: Teaching First General Physics include Laboratory instruction in November 1996-1998. The author published Associate general physics textbook edition for second level education.

Since October 1998, the author has been pursuing his Ph.D. study in the Dublin City University School of mechanical and manufacturing engineering.

This work has been published in the following conferences:

- Paper in conference AMPT ' 99 Dublin in tittle of Laser scanning inspection system an over view
- Paper in conference in 7^{th} International Conference on Production Engineering, Design and Control 2000 Alexandria in tittle of In process of laser scanning system for surface defect recognition
- Paper in conference in AMPT 2001 Madrid in tittle of A novel fibre-optic laser scanning system for surface defect recognition.
- The last one was accepted in the Journal of Mat. Process and Technology

HIGH-SPEED FIBRE-OPTIC LASER SCANNING INSPECTION SYSTEM FOR SURFACE DEFECT RECOGNITION

ABDULBASET ABUAZZA

ABSTRACT

High-speed fibre-optic laser scanning systems are being used in automated industrial manufacturing environments to determine surface defects. Recent methods of surface defect detection involve the use of fibre-optic light emitting and detection assemblies. This thesis deals with the design and development of a new high-speed photoelectronic system. In this work, two sources of emitting diode were examined, LED (light emitting diode) and laser diode. A line of five emitting diodes and five receiving photodiodes were used as light sources and detectors respectively. These arrays of emitting diodes and photodectectors were positioned opposite each other. Data capture was controlled and analysed by PC using Labview software.

The system was used to measure the dimensions of the surface defects, such as holes (1 mm), blind holes (2 mm) and notches in different materials. The achieved results show that even though this system was used mainly for 2-D scanning, it may also be operated as a limited 3-D vision inspection system. This system furthermore showed that all the metal materials examined were able to reflect a signal of the infrared wavelength.

A newly developed technique of using an angled array of fibres allows an adjustable resolution to be obtained with the system, with a maximum system resolution of approximately 100 μm (the diameter of the collecting fibre core).

This system was successfully used to measure various materials surface profile, surface roughness, thickness, and reflectivity. Aluminum, stainless steel, brass, copper, tufnol, and polycarbonate materials were all capable of being examined with the system. The advantages of this new system may be seen as faster detection, lower cost, less bulky, greater resolution and flexibility.

Table of Contents

Last of Tables

Last of Figures

Chapter 1

Introduction

There are many ways in which fibre optics can be used in industry. The tasks they are used for range from being incorporated into a very simple information unit to the most sophisticated process control systems. The automotive industry is one of the biggest users of this technology. This industry has an annual production of several million units, which makes it an attractive target for the fibre optics industry to focus on. The basic principle behind all light-display systems employing fibre optics is to use a complex light guide which receives light from one or more light sources and output it to display the information in any desired manner. The ability of fibres to alter shape and the distribution of light adds to the flexibility of the display. One of the most effective sensory devices currently available for smart structure applications is the fibre-optic sensor. The response of an optical fibre can be affected by very small changes in fibre geometry caused by elongation, bending, or twisting. The advantages of using fibre optics for an on-line laser scanning system are that they reduce the time of scan, have high resolution, are low cost, have small space needs, and are flexible to increase the area of the scan. Further advantages of fibre-optic applications may include high speed, improved quality, and non-contact operation. The main drive of research in this area today has been to produce a range of optical fibre based techniques. These techniques can be used for a variety of different sensor purposes, providing a foundation for an effective measurement technology. This technology is small in size and compatible with conventional measurement equipment. Therein lies the recipe for the success of optical fibre sensor by application to difficult measurement situations where conventional sensors are not well suited.

Most component manufacturing cycles include an inspection stage to ensure an agreement with design requirements. Mechanical systems incorporating a rotating

mirror or polygon is limited in terms of scanning speed. A further disadvantage of these systems is that they can be quite expensive.

To build a low-cost optical module, the number of elements in an optical device package should be kept low. In the most cases, the optical modules are composed of laser diodes (LDs), photo detectors, and waveguides (i.e. fibres). In order to achieve a laser scanning inspection system for surface defect recognition two optical beams the emitted and the received must be considered. Table 1 gives some details (characteristics and applications) of the present system.

Table 1

High speed fibre-optic laser scanning system for surface defect recognition	
Operating principle and characteristics:	**Applications:**
• Light sources light emitting diode (850nm) and Multimode laser diodes (1300nm)	• Surface notch measurement (brass, tufnol, aluminum and transparent polycarbonate)
• Fibre optic with core/cladding 62.5/125 & 100/140 μm	• Surface roughness measurement (stainless steel and aluminum)
Photodetectors response from 650 to 950nm and from 900 to 1700nm	• Material reflectivity measurement (stainless steel, plastic, aluminum and polycarbonate)
Incident angle 30 degree	• Material thickness measurement
• Driving circuit (constant)	• Automated material surface profile measurement with an adjustable resolution
• Transimpedance Amplifier	• Coloured surface measurement
• Resolution of the system 100μm	
• Spatial resolution is 9.5 μm and DAQ rate is 200 Hz	

The research presented in this thesis details the design and development of a new high-speed photoelectronic system. Results from two sources of emitting diode (Light Emitting Diode (LED) and LD) are presented. In the system, arrays of emitting diodes and photodectectors are positioned in parallel opposite each other. The output signals are interfaced with a data acquisition card.

The initial system consisted of one LED (850nm wavelength). Light from the LED was transmitted through a fibre with core/cladding dimensions of 100/140 μm. This emitting signal was reflected from the material samples. The signal was collected by a receiving fibre with core/cladding dimensions of 100/140 μm. The light detector received the reflected light from this fibre and converted it to the electric signal. The resolution achieved in this system was 100 μm. Holes of 1mm and 2mm in different materials (stainless steel, brass, copper and polycarbonate) were analysed with this system. Disadvantages for using an LED system include the low intensity of the signal and the small distance required between the surface and the end face of the fibre.

The system described above was extended to a line of five emitting laser diodes and five receiving photodiodes. These arrays of emitting diodes and photodectectors were positioned opposite each other. As with the above system a data acquisition card was used to capture the output signals from the photodiodes. Data capture was controlled and analysed in real time for this set-up, using Labview software. The experimentally obtained results from several materials show the system's ability to recognise defects. The achieved results show that even though this system is capable of 2-D scanning it may also be operated as a limited 3-D vision inspection system

This sensor system was designed to operate as a photoelectric sensor and used to recognize the surface defects on products on a line during manufacturing. Five laser diodes (1300 nm-wavelength) were used as light sources. The fibres connected to these diodes had a dimension of core/cladding ratio 65/125 μm. Five optic fibres with a dimension of core/cladding ratio 100/140 μm collected the reflected beams from the surface. Five PIN photodiodes collected the light reflected by the sample under inspection. These photodiodes have high responsivity within the wavelength (λ) range 900 to 1700 nm and supply analog outputs. A data acquisition card was used for analog to digital conversion for these outputs. Labview software was developed to aid data analysis.

The five fibres used covered a distance of 4.15 mm. A production line was simulated by moving the samples under the sensor at a speed of 1.91 mm/s. The resolution of the system was made adjustable by mounting the fibre holder on an adjustable rotation stage. This system successfully detected the defects for both high reflectivity surfaces and diffuses surfaces. This system has advantages related to the measurement of the following:

- Surface roughness measurement
- Material reflectivity measurement
- Material thickness measurement
- Coloured surfaces measurement

Chapter two gives the literature survey of the laser technology. It deals with the properties of laser light, which make lasers such useful tools. Low and high power laser applications are discussed. Also it reviews the basic characteristics of the fibre optics. It furthermore provides an overview of progress and developments in the field of fibre-optic technology.

Technology that has been developed especially within the last decade is reviewed. The most common technique used in laser defect inspection systems is the triangulation method. This chapter also includes a description of he designed and development of a fibre-optic sensor for surface defect recognition.

Chapter three describes the experimental equipment and the technique, which was used in this project. Details of the main system components are given. These include the fibre-optic transmitter, the fibre-optic receiver, the fibre itself, D/A conversion and data analysis. The design of the holders to achieve a highly accurate measurement system is presented. A novel measurement method, which uses four degree of freedom, is described.

Chapter four presents the results recorded from the low intensity beam (LED) system. The LD system with four and five fibres is also presented here. This sensor system measures the existence of a holes in a plate, i.e. the size and position of a hole. The optimisation of the fibre-optic detection system is also included.

Chapter five presents other measurement capabilities of the new system. Most of these results indicate that all the metals are very good reflectors in the infrared

wavelength. In this chapter the reflectivity, roughness, and thickness results from aluminium, transparent polycarbonate and Tufnol plate are presented. A linear guide motor was used to obtain for the results presented at the end of this chapter. The liner guide motor simulated the events on a production line by moving the sample beneath the newly developed inspection sensor. The results from this system at variable resolution are presented.

Chapter six presents a discussion of the results achieved by the system, and conclusions and recommendations for future work

Chapter 2

Literature survey of scanning system technology

2.1 Laser technology

This chapter deals with the properties of laser light, which make lasers such useful tools. The ways in which these properties relate to manufacturing applications are reviewed.

The word laser is an acronym for "light amplification by the stimulated emission of radiation," a phrase which covers most, though not all, of the key physical processes inside a laser [1]. The simple definition for a laser that is more definitive would be "a light-emitting body with a feedback for amplifying the emitted light." Unfortunately, this concise definition may not be very enlightening to the nonspecialist who wants to use a laser but has less concern about the internal physics than the external characteristics. The word laser is generally used in referring to either the radiation produced or the device that produces it. Laser radiation can be produced in the spectral ranges from x-radiations through ultraviolet, visible, and infrared radiation. The laser user is in a position analogous to the electronic circuit designer. A general knowledge of laser physics is as helpful to the laser user as a general understanding of semiconductor physics is to the circuit designer. However, their jobs require them to understand the operating characteristics of complete devices, not to assemble lasers or fabricate integrated circuits.

There are many different kinds of laser, but they all share a crucial element: each contains material capable of amplifying radiation. This material is called the gain medium, because radiation gains energy passing through it. The physical principle responsible for this amplification is called stimulated emission, and was discovered by Albert Einstein in 1917 [2]. It was widely recognized that the laser would represent a scientific and technological step of the greatest magnitude, even before the first one was construction in 1960 by T. H. Maiman [3]. The award of the 1964

Nobel Prize in physics presented to C. H. Towens, N. G. Basov, and A. M. Prokhorov carried the citation "for fundamental work in the field of quantum electronics, which has led to the construction of oscillators and amplifiers based on the maser-laser principle " [4]. These oscillators and amplifiers have since motivated and aided the work of thousands of scientists and engineers. Lasers consist of three basic components.

- An external energy source which is a light from special lamps, light from another laser, an electric current, or a chemical reaction.
- The lasing medium, which is a gas, liquid, semiconductor, or solid that gives off its own light (radiation) when stimulated.
- A cavity or vessel with a fully reflective mirror placed at one end and a partially reflective mirror at the other that permits the light to bounce back and forth between the two mirrors through the lasing medium.

2.2 Properties of laser beam

Many of the properties of laser light are special or extreme in one way or another. This section presents a brief overview of these properties, contrasting them with the properties of light from more ordinary sources when possible.

Laser light is available in all colors from red to violet, and is also available outside these conventional limits of the optical spectrum. Over a wide portion of the available range laser light is "tunable" [4]. This means that some lasers have the property of emitting light at any wavelength chosen within a range of wavelengths. Tunability is primarily a property of dye lasers. The energy of laser photon is not different from the energy of an "ordinary" light photon of the same wavelength.

2.2.1 Monochromaticity

The term monochromatic literally means single colour or single wavelength [5]. It is well known that lasers produce very pure colors. If they could produce exactly one wavelength, laser light would be fully monochromatic. The bandwidth, Δf, of a good

stable laser can be less than 1 kHz compared to a thermal source, which is of the order of 10^{14} Hz.

2.2.2 Coherence

Atoms emit radiation. We see it every day when the "excited" neon atoms in a neon sign emit light. Normally, they radiate their light in random directions at random times. The result is incoherent light a technical term for what you would consider a jumble of photons going in all directions. Lasers on the other hand create and amplify a narrow, intense beam of coherent light.

The way in which coherent light going in one precise direction, is generated by using the right atoms with the right internal energy storage mechanisms. Than an environment is created in which they can all cooperate to give up their light at the right time and all in the same direction [6].

Lasers are sources of temporally and spatially coherent light. Compared with the light generated by a thermal lamp laser light is especially suited for applications in surface and materials science due to its coherence, intensity and due to the possibility to generate short and ultra-short pulses [7]. Spatially two partial waves of a light source are called coherent if their phase differences are constant which leads to superposition, interference phenomenon. 'Temporal coherence' means that the amplitude of the emitted electromagnetic wave energy remains constant over a considerably long time. This is demonstrated in Fig (2.1). In this figure the temporal evolution of the electric field amplitude emitted from a laser source and that emitted from a thermal light source are compared.

The existence of a finite bandwidth $\Delta\nu$ means that the different frequencies present in a laser beam can eventually get out of phase with each other. The corresponding difference in coherence time (periods for the light wave) is as following:

$$\tau_c = L_c / c \qquad (2.1)$$

where c is the speed of light in the investigated medium and the coherence length, L_c. The coherence length is defined as the difference in optical length that results in a

phase difference between two partial waves of less than π. The coherence length of thermal light behind an interference filter with spectral bandwidth of 1 MHz at is about 0.8 mm. The coherent length of a laser with a bandwidth of 10 MHz is about 10 m. Hence the temporal coherence of a laser is many orders of magnitude higher compared with that of light generated by a thermal lamp. This light is well suited for applications, which rely on interference phenomena such as optical holography.

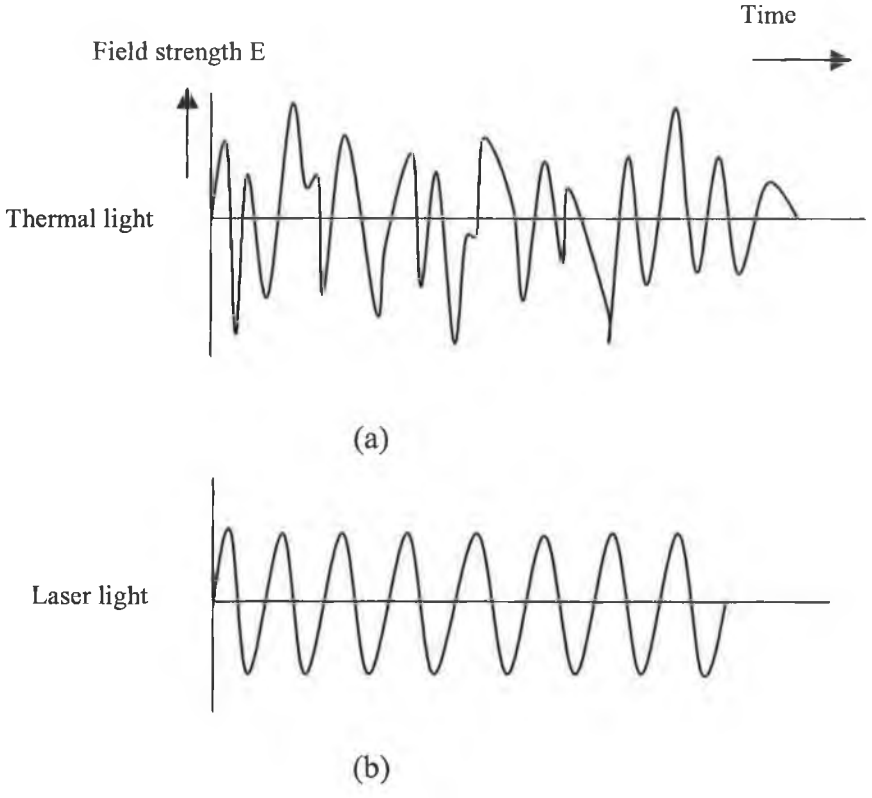

Figure 2.1 Temporal change of the electromagnetic field strength E
a) for a thermal light source b) and a laser light source.

2.2.3 Directionality

The output of a laser can consist of nearly ideal plane wave fronts. Only diffraction imposes a lower limit on the angular spread of a laser beam. The wavelength λ and the area A of the laser output aperture determine the order of magnitude of the change in the beam's solid angle ($\Delta\Omega$) and change in the vertex or planar angle ($\Delta\theta$) of divergence

$$\Delta\Omega \approx \frac{\lambda^2}{A} \approx (\Delta\theta)^2 \qquad (2.2)$$

This represents a very small angular spread indeed if is in the optical range. Figure 2.2 shows the planar and solid angle. For small angle the relation between a planar angle and the solid angle of a cone light source is $\Omega = A/r^2$ where r is the radius at that point of the cone.

Figure 2.2 Cone of light of planar angle θ and solid angle Ω

2.2.4 Brightness

The primary characteristic of laser radiation is that lasers have a higher brightness than any other light source. The brightness of a source is given by the power output per steradian of solid angle and per hertz of bandwidth. For a laser with output power, p, the brightness is given by [8]:

$$B_{laser} = \frac{p}{A\Delta\Omega\Delta f} \qquad (2.3)$$

$$Spectral\ \text{int}ensity = \frac{P_v}{A\Delta f} \qquad (2.4)$$

where h is the Planck's and the spectral intensity (watts/cm^2-Hz).

For the ordinary non-laser optical source, brightness can be estimated directly from the blackbody formula for which given by:

$$\beta_v = \frac{2v^2}{C^2} \frac{hv}{e^{hv/kT} - 1} \tag{2.5}$$

The brightness of the sun is $B_{sun} \approx 1.5x10^{-12}$ W/cm^2-steradian-Hz and the brightness of the Nd: is glass laser is $B_{laser} \approx 2x10^8$ W/cm^2-steradian-Hz [4].

It clears that in terms of brightness there is practically no comparison possible between lasers and thermal light.

High brightness is essential for the delivery of a light power per unit area to a target. This in turn depends on the size of the spot to which the beam can be focused [9].

Other properties of laser light are:

- Its speed is the highest speed possible.
- In a vacuum travels in a straight line
- It can carry information.
- It can be readily manipulated by mirrors and can be switched on and off quickly.
- It can apply energy to very small areas.
- When pulsed it offers the possibility of power multiplication by releasing energy in very brief pulses.

Directionality may be seen as the most important of the above laser properties to obtain an accurate scanning system.

2.3 Laser Types

This section describes the lasers commonly used in manufacturing and their general areas of application. More detail on some of these applications will be presented in later chapters, as will possible future developments in industrial lasers.

Laser types are based on the laser medium used, lasers are generally classified as solid state, gas semiconductor, liquid, free electron, or chemical [4].

2.3.1 Solid-state lasers

The most common solid state laser media are ruby crystals and neodymium-doped glasses and crystals. The ends of the rods are fashioned into two parallel surfaces coated with a highly reflecting multilayer dielective film. Solid state lasers offer the highest power output. They are usually operated in a pulsed manner to generate a burst of light over a short time.

2.3.2 Gas lasers

The medium is usually contained in a cylindrical glass or quartz tube. Two mirrors are located outside the ends of the tube to form the laser cavity. The laser medium of a gas laser can be a pure gas, a mixture of gases or even metal vapor. The Helium-Neon (He-Ne) laser is known for its high frequency stability, colour purity, and minimal beam spread. The HeNe laser is a neutral atom gas laser. Excitation is by means of DC glow discharge. There are a number of wavelengths available for HeNe lasers including, 1.15 μm in the infrared and the visible outputs at 0.543 μm (green), 0.594 μm (yellow), 0.612 μm (orange) and 0.6328 μm (red). The red wavelength is the most commonly used. He-Ne lasers are tunable over several wavelengths. The maximum power output of commercial He-Ne lasers is 50 mW.

2.3.3 Semiconductor lasers

The most compact of lasers, the semiconductor laser, usually consists of a diode junction between layers of semiconductor with different electrical conducting properties. The laser cavity is confined to the junction region by means of two reflective boundaries. Gallium arsenide is the most common semiconductor used. Semiconductor lasers are pumped by the direct application of electric current across the junction, and they are operated in the CW (continuos wave) mode with greater than 50% percent efficiency. A method that permits even more-efficient use of

energy has been devised. The diode laser is a single crystal semiconductor. Commercial devices are compound semiconductor alloys of the III-V type, meaning the main-constituent came from the third and fifth column of the periodic table, e.g. gallium-arsenide (GaAs) and indium phosphide (InP). GaAs/AIGaAs lasers emit wavelength in the 0.78-0.905 μm range depending on composition. InP/InGaAsP type lasers emit in the 1.1-1.6 μm range depending on composition.

2.3.4 Liquid lasers

The most common liquid laser media are inorganic dyes contained in glass vessels. Where the active material is the dye which is contained in a host medium of a liquid solvent, such as ethylene glycol. The advantage of a liquid host is that the concentration of the active ions can easily be changed. However, the gain becomes much higher because of large concentration in liquid lasers. They liquid lasers are pumped by on bright flash lamp in a pulse mode or by another laser such as a Nd: YAG or excimer laser. The frequency of tunable dye lasers can be further adjusted with the help of a prism inside the laser cavity.

2.3.5 Free-electron lasers

The lasers we have discussed so far use a material in which the electrons make a transition from a higher-energy level to produce stimulated emission. Electrons can also radiate when they are accelerated in free space. Lasers using electrons unattached to atoms and pumped to lasing capacity by an array of accelerating magnetic fields were first developed in 1977 and are now becoming important research instruments [4]. They are tunable and in theory could cover the entire wavelength spectrum from infrared to X-rays.

2.3.6 Chemical lasers

Chemical lasers are single pulse lasers wherein the excited state a chemical impulse reaction occurs. Chemical lasers have many attractive features. These lasers produce the highest output power per unit volume and per unit weight. In general, chemical reactions excite vibration levels. If one-shot large power is needed as, for example, in a star war scenario, chemical lasers can produce large amounts of energy without any electric power input.

2.4 Laser applications

The are many applications of lasers in engineering, scientific research, communication, medicine, military, arts, and much more. Laser technology continues to replace many conventional processes in many different industries.

2.4.1 Low-power applications

Applications such as inspections, holography, speckle, measurements and vision, require good spatial and temporal coherence, as well as varying levels of frequency stability and good mode quality. Low power lasers with a 1 to 50 mW range, such as He-Ne laser or diode lasers are common in these applications. Lasers are used to make measurements or to control machines as part of motion systems to within a fraction of a micrometer. The small beam divergence of laser gives them unique capabilities in alignment applications whether for machine set-up or building construction. The high brightness permits the use of low power lasers for accurate triangulation measurements of absolute distance for both measurements and control of machines such as robots.

2.4.2 High-power applications

Powerful laser beams can be focused on small spot with enormous power density. Consequently, the focused beams can readily cut, drill, scribe, etch, weld, or vaporize material in a precise manner. Industry laser systems are used for cutting flat, tubular and three-dimensional metal and non-metal parts. They permit high quality welding by the automotive industry and aerospace manufacturers to be carried out at high speed and without part damage or distortion. Laser systems also provide powerful deep drilling capability in the aerospace and automotive industries, often at angles and with hole diameters not achievable by conventional, non-laser systems.

2.5 Fiber-optic technology

This section presents an overview of progress and developments in the field of fibre optic technology, highlighting the major issues in the area of intensity-based fibre-optic sensors and illustrating a number of important applications.

2.5.1 Optical fibers – introductory theory

An optical waveguide is a structure that can guide a light beam from one place to another. The most extensively used optical waveguide is the step index optical fibre that consists of a cylindrical central dielectric core, clad by a dielectric material of a slightly lower refractive index, n. The refractive index is defined as the ratio of the speed of light in a vacuum to the speed of light in the substance of interest. This number is, of course, always greater than or equal to one. Optical fibres have found widespread use in communications technology, medical endoscopy and in fibre-optic sensing. The characteristics of optic fibres will now be discussed.

2.5.2 Refractive index profile

The refractive index of the fibre optic mediums determines the propagation of light in the waveguide. In fact, it is the refractive index of the core n_1 with respect to refractive index of the cladding n_2, which plays an important role. There are two main fibre types [10]:

(1) Step index (multimode, single mode)

(2) Graded index (multimode)

Step Index Fibre:

Step index fibre (Figure 2.3 and 2.4) is so called because the refractive index of the fibre steps up as we move from the cladding to the core of the fibre. Within the cladding the refractive index is constant, and within the core of the refractive index is constant.

Multimode: Although it may seem that any ray of light can travel down the fibre, in fact, because of the wave nature of light, only certain ray directions can actually travel down the fibre. These are called the "Fibre Mode". In a multimode fibre many different modes are supported by the fibre. This is shown in the diagram below, see Figure 2.3.

Single Mode: Because its core is so narrow Single Mode fibre can support only one mode. This is called the "Lowest Order Mode".

Graded Index Fibre

Graded index fibre has a different core structure from single mode and multimode fibre. Whereas in a step-index fibre the refractive index of the core is constant throughout the core. In a graded index fibre the value of the refractive index changes from the centre of the core onwards. It is called a quadratic profile. This means that the refractive index of the core is proportional to the square of the distance from the centre of the fibre. In a graded index optical fibre, the light has a trajectory that becomes more and more curved as it approaches the cladding (Figure 2.5 and 2.6).

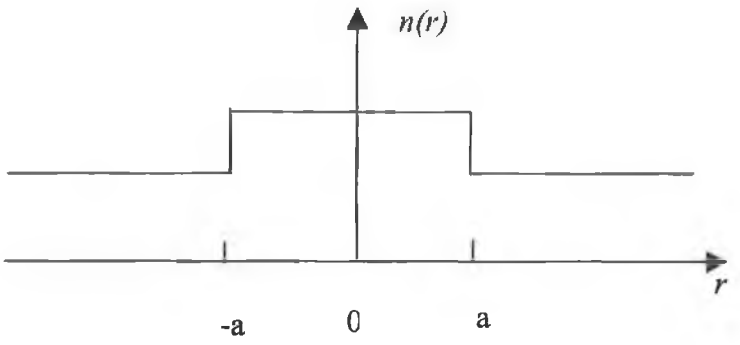

Figure 2.3 Step index profile.

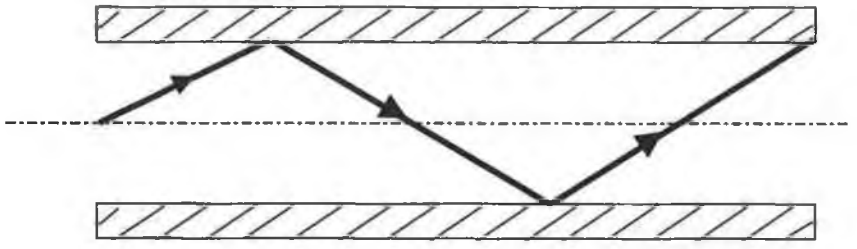

Figure 2.4 Propagation in a step index.

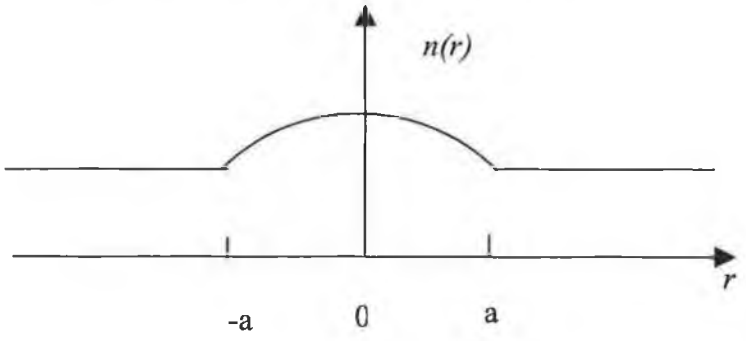

Figure 2.5 Graded index fibre profile.

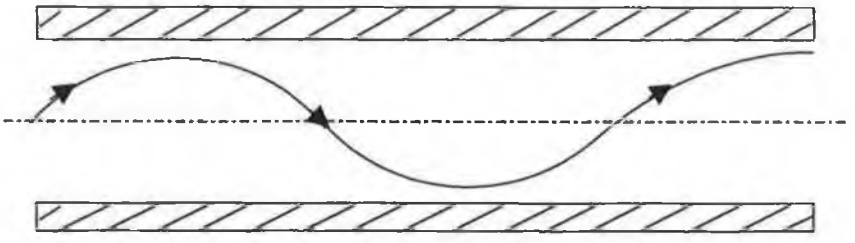

Figure 2.6 Propagation in a graded index fibre.

2.5.3 Numerical aperture

It is of interest to find the angle defining the cone within which light must enter a fibre in order to be guided or accepted (see Figure 2.7). To describe optical fibres more specifically, the definition of a few parameters must be presented [11]. Let n_1 and n_2 be the reflective indices of the core and cladding, respectively.

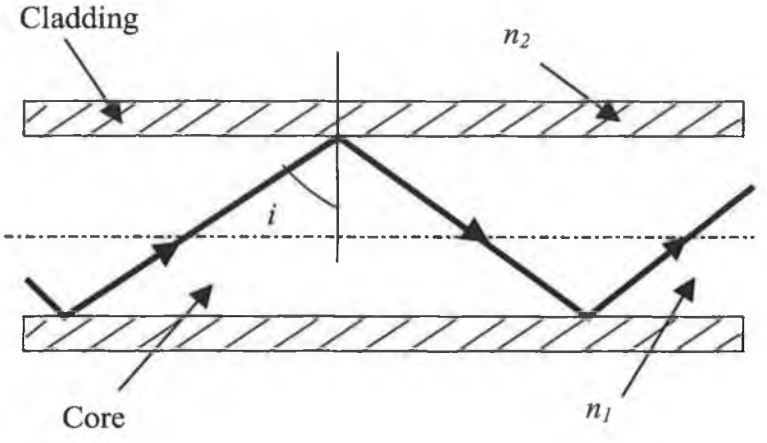

Figure 2.7 Diagram of an optical fiber

Snell's law defines the passage from a medium of refractive index n_1 to a medium of refractive index n_2 by a light ray having an angle of incidence i.

$$n_1 \cdot \sin(i) = n_2 \cdot \sin(r) \qquad (2.6)$$

where r is the angle of the refracted ray in the second medium as shown in Figure 2.8.

As the angle of incidence increases, a point is reached where $r = 90^0$. Angles greater than the critical angle is completely reflected – total reflection. The angle of incidence at this point is called the critical angle, i_c, from Snell's law:

$$i_c = \sin^{-1}(n_2/n_1) \qquad (2.7)$$

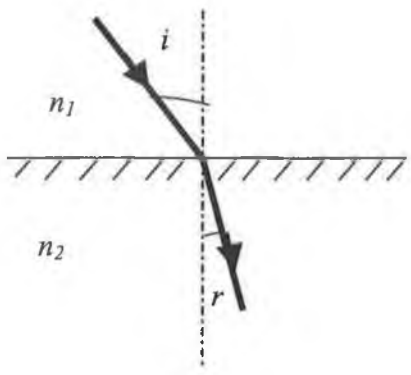

Figure 2.8 Schematic of the radiance angle and reflected angle as a light ray passes from one medium into another

There is a value of the angle of incidence for which the wave is reflected at the medium interface (the Brewster angle), i_m, defined as follows:

$$\text{Sin}(i_m) = n_2 / n_1 \qquad \text{if} \qquad n_2 < n_1 \qquad (2.8)$$

This requires that the second medium have a refractive index less than that of the first. If the angle of incidence i is greater than this limiting angle, the light wave is reflected; this is the case for the optical fibre [12].

The numerical aperture (N_A) is the quantity that is used to measure the acceptance angle for an optical fibre as shown in Figure 2.9. Numerical aperture is defined by this equation:

$$N_A = n_0 \sin(i_0) \qquad (2.9)$$

n_0 is the refractive index of the medium the ray is travelling from, n_0 is considered equal to 1 for air and is defined as 1 for vacuum. Form Snell's law:

$$n_0 \sin(i_0) = n_1 \sin(90\text{-}i_c) = n_1 \cos i_c \qquad (2.10)$$

If follows from the above equation that the numerical aperture is given by:

$$N_A = n_1 (1-\sin^2 i_c)^{1/2} \quad (2.11)$$

Substituting from equation (2.10), the numerical aperture N_A is defined as:

$$N_A = (n_1^2-n_2^2)^{1/2} \quad (2.12)$$

The numerical aperture of an optical fibre is usually of the order of 0.2 to 0.3; the greater the numerical aperture, the greater the luminous power injected into the fibre.

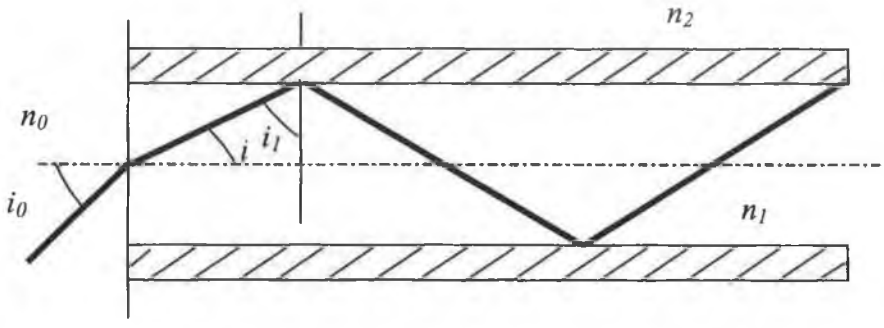

Figure 2.9 Definition of numerical aperture

Once again optical fibre is made of a core and cladding as shown in Figure 2.10 [13]. When we try to inject light into an optical fibre, it needs to strike the core/cladding boundary at less than the critical angle of that boundary, to permit reflection along the core. If the angle is large, the beam will be reflected into the cladding and lost. Therefore a very small light source is used to transmit all the available power into the cable.

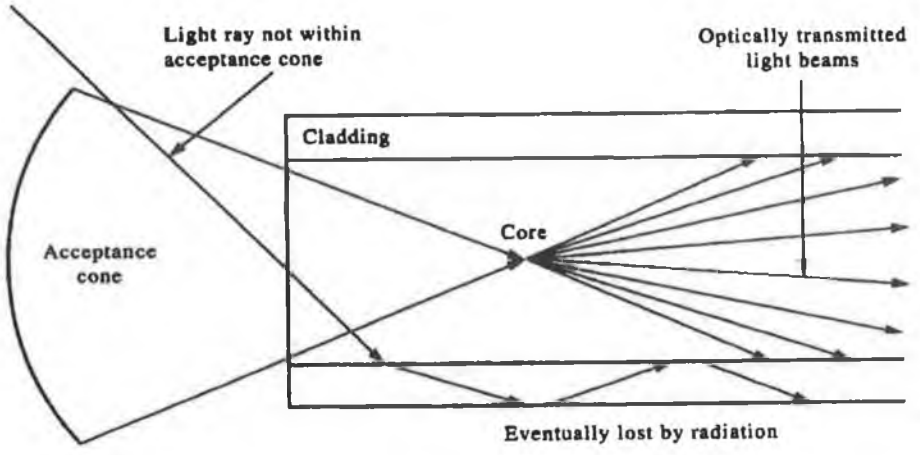

Figure 2.10 Light modes through fibre [14]

2.5.4 Optical fiber dimensions

Typical fibers have core diameters in the range of 8-10 μm for single mode and 50-200 μm for multimode. The outer cladding diameter is typically 125 μm (standard core/cladding ratios: 8/125 μm – lower cladding single-mode; 10/125 μm – matched cladding single-mode; 50/125 μm, 62.5/125 μm, and 85/125 μm graded index). The protective overlayer jacketing will increase the physical size of the fibre by several tens of μm or more (250 μm is a typical overall diameter).

Fibre cable, which includes the fibre, strengthening members and sometimes ancillary conductors as well as a tough abrasion and water resistant sheath, may be as small as a micro-meter for single fibre, and as large as an inch or so in diameter for several hundred fibre [15]. An important additional function of such cables is to limit bending radius to protect the fibre. Special cables such as submarine types tend to be relatively massive because of the need for special strengthening.

Fibre optic basic types, multimode step index, single mode step index and multimode graded index. In the case of this project types of fibre optic used are multimode and

have core/cladding ratio are 125/62.5 and 140/100 as an emitting and receiving the signal.

2.6 Characteristics

This section describes the characteristics of fibres that are of interest to the designer. These range from its transmission parameters to its mechanical properties, all of which are unique in comparison to wire transmission.

2.6.1 Attenuation

Attenuation loss is a logarithmic relationship between the optical output power and the optical input power in a fibre optic system. It is a measure of the decay of signal strength, or loss of light power that occurs as light pulses propagate through the length of the fibre. The decay along the fibre is exponential and can be expresses as:

$$P(z) = P_0 . \text{Exp.} (-\alpha' z) \qquad (2.13)$$

where:

P (z) = optical power at distance z from the input.

P_0 = optical power at fibre input

α' = fiber attenuation coefficient, [1/km].

Engineers usually think of attenuation in terms of decibels; therefore, the equation may be rewritten using $\alpha = 4.343\ \alpha'$, and converting of base 'e' to base 10, as follows [15]:

$$P(z) = P_0\ 10^{-\alpha z} \qquad (2.14)$$

$$\log(z) = -\alpha z/\log 10 + \log P_0 \qquad (2.15)$$

$$\alpha = \alpha_{\text{Scattering}} + \alpha_{\text{absorption}} + \alpha_{\text{bending}} \qquad (2.16)$$

where:

α = fibre loss, [dB/km].

Attenuation in optical fibre is caused by several intrinsic and extrinsic factors. Two intrinsic factors are scattering and absorption. Extrinsic factors are discussed below.

2.6.2 Bending

Extrinsic causes of attenuation include cable manufacturing stresses, environmental effects, and physical bends in the fibre. Physical bends break down into two categories: microbending and macrobending (Figures 2.11 and 2.12). Microbending is the result of microscopic imperfections in the geometry of the core diameter, rough boundaries between the core and cladding, a result of the manufacturing process itself, or mechanical stress, pressure, tension, or twisting. Macrobending describes fibre curvatures with diameter on the order of centimeter. The loss of optical power is the result of less-than-total reflection at the core-to-cladding boundary. In single-mode fibre, the fundamental mode is partially converted to radiating mode due to the bends in the fibre.

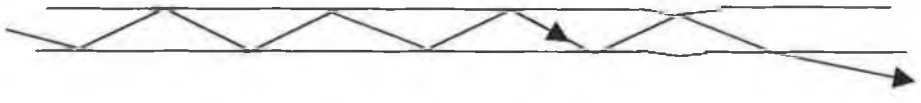

Figure 2.11 Effect of microbend in optical fibre.

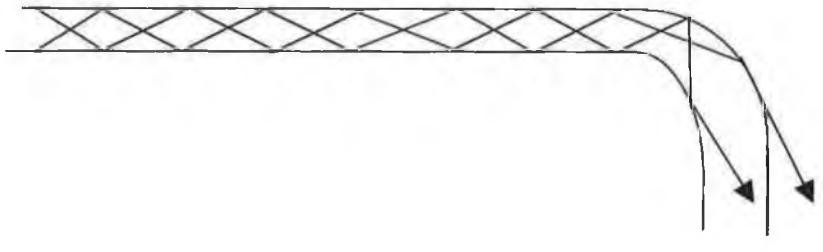

Figure 2.12 Effect of macrobend in optical fibre.

The length of the optical fibre and the wavelength of the light traveling through it primarily determine the amount of attenuation experienced by the optical fibre. There are also many secondary and tertiary factors that contribute. Figure 2.13 shows the loss per unit length of a typical modern optical fibre. The plot covers wavelengths from 0.5 μm to 1.9 μm. As a point of reference, the human eye sees light in the range from 0.4 μm (blue) to 0.7 μm (red). Most modern fibre optic transmission takes place at wavelengths longer than red, in the infrared region. There are three important fibre optic wavelength region, 850 nm, 1300 nm, and 1500 nm. These particular wavelengths were chosen because the loss of the fibre is lowest at these wavelengths. There are three primary mechanisms that influence a fibre's loss at various wavelengths. At shorter wavelength, Rayliegh scattering is important, increasing as λ^{-4}. At longer wavelength, absorption becomes dominant as the molecules in the glass start to resonate. In between, absorption by impurities is also important. The dashed curve in Figure 2.13 shows the approximate location of the absorption caused by the OH^- ions. This is often the most harmful impurity in fibre. When these three loss mechanisms are considered together, there are only a few dips. The plot shows that there are really four dips. The 1060 nm region is a low spot that was skipped over and never became significant although a few companies did produce fibre links in the early 1980's that used this region [16].

The 850 nm region, called the first window, was the first to be widely exploited because of the LED and detector technology that was available in these early days. The 1300 nm region, the second window, is very popular today because of its dramatically lower loss.

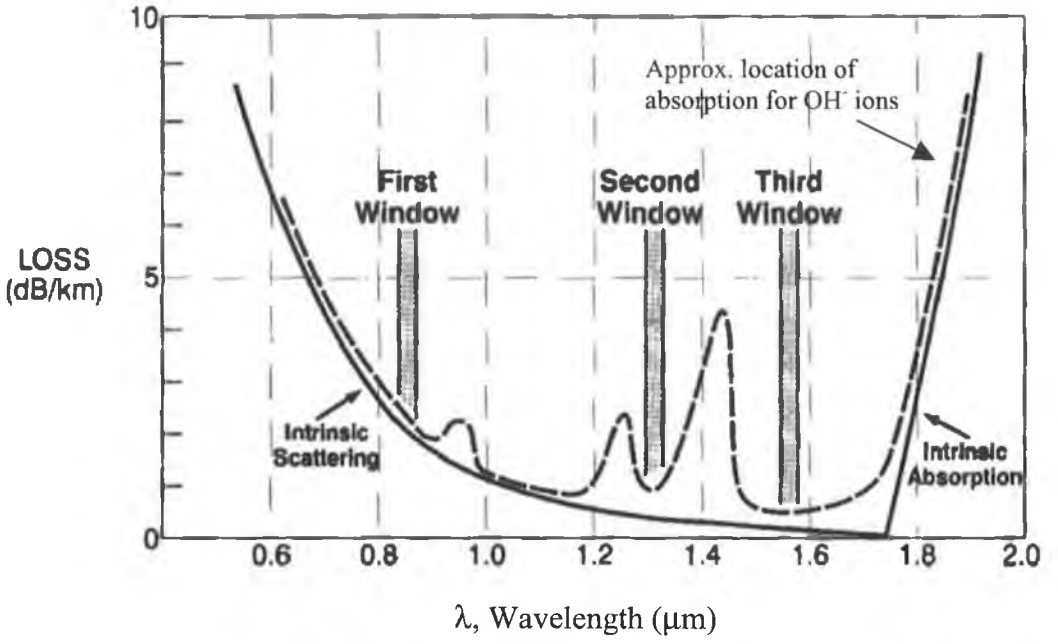

Figure 2.13 Optical loss versus wavelength [16]

The 1550 nm region, the third window, is generally used only in cases where the use of repeaters might otherwise be required or in conjunction with other wavelength as in wavelength-division multiplexed system. A good rule thumb is that performance and cost increase as wavelength increases. A fourth wavelength, 780 nm, is also used. Low-cost short wavelength lasers; 'CD' lasers in this wavelength are manufactured in high volume, making them very economical.

2.6.3 Absorption

Absorption can be caused by the molecular structure of the material, impurities in the fibre such as metal ion and OH^- ions (water), and atomic defects such as unwanted oxidized elements in the glass composition. These impurities absorb the optical energy and dissipate it as a small amount of heat. As this energy dissipates, the light becomes dimmer. At 1.25 μm and 1.39 μm wavelength, optical loss occurs because of the presence of OH^- ions in the fibre. Above a wavelength of 1.7 μm, glass starts absorbing light energy due to the molecular resonance of the SiO_2 molecule.

2.6.4 Scattering

The most common from of scattering, Rayleigh Scattering (Figure 2.14) is caused by microscopic non-uniformities in the optical fibre. These non-uniformities cause rays of light to partially scatter as they travel along the fibre, thus some light energy is lost. Rayleigh scattering represents the strongest attenuation mechanism in most modern optical fibre; nearly 90% of the total attenuation can be attributed to it. It becomes important when the size of the structures in the glass itself are comparable in size to the wavelength of light traveling through the glass. Thus, longer wavelengths are less affected than short wavelengths. The attenuation coefficient (α) decreases as the wavelength (λ) increases and is proportional to λ^{-4}. Rayleigh scattering therefore increases sharply at short wavelengths.

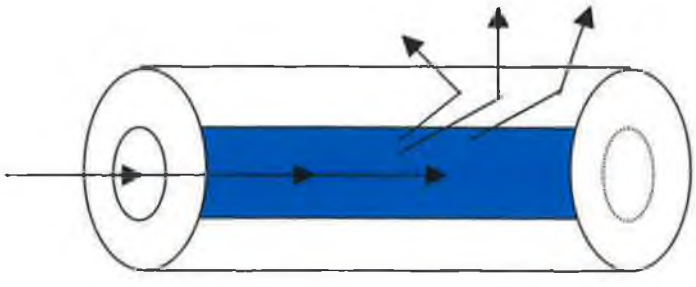

Figure 2.14 Scattering effect in optical fibre.

2.6.5 Dispersion

Dispersion is the mechanism, which limits the bandwidth of the fibre. It is the result of either a wavelength-sensitive effective propagation velocity which causes, for example, a pulse of light composed of a multiplicity of wavelengths to arrive dispersed in time (material dispersion), or a geometrical, flight-path length difference between element of light, even if at the same wavelength, causing them to arrive at the receiving end at different time if they entered the fibre at different angles. Dispersion is a quantity that affects the signal carrying properties of optical fibre. It

is the degradation of the input signal as it travels through the fibre, the pulse becomes longer in duration and generally loses shape.
Dispersion can be divided into material dispersion, waveguide dispersion and modal dispersion.

Material dispersion

Material dispersion is an intrinsic material property, which is a function of wavelength. It is more pronounced when the light source has a broad spectrum such as of Light Emitting Diodes (LEDs) (typically 30 to 100 nm between half-power points). Injection Laser Diodes (ILDs), in contrast, have very narrow spectra (typically 3nm), and their emissions are consequently much less affected by material dispersion. Light launched by very high quality, single longitudinal mode lasers that produce extremely narrow spectra (e.g., 0.1 nm range) is virtually immune to this effect.

Waveguides dispersion

Another wavelength-dependent dispersion mechanism is waveguide dispersion, which is due to the wavelength dependence of modal group velocity [17]. By altering the fibre compassion slightly it so possible to shift the point at which dispersion occurs to higher or lower wavelengths shifting the operational wavelength enables lower light attenuation to be obtain.

Modal dispersion

The differing velocities of modes in a multimode optical fibre cause modal dispersion. Prior to this light has been presented as rays. Light however also acts with a wave nature. For a fibre a certain number of modes are supported. The number of modes a fibre supports changes with variation in the core diameter, optical wavelength and the refractive indices of core and cladding. As the core diameter increases many modes are supported in a fibre and the ray optical analysis proves adequate, unless mode coupling in multimode fibre is of interest. Figure 2.15 shows how a beam travelling along the centerline of a step index multimode fibre reaches the end of the fibre more quickly thus dispersing the input signal. Singlemode fibers do not suffer from modal dispersion

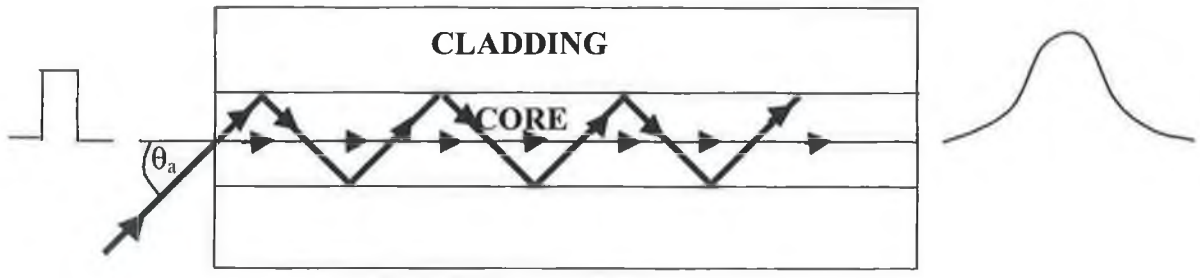

Figure 2.15 Optical fibre modal dispersion.

2.7 Classification of optical fibres

There are two basic types of optical fibre: multimode fibre and single mode fibre. Multimode fibre (Figure 2.16) was the first type to be commercialized. Its core is much larger than that of single mode fibre (Figure 2.17), allowing hundred of rays (modes) of light to move through the fibre simultaneously. Single mode fibre, on the other hand, has a much smaller core. While it would seem that a larger core would allow for a higher bandwidth or higher capacity to transmit information, this is not true. Single mode fibres are better at retaining the fidelity of each light pulse over longer distance, and they exhibit less dispersion caused by multiple rays or modes. Thus, more information is transmitted per unit time. This gives single mode fibre higher bandwidth compared to multimode fibre. Single mode fibres are generally characterized as step-index fibre meaning the refractive index of the fibre core is a step above that of the cladding rather than graduated as it is in graded-index fibre. Single mode fibres also experience lower attenuation than multimode fibres.

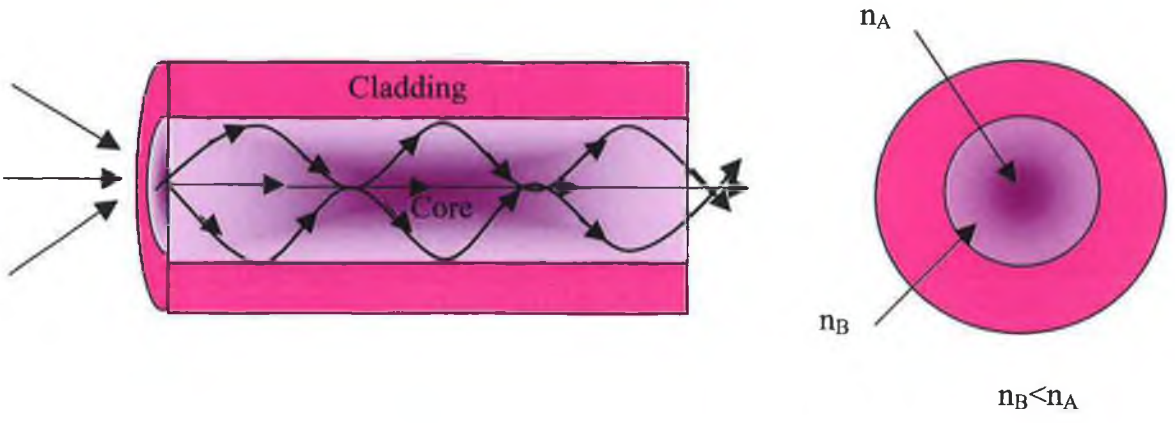

Figure 2.16 Multimode graded index fibre

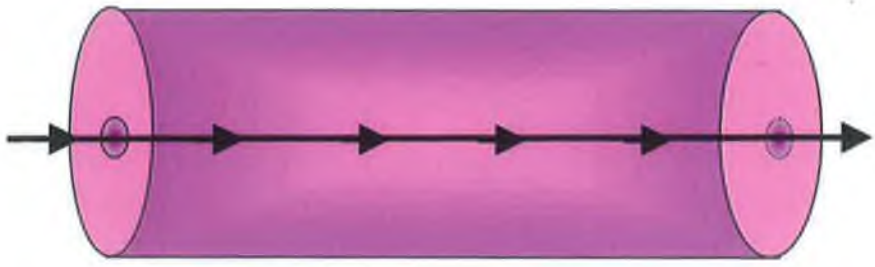

Figure 2.17 Single mode fibre

Single mode fibers however also have some disadvantages. The smaller core diameter makes coupling light into the core difficult. The tolerances for single mode connectors and splices are also much more demanding.

Multimode fibre may be categorized as step index or graded index fibre. The term multimode simply refers to the fact that numerous modes of light rays are carried simultaneously through the waveguide. The larger core diameter increases coupling ease and generally multimode fibre can be coupled to lower cost light sources.

2.8 Laser based fibre optic safety

In order to use laser system safety, there are a few basic rules that are must be observed to limit exposure to laser radiation. Laser radiation will damage eyesight under certain conditions.

The following guidelines are important in laser safety:

- Always read the product data sheet and laser safety label before applying power.
- If safety goggles or other eye protection are used, be certain that the protection is effective at the wavelength emitted by the device under test before applying power.
- Always connect a fibre to the output of the device before power applied.
- Never look in the end of a fibre to see if light is coming out. Most fibre optic laser wavelengths (1300nm and 1550nm) are totally invisible to the unaided eye and will cause permanent damage. Shorter wavelength lasers (780nm) are visible and are potentially very damaging. Always use an optical power meter, to verify light output.

- Never look into the end of a fibre on a powered device with any sort of magnifying device. This includes microscopes, and magnifying glasses.

2.9 Principles fiber optical sensor

In this section, the fibre optic transmission system will be described. Modern optical fiber sensors owe their development to two of the most important scientific advances made in the 1960's - the laser (1960) and the modern low loss optical fiber (1966). Both equally had origins of work the previous decades. In particular development the microwave predecessor of the laser (the maser) and the short-length low transparency fibres used in early endoscopes for medical and industrial applications were significant. Thus, the early 1970s saw some of the first experiments on low-loss optical fibres being used, not for telecommunications, as had been the prime motivation for their development but for sensor purposes [17]. This pioneering work quickly led to the growth of a number of research groups, which had a strong focus on the exploitation of this new technology in sensing and measurement. The field has continued to progress and has developed enormously since that time.

The main drive of research in this area has been to produce a range optical-fibre based techniques which can be used for a variety of different sensor purposes, providing a foundation for an effective measurement technology which can complete with conventional methods, usually in niche areas. Therein lies the recipe for the success of fibre sensor – in tackling difficult measurement situations where conventional sensor is not well suited. The resulting sensors have a series of characteristics that are familiar. They are compact and lightweight, in general, minimally invasive and offer the prospect that they can be multiplexed effectively on a single fiber network [18].

Fiber optic sensors have the advantages that they are relatively immune from electromagnetic interference, have low power consumption, high sensitivity in some cases and are compatibility with electronic control and modulation. Measurement can be made in hostile environments and the fibre can transmit the signal remotely.

2.9.1 Elements of a fiber optic sensor

Fibre optic components transmit information by turning electronic signals into light. Light refers to more than the portion of the electromagnetic spectrum that is visible to the human eye.

The term wavelength refers to the wavelike property of light, a characteristic shared by all forms of electromagnetic radiation. The wavelength of light used in fibre optic applications can be broken into two main categories: near infrared and visible. The visible light has a wavelength range from 400 to 700 nanometers (nm) and has very limited uses in fibre optic applications, due to the high optical loss. Near-infrared wavelengths range is from 700 to 2000 nanometers are almost always used in modern fibre optic systems. The principles behind fibre optic systems are relatively simple. As shown in Figure 2.18, fiber optic links contain three basic elements: the transmitter that allows for data input and outputs an optical signal, the optical fibre that carries the data, and the receiver that decodes the optic signal to output the data.

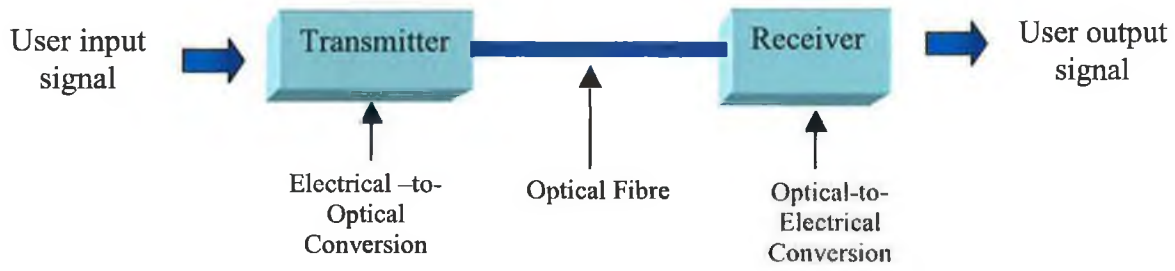

Figure 2.18 Element of a fiber optic sensor

2.9.2 Fiber optical transmitter

The transmitter shown in Figure 2.19 uses an electrical interface, either video, audio data, or other forms of electrical input, to encode the user's information through modulation. The electrical output of the modulation is usually transformed into light either by means of a light-emitting diode (LED) or laser diode (LD). The wavelengths of this light sources range from 660 nm to 1550 nm for most fibre optic

applications [16]. Laser diodes can be selected for photoelectric sensing having most of the advantages of LED's. Laser diodes emit higher intensity, which increases the range of the sensor and also increases the effectiveness, an object that has low reflectivity [19].

An LED with 850 nm and laser diode with 1300 nm wavelength where chosen for the work in this thesis for comparison proposes.

Figure 2.19 Elements of a fiber optic transmitter

2.9.3 Fiber optical receiver

The receiver, illustrated in Figure 2.20, decodes the light signal back into an electrical signal. Two types of light detector are typically used: PIN photodiode or the avalanche photodiode (APD). Typically, these detectors are made from silicon (Si), indium gallium arsenide (InGaAs), or germanium (Ge). The amplified electrical signal is then sent through a data decoder or demodulator that converts the electrical signals back into video, audio, data, or other forms of user information.

The wavelength characteristics of light source should match the wavelength characteristics of the photodetector [13]. The PIN photodiodes are the most suitable devices for long-wavelength optical communications system due to their high efficiency and their capability for high-speed operation. In optical receiver circuit terminal, a PIN photodiodes were chosen as the photodetector device because of its excellent linearity, simplicity and operational stability combined with a sufficiently fast response and low cost. While presenting a maximum responsivity in the 650-950 nm and 900-1700 nm regions, hence begin matched to the LED and laser diode of

the transmitters respectively. PIN photodiodes were used in this work because of these reasons.

Figure 2.20 Elements of a fiber optic receiver

2.10 Scanning system technology

Over the last three decades the attention which has been given to the laser technology has increased. The light beam from a laser is monochromatic, coherenent and highly directed [20]. These properties have motivated a growing list of laser applications in the fields of measurement and inspection. The major advantages of laser scanning systems are listed as [21]: higher resolution, faster scanning speed and high contrast image acquisition. The laser scanning inspection system using triangulation technology is one of the most common and useful methods for 2D-and 3-D profiling where accurate repeatable height measurements are required [22]. Laser scanning has been successfully implemented in the inspection of widely varied material surfaces. Continuous on-line inspection of moving sheet is one of the most active fields of optical inspection [23]. Examples of sheet materials for which optical inspection systems have been reported include paper webs, textile fabric, glass material, hot slabs and cold-rolled metal strip [24]. These systems are essential tools for the implementation of modern statistical process control procedures. Non contact methods of measuring thickness and distance with laser sensors have already been widely reported in the literature [25-28]. Very high orders of accuracy in the measurement of lengths at close ranges of up to several meters are achieved by interferomtric methods [29,30]. These methods are however mostly too complicated to be practical for application in production [31]. An intensity-based sensor requires a much simpler optical system, and therefore, can be made very small. The working

principle of these sensors is based on the correlation between the detected intensity of the reflected light and the average roughness of the surface. The essential problem with intensity-based sensors is that the detected intensity is strongly dependent on the gap distance between the sensor and the surface and on the surface reflectivity. The intensity of the detected light depends upon how far the reflecting surface is from the fibre optic sensor [32]. Light scattering of a test surface may be a changed by different microstructures encountered [33]. However, a sudden change in the light intensity would occur when the incident light beam encounters a defect [34].

Most previous research efforts on this area have been focused on the development of the path planning of commercial laser scanning system [35]. Laser scanning systems have been successfully used in the inspection of widely varied material surfaces, from metals of all types to paper, glass, plastics, films, textiles, as well as magnetic and optical discs [34]. A laser scanner consists of two parts: an illumination part and on imaging part [37]. One of the most effective sensor devices currently available is the fibre optic sensor [38]. The response of an optical fibre can be affected by very small change in fibre geometry caused by conditions such as elongation, bending, or twisting [39]. These changes in response can be used to detect strains in different materials. However industrially photoelectric displacements sensing is the most common application of fibre-optic sensing [36].

2.11 Triangulation method

Vision systems often are suitable for on-line production measurement applications. For height or displacement measurements though, laser-triangulation sensors provide more detailed and repeatable data than conventional vision systems. For this reason, system integrators incorporate triangulation sensors into automated assemblies to provide on-line gauging or position sensing.

Laser triangulation is frequently the best solution for these types of applications because it combines the advantage of non-contact inspection with the ability to measure with sub-micrometer resolution. Recently, the importance of 3-D vision in robotics was recognised and research activities in this field are growing [40,41].

The sensor's laser diode projects a beam of light onto the target object. Some of the light is reflected off the object onto a light-sensitive detector built into the sensor. The detector records the position of the reflected beam and reports a height measurement. If the target or the sensor moves, the position of the reflection on the detector changes. The sensor calculates the amount of change based on the new spot position on the detector [42]

Among different techniques described, the triangulation method seems to be an attractive approach that can lead to low-cost 3-D camera [43-46]. Basic elements of such a range finding system are: a light source, a scanning mechanism to project the light spot onto the object surface, a collecting lens and a position sensitive photodetector [47]. Optical triangulation provides a non contact method of determining the displacement of a diffuse surface. Figure 2.21 shows the diagram of a laser-based system that is successfully used in many industrial applications. A low power He-Ne or diode laser projects a spot of light on a diffusive surface. A portion of the light is scattered from the surface and is imaged by a converging lens on a linear diode array or linear position detector. Many triangulation systems are built with detector perpendicular to the axis of the detector lens. The displacement Δd of the image on the detector in terms of the displacement of the diffusive surface Δz, parallel to the incident beam is approximately:

$$\Delta d = \Delta z \, m \sin\theta \qquad (2.17)$$

where m is the magnification factor and θ is the angle between a line normal to the surface and the light scattered to the imaging lens.

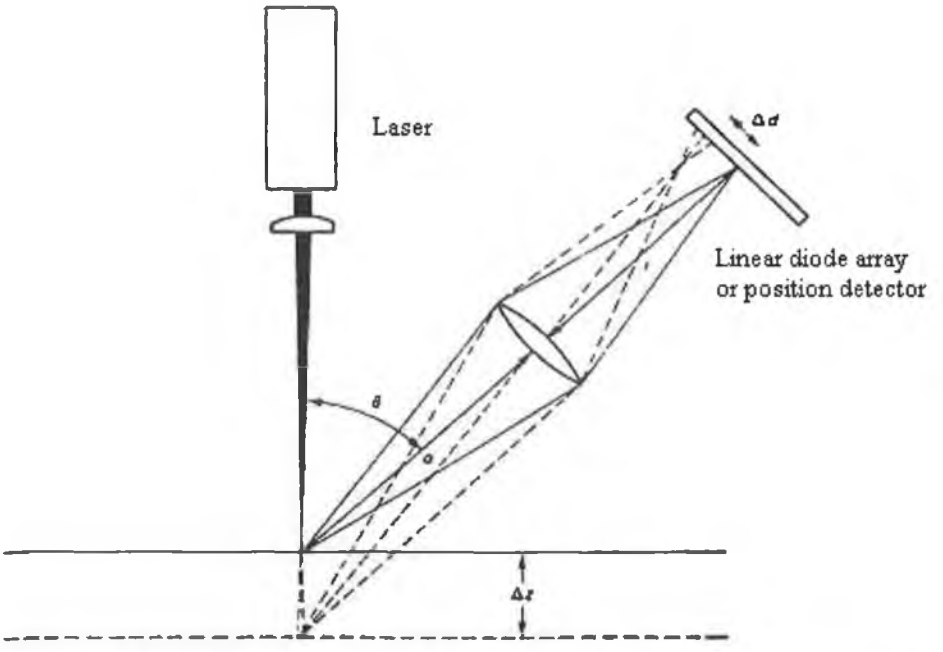

Figure 2.21 Diagram of a laser based optical triangulation system [37]

Optical triangulation is one of the most common methods for acquiring range data. Although this technology has been in use for over twenty years, its speed and accuracy has increased dramatically in recent years with the development of geometrically stable imaging sensors such as CCD's and lateral effect photodiodes. The range acquisition literature contains many descriptions of optical triangulation range scanners [48-53]. The variety of methods differ primarily in the structure of the illuminate (typically point, strip, multi-point, or multi-strip), the dimensionality of the sensor (linear array or CCD grid), and the scanning method (move the object or move the scanner hardware). For optical triangulation systems that extract range data from single imaged pulses, variations in surface reflectance and shape result in systematic range errors. Several researchers have observed one or both of these accuracy limitations [54,55]. For the case of coherent illumination, the images of reflections from rough surfaces are also subject to laser speckle noise which, introducing noise into the range measurement data. Researchers have studied the effect of speckle on range determination and have indicated that it is a fundamental limit to the accuracy of laser range triangulation, though its effects can be reduced with well-known speckle reduction techniques [56,57]. These attempt to correct for variations in surface reflectance by noting that two imaged pulses, differing in position or wavelength are sufficient to overcome the reflectance errors. Some

restrictive assumptions are however necessary for the case of differing wavelengths. [14].

Digital arrays are composed of rows of individual detectors, each reporting a separate voltage reading. They generate more data than analog sensors, so the data rate is slower, but post-processing provides more detailed information. Using an algorithm to analyze the data, the digital sensor locates the center of the laser spot to within a fraction of a pixel, identifies multiple spots when more than one reflection is recorded, and reports the location and intensity of each spot. Digital data processing allows the user to set thresholds that filter irregularities and eliminate spurious data, thereby improving the readings' quality.

2.11.1 Triangulation method applications

Today's measurement requirements include smaller components, tighter tolerances, and lower inspection time, increasing the need for precision-measurement tools to perform tasks such as:

- measuring fragile, etched metal parts such as disk-drive suspension arms
- scanning laser-printer drums and other components that can be damaged by contact methods
- inspecting integrated circuits, connectors, and other electronic components with easily damaged wire contacts
- checking materials that must be measured when still wet or soft, such as adhesives, sealants, and solder pastes.
- Pairs of sensors can be used on-line web systems where manufacturing involves a continuous roll of material passing through a number of steps before being cut into the final product. By mounting one sensor above and another at roller level or below the web, material thickness can be monitored in real-time as the process operates.
- Triangulation sensors are also used to inspect the delicate wire leads on integrated-circuit devices. The leads are easily bent or damaged by handling, which can cause defects in finished circuit boards. The best time to inspect devices is immediately prior to placement. Many of the leading manufacturers of

high-speed component placement systems use a specially designed triangulation sensor that fits on the placement head and performs on-the-fly inspection as the head travels around the board to place components.

- Triangulation sensors excel at collecting high-resolution measurements over a relatively small working range. This makes the technology a good fit for the electronics industry, where small, fragile components are the norm and touchless inspection is preferred. Triangulation sensors are used on-line and off-line for process control in a variety of inspection systems.
- Besides being suitable for inspecting integrated circuit devices, triangulation sensors have proven to be ideal for inspecting soft or wet materials such as solder paste and thick film ink. When evaluating paste or ink deposits, height is the critical measurement, so triangulation is preferred over other measurement methodologies.
- Triangulation sensors are used on non-contact scanning stations that diagram and analyze a target object's co-ordinates. A single row of data points collected by the sensor form a line show the object's 2-D profile. When the height data from a parallel series of scans is in the z-direction combined with x and y data, the scanning system can generate a 3-D graph or wire diagram showing the topography of the entire measurement area.

2.11.2 Error in triangulation systems

For optical triangulation systems, the accuracy of the range data depends on proper interpretation of imaged light reflections. The most common approach is to reduce the problem to one of finding the "center" of a one-dimensional pulse, where the "center" refers to the position on the sensor, which hopefully maps to the center of the illuminate. Typically, researchers have opted for a statistic such as mean, median or peak of the imaged light as representative of the center. These statistics give the correct answer when the surface is perfectly planar, but they are generally inaccurate whenever the surface perturbs the shape of the illuminate.

2.12 Displacement measurement using fibre optic laser scanning system

Fibre-optic displacement sensors were among the first implementation of fibre-optic sensing they have also been used to measure other parameters such as pressure, strain and vibration [58]. There are three methods of measuring displacement using fiber-optic sensors: coherent interferometry [59], low coherence interferometry [60,61] and intensity modulated sensors [62]. In the intensity modulated sensors the parameters of interest affects the intensity of the signal collected by the photodetector. Of these methods the intensity modulated sensor is the simplest and cheapest to implement but is limited to highly reflective surface. The other two methods prefer reflective surfaces but their principle of operation is not absolutely reliant on the reflectivity of the surface in question being based on the wavelength of light.

For displacement measurement in intensity based fibre-optic sensors there are two basic set-ups: one uses a bifurcated fibre-optic bundle the other uses arrangements of single fibres. A bifurcated bundle fibre-optic sensor identical to photoelectric sensors can measure displacement from a reflective surface if it has an analogue output [58]. Modelled the operation of these bundle type displacement sensors by [63], for different distribution of sensing and emitting fibres in the sensing head of the bundle and compared with experiment.

Using single fibres to deliver and collect light in a fibre-optic sensor uses the internal reflection properties of optical fibres. These sensors have very high sensitivity to displacement but with the disadvantages of close stand off distance to the surface and short ranges. Some different arrangements of single fibre displacement sensors are shown in Figure 2.22 [64].

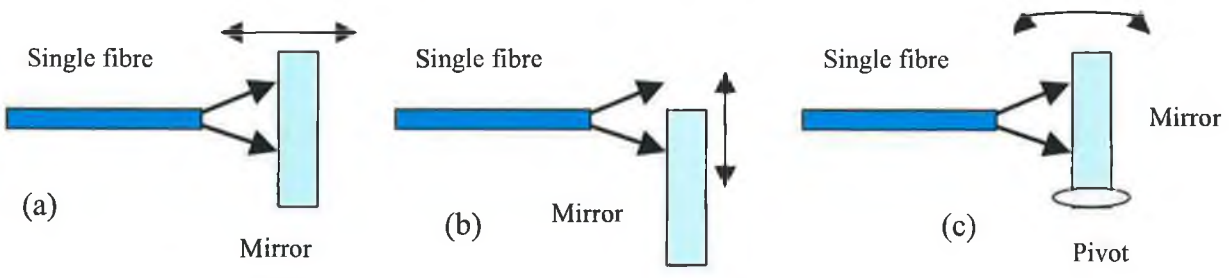

Figure 2.22 (a) Horizontal displacement (b) Vertical displacement (c) angular displacement

These arrangements have the same fibre emitting and receiving light, Figure 2.23 shows an arrangement with separate fibres for emitting and receiving light.

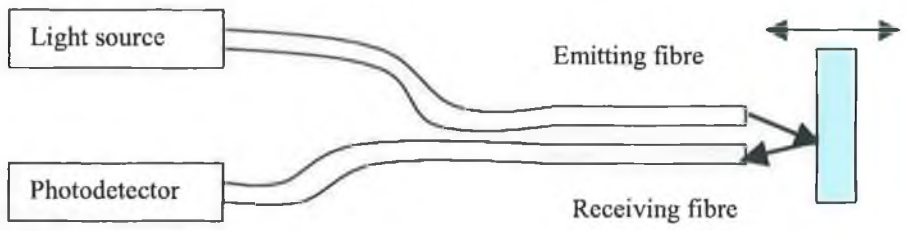

Figure 2.23 (a) Schematic diagram of basic fibre-optic displacement

Fibre-optic sensors can be integrated with silicon micro machining [65,66] to provide mechanical assemblies for sensors based on these principles among others. This is an interesting area, which may lead to low cost sensors for many instrumentation applications.

2.13 Fiber optic surface roughness sensor

Generally sensors that can be used to measure surface roughness can be classified into three categories: interferomtric sensors, polarimetric sensors, and intensity based sensors. An interferomtric fiber sensor for surface roughness measurement was recently developed [67]. This sensor employs a fiber optic guide and lens arrangement that forms an interferomtric cavity between the lens front and the surface to be measured [68]. A typical polarization-based surface roughness sensor was previously presented [69]. Their sensor is based on the polarization changes in the light scattered from a target surface. The data obtained from the polarization measurement have been correlated with some parameters of surface roughness. Both interferomtric sensors and polarimetric sensors require relatively complicated optical system [68]. Intensity based sensor, on the other hand usually requires a much simpler optical system, and therefore, can be made very small. In addition, the

working principle of intensity based sensors is also very simple. Research on surface roughness measurements using intensity-based fiber optic sensors was previously conducted [70,71]. They used either one or two fiber bundles to deliver light to the surface and collect the reflected light and guide it to a photodetector.

Surface roughness is of great importance in engineering industry [14]. The traditional method for measuring surface roughness is the contact stylus method [72,73]. Optical methods due to their non-contact nature can perform measurements of surface roughness very quickly, often while the sample is in motion. Several optical methods are applicable to surface-roughness measurement. The most common of these is interferometry [74]. The main advantages of optical methods are long area covering measurement capability, applicability to in-process measurement, and fast measurement. The absences of mechanical contact with the measured surface and its non-destructiveness make the optical method in high demand by industry [75]. There are other non-contacting methods such as capacitance, pneumatic and ultrasonic, but these are not in general use and do not offer the same versatility [76].

Surface roughness can be measured through the effect of light scattering from the surface [77,78]. In the transition from a smooth surface, which transmits light specularly, to a rough surface, a higher proportion of incident light is scattered diffusely. This transition can be related to surface roughness.

Roughness measurements and microtopographic inspection of rough surface requiring measuring ranges from a few micrometers to a few millimeters.

Among the quality control tasks, surface inspection is a major one. For a long time, invasive stylus-based systems were widely accepted. Today the new standards and the huge new variety of surfaces and materials to be inspected often all in the same industry, require the use of a versatile, non-contact system. Optical or laser-based systems have clearly proved their merits in this area [79,80].

Reflection from a surface depends on the wavelength and incident of angle of the incident beam and also the properties of the surface; electrical properties (permittivity, permeability and conductivity) and surface features [58]. Surface features include surface roughness, shape parameters, surface spatial frequency, lay, directionality, and surface slope. It is possible to infer some of these surface features from the light scattering characteristic of the surface. Equation 2.18, taken from

Becklmann & Spizzichino [78], describes the scattering electromagnetic radiation from a random rough surface:

$$\frac{I_s}{I_o} \propto \exp[-(\frac{4\pi R_q \cos\theta}{\lambda})^2] \qquad (2.18)$$

where I_s is the specular reflectance, I_o is the total reflectance, θ is the incident angle, R_q is the rms surface roughness and λ is the wavelength. This equation also indicates how the incident angle and light wavelength affect the reflectivity. To estimate roughness from this equation the scattering ratios I_s/I_0 must be above 0.6. This equation describes how in the transition from a mirror like surface to a rougher surface what fraction of light intensity is transmitted specularly. The equation was shown to be valid by Hensler [81].

Chapter 3

Experimental design and set-up of laser scanning system

3.1 Introduction

The main system-level components of the fibre optic sensor used in this work were the light emitter, the photo detector, the fibre waveguides, data acquisition and analysis, using Labview software. Each component plays a vital role in the quality of transmission. Careful decisions, based on system requirements, must be made for each component of the system if high-quality sensing is to be achieved. This chapter is mainly devoted to a system description covering the following main areas:

1) System configuration
2) Labview
3) Mechanical design
4) Resolution
5) Electronic design

3.2 System configuration

The effective application of a fibre optic system requires consideration of entire system: the transmitter (light emitter diode LED and laser diode), travelling signal (fibre optics, length, characteristics, and connectors), receiving detector (PIN photodiode, preamplifier). This section will describe and detail the following three main parts of the system:

1) Signal sources
2) Signal travelling
3) Received signal

3.2.1 Signal sources

Light emitters are a key element in any fibre system. These components convert the electrical signal in to a corresponding light signal that can be projected into the fibre. The light emitter is important because it is often one of the most costly elements in the system, and its characteristics often strongly influence the final performance limits of a given fibre optic link.

Two types of light emitters in widespread use in modern fibre optic systems are laser diodes (LD's) and light emitting diodes (LED's). Laser diodes may either a Fabry-Perot or distributed feedback's (DFB) type while LED's are usually specified as surface-emitting diodes. These different classifications will be discussed in detail later in the chapter. All light emitters are complex semiconductors that convert an electrical current into light. LED's and laser diode have been of interest for fibre optic application because of five inherent characteristics:

- Small size
- High radiance (emit a lot of light in a small area)
- The emitting area is comparable to the diameter of optical fibre cores
- They offer high reliability and have long life.
- High modulation speed (can be turned ON and OFF very quickly)

The light sources selecting considerable to the above characteristics. The practical aspects selecting and using either of the electronic light sources are discussed below.

3.3.1 Light emitting diodes

Light emitting diodes are characterised by their emission of incoherent light due to the random nature of the recombination of the hole-electron pairs. LED's are made of several layers of p-type and n-type semiconductors. A p-n junction generates the photons and several p-p and n-n junctions direct the photons to create a focused emitting light. These later mentioned junctions direct the light by providing energy barriers and a change in the index of refraction. The energy is emitted as infrared radiation or visible light.

Figure 3.1 shows a schematic diagram of a p-n. diode. V_F is the forward voltage, the voltage drop between the p and n terminal of the diode. I_F the forward current, is the current flowing from the p terminal, anode, to the n terminal, cathode, of the diode.

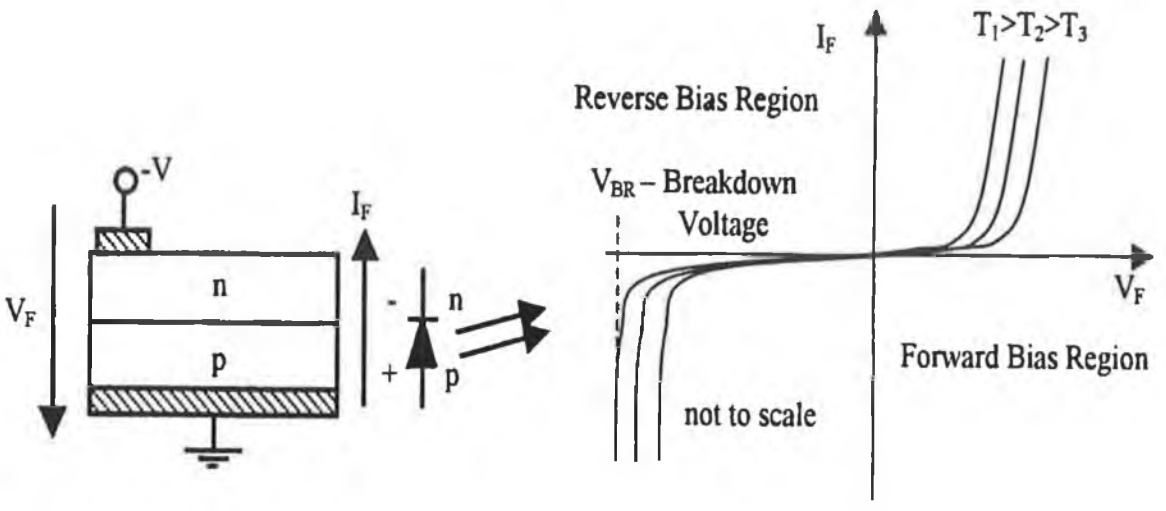

Figure 3.1 Schematic diagram of a p.n. diode [82].

There are two main types of LED's currently being used:

- Surface-emitter
- Edge-emitter

Surface-emitter

Surface emitting devices emit light through a window that is in a plane parallel to the surface of the device [83]. Figure 3.2 shows a schematic of the surface emitter LED. Surface emitters are made of layers of semiconductor material that emit light in a 180^0 arc. They are relatively inexpensive and very reliable, but the emission pattern limits the coupling efficiency with the fibre, and therefore the amount of power that can be transmitted. Surface emitters are the most economical of the two types of LED's but they have low output and are generally slower devices. The emitted light is not directional, with a beam width at half intensity of about 120^0 [84]. Spherical lenses are routinely applied in association with these devices, which couples the beam from a surface emitting LED into a fibre.

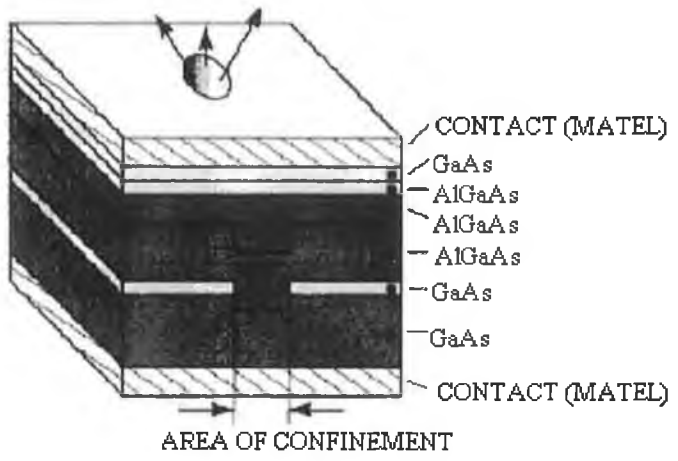

Figure 3.2 Surface-emitter diode [15].

Edge-emitters

In edge-emitting LED's the window is embedded between two layers as shown in the Figure 3.3. Edge emitters are designed to confine the light to a narrow path direction. This focusing of the light gives more emitted power, and more power can be coupled to the fibre because the path is comparably to the size of the optical fibre core. Edge emitters LED's are considerable faster devices than surface-emitting LED's. Surface emitting LED's are however almost always more stable over temperature ranges than the edge-emitting type. For edge emitting LED's 850 nm may only drift 0.03 $dB/^0C$, while a 1300 nm source may drift three to five times as much. The optical power drops as the temperature increases as shows in the Figure 3.4. Temperature also affects the peak emission wavelength [15].

Of the two light source types, LED's are the most widely used for short system fibre optic applications. In general, LED's tend to cost less than laser diodes, so they find wider application.

Spectral characteristics in LED's can be important. Spectral characteristics represent the light intensity of the source against its wavelength Figure 3.5 shows the typical optical spectra for LED's. An 850 nm and 1300 nm surface-emitting LED has a FWHM (full width half maximum) of 60 nm and 110 nm respectively. The last

figure shows an edge emitting 1300 nm LED. It has a much more compact spectrum with a FWHM of about 50 nm.

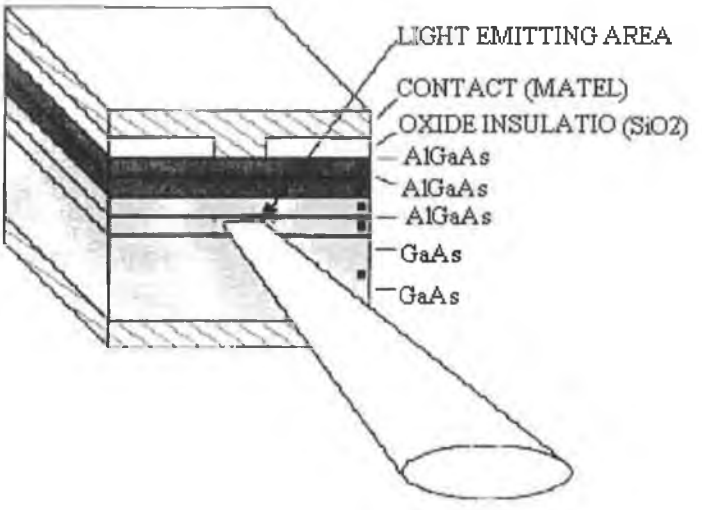

Figure 3.3 Edge-emitter diode.

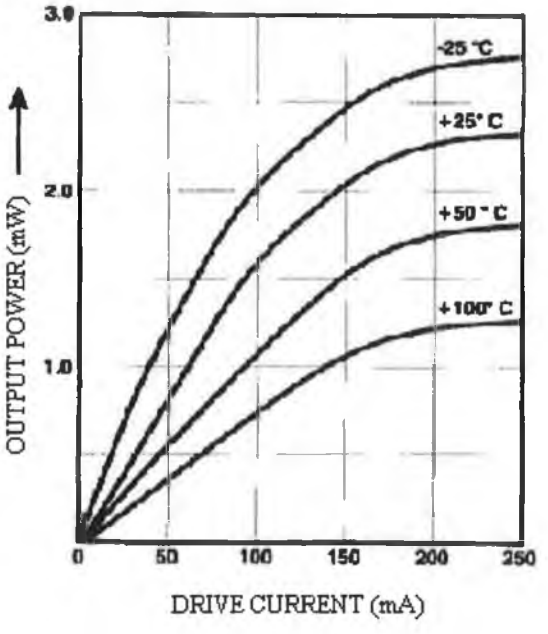

Figure 3.4 Typical LED behaviour versus temperature [15].

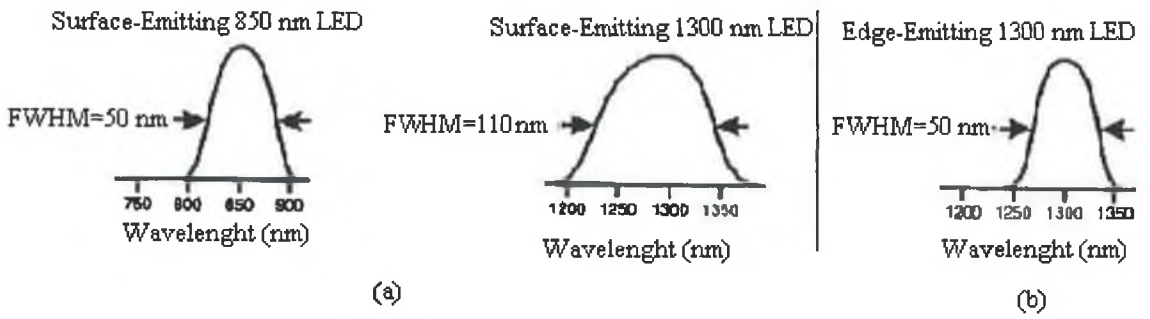

Figure 3.5 Optical spectra for LED's. (a) Surface-emitting 850 and 1300 nm (b) Edge emitting 1300 nm [15].

3.3. 2 Laser diode

Laser diodes are semiconductors in which an amplifying medium has been created together with a resonant cavity as shown in Figure 3.6 and in which population inversion is achieved by means of a current. As long as the current remains below a threshold value, the laser diode behaves as a conventional light-emitting diode. As soon as the threshold is reached, population inversion is achieved and the laser effect is initiated

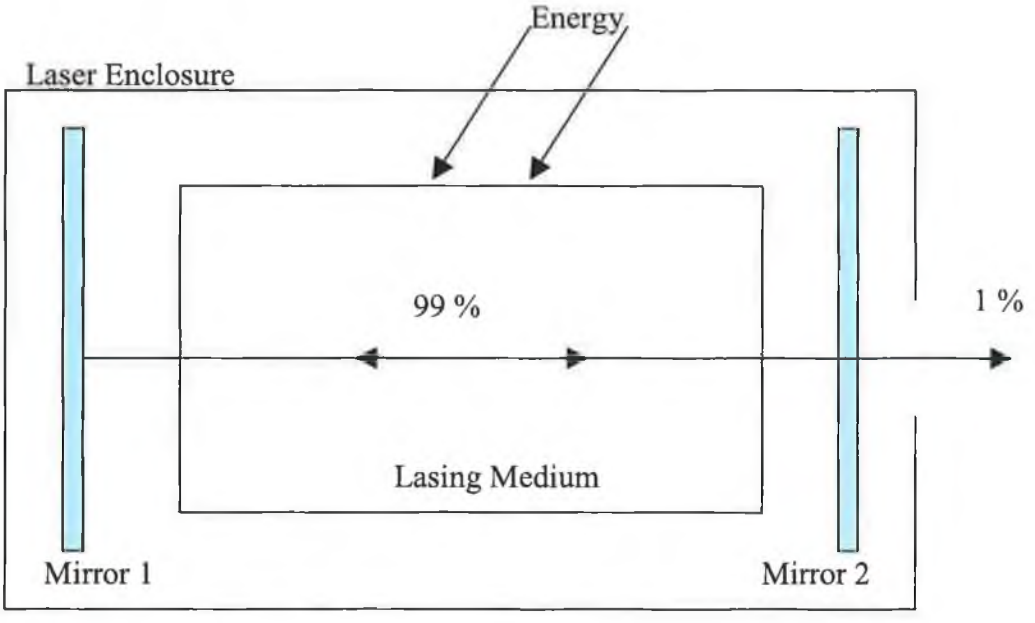

Figure 3.6 Light amplification in a laser cavity

Figure 3.7 shows the layer structure of an AlGaAs laser. The shaded layer indicates the laser cavity. As this occurs at both ends of the cavity, it is common to include a monitor photodiode at the inactive side.

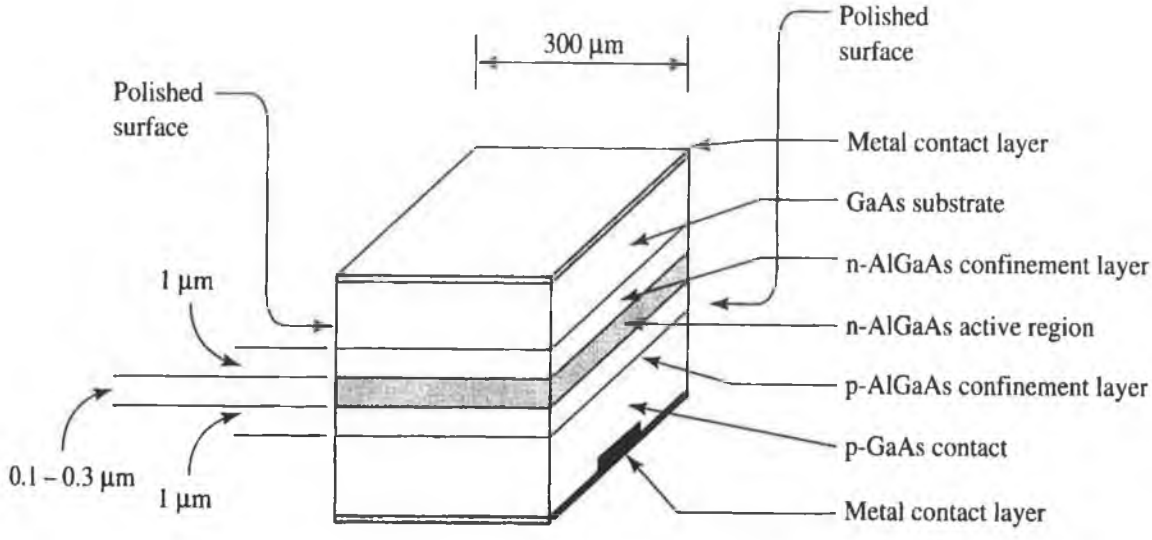

Figure 3.7 Layer structure of an AlGaAs laser [85].

The output power versus forward current curves of typical AlGaAs laser and the forward current versus the forward voltage characteristics are shown in Figure 3.8 (a) and (b) respectively.

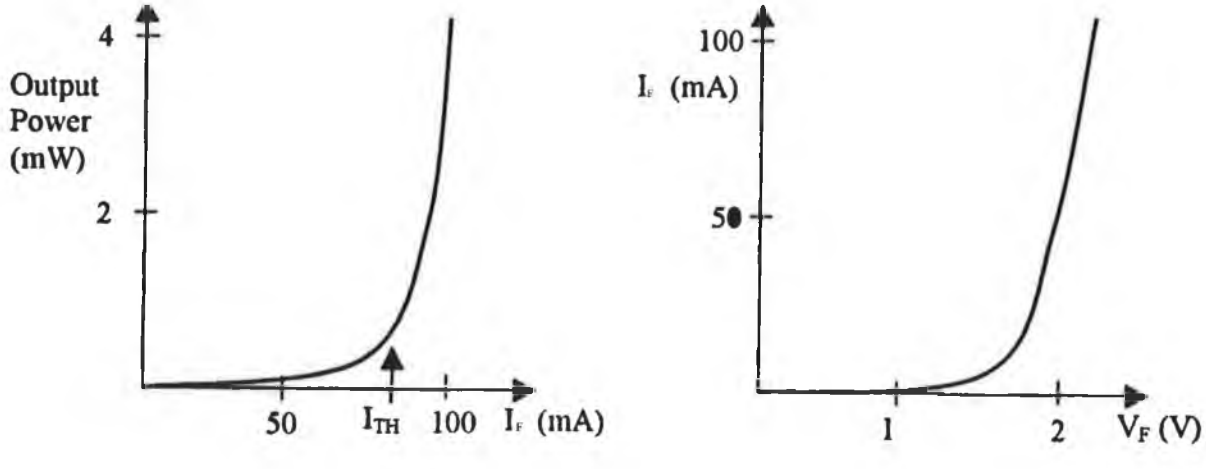

Figure 3.8 (a) Output power versus current and (b) forward current versus voltage [86].

Laser diodes are available as single mode and multimode devices. The spectra pattern of a multimode laser is multiple peaks at a range of wavelengths. A single mode laser operates with a single wavelength peak. It is also possible to make a single mode laser diode, but it is more expensive to do so. A multimode laser diode was seen to be much better for the fibre optic defect sensing applications.

There are two main types of laser diode structures, Fabry-Perot (FP) and distributed feedback (DFB). First, 130nm Fabry-Perot laser as showed in Figure 3.9. The spectrum consists of nine discrete lines. This would properly be called a multimode laser, not referring to multimode fibre, but to the fact that the laser emits light at a number of discrete frequencies. Figure 3.9 b shows the spectra of DFB 1300 nm laser diode. Generally multimode lasers are a better choice when used with multimode fibre since they are less coherent and produce a lower contrast speckle pattern.

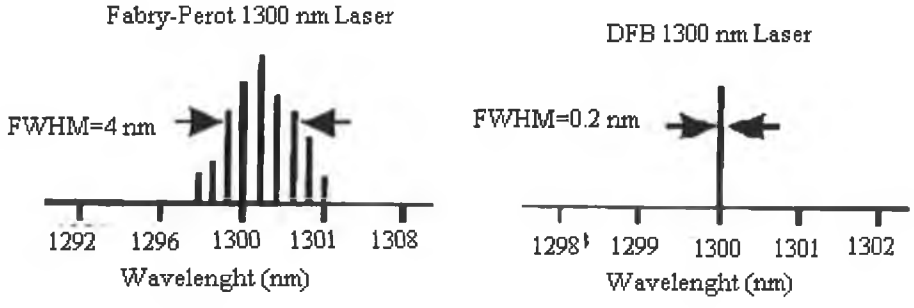

Figure 3.9 (a) Spectra of Fabry-Perot and (b) DFB 1300 nm laser diode [15].

Lasers can survive wide temperature ranges up to full industrial specification, -40^0C to 85^0C. Temperature affects the peak emission wavelength as well as the threshold current and the slope efficiency of the laser. Most lasers exhibit a 0.3-0.6 dB/^{0}C drift in the peak emission wavelength as temperature varies. Generally, laser optical output is approximately proportional to the drive current above the threshold current. Below the threshold current, the output is from the LED action of the device. Above the threshold, the output dramatically increases as the laser gain increases. Figure 3.10 shows the typical behaviour of a laser diode. As operating temperature change, two effects can occur.

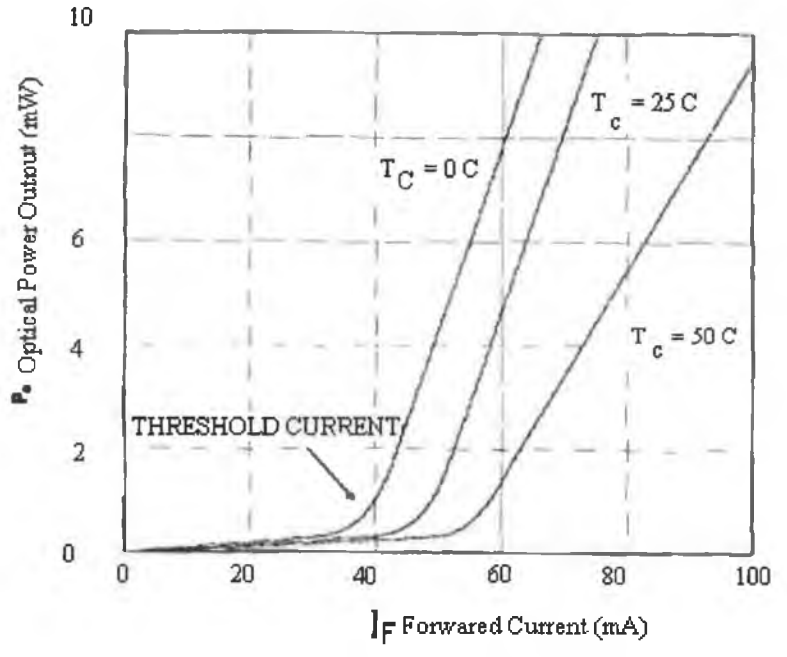

Figure 3.10 Laser optical power output versus forward current [15].

- First, the threshold current changes, and
- The second change is the efficiency slope

Table 3.1 compares the properties of laser diodes and LED's. Both types of light sources use the same key materials. Laser diodes have faster rise switches ON and OFF times, narrower spectral bandwidth, and higher modulation bandwidth. High performance laser diodes have been designed for optical communications where these quantities are critical.

For a multimode fibre optic sensing application, the performance of LED's with regard to these quantities is often adequate. The stability and low temperature sensitivity of LED's are highly important for sensing applications, as is their low cost.

For these reasons, an LED's have been chosen as the light source for the surface roughness sensing and surface defect detection [15,86,].

Parameter	Light-emitting diode (LED)	Laser Diode (LD)
Output Power	Linearly proportional to drive current.	Proportional to current above the threshold.
Current	Drive Current: 50-100 mA peak.	Threshold Current: 5-40 mA
Coupled Power	Moderate	High
Bandwidth	Moderate	High
Wavelength Available	0.66-1.55 μm	0.78-1.55 μm
Emission Spectrum	40 nm-190 nm FWHM	0.1 nm-10 nm FWHM
Cost	Low (32 EU)	High (56 EU)
Temperature Sensitivity	Low	High

Table 3.1 Compares the properties of laser diodes and LED's [15,87].

These diodes were chosen because their small size enabled them to be coupled to the optical fibres. The low power emitted by these diodes also ensured no damage to scanned surfaces.

3.4 Optical fibres

One of the main components of a fibre optical sensor is the fibre itself. Careful of choosing of fibres, based on operating parameters must be made to achieve a high-quality system. It is impossible to say which fibre type is best without examining the specific problem to be solved. Figure 3.11 illustrates the some of the most popular fibre sizes. There are:

- Single-mode: Widely used for high data rate and long distance application.
- 62.5/125 μm: Very popular in most commercial application; it has wide uses with low to moderate speed data links and video links.
- 50/125 μm: This fibre type is mainly used for military application.
- 100/140 μm: Once a very popular sizes, there are only a few remaining applications.

Figure 3.11 Fibre sizes used in this work.

They are designed to interface with fibre-optic devices using standard fibre-optic connectors; ST and FC connectors are shown in Appendix B_6. ST connectors are very widespread and are used predominately with multimode fibre. The design features a spring loading twist and lock bayonet coupling that keeps the fibre ferrule (clamping ring) from rotating during multiple connections. The cylindrical ferrule may be made of plastic, ceramic, or stainless steel. ST connectors offer very good features, cost, and performance. The FC connector has a flat end face on the ferrule that provides "face contact" between joining connectors. The FC designed with very good performance and features but these come at a relatively high cost. It offers very good single-mode and multimode performance and was one of the first connectors to address the problem of backreflection. FC's are often used for analog systems or high bit rate systems. FC/PC connectors incorporate a "physical contact" curved polished fibre end face that greatly reduces backreflection.

Many factors will dictate the choice of fibre type. Transmission bandwidth, maximising distance between amplifiers and cost of splicing (or connectorizing), sensitivity to temperature fluctuation, strength and flexibility are just some of these factors.

In choosing the size of fibre, the three important criteria are the following; coupling intensity from light source, collecting reflecting intensity and stand-off distance from the surface. Coupling light intensity to a fibre from a laser diode is relatively simple as the laser emits a narrow beam from a small area. Coupling from an LED is more troublesome as an LED emits a wider beam larger area. Connectors provide mechanical security and optical alignment for the fibres. Honeywell LED's are designed to interface with multimode fibres. Their modules have a ball lens, which focuses light from an LED more efficiently into a fibre pigtail. A fibre optic pigtail consists of a buffered fibre with an end connector see Figure 3.12. Table 3.2 shows

typical coupled power from a Honeywell HFE4050-014 LED into a variety of optical fibres, for a drive current of 100mA.

Core/Cladding Ratio (μm/μm)	Fibre type	Numerical Aperture	Coupled Power (μW)
8/125	Step Index	-----	1.8
50/125	Graded Index	0.20	70
62.5/125	Graded Index	0.28	153
100/140	Graded Index	0.29	406

Table 3.2 Typical coupled power from a Honeywell HFE 4050-014 LED into a variety of optical fibres, for a drive current of 100 mA [88].

Telecommunications fibres are normally surrounded by a buffer of ≈ 0.9 mm diameter, with a thin layer of gel between the fibre and buffer. A patchcord is a pigtail that has a further PVC coating, cable jacket, 2.9 mm diameter, for protection. Typically, Kevlar fibres are inserted between the patchcord jacket and buffer for added strength and protection. Figure 3.12 shows the structure of fibre-optic patchcord.

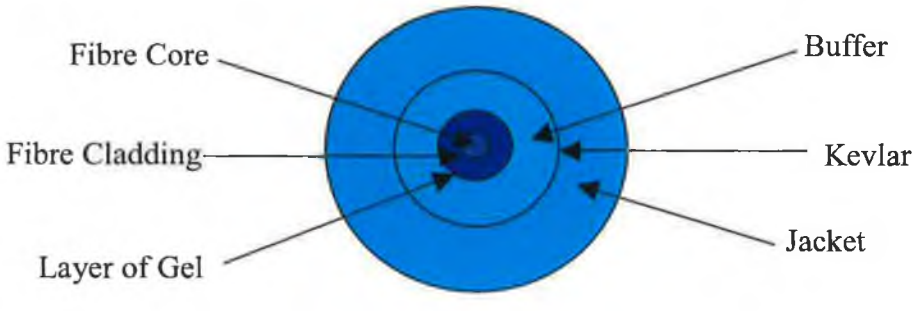

Figure 3.12 The structure of a typical of fibre optic patchcord.

Fibre-optic strippers are used to strip the outer jacket and the buffer. An optical fibre will not couple or emit light efficiently without fibre endface preparation.

3.4.1 Preparation of the fibre ends

It has been seen that three types of losses are associated with the surface state of the fibre endface:

- The orthogonality of the face with respect to the axis of the fibre
- Convexity
- Roughness

The quality criteria are a surface that is as flat as possible, orthogonal to the axis of the fibre and of optical polish. Two techniques enable the ideal state to be approached – cleaving and cleaning.

3.4.2 Cleaving and cleaning fibres

While cleaving might be done by hand, a cleaver tool, available from such manufacturers such as Fujikura, allows for a more consistent finish and reduces the overall skill required. The steps listed below outline one procedure for producing good, consistent cleaves with an optical fibre cleaver see shown in Figure 3.13.

- The buffer is stripped to an appropriate length
- The fibre is positioned in the guide and the buffer is butted against a stopper

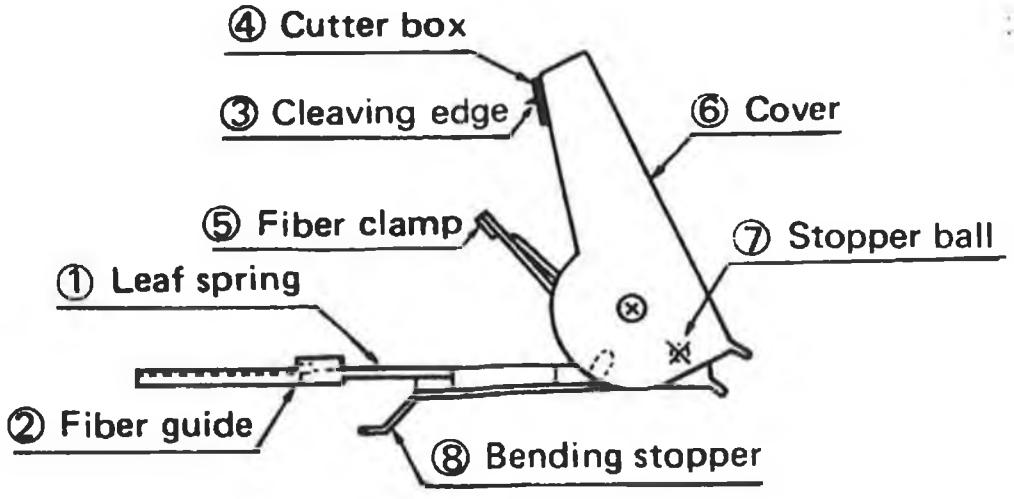

Figure 3.13 Schematic of the optical fibre cleaver [89].

- The uncleaved end of the fibre is clamped, and then the fibre is scratched by the cleaving edge
- As a little force as possible is used in scratching the fibre and releasing the cleaving edge (the fibre still clamped)
- The leaf spring is bent down, causing the scratch on the fibre surface to propagate resulting in cleaved fibre endface

An advanced manual fibre-optic cleaver is shown in Figure 3.14. The steps listed below outline the second procedure:

- Place the blade of the cleaver tool at the tip of the fibre
- Gently score the fibre across the cladding region in one direction. If the scoring is not done lightly, the fibre may break, making it necessary to reterminate the fibre.
- Pull excess, cleaved fibre up and away from the endface

Figure 3.14 A Fujikura fibre-optic cleaver [89].

Once Appendix A_1 shows the photograph of the cleaved fibre but not cleaning.

There are two types of cleaning techniques.

- Denatured alcohol and lint-free tissue (not found to be satisfactory in this work)
- Electric spark by using microscope

The fibre may be cleaved using the BFS-50 (single mode fusion splicer) shown in Figure 3.15 which uses a cleaning arc. It is imperative that the fibres prior to use have absolutely no dirt on them.

Figure 3.15 BFS-50 fusion splicer with integral microscope.

The cleaning cycle is not intended to clean away dirt that can be seen, rather it is intended to sonically displace minute particles of dirt that cannot be seen even through the integral microscope. Figure 3.16 shows a simple diagram of the cleaning cycle, which is recommended to be used each time after fibre cleaving.

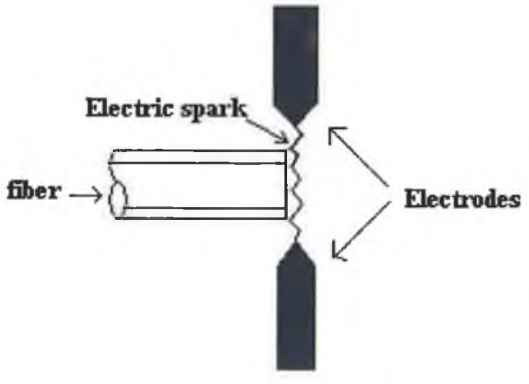

Figure 3.16 Schematic of electric arc cleaning cycle.

The cleaning cycle does not have enough energy to deform the prepared cleaves so it is quite in order to clean more than once if this is thought necessary.

3.5 Receiving signal

Conversion from the optical to the electrical domain requires a device, which can efficiently collect incident photons and cause them to generate hole-electron pairs which can in turn be detected electrically. They enable the optical signal to be converted back into electrical impulses that are detected at the receiving end of the fibre. Light detectors perform the opposite function of light emitters. The most common detector is the semiconductor photodiode, which produces current in response to incident light.

In an LED, the energy emitted during the recombination of electron-hole pairs is in the form of light. In a photodiode, the opposite phenomenon occurs. Many different photodetectors are commercially available but PIN (p-i-n) photodiode are most commonly used with optical fibres [88,90,]. The following considered when selecting a photodetector:

- responsivity (wavelength and intensity),
- cost,
- signal to noise ratio, and
- speed of response

3.5.1 PIN Photodiode

The diode consists of the semiconductor structure. Figure 3.17 shows the cross section and operation of a PIN photodiode. A PIN diode differs from a p-n. diode as between the positively doped, p region and negatively doped n region there is an intrinsic, undoped, I region [90]. The diode's name comes from the layering of these materials Positive, Intrinsic, Negative. Photons incident through the anti-reflection coating and the p layer are absorbed by the intrinsic layer causing a current, I_D to flow through the diode as shown. In the absence of light, PIN photodiodes behave electrically just like an ordinary rectifier diode. PIN detectors can be operated in two modes: photovoltaic and photoconductive. In the photovoltaic mode, no bias is applied to the detector. In that case the detector will be very slow and the detector output is a voltage that is approximately logarithmic to the input light level. Real-

world fibre optic receivers never use the photovoltaic mode. In the photoconductive mode, the detector is reversing biased. The output in this case is a current that is very linear with the input light power. A PIN detector can be linear over seven or more decades of input light intensity.

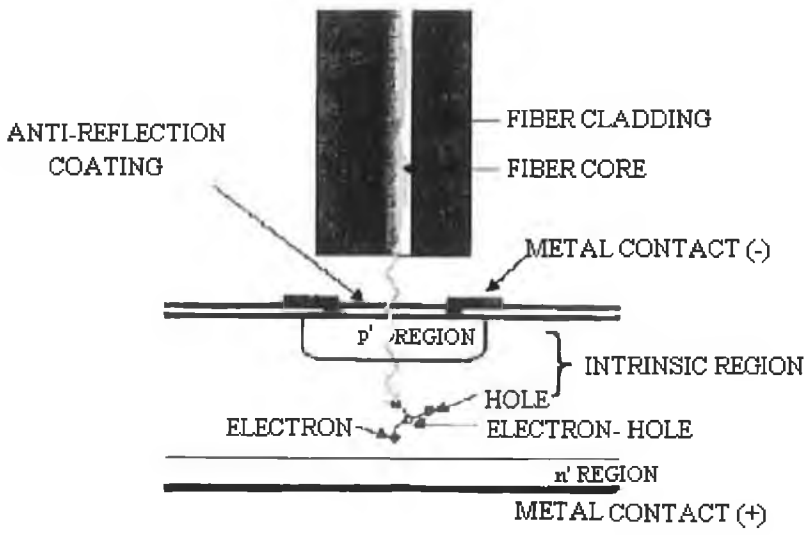

Figure 3.17 Cross section and operation of a PIN photodiode [15].

3.5.2 Important photodetector parameters

Responsivity The responsivity of a photodetector is the ratio of the current output to the light input. Other factors being equal, the higher the responsivity of the photodetector, the better the sensitivity of the receiver. For most applications, responsivity is the most important characteristics of each detector because it defines the relationship between optical input and electrical output. The theoretical maximum responsivity is about 1.05 A/W and 0.68 A/W at a wavelength of 1300 nm and 850nm respectively. Commercial InGaAs detectors provide typical responsivity of 0.8 to 0.9 A/W at a wavelength of 1300 nm.

Different semiconductor device designs and semiconductor material are responsive at the various wavelength used with fibre-optic light source. Figure 3.18 shows a typical response of various detector materials.

The theoretical maximum responsivity of a photodetector occurs when the quantum efficiency of the detector is 100% (means every absorbed photo creates an electron hole pair).

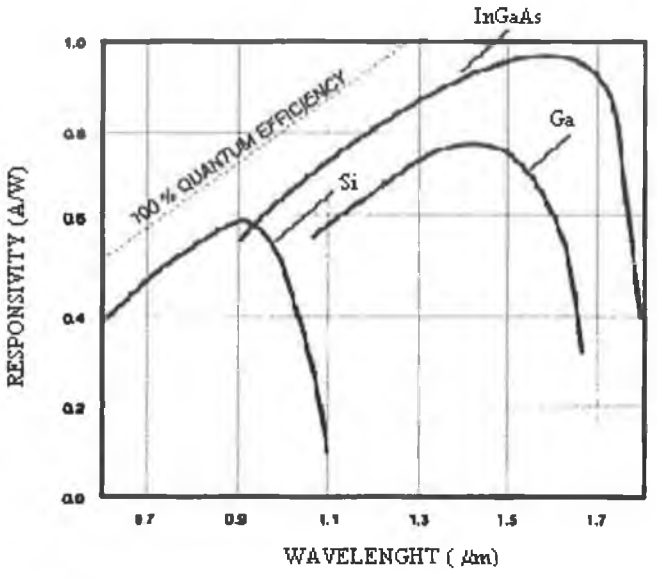

Figure 3.18 Typical spectral response of various detector materials [15].

Quantum efficiency is the ratio of primary electron-hole pair created by incident photons to the photons incident on the diode material. Factors that prevent the quantum efficiency from being 100% included coupling losses from the fibre to the detector, absorption of light in the p or n region, and leakage currents in the detector.

Capacitance of the detector is dependent upon the active area of the device and the reverse voltage across the device. A small active diameter allows for lower capacitance.

Photodiode capacitance decreases with increasing reverse voltage. Figure 3.19 shows a typical capacitance voltage curve for a high-speed photodiode.

Response time represents the time needed for the photodiode to respond to optical input and produce an external current. The combination of the photodiode capacitance and the load resistance, along with the design of the photodiode sets the response time. The response time is influenced by the design of the photodiode as well as its applications parameters.

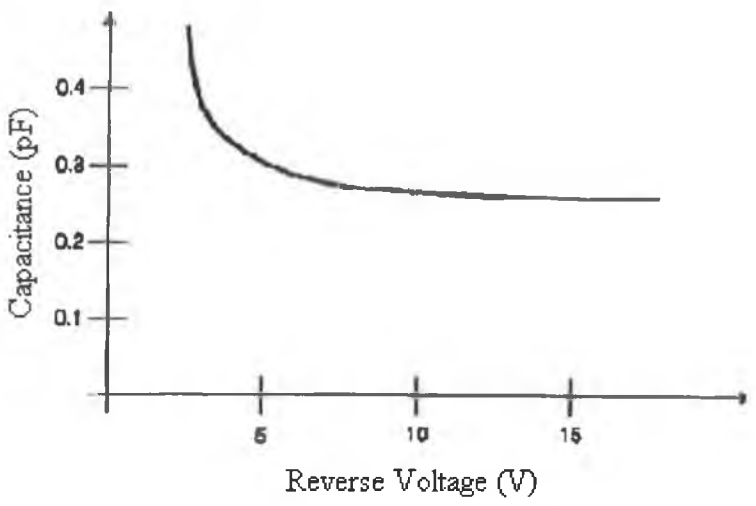

Figure 3.19 Capacitance versus reverse voltage [15]

Dark current Is some what of a misnomer for this phenomenon. It implies that somehow the detector manages to put out a current when there is no light. What really happens is that a current flow through the detector in the absence of light because of the intrinsic resistance of the detector and the applied reverse voltage. The voltage acting on the bulk resistance of the detector causes a small current to flow. This current is very temperature sensitive and may double every 5^0 to 10^0C. Dark current contributes to the detector noise and also creates difficulties for DC coupled amplifier stages.

Linearity and backreflection All PIN photodiodes are inherently linear devices. However, for most demanding applications special care must be taken to reduce distortion to very low levels. These so called analog PIN detectors often have a distortion below 60 dB. Another factor that is very important for analog applications is the backreflection of the detector. Generally the fibre is coupled to the detector at a perpendicular angle. For a low backreflection detector, the detector may be tilted by 7^0 to 10^0.

Noise Is an ever present phenomenon that limits a detector's performance. It is any electrical and optical energy other than the signal itself. Noise appears in all elements of the of the communication system; however, it is usually most critical to the receiver. This is because the receiver is trying to interpret an already weak signal.

Detection noise sources result from photodiode noise and amplifier noise. Photodiode noise is due to shot noise and Johnson noise [91,92]. The input bias current of the op amp and Johnson noise in the load resistor cause amplifier noise, for an unbiased transimpedance amplifier [93].

Shot (discontinuous) noise occurs because the process of creating the current is a set of discrete occurrences rather than a continuous flow. Noise also increases with current and bandwidth.

The shot noise may be minimized by keeping any DC component to the current small, especially the dark current, and by keeping the bandwidth of the amplification system small.

Johnson noise occurs in resistors and is proportional to the square root of absolute temperature divided by the resistance. Thus, Johnson noise increases with temperature and decreases with increasing photodiode shunt resistance.

3.6 Labview-based data acquisition and data analysis system

This section explains the procedure and algorithms that were implemented for data acquisition and data analysis. A National Instrument AT-MIO-16XE-10 data acquisition card [94] was used for analog to digital conversion. It has 12-bit resolution and a maximum sampling speed of 100,000 sample/second. Labview software interfaces with the data acquisition card and provides a graphical user interface to control data acquisition and to perform data analysis [95].

3.6.1 Labview for sensor data acquisition

Labview by [96] is a universal programming system, with both a graphical user interface 'Front Panel' and a graphical program code 'Block Diagram'. It was designed for programming data acquisition, data analysis and data display. "The software in Instrument" is not just an advertisement but describes the aim of the software package: to integrate external measurement devices and a graphical user interface into a personal computer-based measurement instrument [97]. The development of a graphical user interface (GUI) in conventional text-based software

packages is a very time consuming task. Labview offers a wide selection of graphical objects (controls and indicators) that can be dragged onto control panels as shown in Figure 3.20.

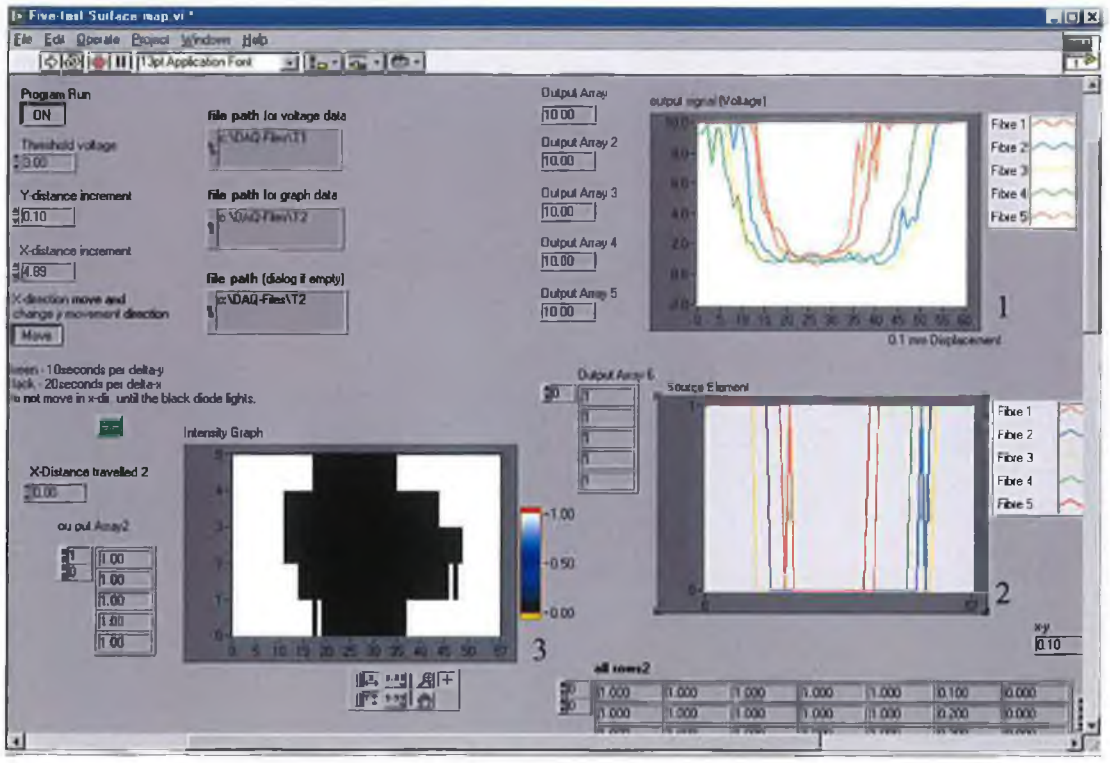

Figure 3.20 A screen captured image of a data acquisition system. One graph is the output signals, the second shows the applied cut-off voltage and the third is a representative the sample surface map.

Each object placed on the front panel automatically appears as a symbol in the block diagram window where its input and output are connected to other program elements Figure 3.21. For example, an X-Y plot of a histogram can be implemented simply by dragging an icon onto the front panel and connecting the histogram array to the corresponding symbol on the wiring diagram. In a similar manner, connecting the 2D X and Y array to an intensity plot can display a surface map. The intensity graph represents points in the surface map and is generated after applying the cut-off voltage.

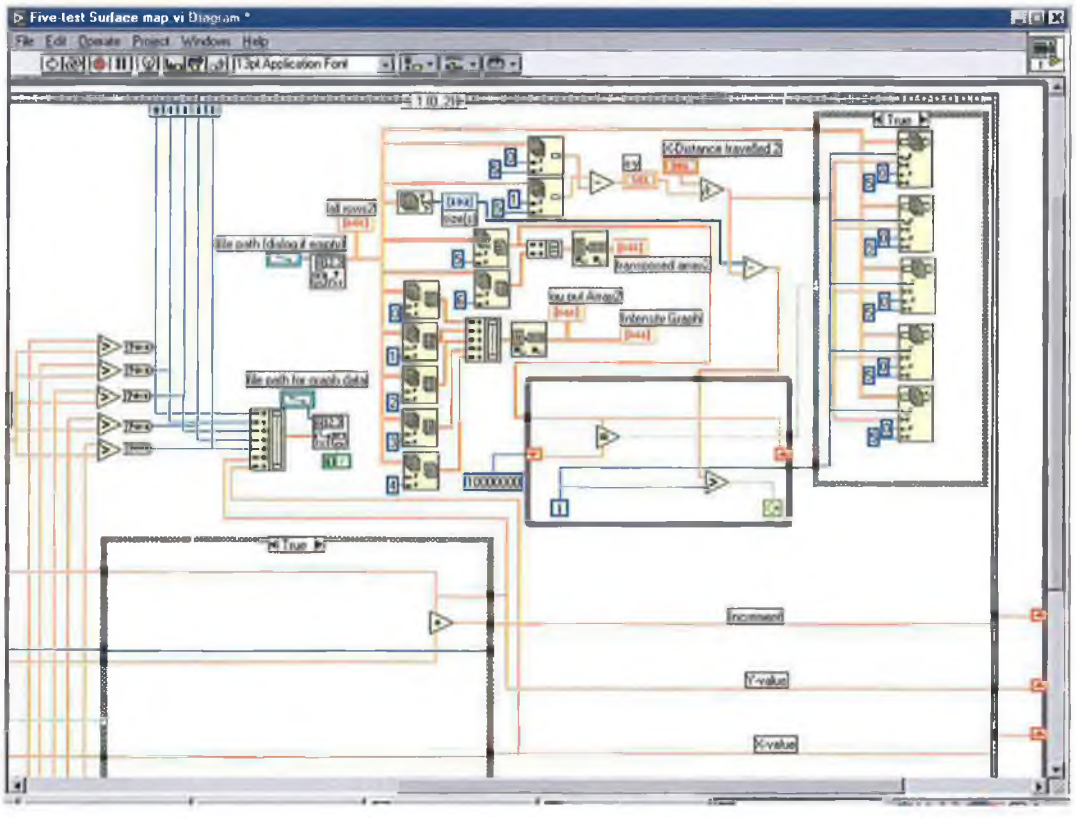

Figure 3.21 Program code of the application of Figure 3.20. The cut-off voltage and the surface map are applied here.

3.6.2 Surface defect sensing

A flow chart depicting the programmes developed for data acquisition in Labview is shown in Figure 3.22. This system is more directly implemented when the cut-off voltage is applied as a part of measurement. Figure 3.23 shows the program that generates a surface map. The voltage level at each point (x, y), P_{xy} is compared to the cut-off voltage, V_c. If it is less than V_c. the point (x , y) is added to the surface map, if it exceeds V_c it is ignored. In this way the surface map displays the areas of the surface that are below the cut-off level. Points that deviate from the displacement cut-off defined by the cut-off voltage or that reflects light irregularly for some other reason. The front panel and block diagram of the display data file, which were developed by the Labview software, which consists of the block diagram and front panel.

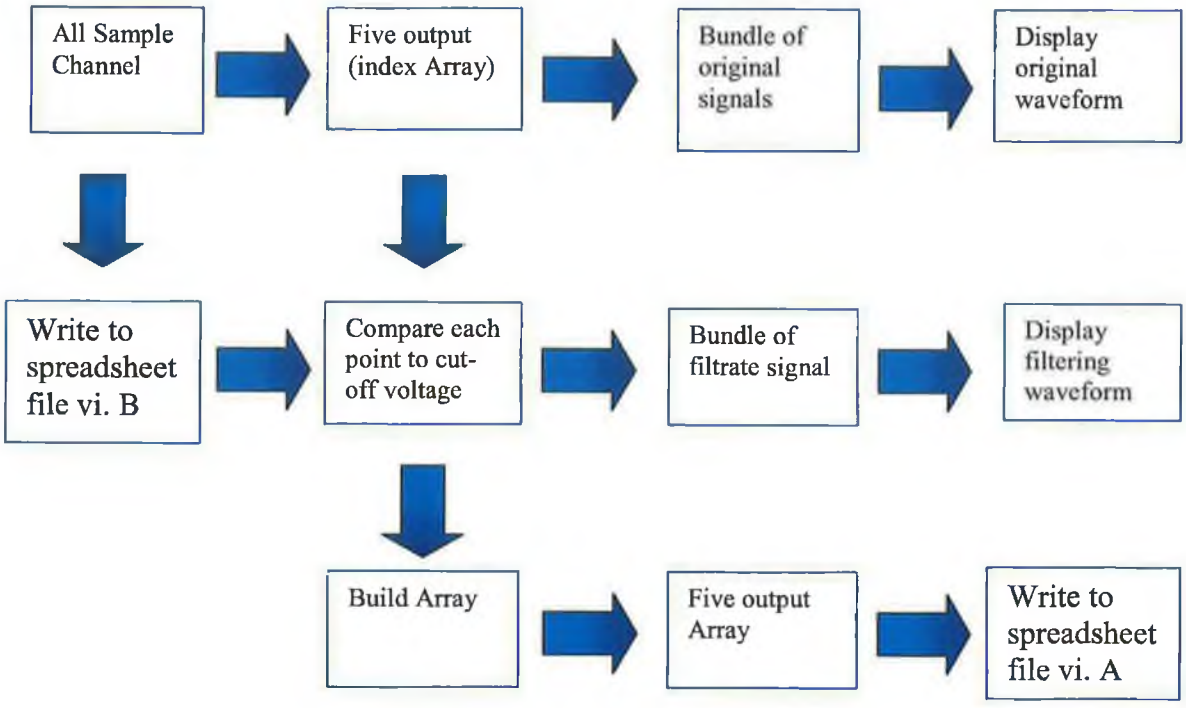

Figure 3.22 Surface defect sensor data acquisition programme which displays and logs the captured data.

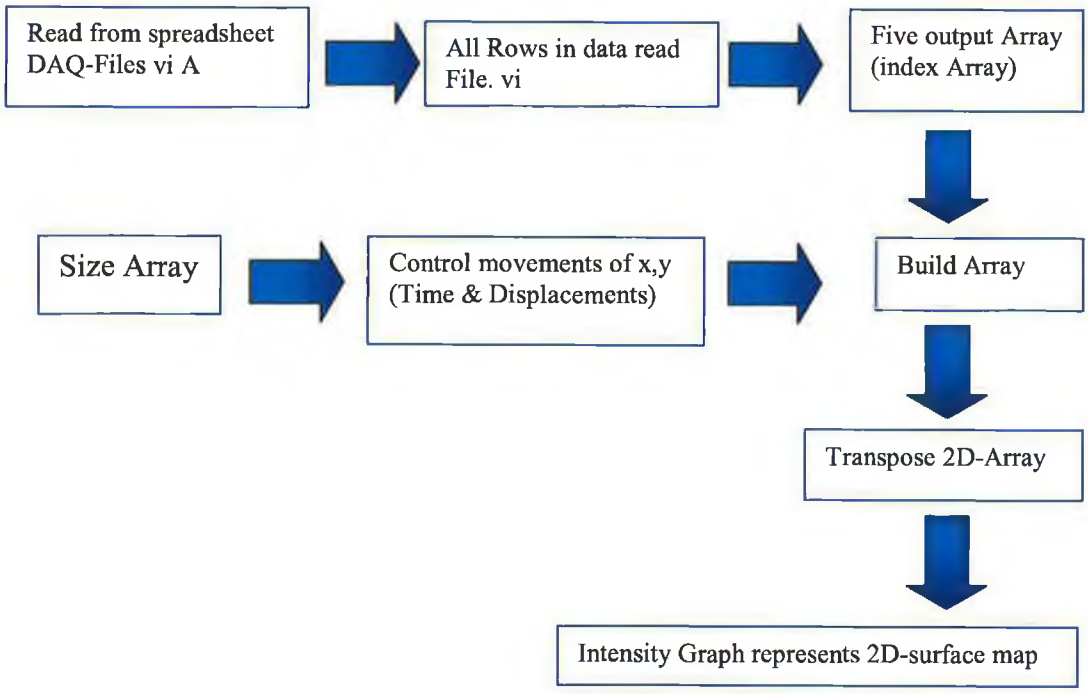

Figure 3.23 Surface defect surface map generation.

Other X-Y plots representing the light displacements against output signals (voltages) could be displayed to show the five output signals. All the plots except the histogram are display on separate graphs to a void clutter on the main screen. The function and appearance of any Labview display can be set by the programmer

3.7 Mechanical design

This section describes the design of the mechanical tools, which were, used for this system such as fibre holder and x-y-z stages

3.7.1 Fibre holders

Two types of holder were used there were a Newport single fibre holder and a multi fibre holder. These holders were designed to achieve highly accurate measurements and high resolution system. The first holder used for this project was to accommodate one fibre. Early stage Newport fibre holder, FPH-S [98], designed to hold bare fibres of outside diameter between 80-200 μm was used. A fixturing and flexing rig was required to position the fibres. The fixturing was designed to hold the fibre holders at incident angle of change 60^0 for LED and to 30^0 for laser diode to the normal. Each fibre holder fits tightly to the fixturing plates and is held in place by a plastic screw. The disadvantage of this system was that the fibres were manually adjusted to be at the same height off the sample surface and the fibres were not in a straight line. Figure 3.24 shows photograph and the dimension of the optical fibre holder

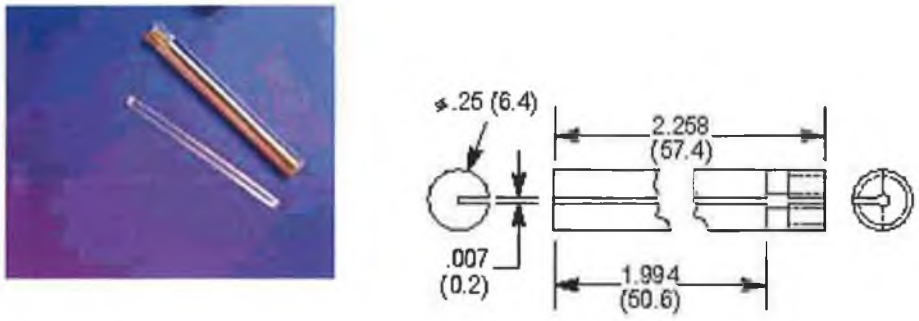

Figure 3.24 (a) Photography of the holder and (b) dimensions of the holder [97].

A new holder was designed and developed to hold a set of five emitting and receiving fibres. The holder consisted of two aluminium plates of 1 mm thickness. The dimension of the holder was shown in Figure 3.25. The plates of the holder fixed together with metal screws. One of the plates of each holder has a soft material to protect the fibre from any damage can be happened. Each fibre holder fits tightly to the fixturing plates and is held in place by two plastic screws. The fixturing was redesigned to hold the fibres at incident angle of 30^0 to the normal.

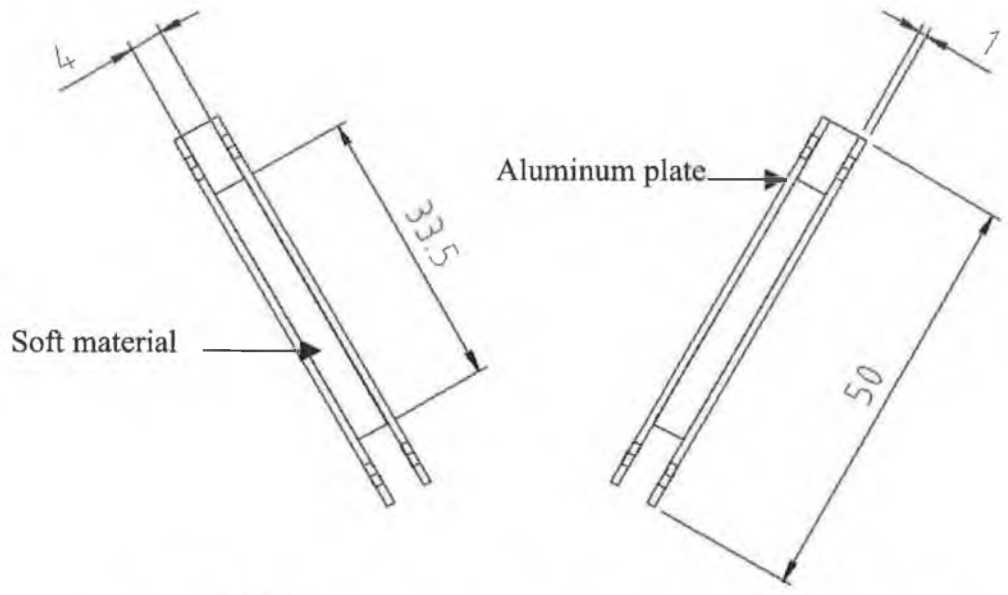

Figure 3.25 Dimensions (mm) of the early fibre optical holder.

The final fibre optic holder was designed carefully achieve the highest resolution and more accurate measurements. Figure 3.26 shows the diagram of the holder and the rotation plate and all the dimension of both the fibre optic holder and the rotation plate. The rotation plate can be used as a rotate stage to control the scan angle. The rotation plate was fixed by one metal screw on the side of the z stage, which allowed adjustment.

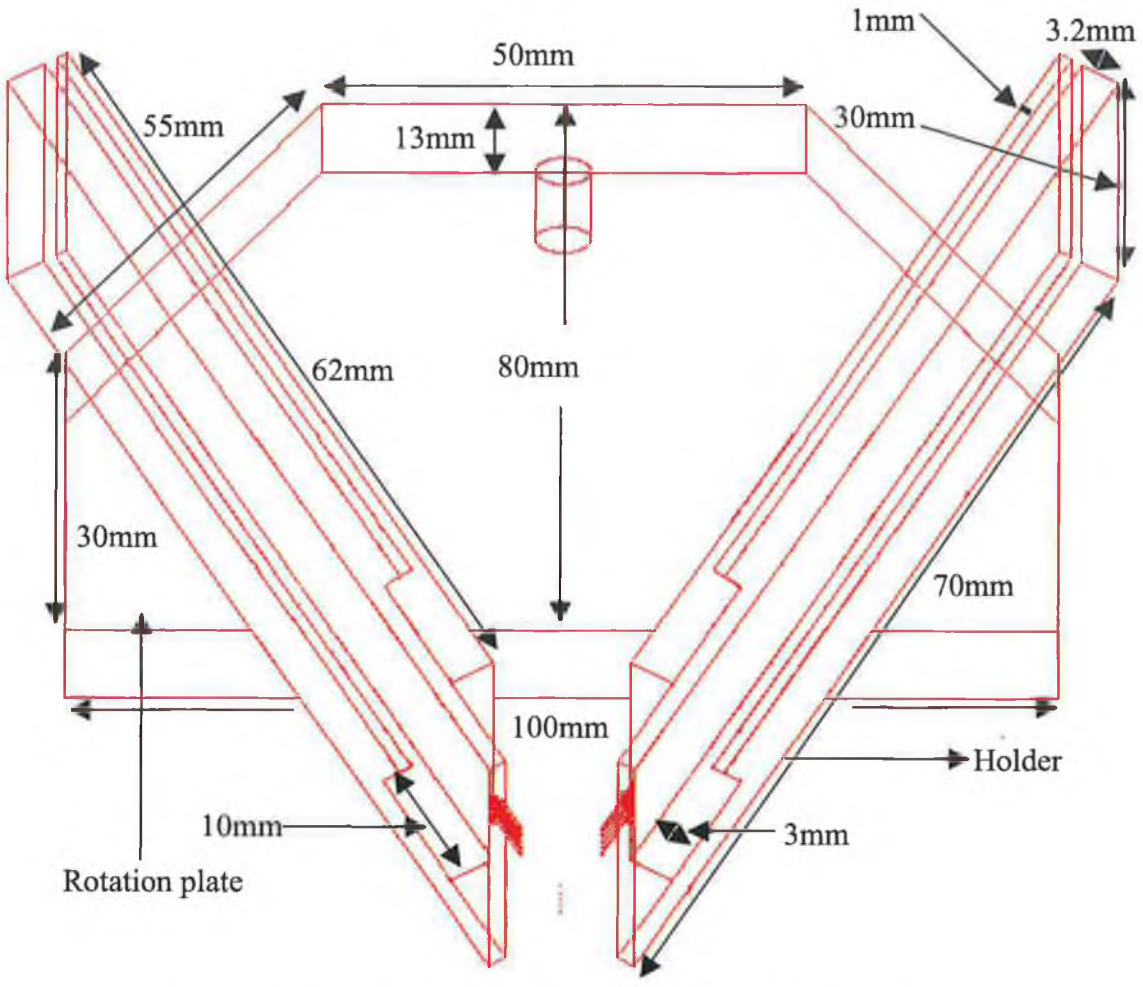

Figure 3.26 Fiber optic holder and rotation plate dimension

The final design was consisted of two Aluminum plates with different step thickness. One of the plates was drilled by five holes to accommodate the fibres. The plates of the holder were fixed together with six metal screws. The fibre optic holder was designed to protect the end face of the fibre optic from any damage. Figure 3.27 shows the five end faces of the fibre optic and distance between the fibres.

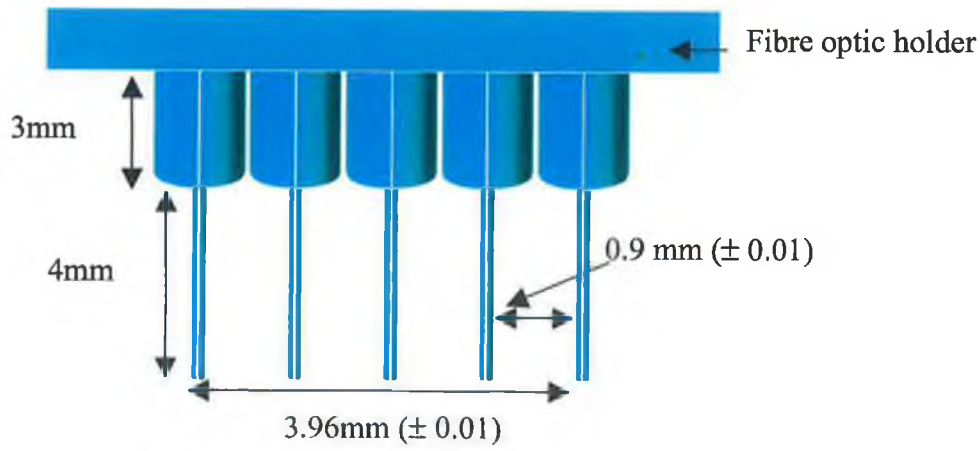

Figure 3.27 Five-fiber optics in holder

Figure 3.28 presents the side view of the rotation plate and the fiber optic holder. Each fiber optic holder fits tightly to the fixturing rotation plates and is held in place by two nylon screws.

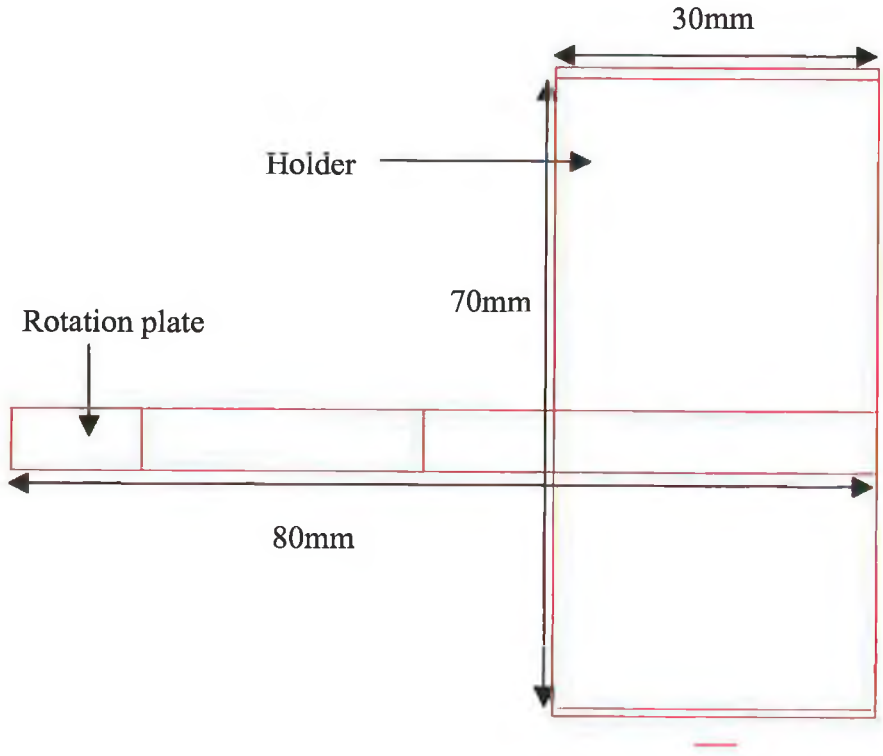

Figure 3.28 Side view of the rotation plate and fiber optic holder.

Front view of the fibre optic holder and the rotation plate are shown in Figure 3.29. The holder was fixed on the rotation plate can be moved up and down depending upon how far the fibres to be needed from the surface plate. Figure 3.30 shows the most important part of the fibre optic holder.

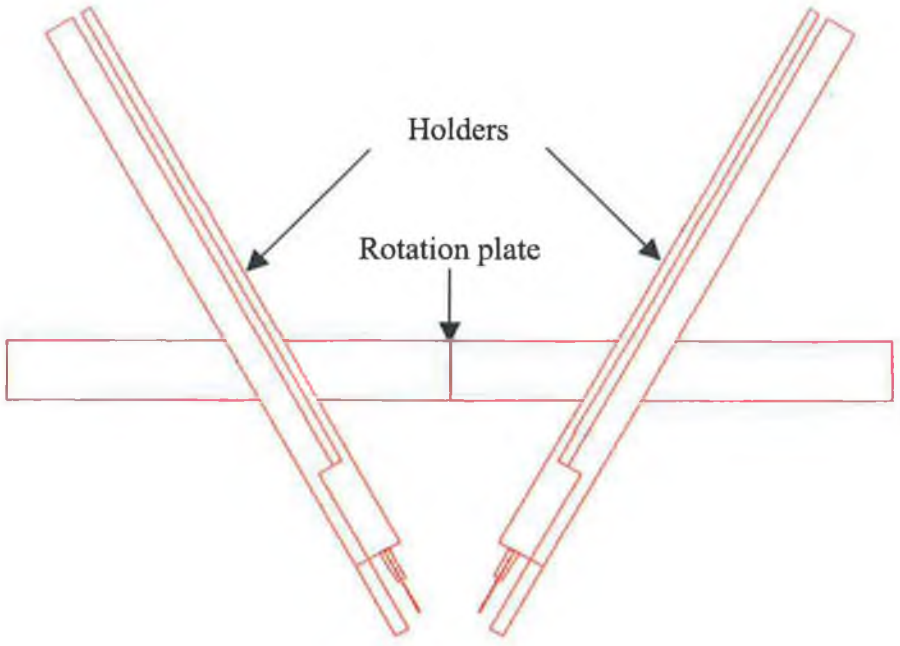

Figure 3.29 Front view of the optical fiber holder and the rotation plate.

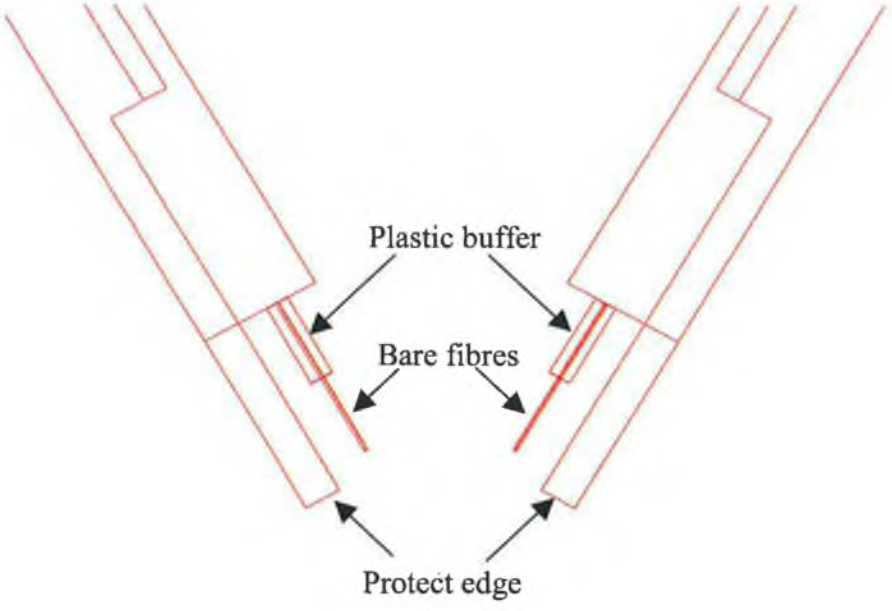

Figure 3.30 Close up of fibre optic holder in Figure 3.29.

3.7.2 Translation stage

Three perpendicular micrometer driving stages (Newport precision steel stages, Appendix B_1, M-UMR8.25 [98]) were used as translation stage. They have travel length 25 mm with a vernier deviation of 10 μm, see, Appendix B_2, –BM11.25 [98]. The bottom stage is mounted on an aluminum base plate.

3.7.3 Circuit boxes

Electronic boxes were used to hold the electronic circuits such as the feeding circuit, the laser diodes driving circuit, the photodetectors circuit and divided circuit. Five laser diodes were held on one side and on the other side five photodiodes and the switches (ON/OFF). The third side held three power supply plugs (±15 volt and the ground) and the opposite side contained output ports as shows in Appendix A_2. The dimension and the designed of the small box are also shown in the Appendix A_3.

3.8 Resolution

This section describes a developed technique, developed by the author, to achieve high resolution for the present system. The novel method used four degree of freedom. Figure 3.26 shows the dimensions of the holder. Metal screws are used to fix the fibre one beside the other to achieve a fixed distance between the fibres (0.91mm).

The novel method, used to reach high resolution, is dependent on the displacement projection of the spots on the x-axis. Figure 3.31 (a) shows that the spots are elliptical due to the incidence angle of the light on the surface. It also shows the total distance between the spots, and the distance between any two spots of the set and x-y plane. Two diameters of the fibre spot depending on fibre, small diameter (d = 62.50 μm) and large diameter (D = 72.12 μm) were used.

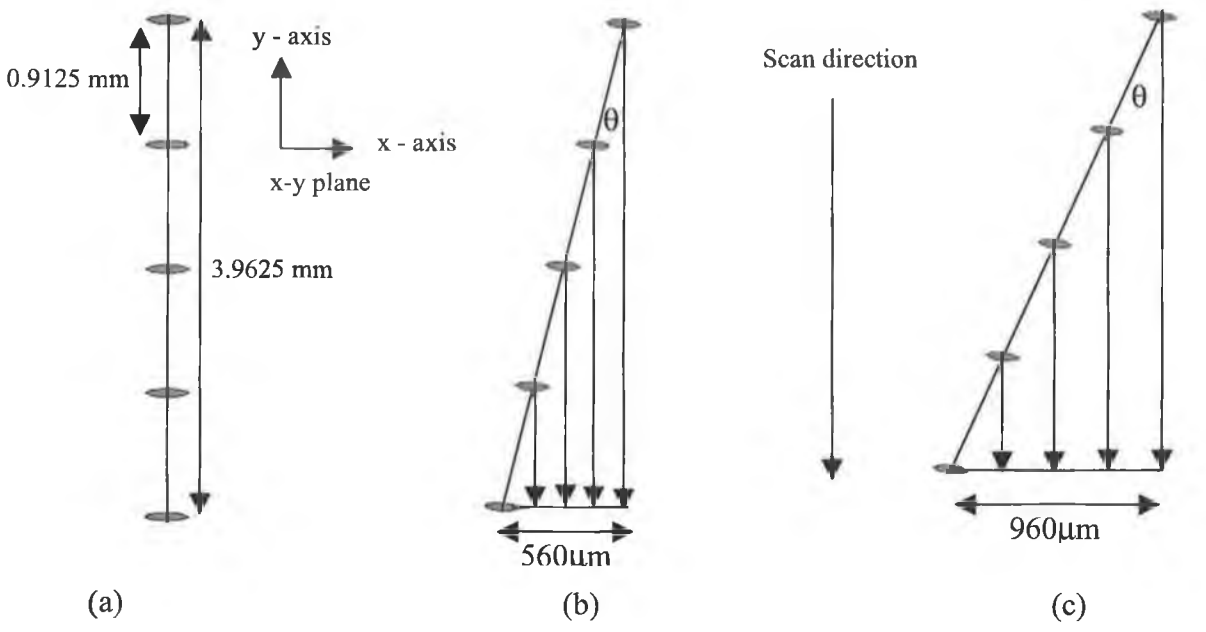

Figure 3.31 Using different rotation plate angles to show the difference in resolution a) $\theta = 0$, b) $\theta \approx 8^0$, c) $\theta \approx 14^0$.

The rotation plate was rotated in x-y plane by angle θ as shown in Figure 3.31. The angle should be greater than five degree ($\theta \approx 8^0$) to achieve a projection distance 560 µm. The direction of the scan is presented in y-axis on x-y plane. Figure 3.31 (c) shows the scan direction with angle ($\theta \approx 14^0$), which delivers a 100 µm displacement between any two spots. Table 3.1 shows different values of the scan angle the corresponding theoretical projection of scan and the experimental of scan projection. The experimental projections have been measured manually by recording the first and the last signal drops down when the five fibres passes the sample plate.

Scan angle (θ^0)	Theoretical projection	Experimental projection
5	0.3454	0.3617
6	0.4142	4338
7	0.4829	0.5058
8	0.5514	0.5776
9	0.6492	0.6573
10	0.6881	0.7210
11	0.7561	0.7920
12	0.8239	0.8630
13	0.8914	0.9340
14	0.9586	1.0040
15	1.0256	1.0741

Table 3.3 Comparison between the theoretical and experimental projection.

The resolution curve (Figure 3.32) presents the relation between the angle (θ) and the projected distance. The equation and this curve gives the relationship between the angle (θ) and the projection (resolution).

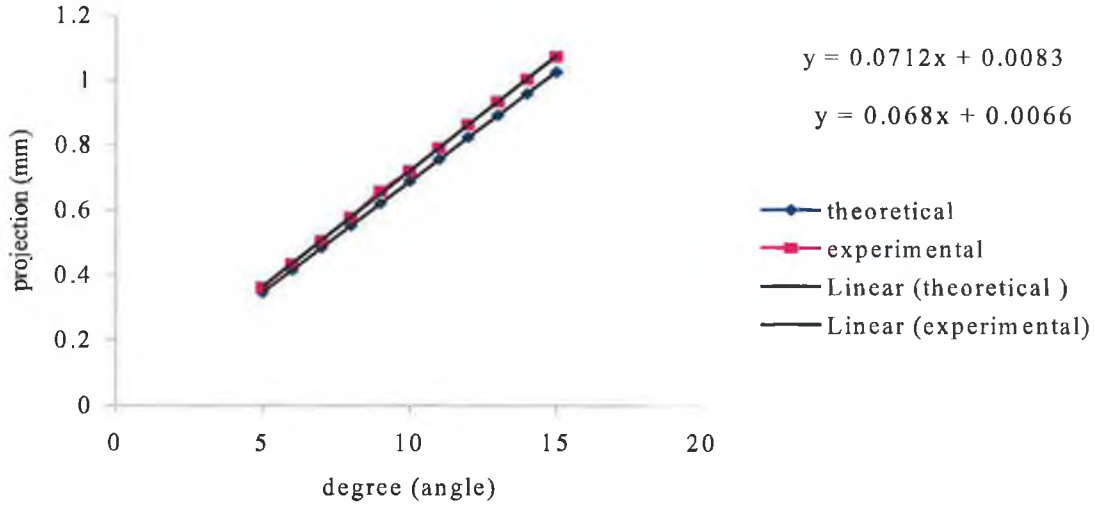

Figure 3.32 Theoretical, experimental and the fitted resolution curves

3.8.1 Scanning methodology

In order to prepare the system to start scanning the object, the system is positioned at the scanning angle needed ($\theta = 8^0$).

Choosing the reference point, which is the nearest point from the object (the simulation defect on the surface). In the first stage of the results the sample plate fixed and the fibre moving manually. Once the last stage of the results the fibres fixed and the sample plate moving using a motor guide. The signals started scanning by reaching the first spot the object and following the other spots one by one until all the spots pass the object. Within the scanning rotational and after the first spot reached the object, the following spots reach the object with a distance less than the original distance of the spots. Once again all spots pass the object with different time and different position. Subsequently the spots pass the object that is means the scan of the object is finish. According to the scanning angle chosen the system can produce a high resolution and it can detect very small defects. This new method it is simple and highly accurate. The system also only takes a small space.

3.9 Electronic Design

The electronic circuitry that drives the light sources such as LED, laser diodes and the detection signals

3.9.1 Light sources driving circuits

The simplest LED and laser diode drive circuit is unquestionably the resistor-driving circuit, which uses only one resistor. Figure 3.33 shows an LED and resistor connected in series across the terminal of voltage supply. With a few more components and a transistor, we can design a constant current drive that guarantees a predictable and stable current through a single LED or any array.

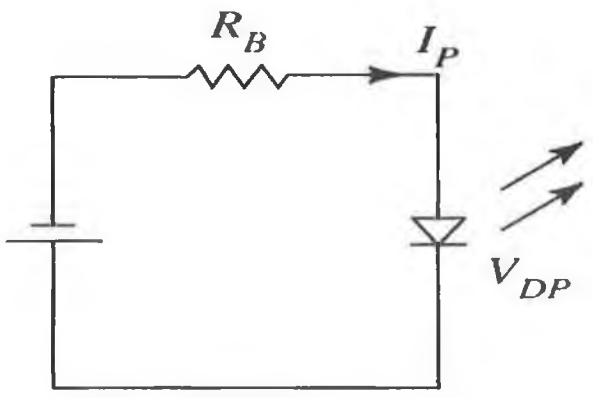

Figure 3.33 Resistor driving circuit

The advantage of this circuit is that the current is not at the mercy of LED characteristic variations. This circuit is shown in Figure 3.34. It can be used for many LEDs in series, as long as the total voltage drop across the LEDs does not exceed the available collector voltage Vcc.

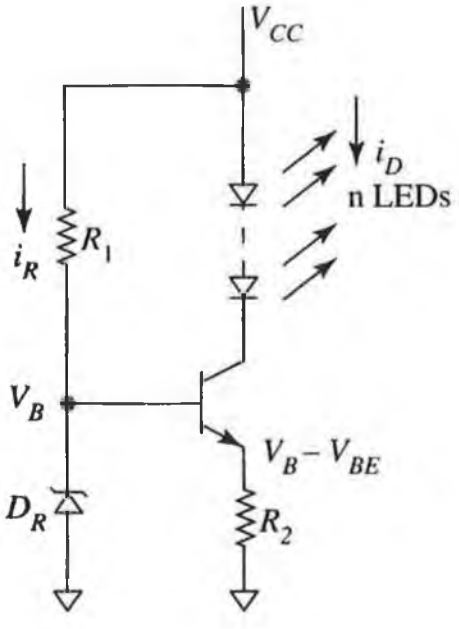

Figure 3.34 Transistor constant current drive

The circuit can be designed using the following relationship [85]:

$$R_1 = (V_{CC}\text{-}V_B)/\, i_R \qquad (3.1)$$

Where V_{CC} = supply voltage (V)

V_B = voltage of the reference diode (V)

i_B = current through the reference diode (A).

$$R_2 = (V_B\text{-}V_{BE})/i_D \qquad (3.2)$$

Where V_{BE} = base-emitter voltage drop V_{BE} =0.7 (V)

i_D =desired LED current (A).

For the circuit to operate properly, the following condition must be met:

$$V_{CC} > nV_P + (V_B\text{-}V_{BE}) + 0.2\ V \qquad (3.3)$$

The main light sources (laser diode) of the data acquisition system driving by a simple single resistor for each laser diodes driving circuit. It was used to drive laser diodes with respect this system accommodated any thermal variations in power output as shows in figure 3.33. Electronic circuit, Appendix C_1, represents the five laser diodes driving circuit, which were connected with 12 volt from the feeding circuit. The feeding circuit is connected with voltage supply (±15V). The circuit is dependent on the two voltage regulators to achieve stability feeding (±12V).

3.9.2 Signal detection circuit

The basic power supply for a photodetector consists of a bias voltage applied to the detector and a load resistor in series with it. The basic circuit for a photoconductive detector is shown in Figure 3.35 (a). As the irradiance on the detector element changes, its conductance changes because of the free carriers generated within it. A change in the conductance increases the total current in the circuit and decreases the voltage drop across the detector. The load resistor is necessary to obtain an output signal. The internal shunt resistance of the photodiode further limits amplification [98]. If the load resistor was zeroing, all of the bias voltage would appear across the detector and there would be no signal voltage available. In the circuit shown, an increase in light intensity increases the voltage drop across the resistor, yielding a signal that may easily be monitored.

The magnitude of the available signal increases as the value of the load resistor increases. But this increase in available signal must be balanced against possible increase in Johnson noise and possible increase in rise time, because of the increased RC time constant of the circuit. The designer must trade these effects against each other to obtain the best result for the particular application.

A photovoltaic detector requires no bias voltage; it is a voltage generator itself. The basic circuit for a photovoltaic detector is shown in Figure 3.35 (b). This shows the conventional symbol for a photodiode at the left. The symbol includes the arrow representing incident light. The incident light generates a voltage from the photodiode, which causes current to flow through the load resistor. The resulting IR drop across the resistor again is available as a signal to be monitored.

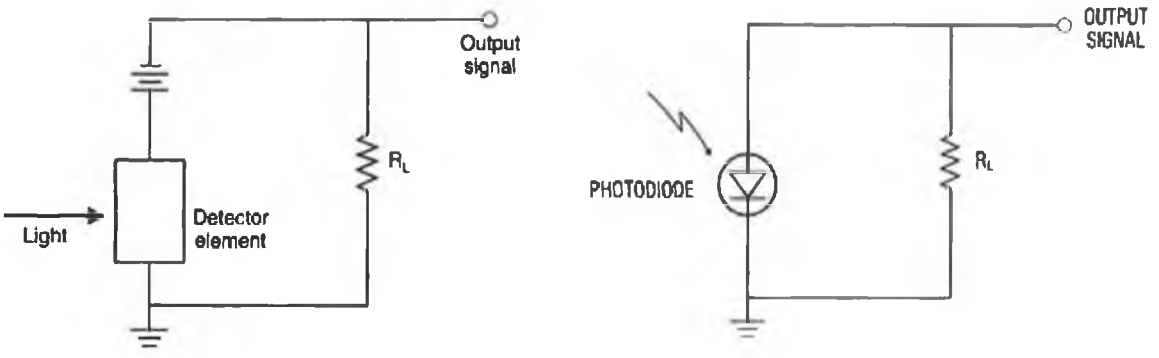

Figure 3.35 Basic circuits of operation for (a) photoconductive detector (b) Photovoltaic detector.

Disadvantages of this circuit are the nonlinear nature of the response and the fact that the signal depends on the shunt resistance of the detector, which may have a spread in values from different production batches of detectors.

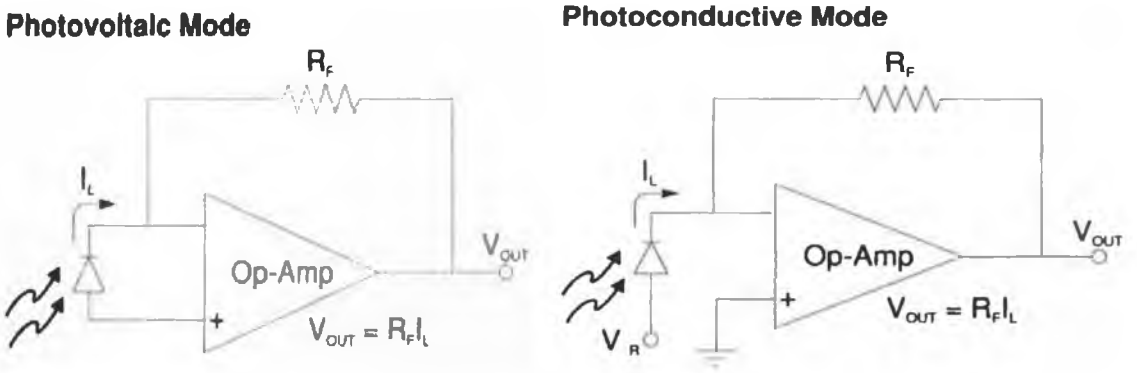

Figure 3.36 Transimpedance amplifier (a) unbiased and (b) reverse biased circuit [99].

Unbiased transimpedance amplifier, Figure 3.36 (a), uses a high-gain operational amplifier to effectively short circuit the photodiode. The gain and the feedback of the amplifier force both positive and negative terminal to the same voltage. Thus, the voltage across the photodiode is clamped to 0V. All the photocurrent flow through the load resistor is given by equation 3.2 above. The value of the load resistor, R, is unlimited by the diode characteristics increasing output voltage. Clamping diode voltage to 0 V improves the range and linearity of the amplifier. This circuit has no dark current noise.

The noise characteristics of the circuit are outlined in the next section. For practical reasons, a single detection circuit is usually constructed for both systems, with only the photodiodes differing between the systems [17].

3.9.3 System noise

The LED light source is sensitive to thermal variation. A HFE4050 high-power fibre optic LED claims a temperature sensitivity of $0.01 dB/^{0}C$.

The op-amp used in the transimpedance amplifier, OP37GP, was chosen in this work for its low input bias current and consequent low input bias current noise and its high speed, high slew rate, high gain and low drift. The load resistor was made as high as possible, 10MΩ to minimise Johnson noise and to give a large stand-off distance, due to the high gain.

A divided voltage output circuit was therefore used, Appendix C_2, to reduce the voltage output. This circuit was connected between the photodetector circuit and the data acquisition cord. The data acquisition card could not read voltage larger than 10V and the output signals are around 12 V.

3.11 Fibre optic laser scanning inspection system for surface defect

This project was concerned with the design and the development of a fibre optic sensor to recognise surface defects. The block diagram of the apparatus designed in this project is shown in Figure 3.37. The system includes an LED as the primary light source and five laser diodes as a main source. Multimode fibre optics with core/cladding ratios of 62.5/125 and 100/140 were used as emitting and receiving fibres respectively. PIN photodiodes were used as the photodetection to converted the light received to on electric signal

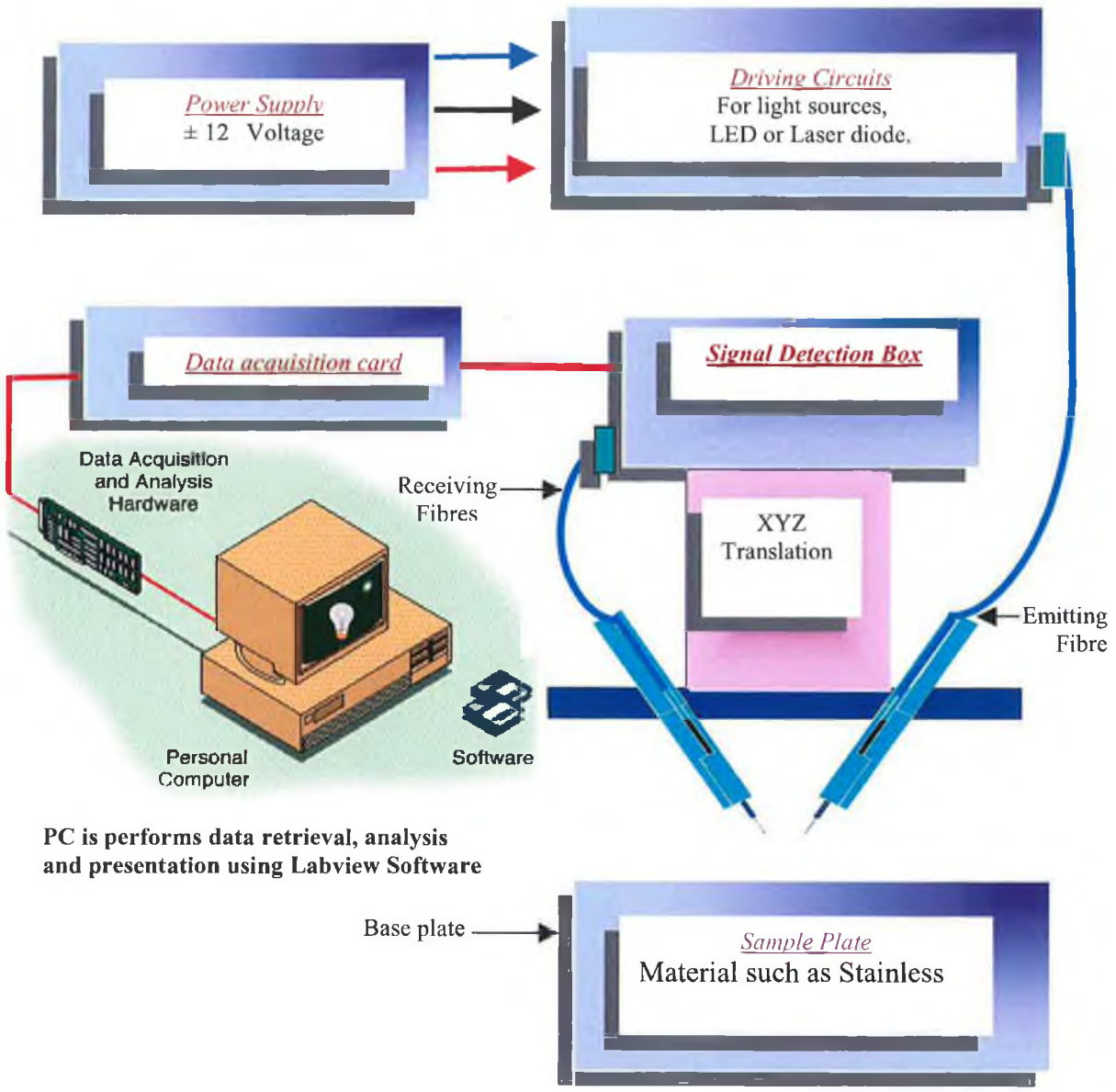

Figure 3.37 Block diagram of fibre optic laser scanning inspection system

All the signals from the photodiodes are converted from analog to digital and amplified before reaching the data acquisition system, which continuously reads their values. Labview software is a high level, modular graphical programming language that is often used to program real time data acquisition and data analysis systems. It was used to capture analyse and display the system data

For the purpose of this project, a surface defect was defined as a hole and blind holes in a sheet of metal such as stainless steel, brass, copper, aluminium and polycarbonate.

Figure 3.38 shows an oblique side view of the emitting and receiving optical fibres. The emitting fibres carry signals from laser diodes emitting light with wavelength 1.3 μm. This light was collected by the receiving fibre and thereby conveyed to the PIN photodiodes.

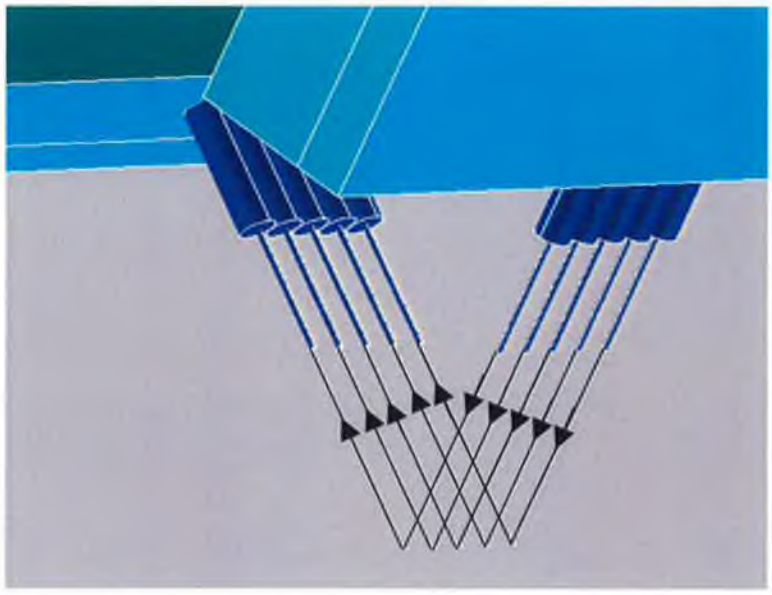

Figure 3.38 Side view of fibres and signals emitting and receiving

The drawing in figure 3.39 shows the fibre held at incident angle to the normal. The basic measurement of this surface sensor is the presence or absence of a surface within a certain range.

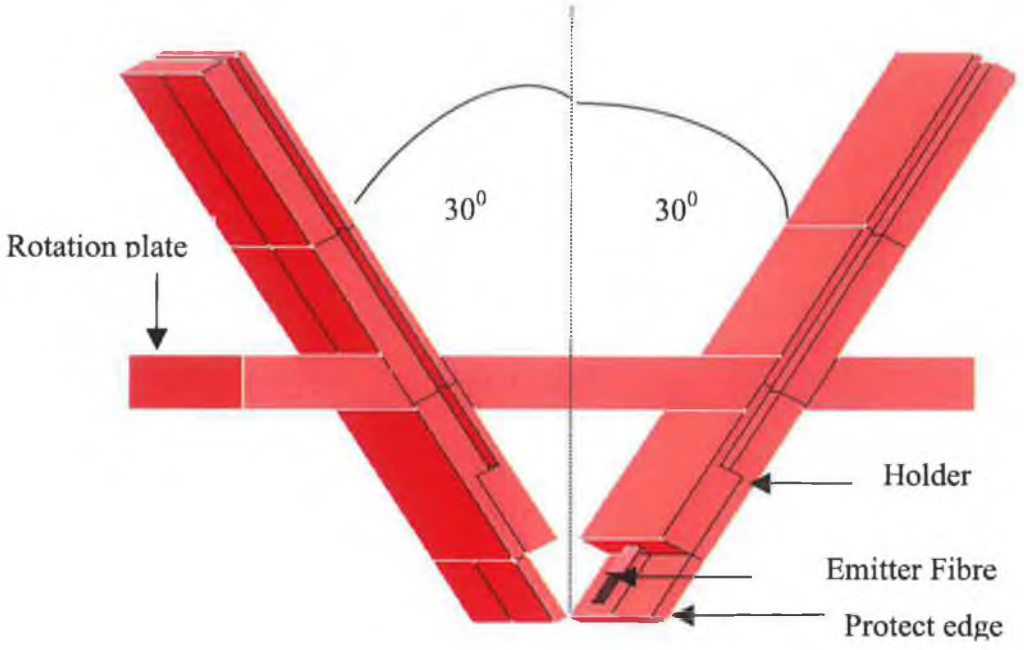

Figure 3.39 Side view of fibre optic holders

This sensor could create the surface map of the defects and the position of the defects in different sample material plates, which were tested by this system.

Chapter 4

LED and LD results for fibre-optic scanning systems

4.1 Introduction

The results of the fibre optic detection system were obtained using two emitter diodes (light emitting diode and laser diode). Primary and advance fibre optic systems have been described in the previous chapters. The block diagram of the apparatus designed in this work is shown in Figure 4.1. The experimental set up includes and consists of an LED or LD, the emitting and receiving fibre optic, and photodetectors. Photographs of the system are shown in the Appendix C_3.

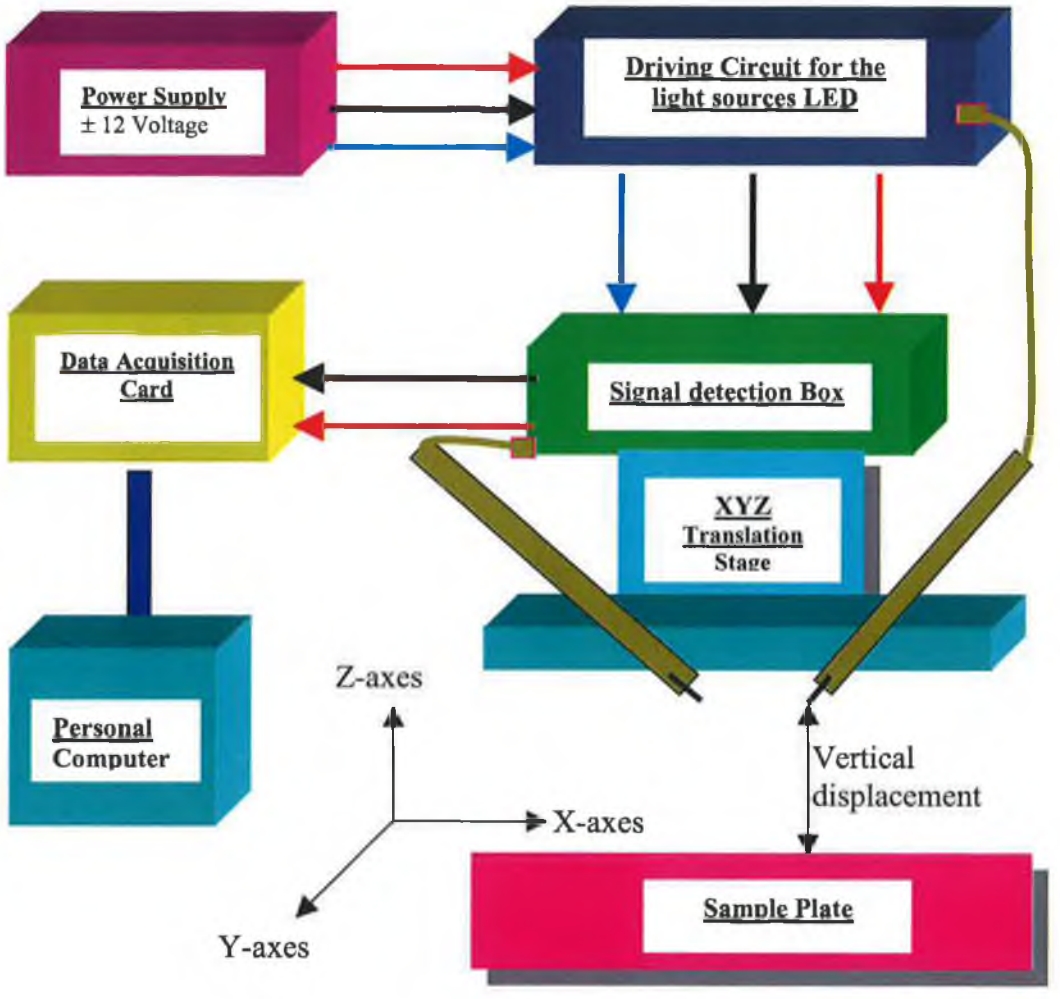

Figure 4.1 The experimental rig for the fiber-optic sensor system.

Basic surface sensing was set up as follows:

- Light sources such as LED and LD emit a light signal into the optical fibre
- Signal passes to the optical fibre and travels through it
- Light beam exits the optical fibre and arrives at the sample surface
- The beam is reflected from the sample surface
- Light is received by the juxtaposed light detector
- Light detectors perform the opposite function of light emitters
- Data acquisition card was used for analog to digital conversion
- Data analysis was performed using Labview software

4.2 Results achieved from signal beam (light emitting diode)

For the work reported in this section here, a fibre optic sensor system with an LED was used. Design and construction to control the system was described in the previous chapter.

4.2.1 System Configuration

The system was initially configured to record displacement. The high power LED, Appendix B_3, driven by constant circuit provided the light source. The receiving fibre collected the reflected optical radiation from the sample surface. This light was detected by a PIN photodiode attached to other end of the fibre. The PIN photodiode was mounted in low profile ST fibre optic connector (HFE3022/002BBA Honeywell Appendix B_4) with an integral preamplifier. These PIN photodiodes are sensitive to radiation between 650 to 950 nanometers wavelength, giving an analog output, which was converted to digital form, by a picolog data logger. This sensor used fibres with a core/cladding ratio of 100/140 and the optical fibres were oriented at the incident angle of 60^0.

The surface defect sensor operates by using an 850 nm wavelength LED. A National Instruments data acquisition card was used for analog to digital conversion. Data analysis was performed using Labview software, which interfaced with the data

acquisition card to provides a graphical user interface (GUI) to control display and analyse the captured data.

This sensor system measures the existence of a hole in a plate, i.e. the size and position of a hole. This estimation of the size of a hole was able to discriminate between, for example, a hole drilled with a 1mm or 2mm drill bit. This system was designed for high accuracy measurement and to enable operation as a high-speed photoelectric sensor.

4.2.2 Sample surfaces

This section presents the scanned samples, which are made from materials such as stainless steel, brass, copper, and polycarbonate. The design and the dimension of these plates are shown in Figure 4.2.

Figure. 4.2 Sample plate of material such as stainless steel, copper, polycarbonate, and brass.

The polycarbonate sample was machined from a moulded plate. It was dull white in colour. The copper plate had a blotched grainy surface as a result of rolling, where the surface colour varied. It was the roughest of the samples. The rolled brass plate had a tarnished surface, which would tend to decrease the reflectivity. The holes in these plates, the area surrounding these hole, the smallest blind hole and the smallest through

hole were examined by this system. Figure 4.3 shows the dimension of the smallest through hole on each plate.

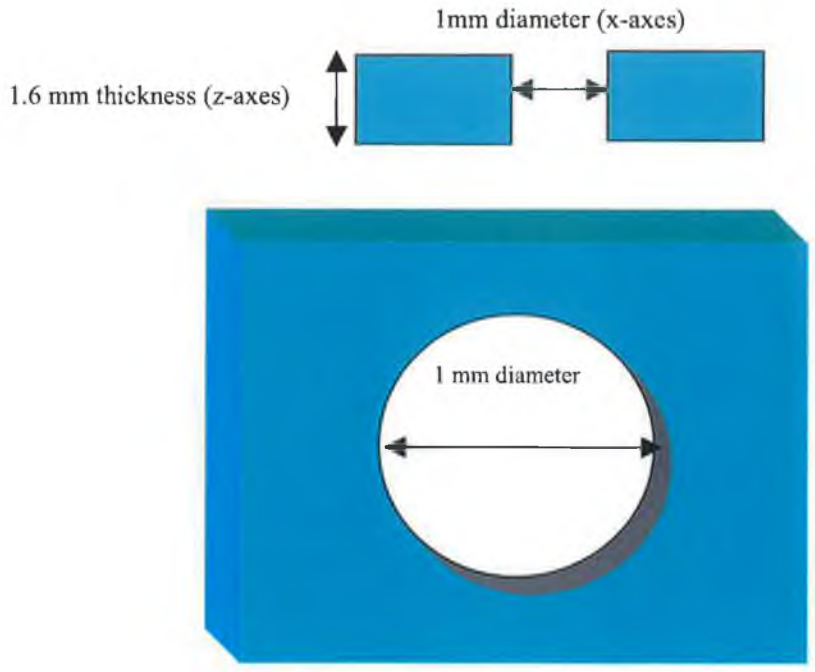

Figure 4.3 Through hole of 1mm diameter.

The dimensions of the smallest blind hole these were the same on every plate (except the stainless steel plate). The system was able to detect a stainless steel blind hole with a central island, Figure 4.4.

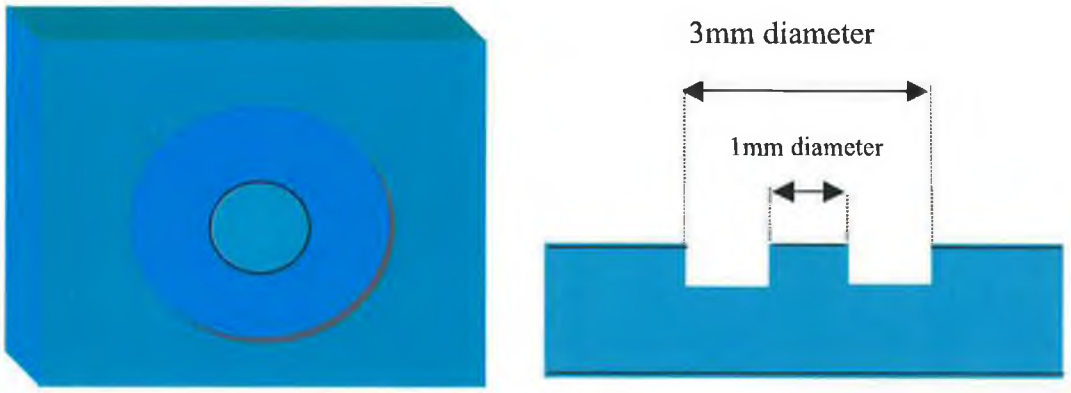

Figure 4.4 Stainless steel 3mm diameter blind hole in a plate of depth 0.6mm with island of 1mm diameter.

Note the island of 1mm diameter that is left by the end-milling operation. A photograph of the four samples is shown in Figure 4.5.

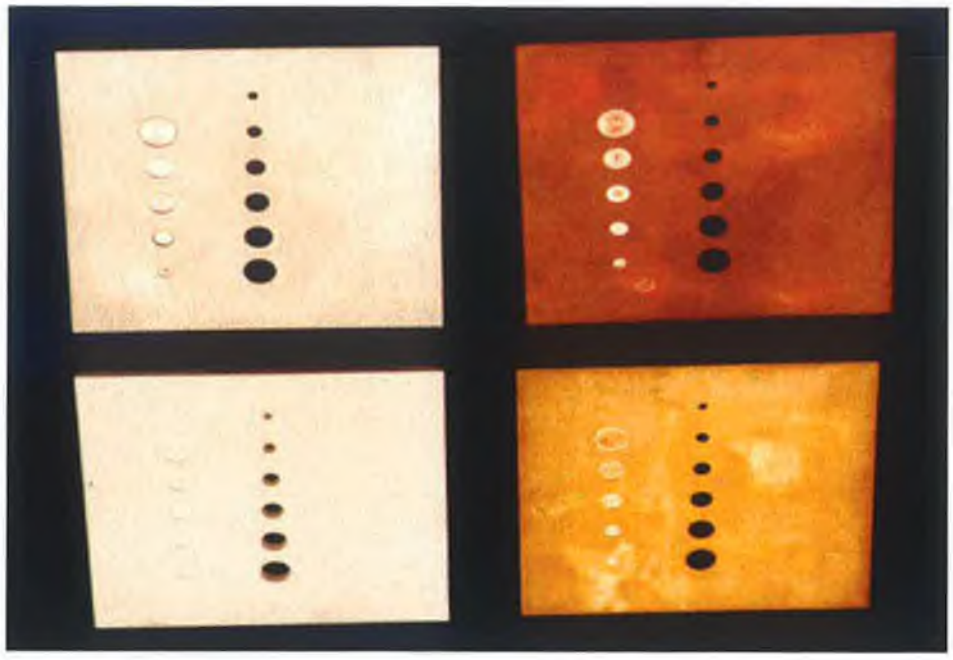

Figure 4.5 A photograph of four sample plates.

4.2.3 Measurement steps

The translation stage was fixed on the optical bench. An adhesive pad was used to position the sample plate for each surface on the translation stage. The XY translation stage was arranged to start from the beginning of the scale so that a surface map containing all of the area of the hole and surrounding surface area could be recorded. The vertical displacement of the Z-stage, for the remainder of the measurement, was chosen very carefully and set close to the peak of the displacement characteristic. A first translation displacement characteristic or scan was taken by displacing the X-stage through a certain number of 0.1 mm increments. After the completion of a scan, the Y-stage was translated through an increment of 0.1 mm for 1, 2 and 3 mm holes and a blind hole in stainless steel plate. The X-stage was then translated through the same number of increment in the reverse direction.

This cycle continued until the area around the hole or blind hole was mapped. Each reading was compared with a cut-off voltage level. Any point below the cut-off voltage was displayed on the surface map.

4.2.4 Measurement details

The measurement surfaces were obtained when using one fibre transmitting light with wavelength 850 nm. The maximum voltage recordable at this stage of the work by data acquisition equipment was 10 V. some of the following graphs are therefor truncated. The danger of blowing the data acquisition card was reduced by insuring that the preamplification level of the transimpedance amplifier did not rise above 12 V, which is the voltage level of the supply. The displacement characteristic seen in Figure 4.6 for the brass sample shows the effect of the different z, y position (Figure 4.1) of the fibres.

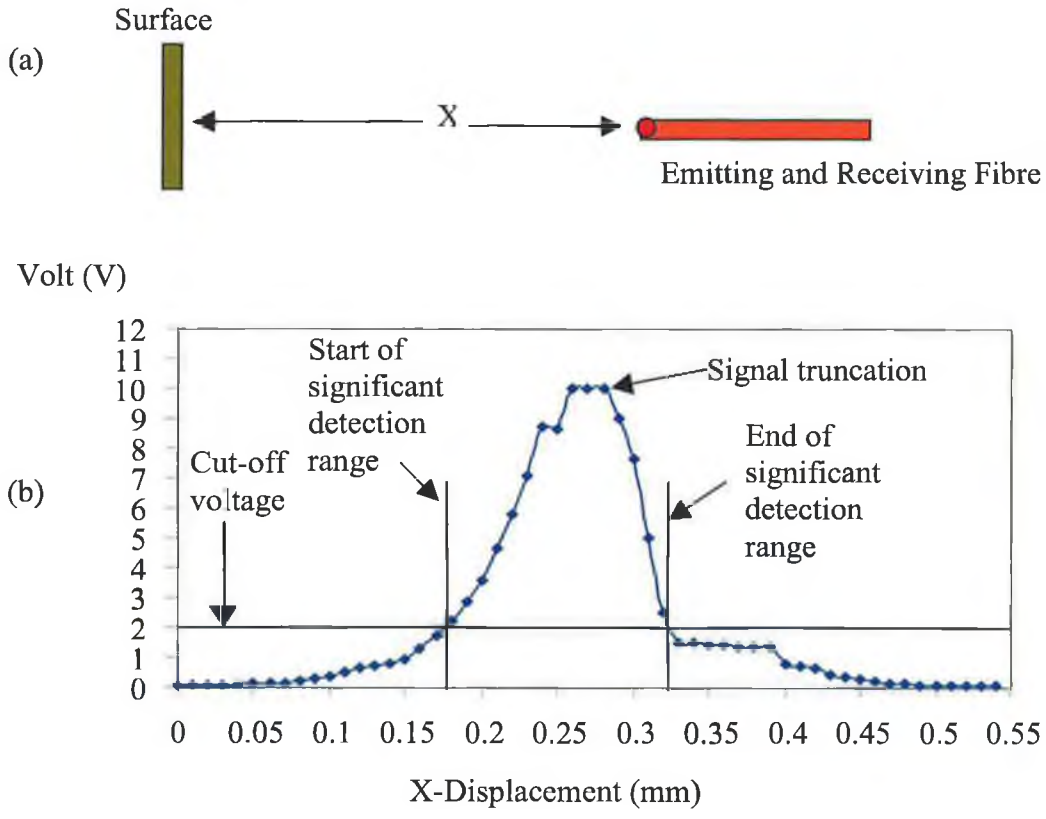

Figure 4.6 (a) Scanning set-up and (b) corresponding recorded vertical displacement characteristics for a brass surface using an LED light source.

Several sets of readings from the experiment were taken. Any defect on the surface or irregular shapes could also can be scanned using the same procedure.

4.2.5 Vertical displacement characteristic of each sample plate

The results obtained for sample plates surfaces are present here. A vertical displacement characteristic of each plate is shown in Figures 4.6 to 4.9. These diagrams illustrate the reflected signal at each vertical displacement from the particular sample plate. The curves are seen to be not very symmetrical about the peak voltage response. This variability was due to particular material surface properties (roughness and reflectivity). On the other hand the cleaving fibres can have large affect and change the stand-off distance of the fibre from the surface. However the peak response is clearly distinguishable enabling fibre end and surface distance to be set for future measurements.

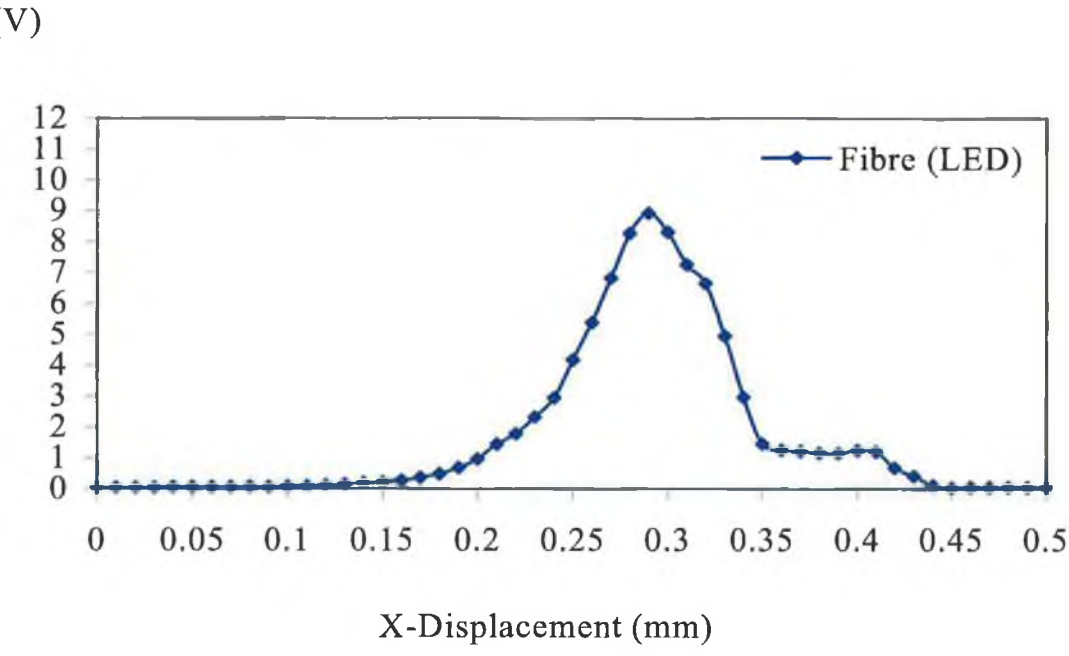

Figure 4.7 Vertical displacement characteristics for a stainless steel surface.

The photosensor was designed to withstand signal voltage variation. This system was designed to measure extremely small changes in light reflection. The principle of

operation was based on reflectivity. Ordinary engineering surfaces generally reflect irregularly. The vertical displacement characteristics can therefore differ between the same plate for different sets of measurement e.g., there was some difference in the peaks of the signals detected from two different points on a given sample's surface. Average curve must therefore be used.

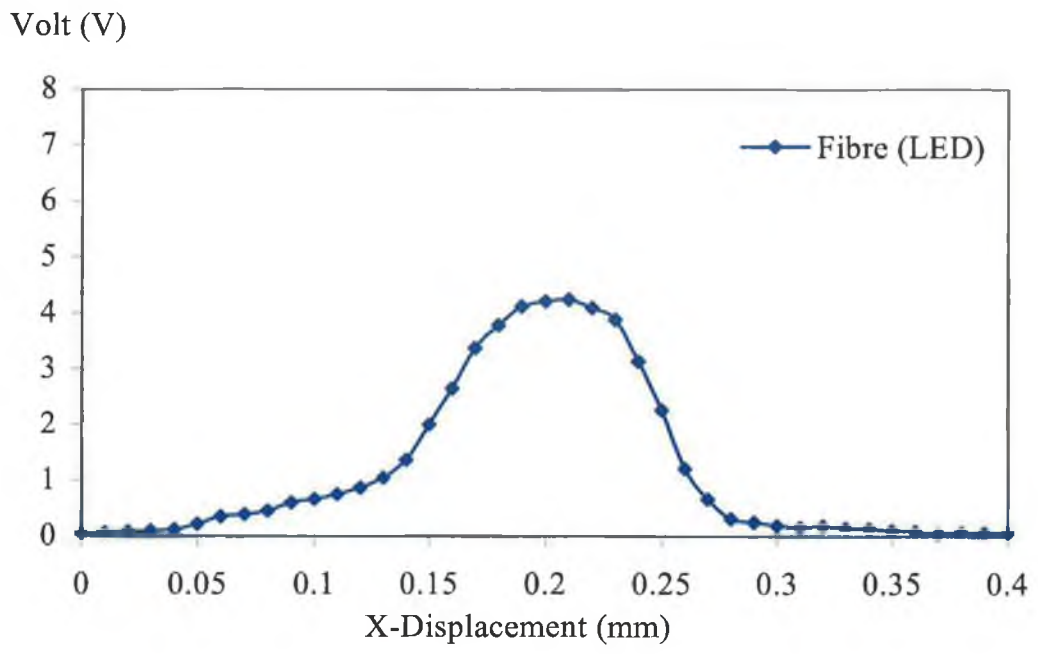

Figure 4.8 Vertical displacement characteristics for a polycarbonate surface.

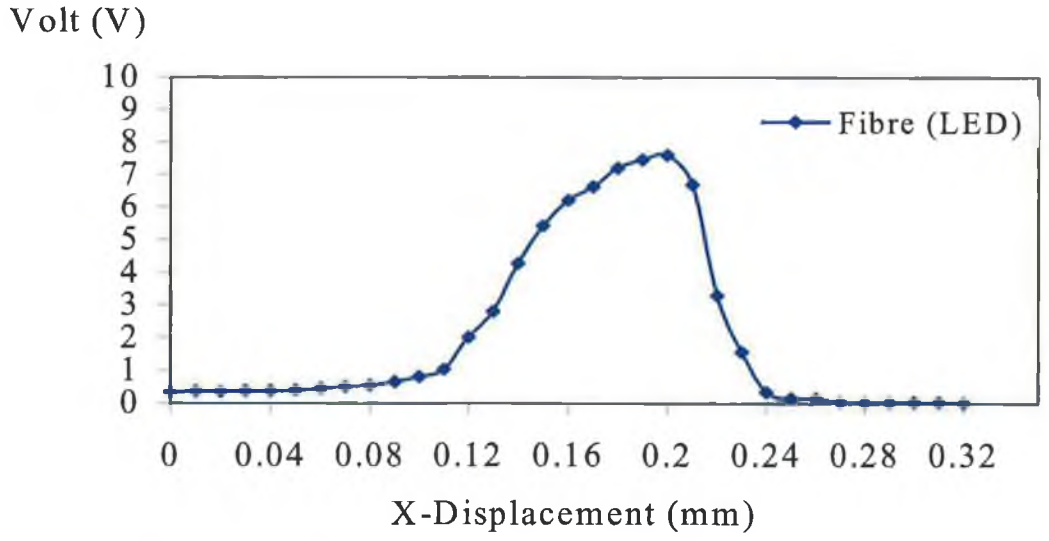

Figure 4.9 Vertical displacement characteristics for a copper surface.

4.2.6 Lateral displacement characteristics of each sample plate

A scan of a sample's lateral displacement characteristic was taken and each set of readings is shown in Figure 4.10 to 4.20. To generate the surface map of the sample plates many other scans were required. For the reasons of space it is impossible to show all these. From inspection of these scans it can be seen which cut-off voltages generates surface maps adequately for each set of results. For scan there was a horizontal line superimposed on the graph (Figure 4.10) to indicate the of cut-off voltage. All the Figures 4.10 to 4.13 shows scans through the holes in the copper plate, polycarbonate plate, brass plate and stainless steel plate respectively. These measurements were obtained from the beam when crossing the centre line of the hole.

In the following graphs it may be seen, when going from left to right, that the signals obtained from the bottom of the hole rises. This is due to slight rise which is physically present in the center of the holes. The fall off in the rise is believed to be missed on the right due to shadow affect.

Excellent contrast is shown between the presence and the absence of a surface. Any cut-off voltage level chosen between 1 V and 9 V will confidently ensure detection of the holes in the samples (stainless steel, copper polycarbonate and brass). An appropriate cut-off voltage is however necessary to correctly determines the hole size. A cut of voltage of 2V gives accurate results for 1 mm hole in the copper plate, see figure 4.10. The smallest through hole in the brass plate, 1 mm, was scanned and showed the high contrast achieved through this method for a smooth and bright surface. Any cut-off voltage between 2V and 9 V will operate successfully for this materials and hole size.

(a)

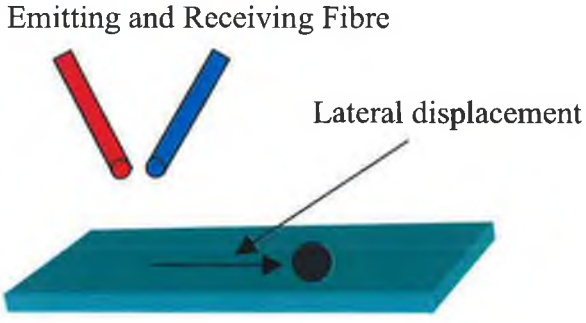

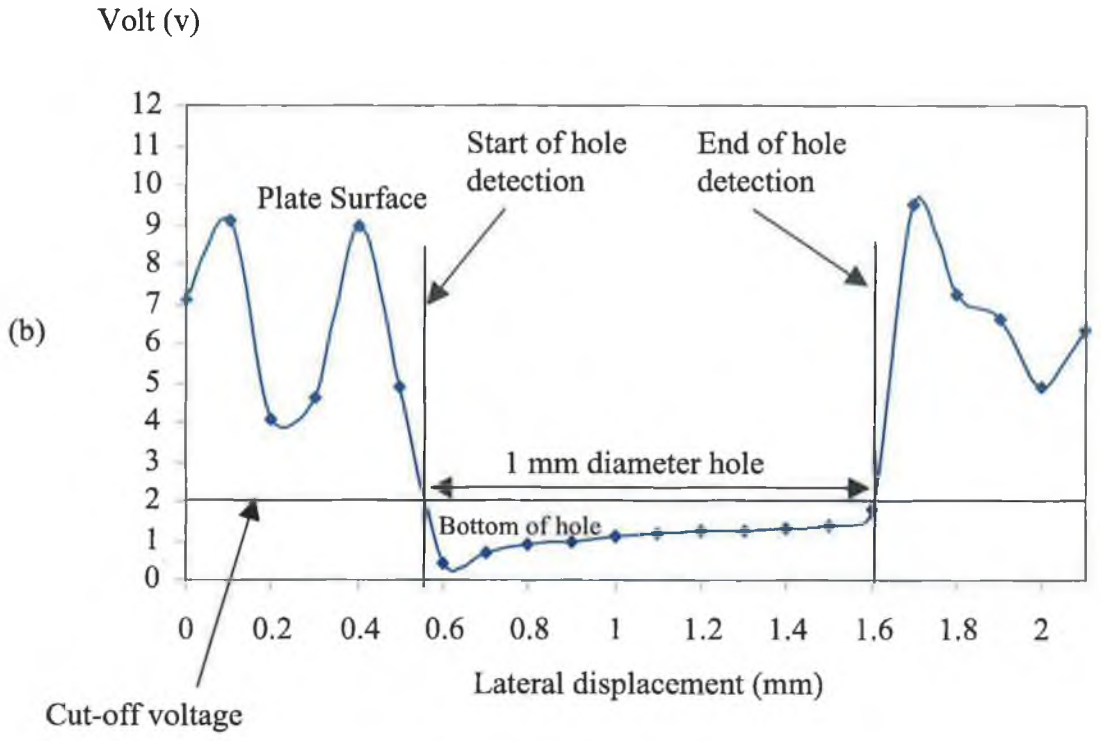

Figure 4.10 (a) Scanning set-up and (b) the sample scan of lateral displacement through a 1 mm hole in a copper plate using an LED light source.

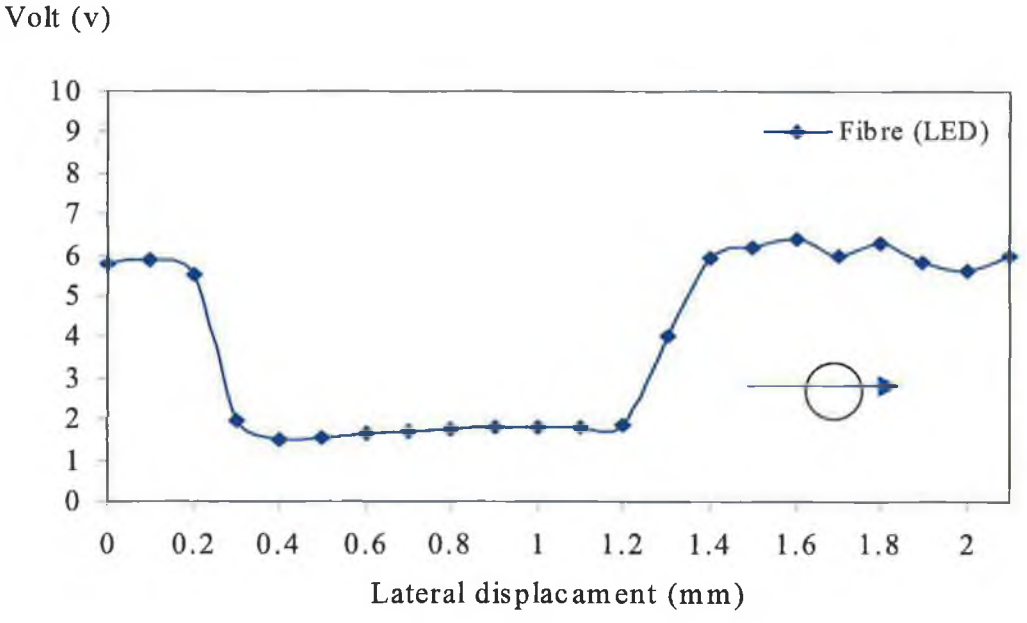

Figure 4.11 Sample scan of through 1 mm hole in a polycarbonate plate.

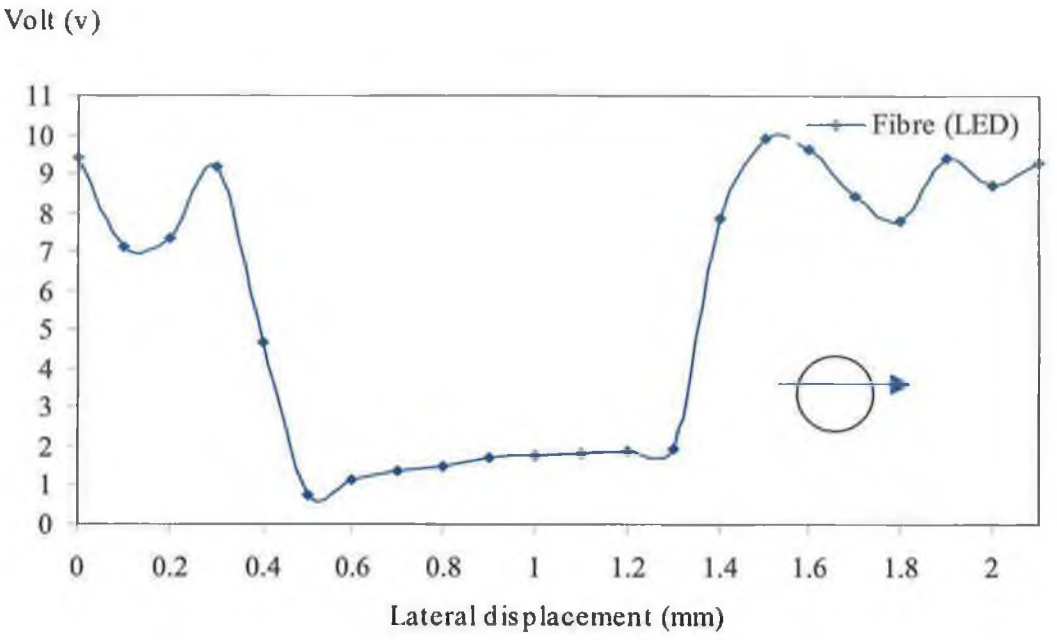

Figure 4.12 Sample scans of brass through 1 mm hole.

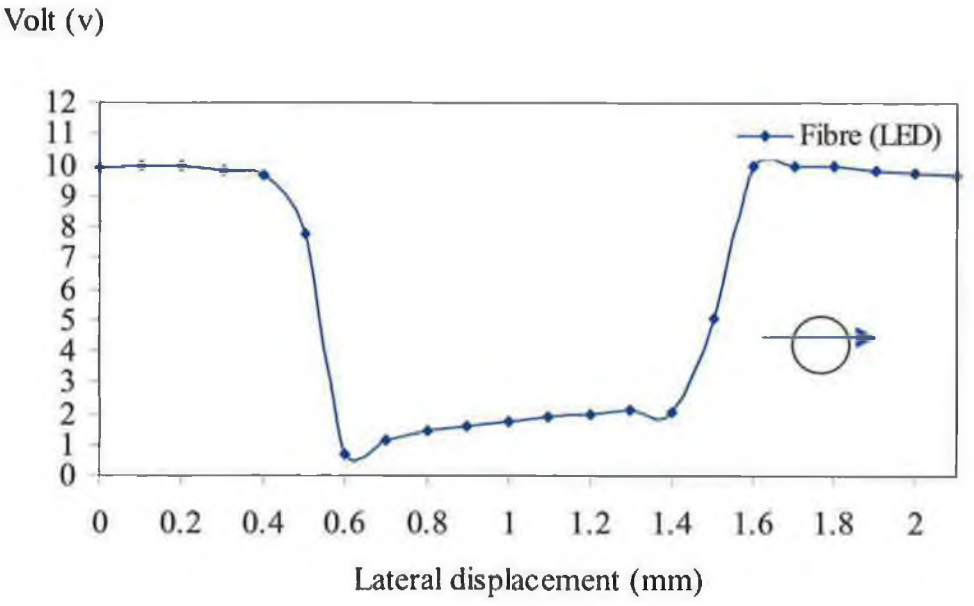

Figure 4.13 Scans of 1 mm through hole in stainless steel plate.

Figure 4.14 to 4.17 shows a scan through the smallest (3 mm) blind hole on the stainless steel plate taken from different positions across the hole. Both the unmachined and machined sections of the blind hole are clearly sensed. The unwanted spikes hinder in the cut-off voltage operating range. In the machined section the surface map of this hole at a cut-off voltage of 2 V operates successfully. This hole was end-milled and an island remains in the centre of the hole.

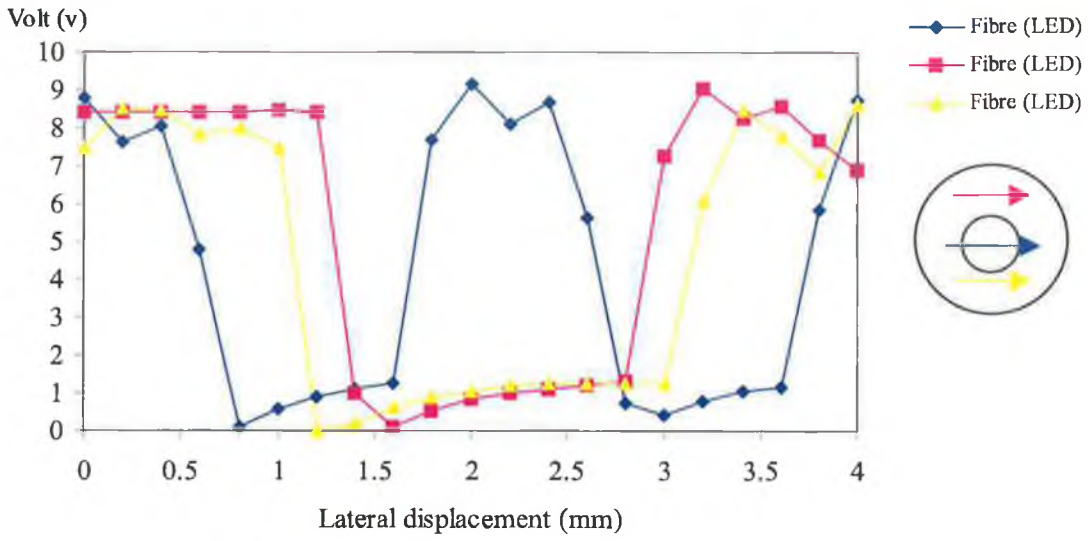

Figure 4.14 Three scans of through 3 mm blind hole with island in stainless steel plate.

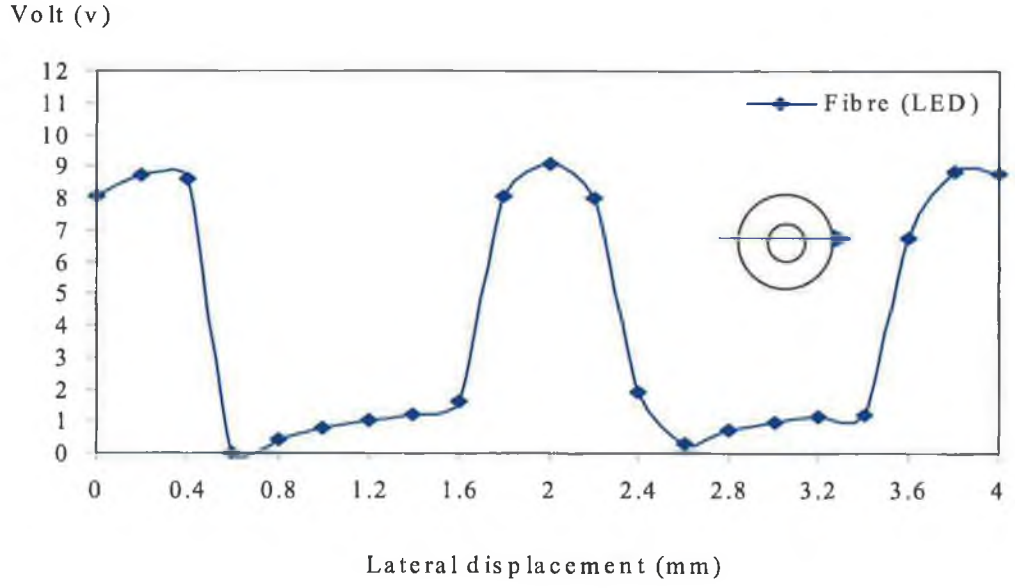

Figure 4.15 Sample scan 3 mm blind hole with island in stainless steel plate.

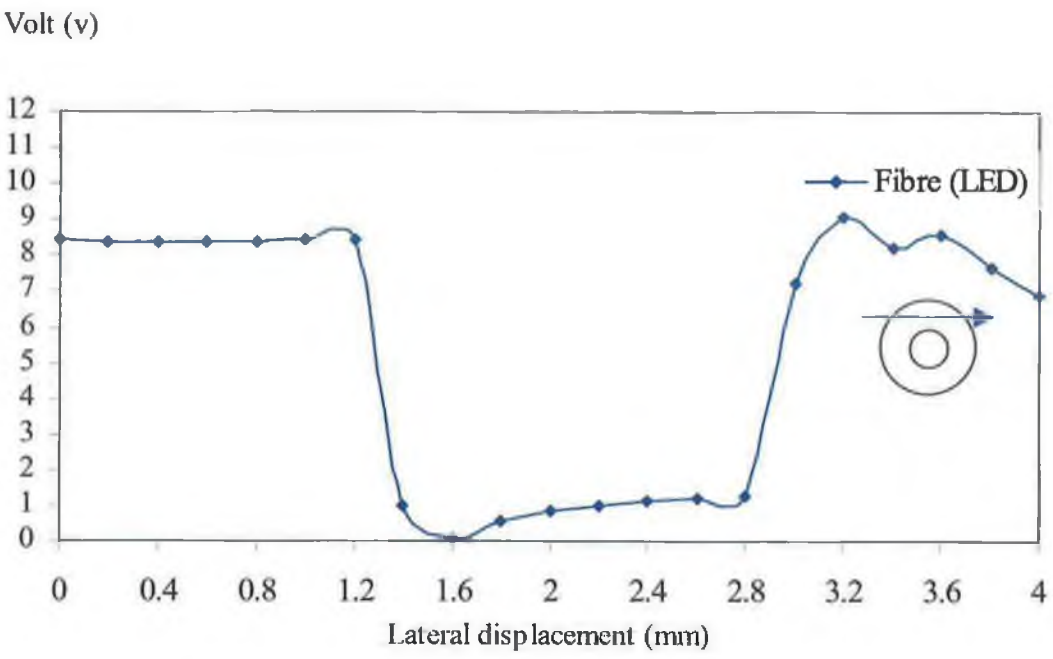

Figure 4.16 Sample scan 3 mm blind hole with island in stainless steel plate taken off center.

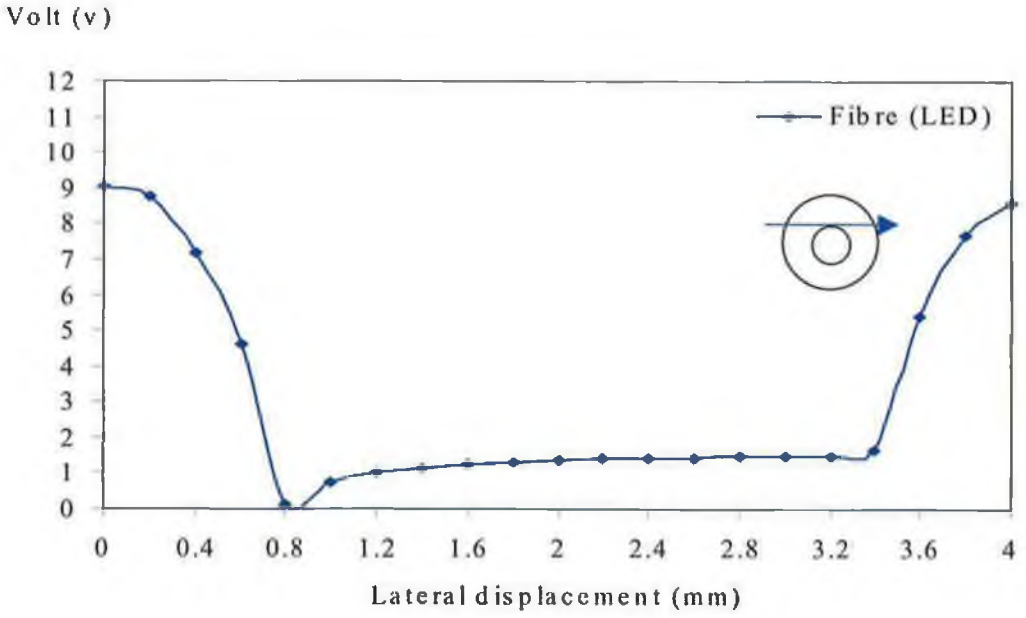

Figure 4.17 Sample scan 3 mm blind hole in stainless steel plate.

For the polycarbonate Figure 4.11, a scan of the smallest through hole shows the disadvantage of using a sensor of this kind with a surface that reflects light diffusely. The variability of the reflection from a surface is clear from this figure and more so from the next. The Figure 4.18 to 4.19 shows a scan through other size through holes (2mm) in stainless steel and copper plates. Figure 4.20 shows the examination of signal drift effect of the system over a period of time. This effect in the system was not seen to be very significant.

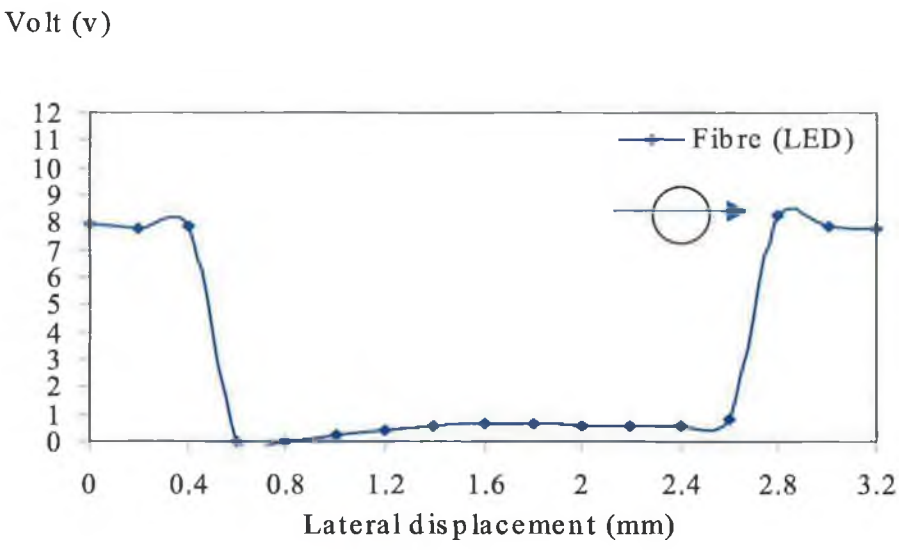

Figure 4.18 Sample scan 2 mm through hole in stainless steel plate.

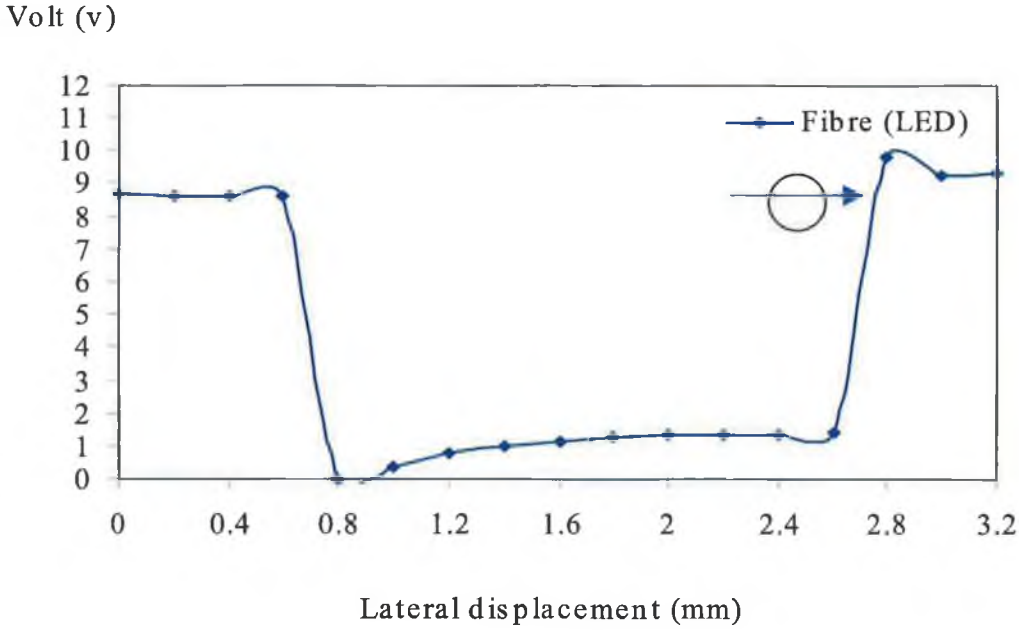

Figure 4.19 Sample scan through 2 mm through hole in copper plate.

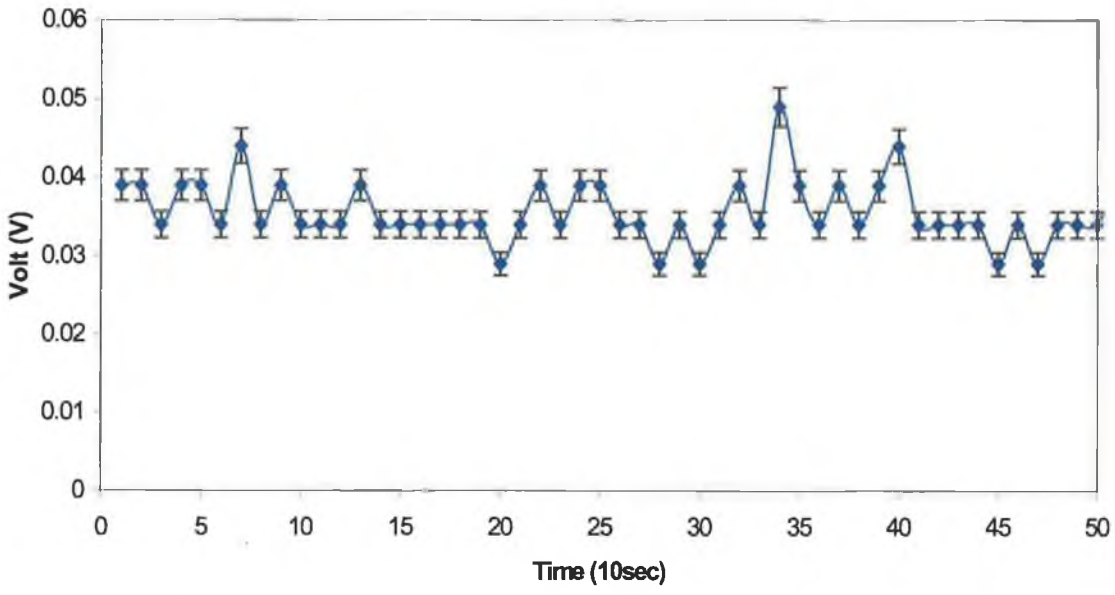

Figure 4.20 Study on voltage of the system over a period of time.

4.2.7 Two dimensional surface map of each sample plate

A cut-off voltage of 2 V was applied to achieve the surface transverse displacement characteristics. Plots of the surface maps produced are shown in Figures 4.21 to 4.27. This cut off voltage was suitable for all the sets of through holes. The detection of through holes relies solely on detecting the presence or absence of a surface.

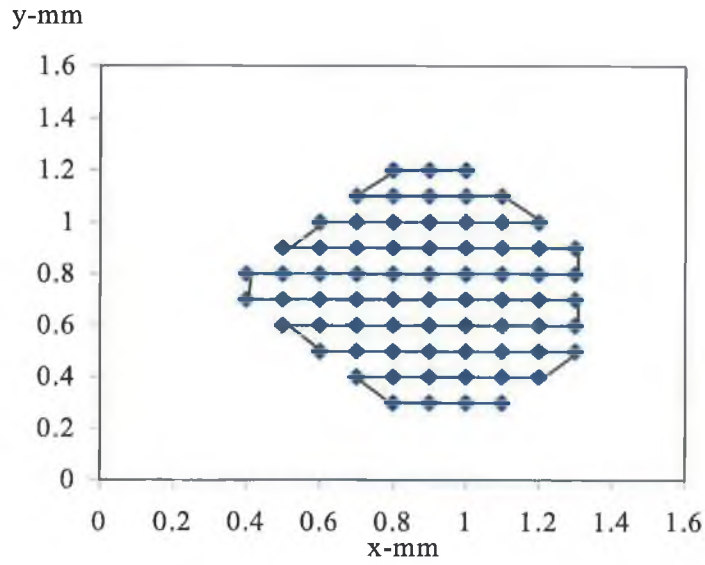

Figure 4.21 Surface maps though a 1 mm hole in stainless steel plate using 2V cut-off voltage.

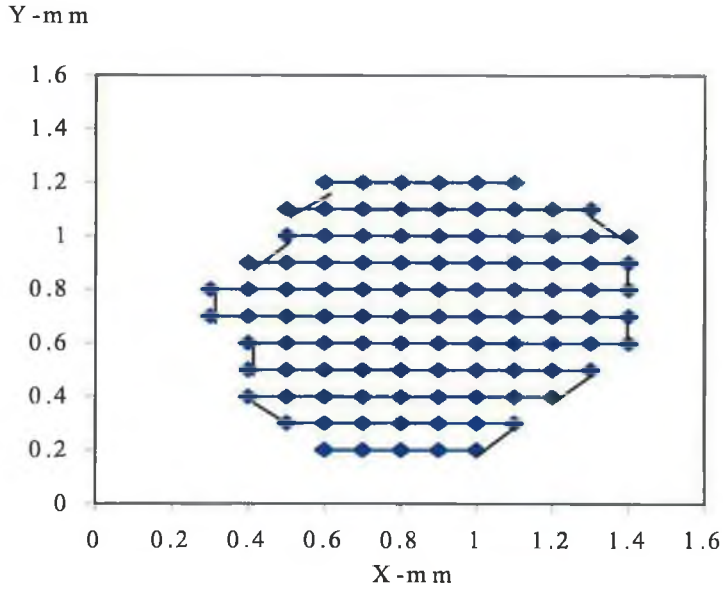

Figure 4.22 Surface map through a 1 mm hole in a copper plate using a 2V cut-off voltage.

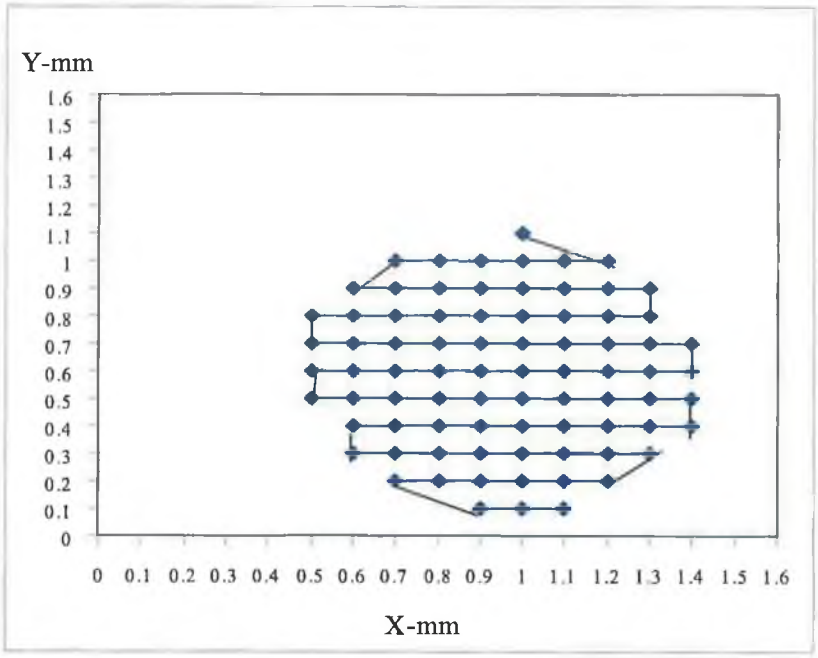

Figure 4.23 Surface map through a 1 mm hole in a polycarbonate plate using a 2V cut-off voltage.

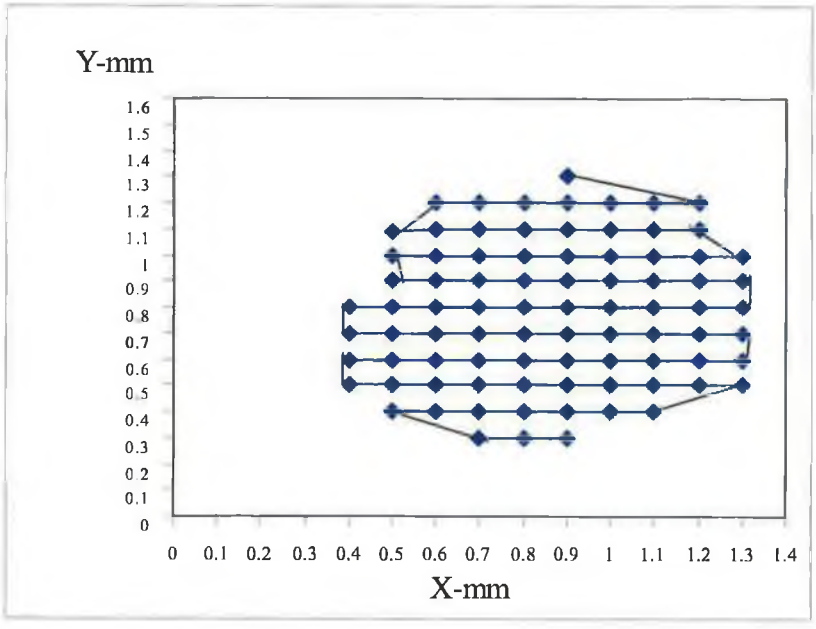

Figure 4.24 Surface map through a 1 mm hole in a brass plate using a 2V cut-off voltage.

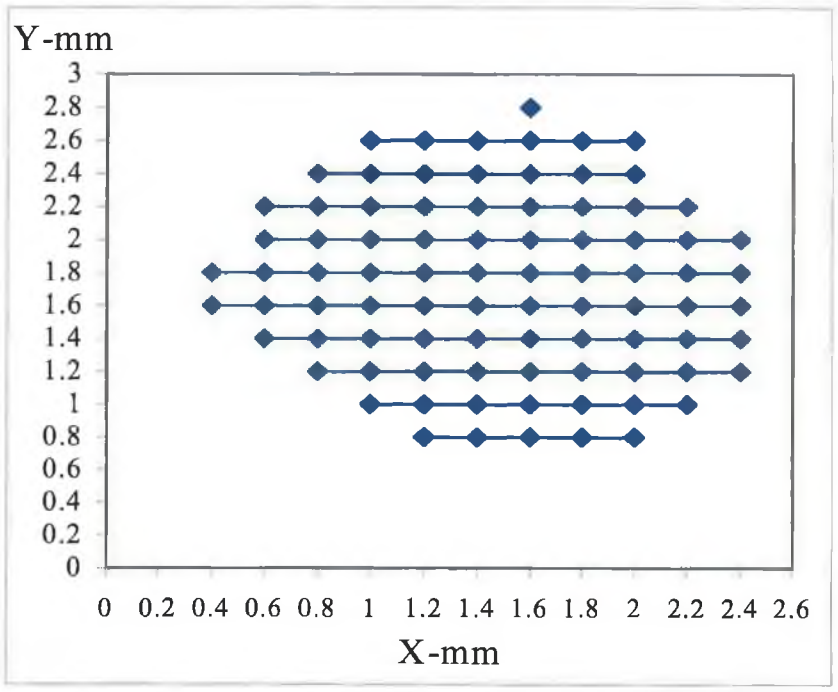

Figure 4.25 Surface map through a 2 mm hole in stainless steel plate using a 2V cut-off voltage.

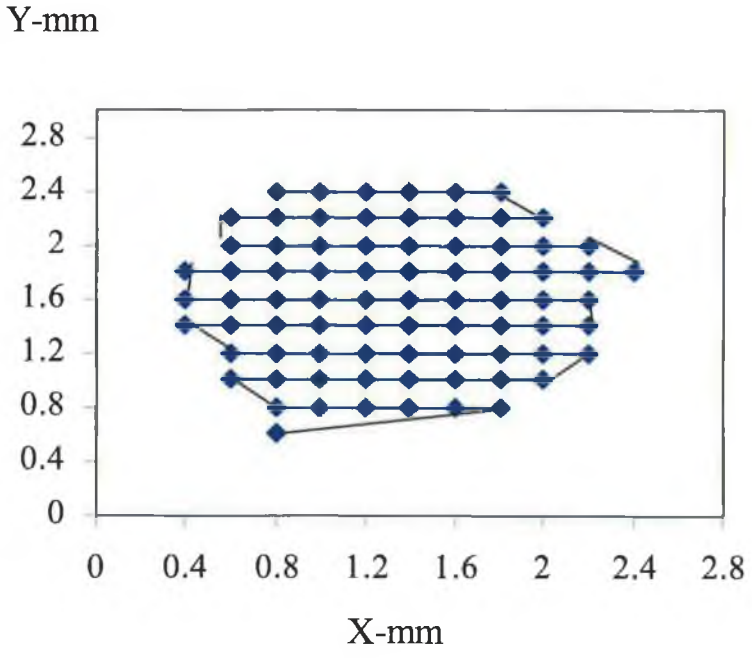

Figure 4.26 Surface map through a 2 mm hole in copper plate using a 2V cut-off voltage.

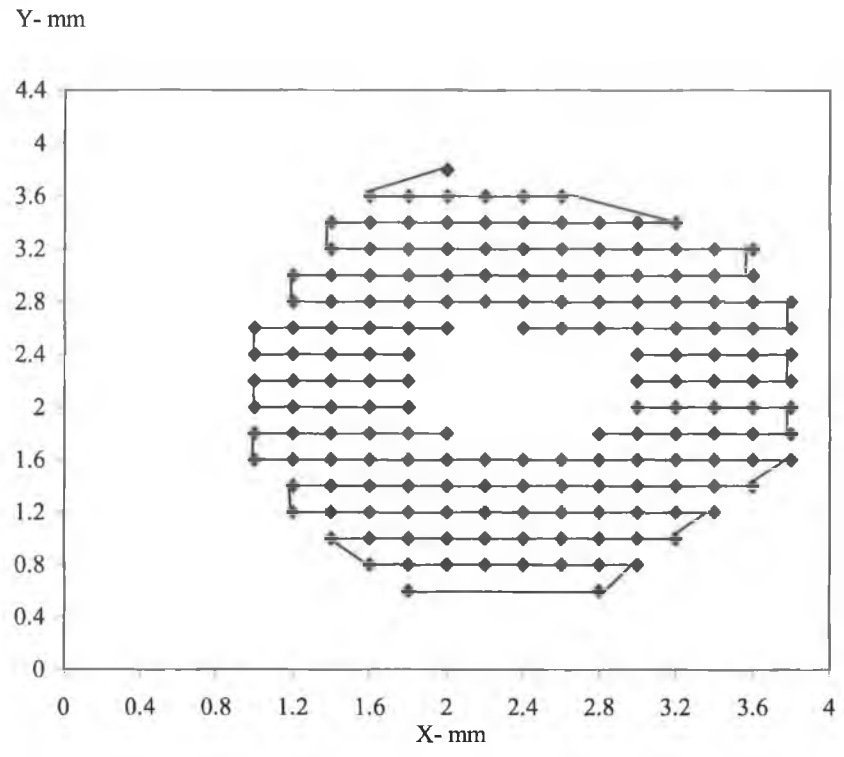

Figure 4.27 Surface map through a 3 mm blind hole in stainless steel plate using a 2V cut-off voltage.

It was more problematic to detect a blind hole as this relies on the detection of a surface within certain displacement limits. This in turn relies on the vertical displacement characteristics discussed in Section 5.2.5 and the choice of vertical stand-off distances. With the blind hole of depth of 0.6 mm, there was no real error. The depth of the shallowest blind hole that could be detected.

4.3 Results achieved from multi-beams (Laser Diode)

The results of the optimisation of the fibre optic detection system showed that the output signal of four and five arrays successfully measured the existence of the size and position of a hole in a plate. This system designed to operate as a high-speed photoelectric sensor.

Figure 4.28 shows the structure of the fibre optic sensor, the sensor was operated using four and five 1300 nm-multimode laser diodes (Mitsubishi FU-17SD-F, Appendix B_5.).

The driving circuit as shown in, Appendix C_1. The light source with a 1300 nm wavelength was chosen in order to reduce surface scattering and maximise the proportion of optical radiation that reflects specularly.

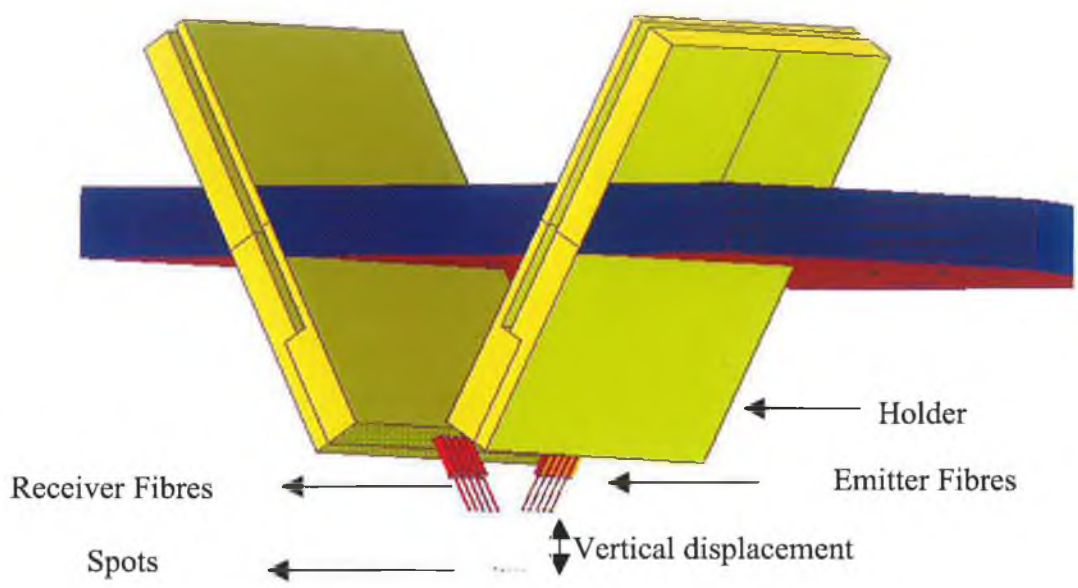

Figure 4.28 Configuration of fibre optics transmission system.

This sensor used fibres of core/cladding ratio of 62.5/125 and 100/140 with ST connectors. The emitting fibres were oriented at an angle of 30^0. The five receiving fibres were positioned in opposite direction of emitting fibres. The signal detection circuit consisted of unbiased transimpedance amplifiers using EG & G PIN photodiodes, (C30617-BST, Appendix B_6). This PIN photodiode's (InGaAs) are sensitive to infrared radiation between 900 nm 1700 nm.

4.3.1 Measurement steps

- Position the translation stage on the optical bench.
- Put the sample plate on the translation stage, arranged so that a surface map containing all the area of the hole and the surround surface area could be recorded.
- The vertical displacement characteristic of the z-stage was set carefully close to the peak.

- A first scan was taken by displacing the x-stage through a certain number of 0.1 mm increments. After the completion a scan the area covered is mapped.
- This reading is compared with a cut-off voltage level, as shown in the previous section. Any points with a voltage below the cut-off voltage level are displayed on the surface map.

4.3.2 Vertical displacement characteristics of each plate

The system used either four or five optic fibre sensors to deliver light from source to the surface and collect the reflected light and guide it to the photodetectors. The intensity of the detected light depends upon how far the reflecting surface is from the fibre optic sensor. Figure 4.29 shows a schematic of the end faces of the fibres, the sample surface and the vertical displacement between the two.

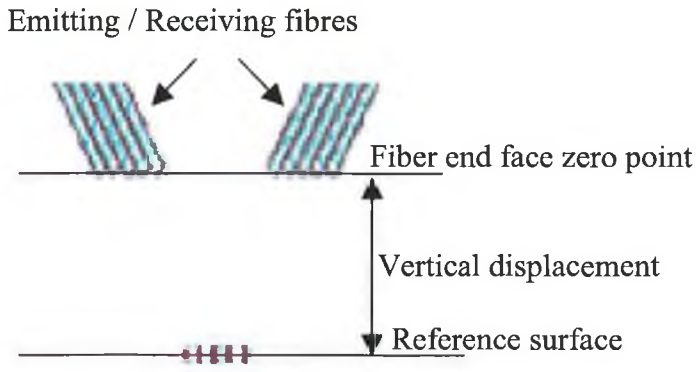

Figure 4.29 Schematic of the system's vertical displacement.

Vertical displacement characteristics for each sample plate are shown in Figure 4.30 to 4.34. These graphs illustrate the strength of reflected light, measured at different distances above the top surface of each sample plate. The four fibres used for the results of Figure 4.30 were not well cleaved or aligned. However the five fibres used to obtain the results of Figure 4.34 were well cleaved, cleaned and aligned. It is clear from the comparison of between Figure 4.30 (four-fibres) and Figure 4.34 (five-fibres) that carefully alignment, well-cleaved and cleaned fibre ends produced much enhanced

sensing results. It is believed that these parameters can be improved further, though precise quantification is difficult.

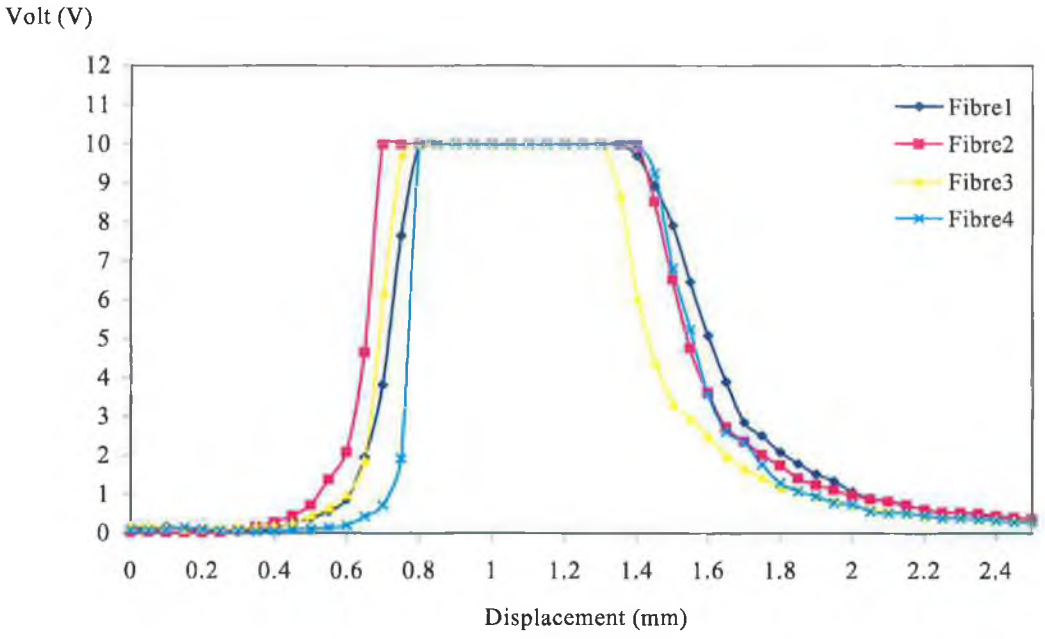

Figure 4.30 Vertical displacement characteristics for a brass surface.

The signal increased as the fibre arrays was brought down to the surface samples plate. When the fibre termination got very close to the surface, however, the signal started to decrease with the distance. Once the fibre termination was closest the surface, the reflected signal from surface scattering was largely excluded, resulting in a significant decrease in the signal. As can be seen the curves are not always symmetrical, and it is meant only as a rough estimate and used to choose a vertical displacement for further complete sets of scan.

Voltage profile differences from the beams were noted for all sample plates tested. At the early stages of the experiment the reflection signal was scattered due to a rough fibre surface as a result of poor mechanical cleaving. Due to the poor initial result factors that could affect the quality of the sensor were examined

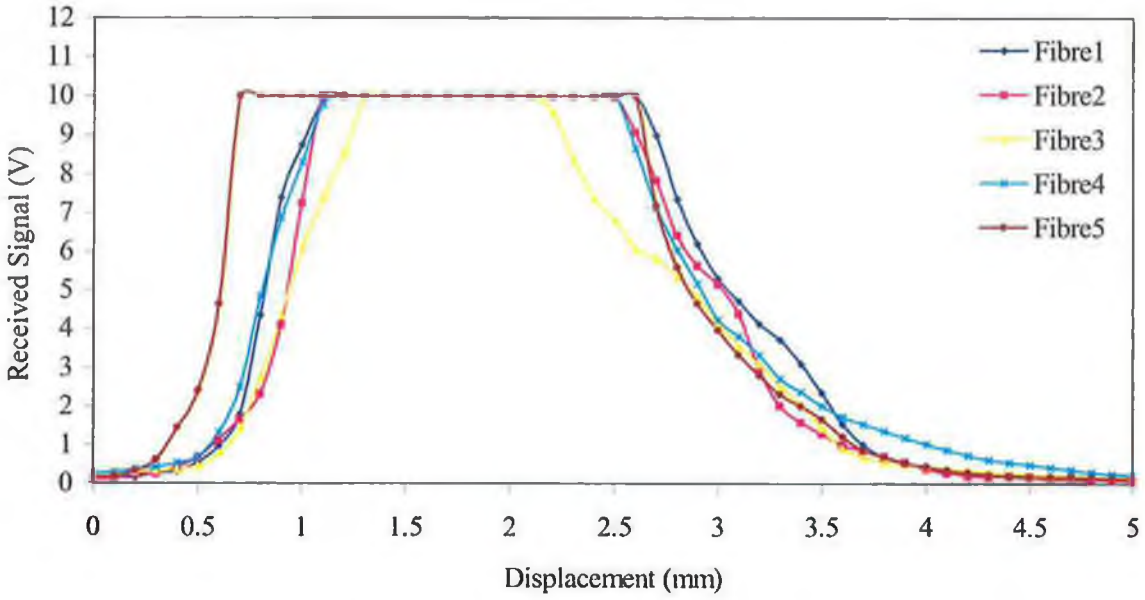

Figure 4.31 Vertical displacement characteristics for a brass surface.

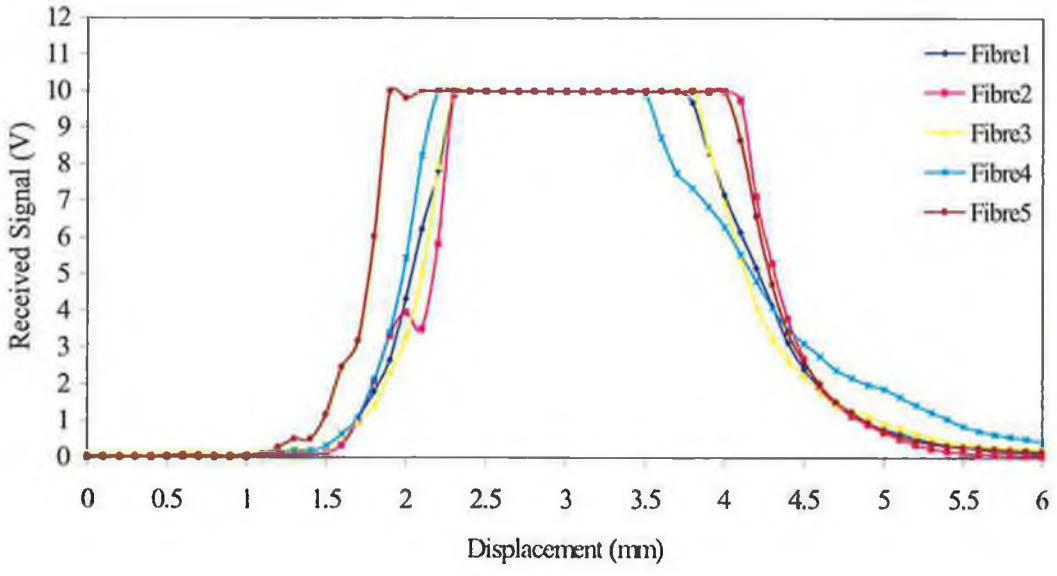

Figure 5.32 Vertical displacement characteristics for a stainless steel surface.

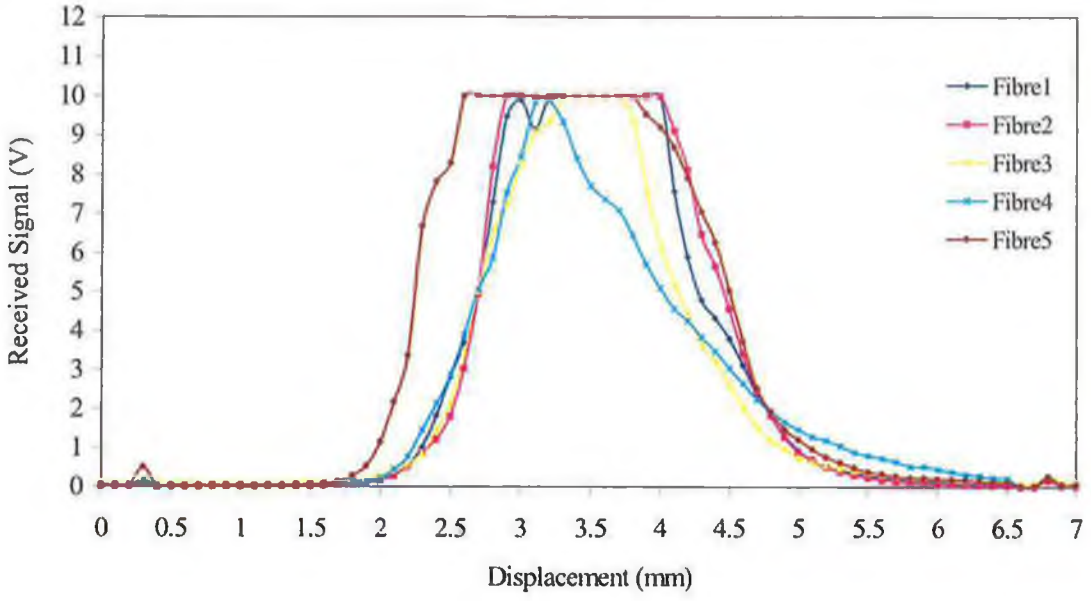

Figure 4.33 Vertical displacement characteristics for a Copper surface.

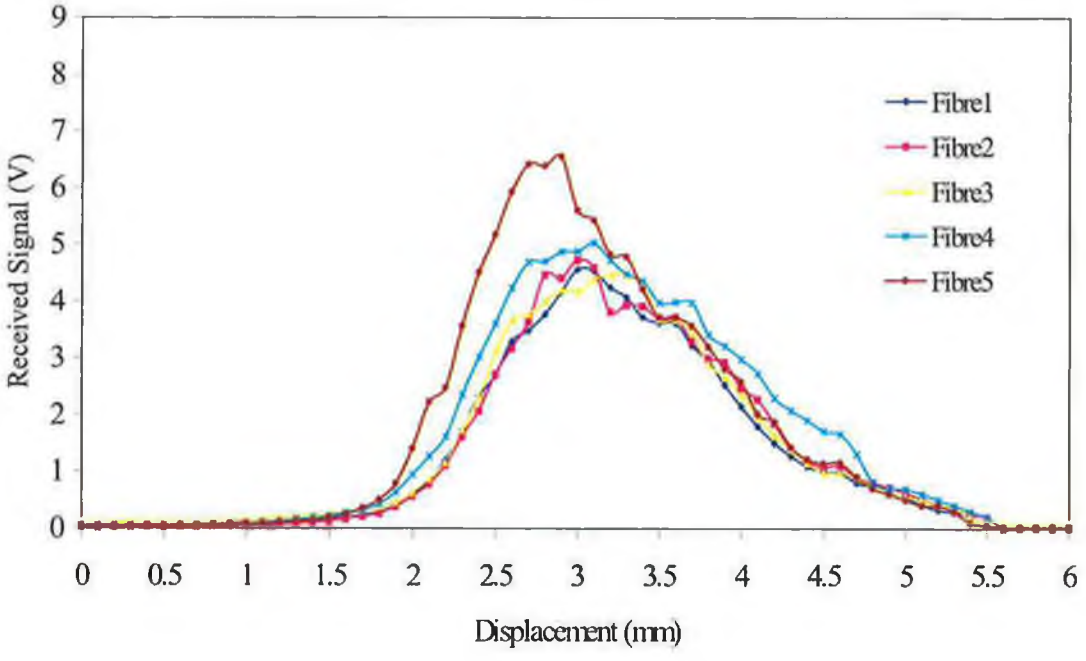

Figure 4.34 Vertical displacement characteristics for a polycarbonate surface.

Besides the previous analysis, there were more factors affecting the operation of the sensor such as alignment fibres, cleaving, cleaning, and polishing of the fibres. Results from the four fibres optic system were affected seriously by these factors.

4.3.3 Displacement characteristics of each sample plate

Sample transverse scans for plate material are shown in Figures 4.35 to 4.38. The surface map was generated by one set of scans. From scrutiny of these scans it can be seen that a range of cut-off voltage adequately generated surface maps.

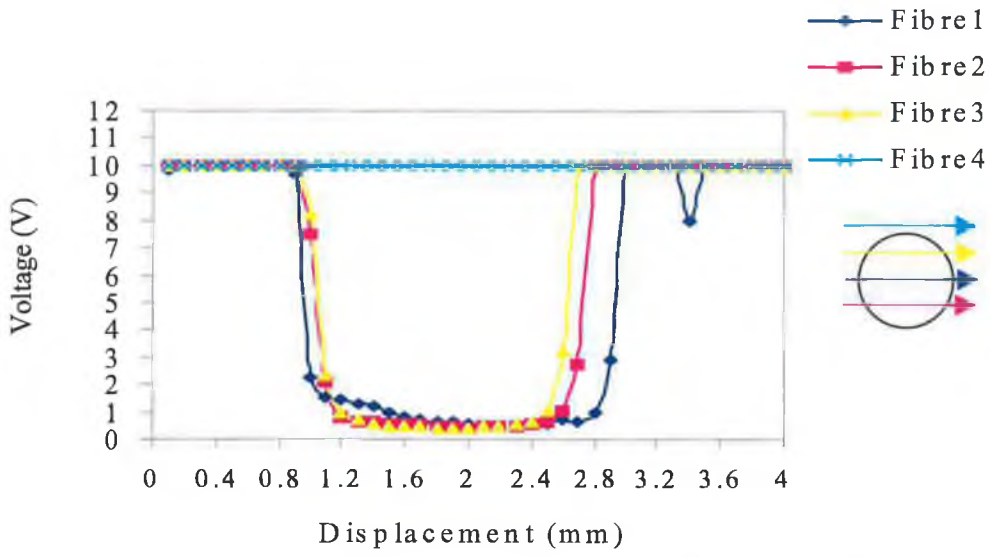

Figure 4.35 Set of scans through a 2 mm hole in brass plate (four fibres emitting).

The graph in Figure 4.39 show scans through hole 7 mm in diameter brass plate. As the first signal reach the edge of the hole, the signal decreased sharply and the other signals followed each other until all of the signals reached their minimum value. The sensors could still detected some light, although the reflected beam was from inside the hole. These indicate that the intensity of the reflected light is very high compared with the previous results (Figure 4.35 to 4.38). The thickness of the brass plate is 0.6 mm and the sensor can detect light from 1mm or more depth.

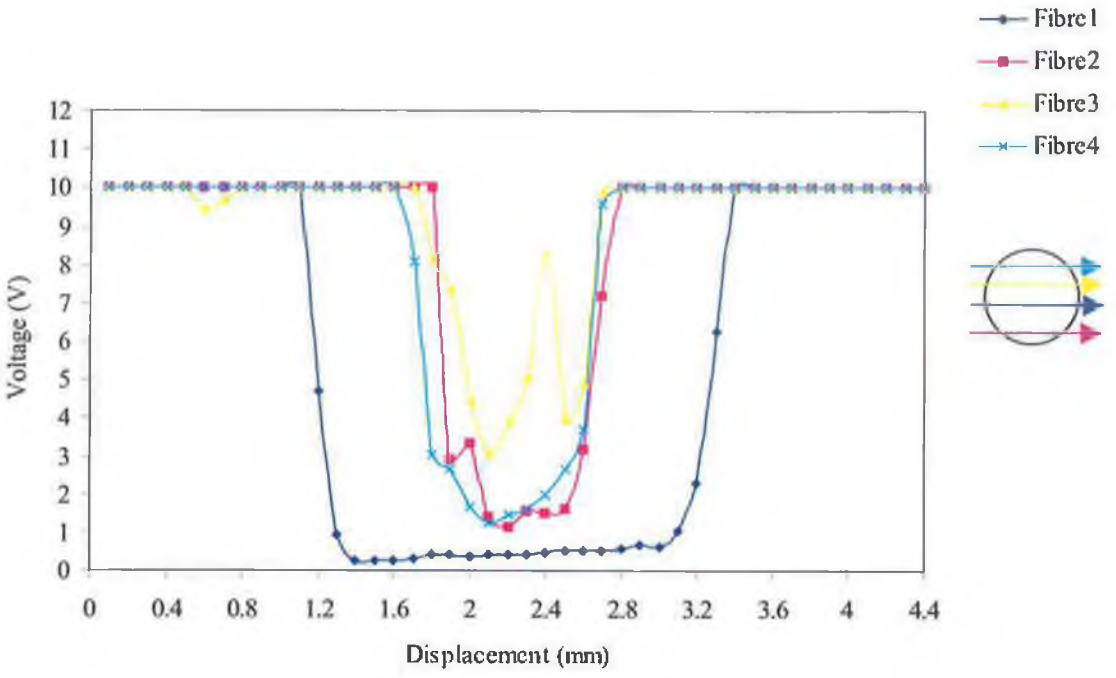

Figure 4.36 Set of scans through a 2mm hole in stainless steel plate (four fibres emitting).

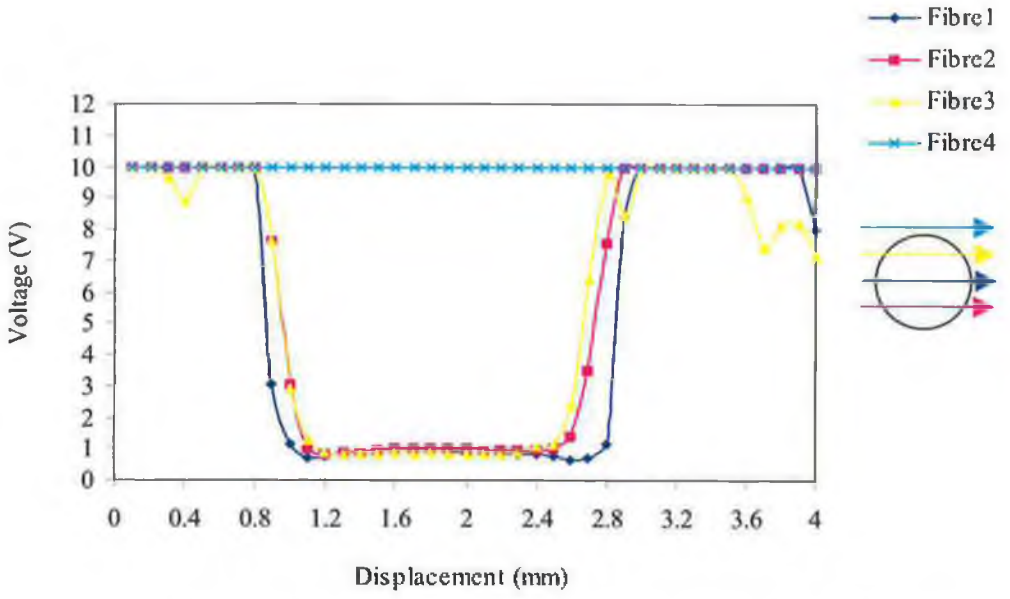

Figure 4.37 Set of scans through a 2mm hole in copper plate (four fibres emitting).

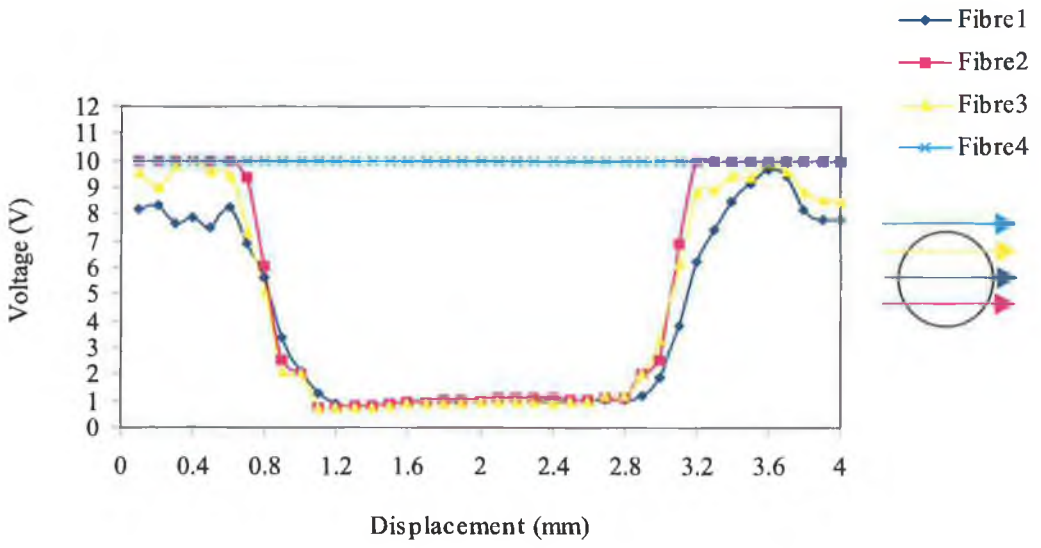

Figure 4.38 Set of scans through a 2 mm hole in polycarbonate plate (four fibres emitting).

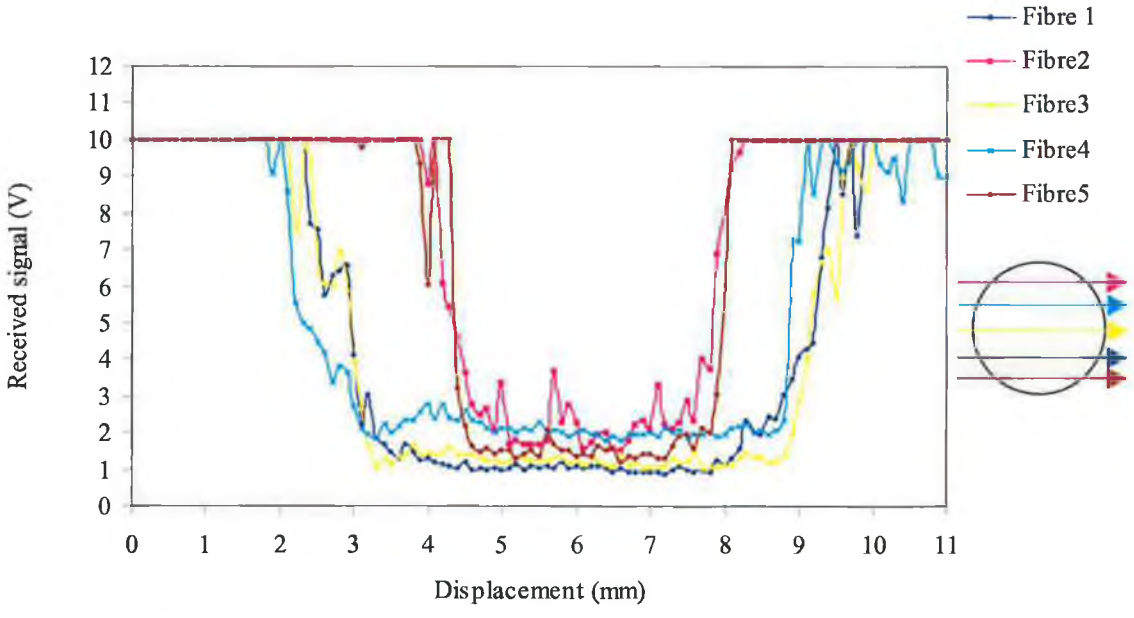

Figure 4.39 Set of scans through a 7 mm hole in brass plate (five fibres emitting).

From Figure 4.40 it can see that, the sensitivity of the system to detect light is quite high. Displacement characteristics of stainless steel plate are shown in Figures 4.41 to 4.43.

The sensor could detect the light through the hole because the thickness of the stainless steel plate is 1.6 mm.

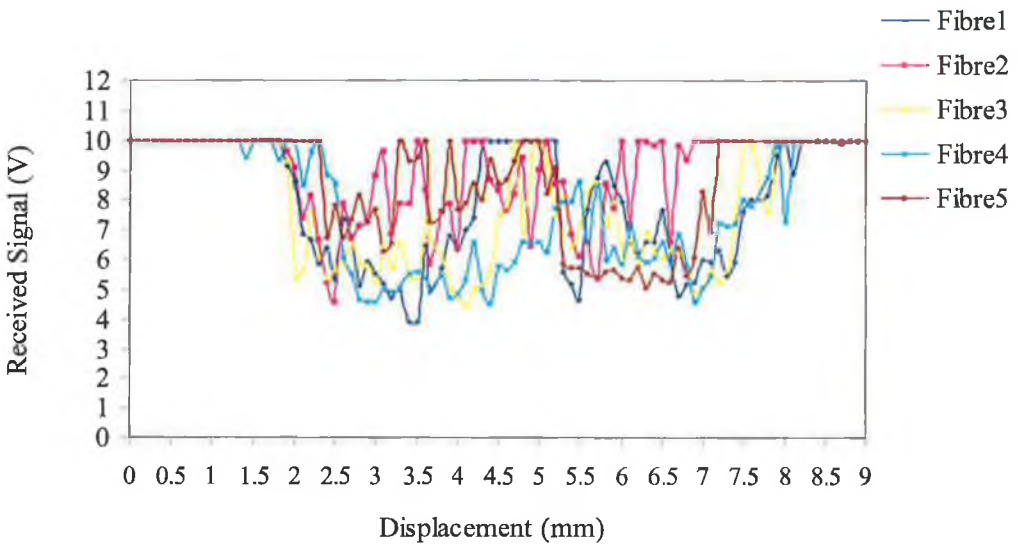

Figure 4.40 Set of scans for a blind hole of 7 mm in diameter in brass 7 mm (five fibres emitting).

Displacement characteristics of the copper plate are shown in Figures 4.44 to 4.47. As we can see from the graphs, the signal beams reflected from the copper surface are quite variable and it is clear that no light is detected through the holes because the thickness of the copper plate is more than 2 mm.

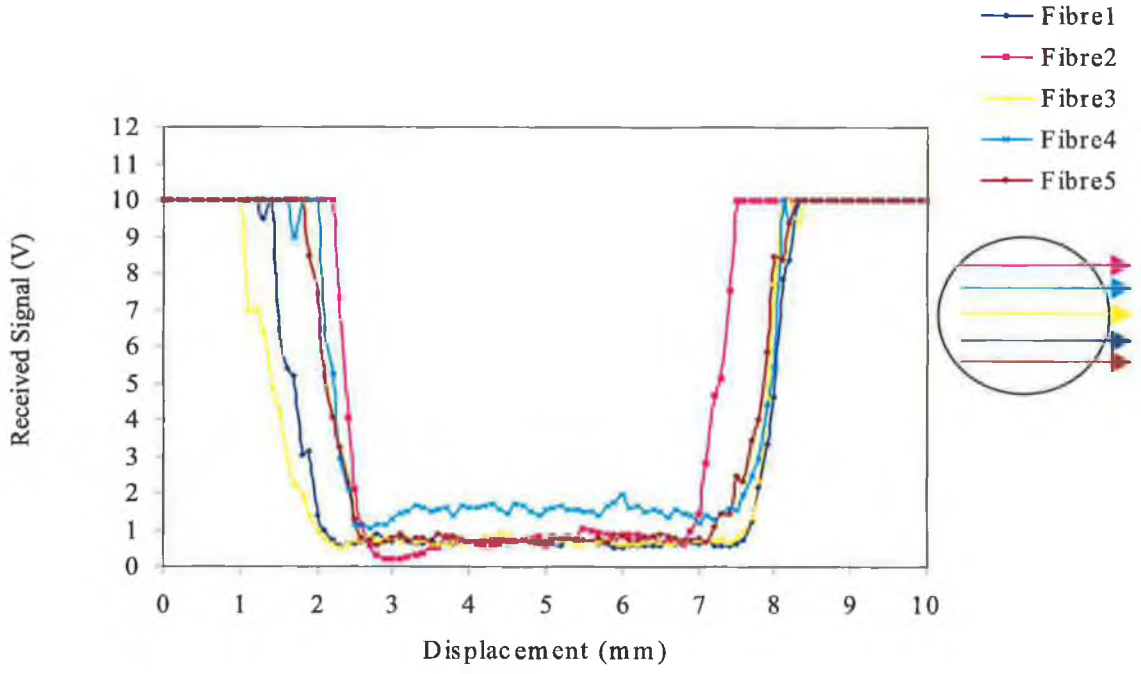

Figure 4.41 Set of scans through a 6 mm hole in stainless steel plate (five fibres emitting).

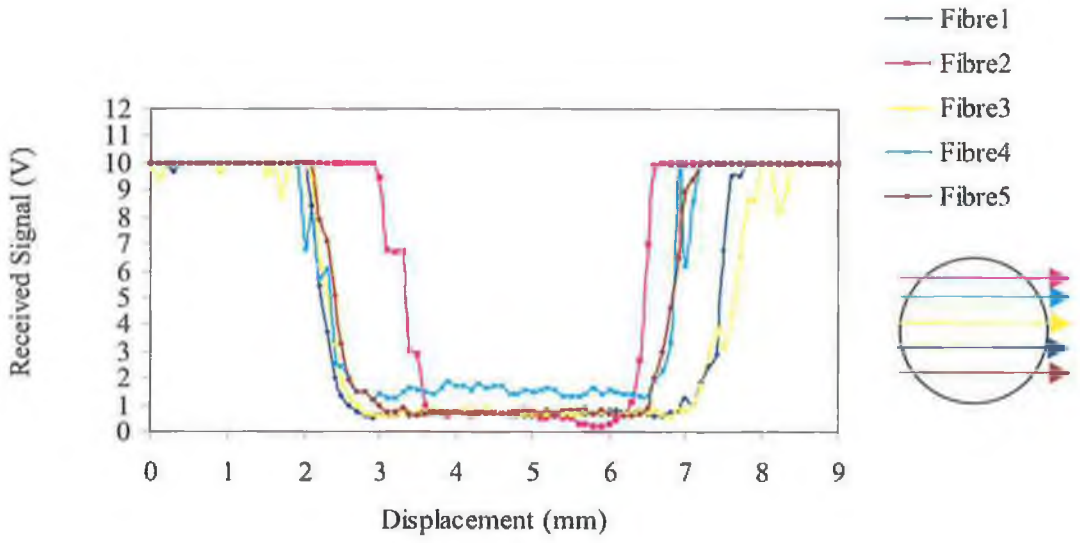

Figure 4.42 Set of scans through a 5 mm hole in stainless steel plate (five fibres emitting).

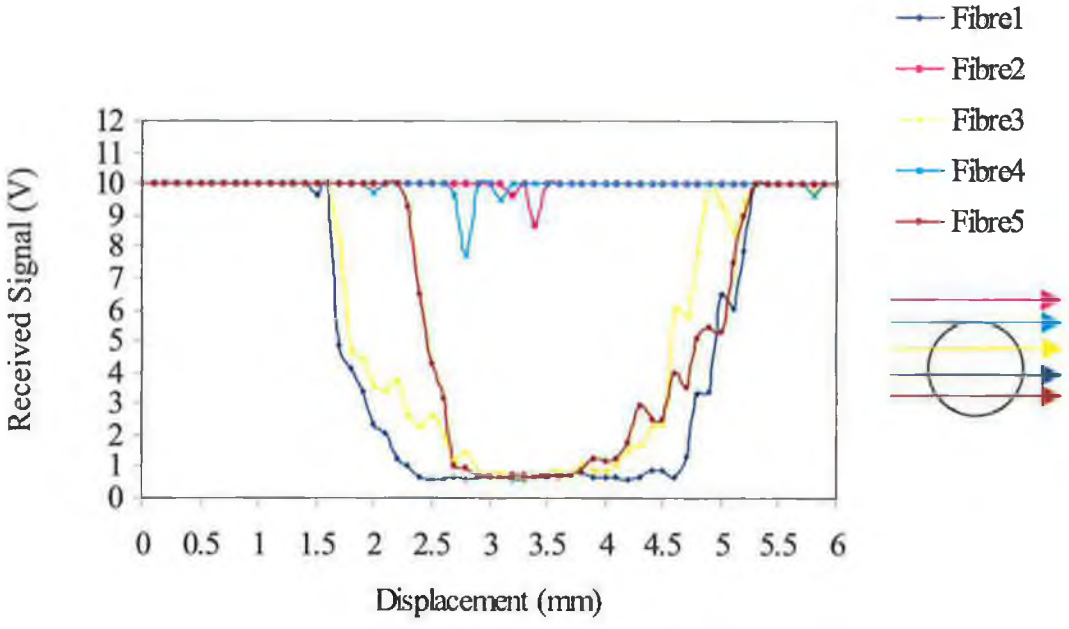

Figure 4.43 Set of scans through a 3 mm hole in stainless steel plate (five fibres emitting).

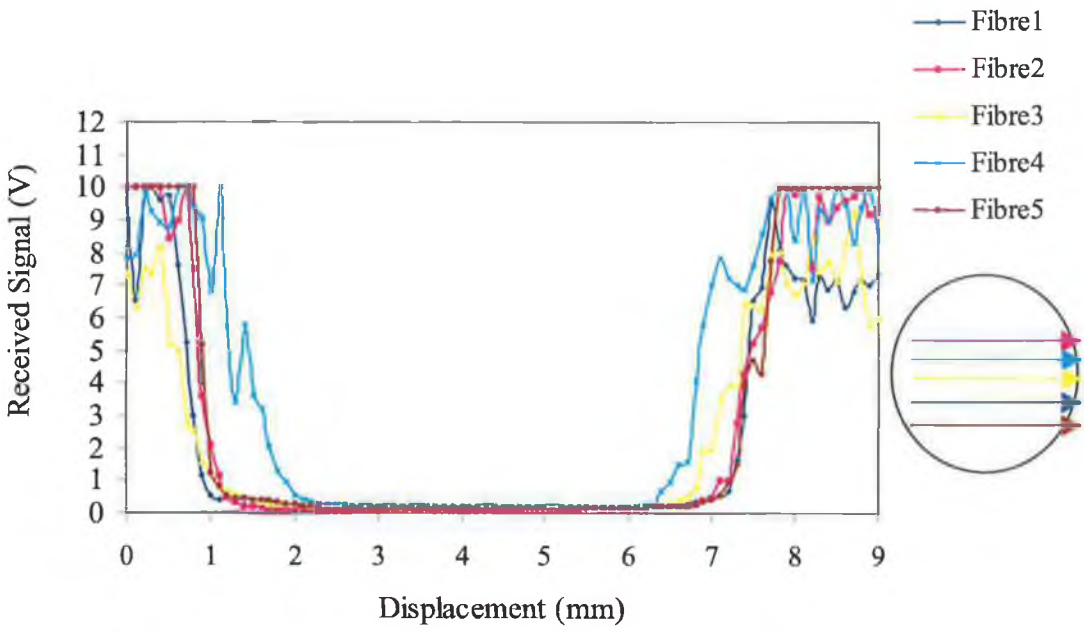

Figure 4.44 Set of scans through a 6 mm hole in copper plate (five fibres emitting).

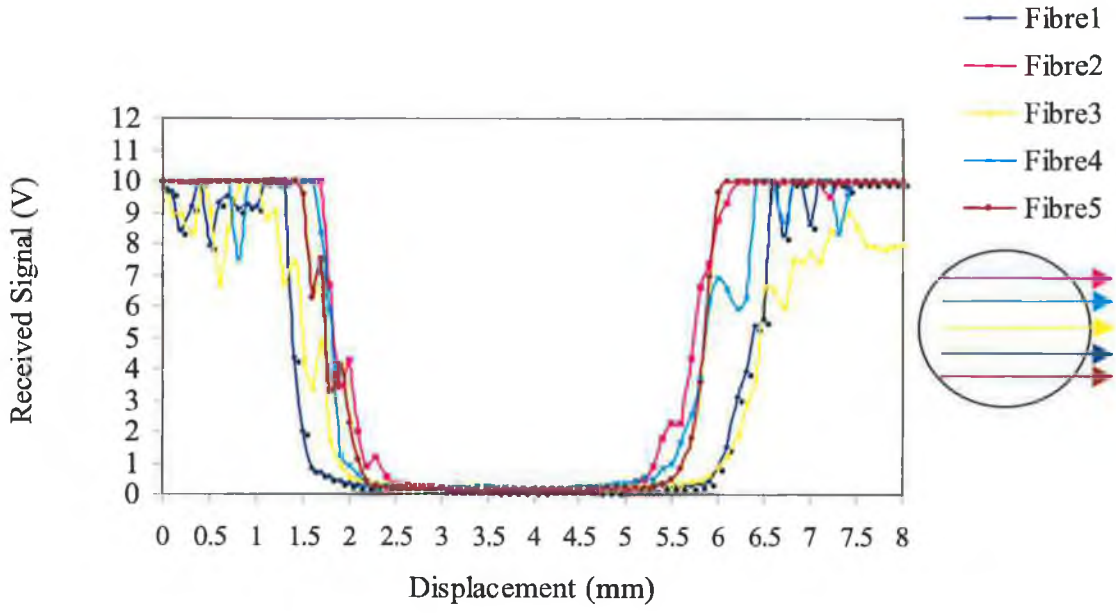

Figure 4.45 Set of scans through a 5 mm hole in copper plate (five fibres emitting).

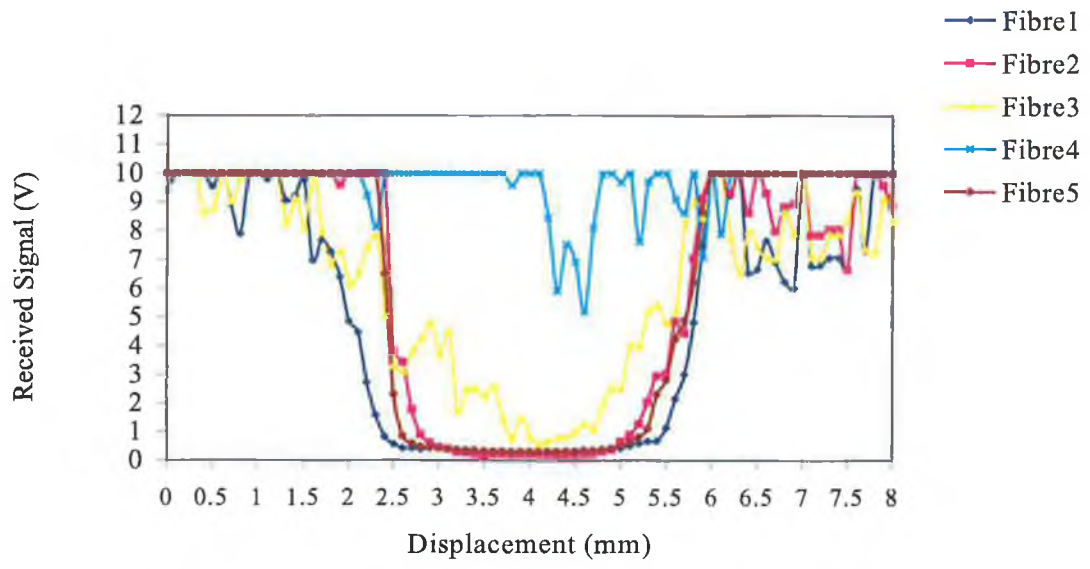

Figure 4.46 Set of scans through a 4 mm hole in copper plate (five fibres emitting).

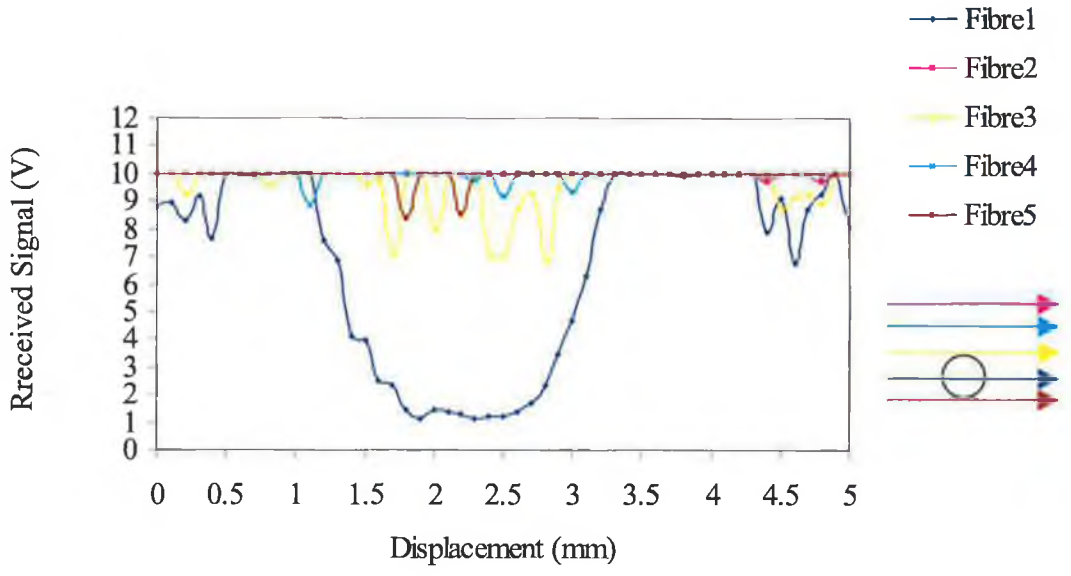

Figure 4.47 Set of scans through a 1 mm hole in copper plate (five fibres emitting).

Figures 4.48 to 4.49, a scan of the different sizes of polycarbonate plate through holes, shows the disadvantages of using this sensor with polycarbonate surface which is

reflects light diffusely. The contrast is much less than that from a copper surface. The variability of the reflected signal from the surface is large and also greater than that from the copper surface. A scan of different sizes of the blind hole was obtained from polycarbonate plate, the depth of the blind hole is 0.6 mm which means the sensor can detect light inside it, Figures 4.50 to 4.51.

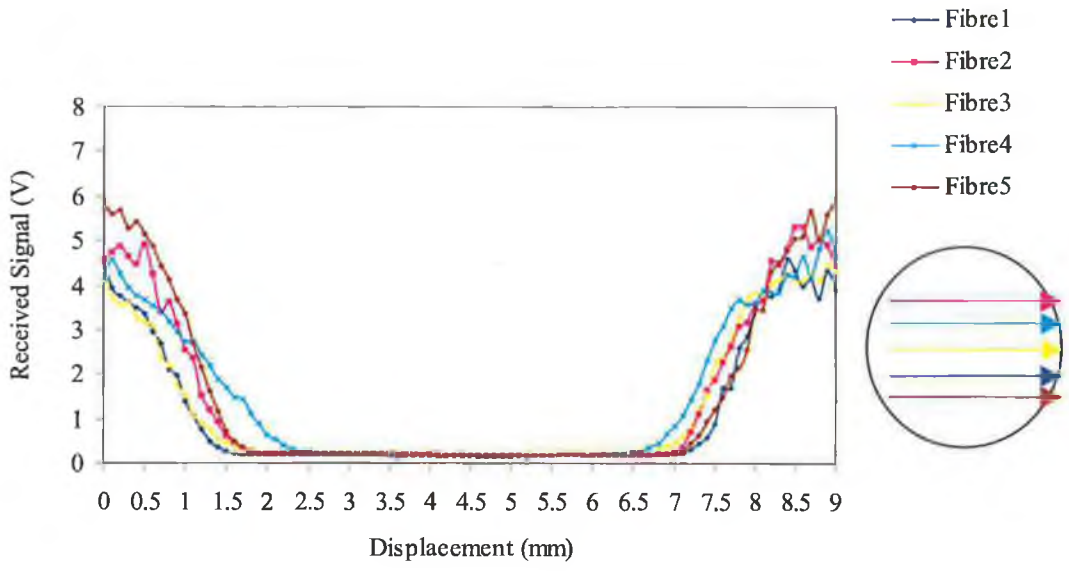

Figure 4.48 Set of scans through a 7 mm hole in polycarbonate plate (five fibres emitting).

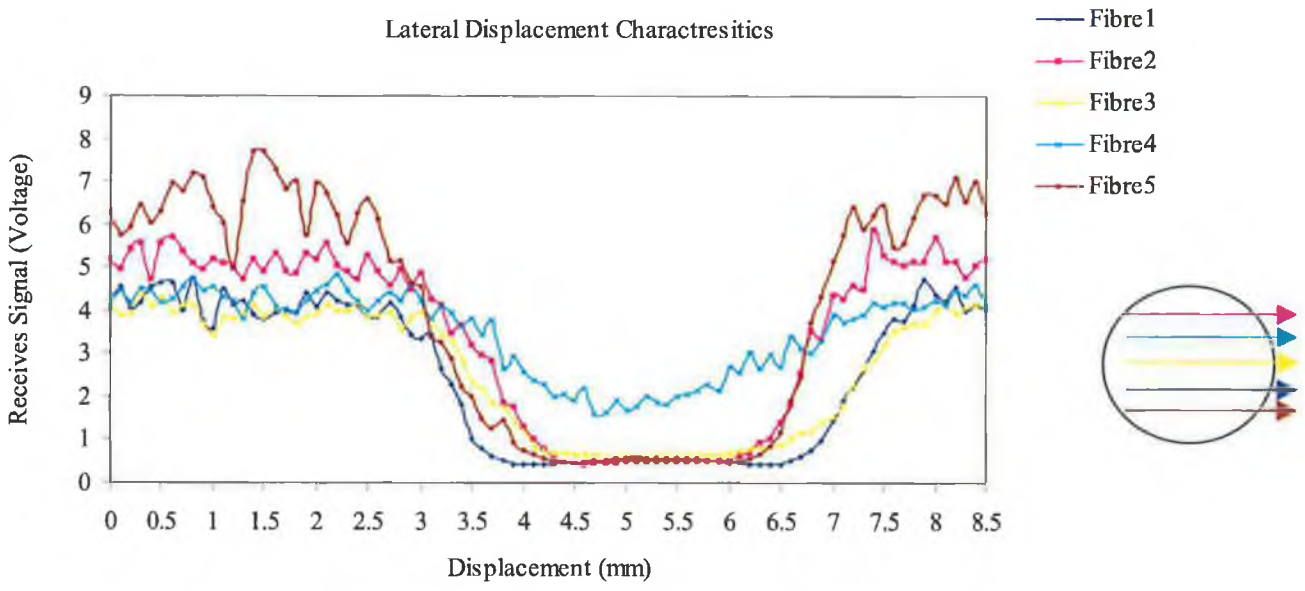

Figure 4.49 Set of scans through a 4 mm hole in polycarbonate plate (five fibres emitting).

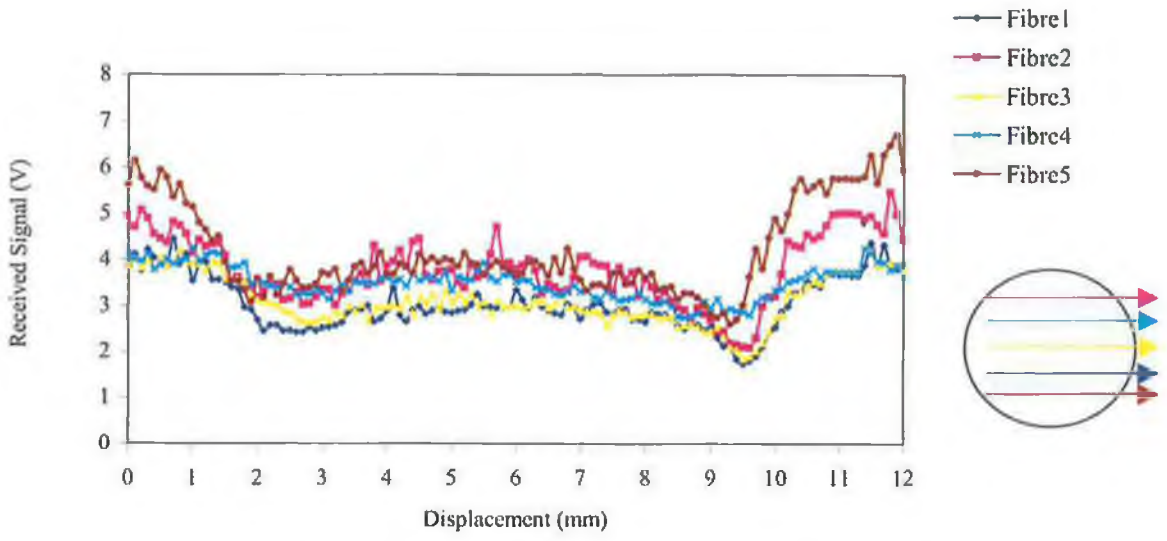

Figure 4.50 Set of scans for a blind hole of 7 mm in diameter in polycarbonate plates (five fibres emitting).

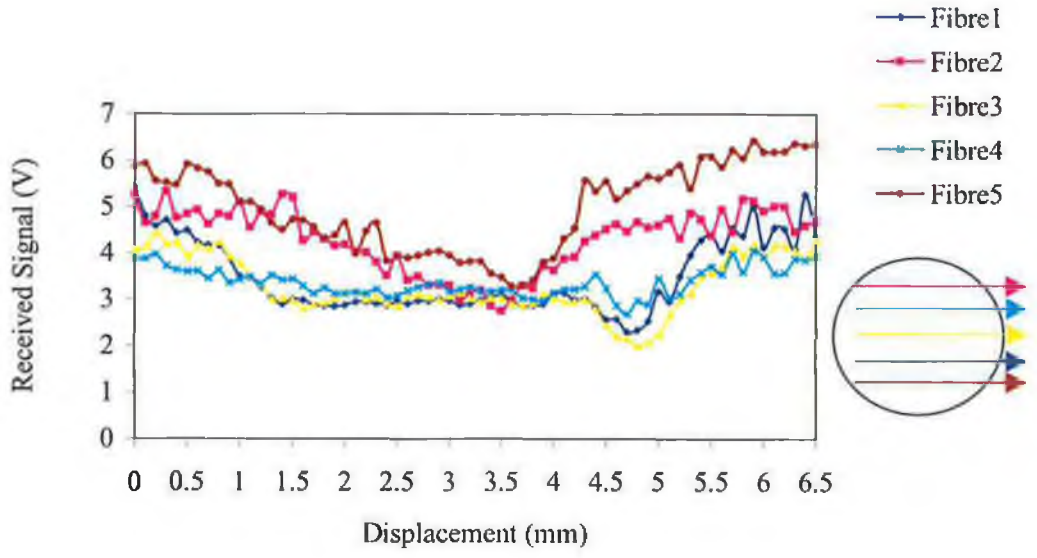

Figure 4.51 Set of scans for a blind hole of 4 mm in diameter in polycarbonate plate (five fibre emitting).

4.3.4 Two-dimension surface map of each sample plate

Each of the surface maps (shown in Figures 4.52 to 4.60) were generated by one set of scans. These were plotted by applying cut-off voltage of 2 V. The cut-off voltage of 2 voltage is not very suitable for the sample plates because, as mentioned previously, the system can detect the light through the hole particularly in the stainless steel plate and brass plate. Detection of blind holes was more problematic as it relied on detecting a surface within certain displacement limits. The intensity of the reflected light from a blind hole was quite high, enabling the cut-off voltage to be applied more successfully to generate the surface maps. The blind holes could be recognised from these transverse displacement curves. A high intensity of reflected light was achieved with brass, stainless steel and copper plate. It is clear that the polycarbonate plate has a diffusely reflecting surface. Measuring blind holes with this sensor does not necessarily achieve good results and from all parameters investigated was most critically affected by the surface properties of the sample plate and fibre stand off distance.

An appropriate cut-off voltage is however necessary to correctly determines the hole size. A cut of voltage of 2V gives accurate results for different sizes holes in different material such as copper, stainless steel, brass and polycarbonate plates.

The length of the fibres scan array was 4.15 mm. Therefore with only one scan pass in Figure 4.57 (b) and 4.58 (b) the scan line only obtained information about the center region of the data.

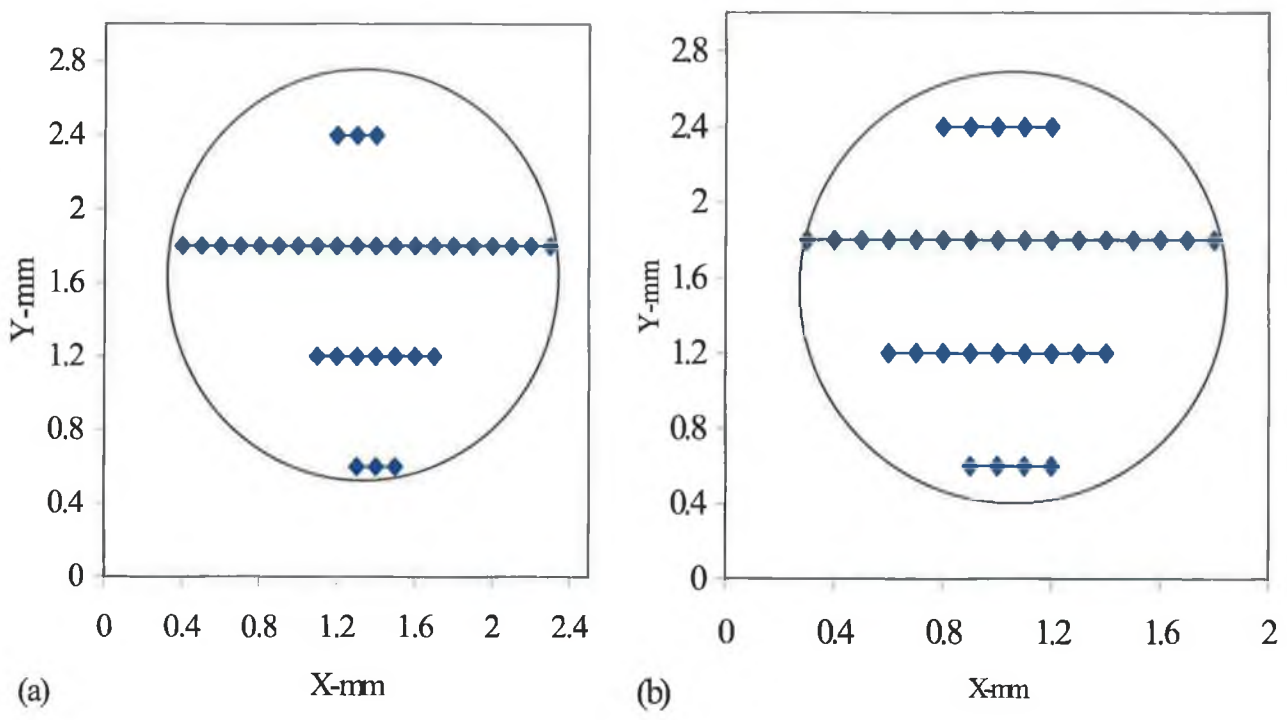

Figure 4.52 Surface maps of through a 2 mm hole in (a) brass, (b) stainless steel.

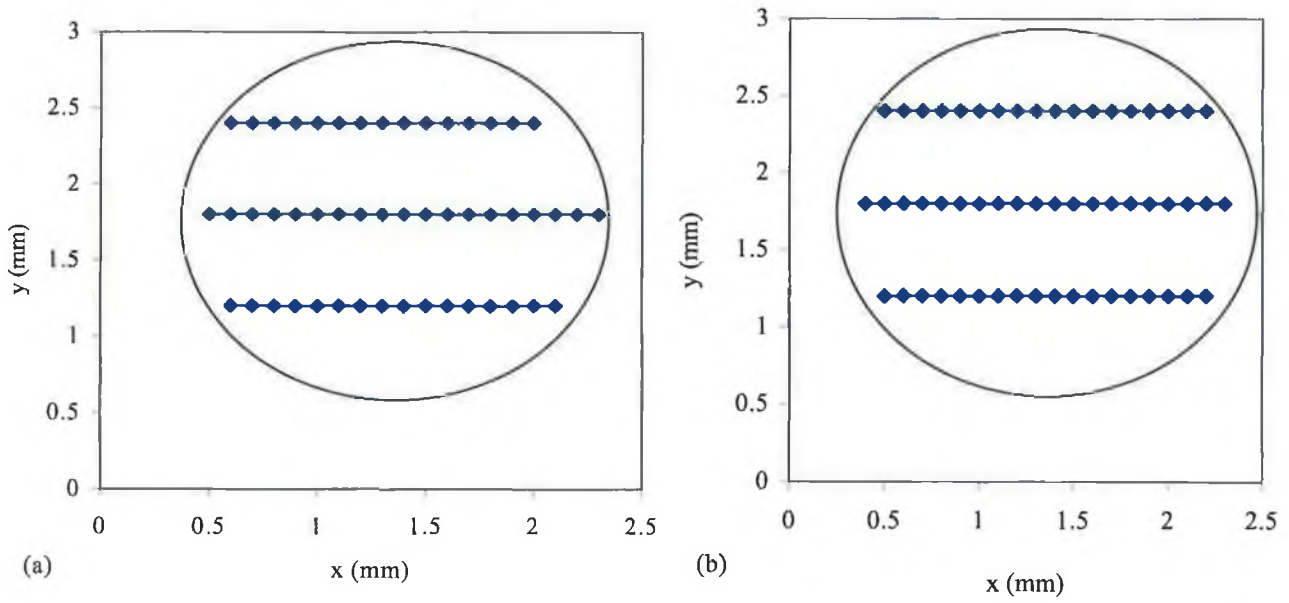

Figure 4.53 Surface maps of through 2 mm hole in diameter (a) copper,
(b) polycarbonate.

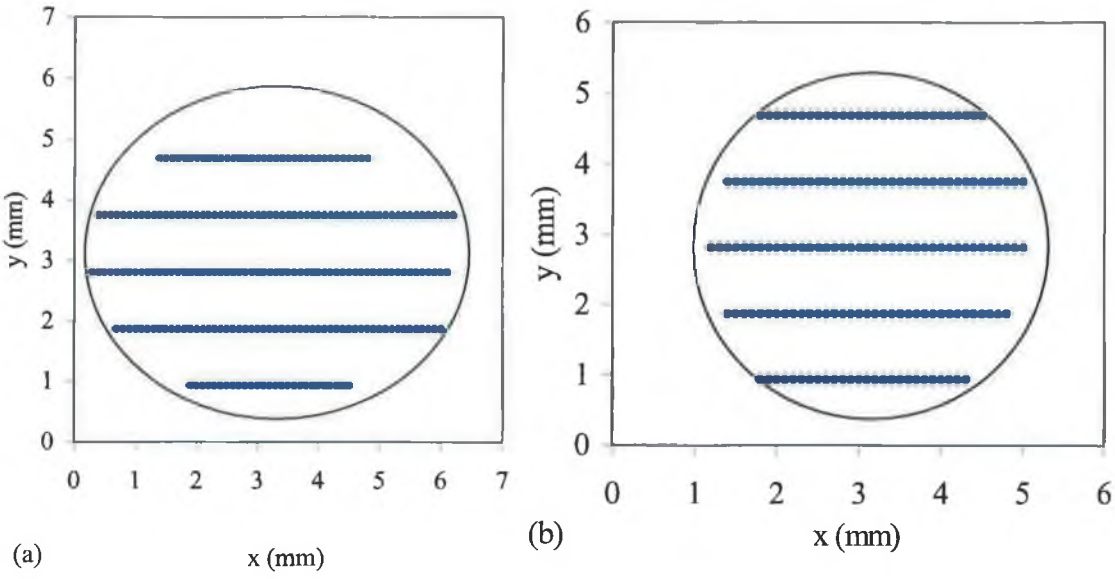

Figure 4.54 Surface maps of through hole in brass in diameter (a) 7 mm (b) 5mm.

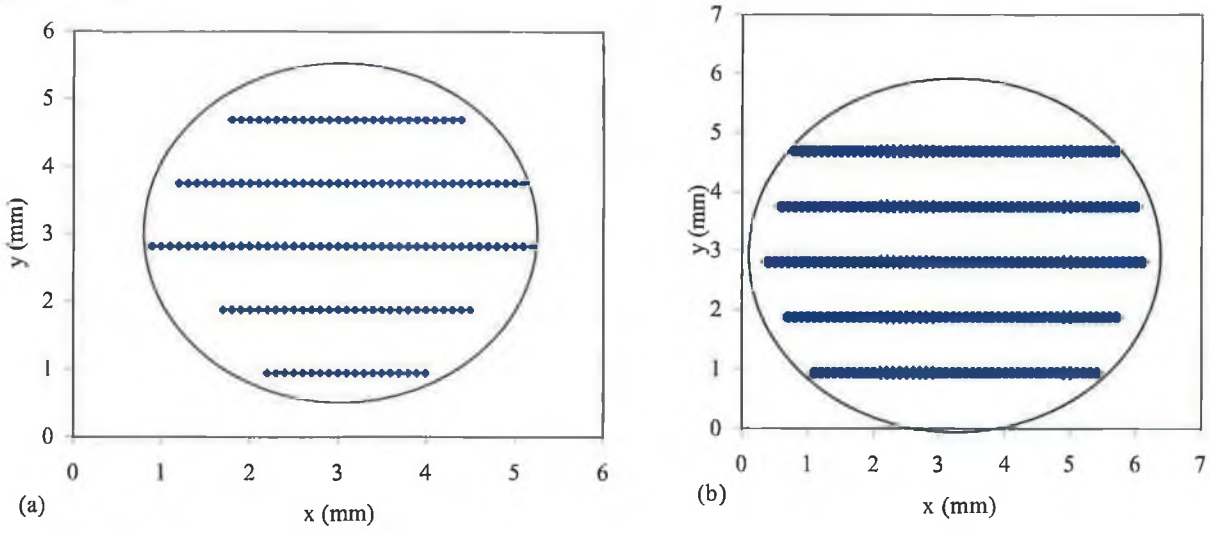

Figures 4.55 Surface maps through hole in (a) 4 mm in diameter in brass,
(b) 6 mm in diameter in stainless steel.

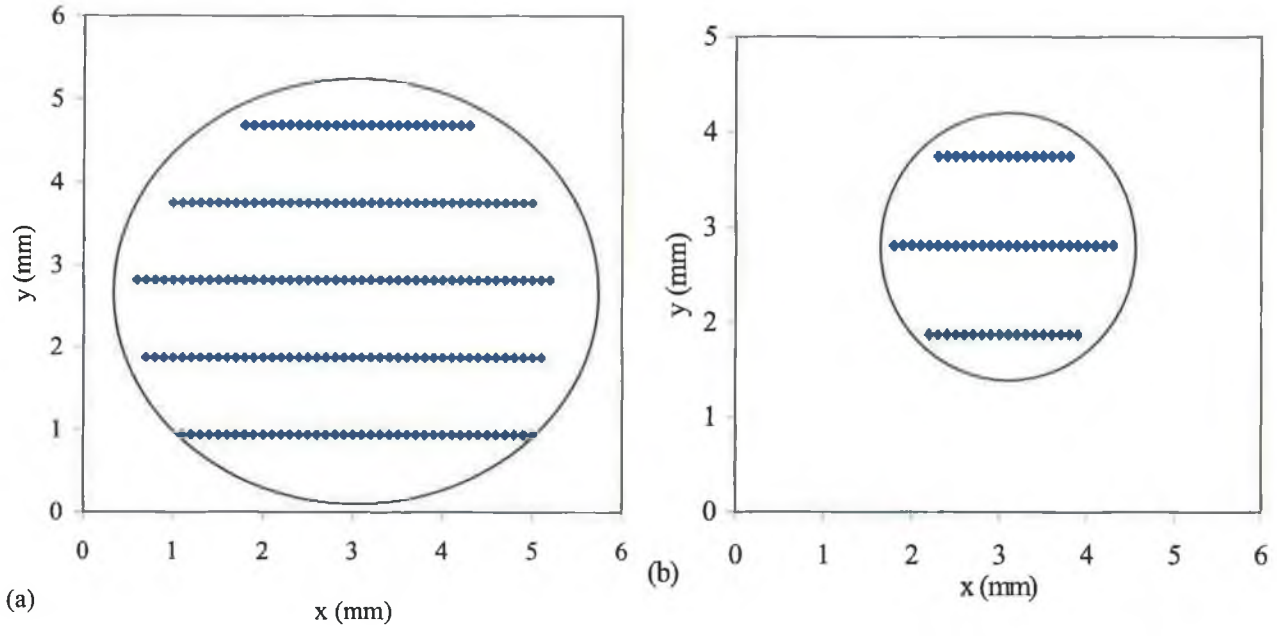

Figure 4.56 Surface maps of through hole in stainless steel in diameter (a) 5mm (b) 3mm.

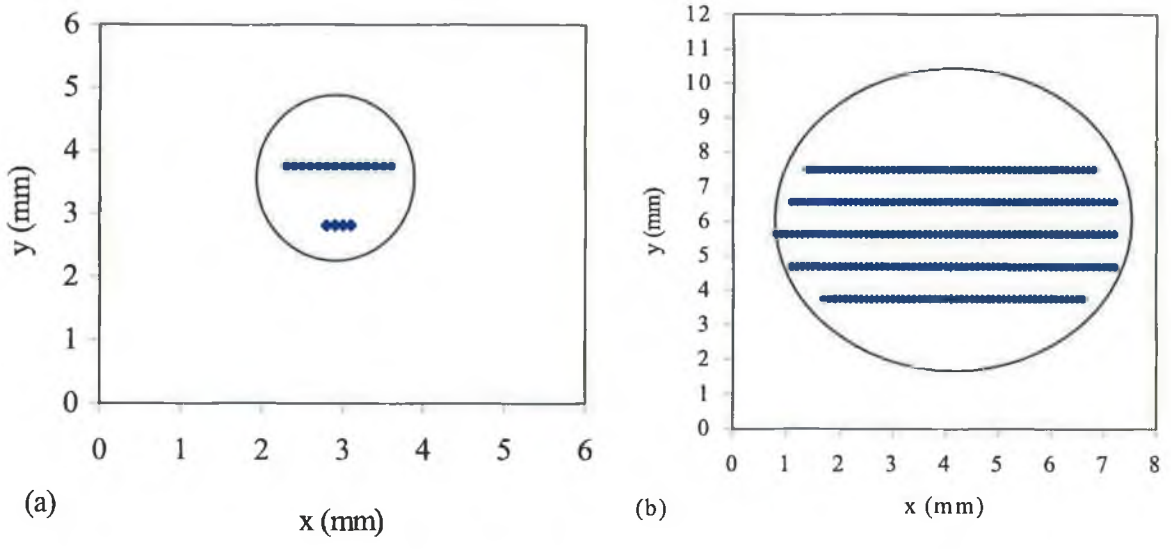

Figures 4.57 Surface maps of through hole in (a) 2 mm in diameter in stainless steel, (b) 7 mm in diameter in copper.

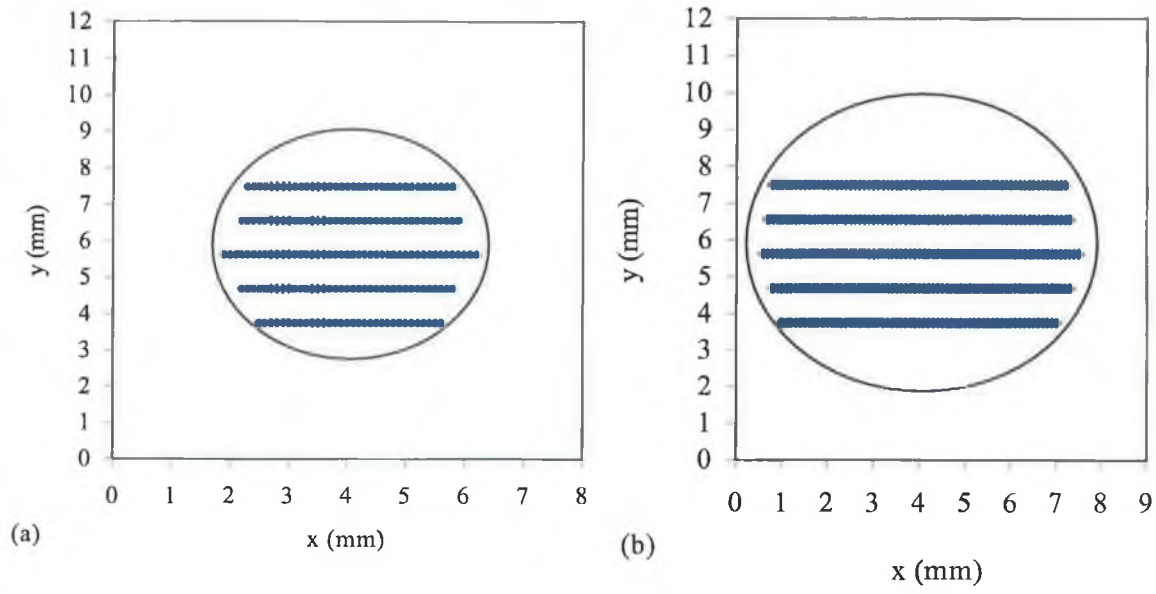

Figure 4.58 Surface maps of through hole in (a) 5 mm in diameter in copper, (b) 7 mm in diameter in polycarbonate.

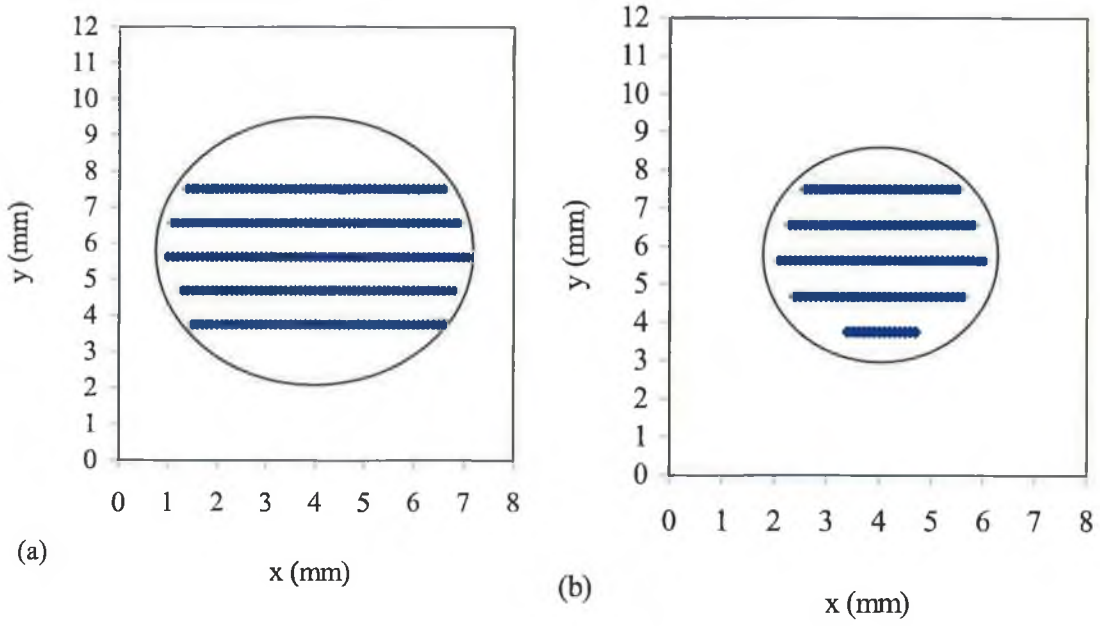

Figure 4.59 Surface maps of through hole in polycarbonate in diameter (a) 5mm (b) 4mm.

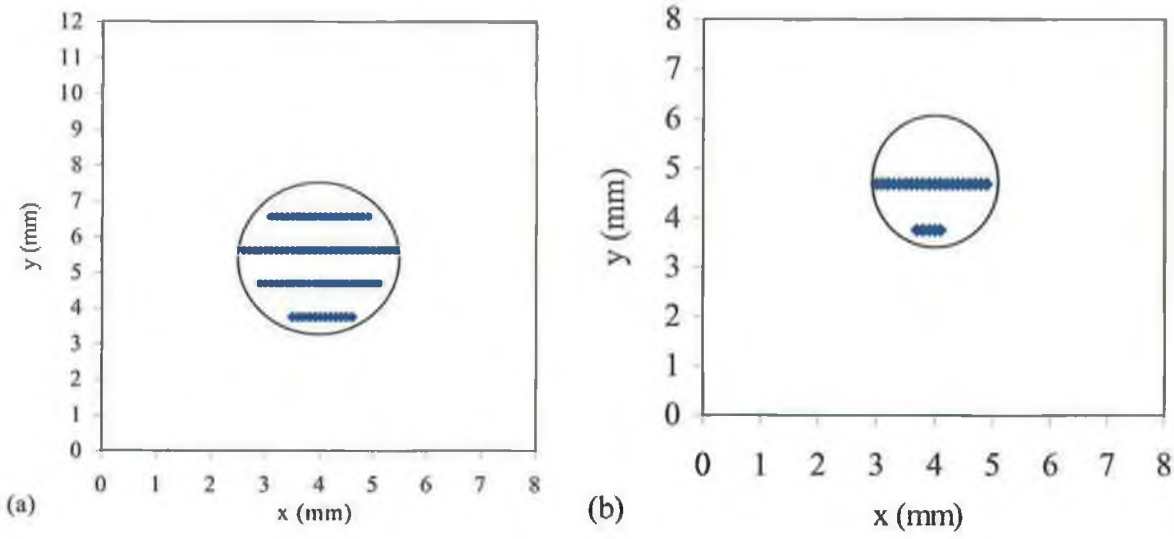

Figure 4.60 Surface maps of through hole in polycarbonate in diameter (a) 3mm (b) 2mm.

Chapter 5

Application results for developed fibre-optic laser scanning system

5.1 Introduction

An intensity based fibre-optic laser scanning system was developed. This chapter describes the following applications of which the system was applied.

1. Surface defect on aluminium, tufnol, and transparent polycarbonate sheets.
2. Reflectivity for plastic, transparent polycarbonate, aluminium and stainless steel sheets.
3. Thickness of aluminium sheet.
4. Surface roughness for aluminium and stainless steel materials

In addition the system was used to perform semi-automated surface profile measurement with adjustable resolution, and the scanning of the coloured surfaces.

5.2 System optimisation

When the surface of the reflecting material was not smooth and polished, the reflection of incident rays was diffuse. The degree of diffusion depended on the roughness of the surface. The intensity of the reflected signals is always less than the intensity of the incident signals. The intensity of a reflection of laser light is related to different refractive indices. For normal incidence, the reflection coefficient, R, is given by [100]:

$$R = \frac{n_1 - n_2}{n_1 + n_2}, \tag{5.1}$$

where n_1 is the refractive index of the material to be processed, and n_2 is the refractive index of the incident medium. For the case of good electrical conductors such as aluminium and steel it my be approximated as follows:

$$n \sim \sqrt{\frac{\sigma}{2\pi\mu f}} \tag{5.2}$$

where σ is the electrical conductivity, μ is the magnetic permeability, and f is the frequency of laser light. The intensity of the reflected lights I_0, is given by:

$$I_0 = (1 - R^2) I_i \tag{5.3}$$

where I_i is the incident radiance.

5.3 Material reflectivity

Different materials were tested for reflectivity such as aluminium, stainless steel, transparent polycarbonate and plastic plates. Figure 5.1 shows the average of the five reflected signals from different material surfaces. The scan was done for each sample plates. These results were taking with respect to the surface roughness, which was constant, at Ra = 0.1 μm, for all the materials tested. It was clear that all the metals tested in are good reflectors. The highest reflectivity was produced from the stainless steel plate, and the lowest from plastic plate.

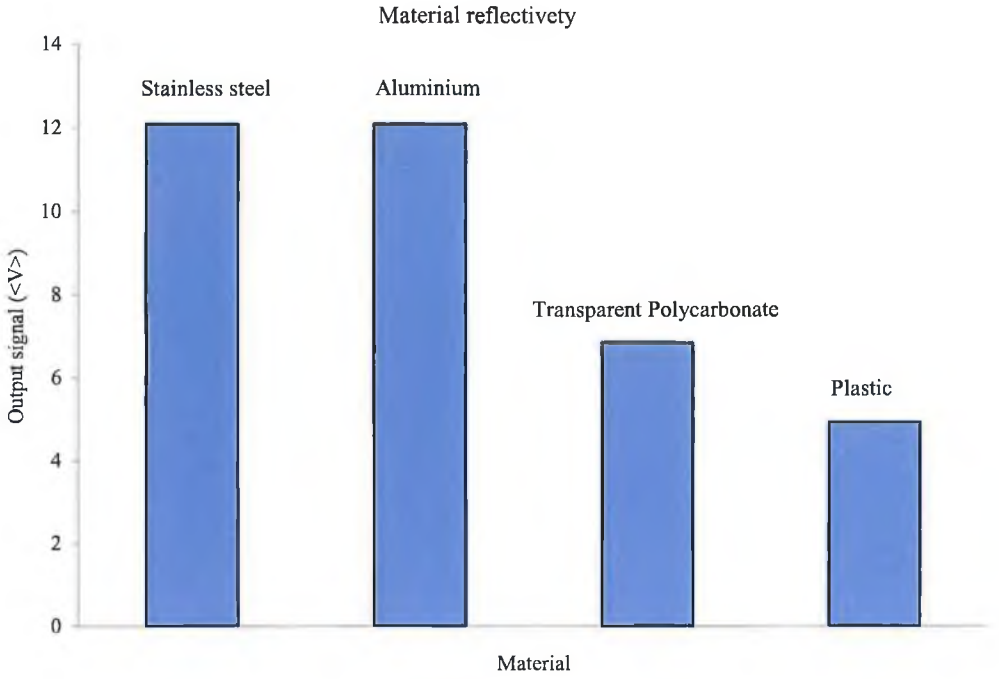

Figure 5.1 Reflectivity signals produced from materials of the same Ra value (0.1μm).

Figure 5.2 Show the actual reflected ray signals from a mirror surface. The five fibres were incident on the surface at an angle of 30^0 and collected the reflected light was captured by the five receiving fibres. A 3-D view of the results of Figure 5.2 is shown in Figure 5.3 (a) and (b) Schematic of the system's vertical displacement. High reflectivity was obtained from the mirror surface. Small differences in the reflected signals were caused by small mis-alignment of the fibres. The vertical position of the fibres was varied from 0 to 16 mm displacement to obtain these intensity signals. From the results the system could be used in the range of about 1.5 to 8 mm off the sample. However highest signal intensities were achieved from about 2 to 8 mm off the surface. When raised above 16 mm off the surface no more light signal could be detected.

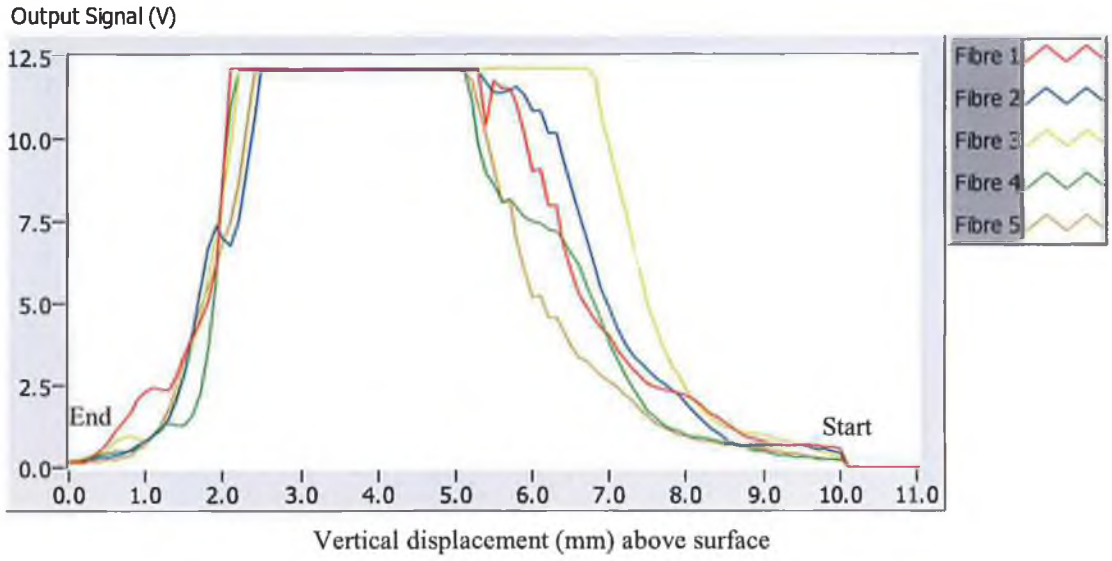

Figure 5.2 Vertical displacement diagram of the reflected array signals from a mirror surface.

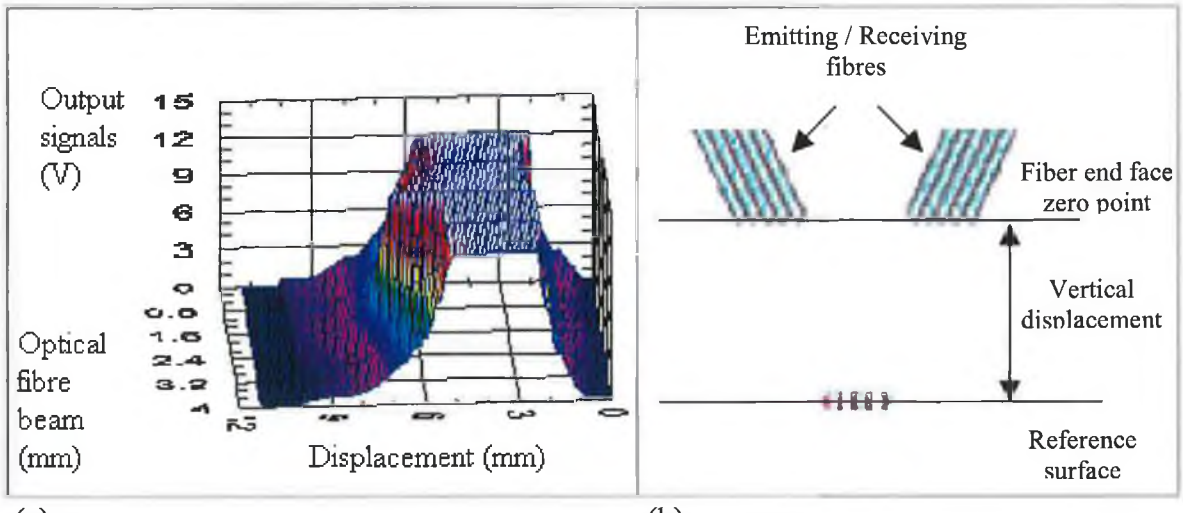

(a) (b)

Figure 5.3 (a) Profile of the reflected signals for the five vertically displacement fibres from the mirror surface (b) Schematic of the system's vertical displacement.

In the last chapter several materials were tested for the vertical displacement. All of these results indicated that all metals are very good reflectors within the infrared

wavelength. In this section the results of various material (Engineering material data sheet, Appendix B_9) are presented such as aluminium plate, transparent polycarbonate plate, brass and tufnol plate, (Appendix C_4 photograph of sample plates).

The system was optimised for each material to produce the highest intensity in reflected signals. Figure 5.4 Shows the actual reflected signals from the sample surface of aluminium. Figure 5.5 shows the profile of the reflected signals from the aluminium sample. Small differences in the reflected signals were caused by small mis-alignment of the fibres and the different points on the scanned surface.

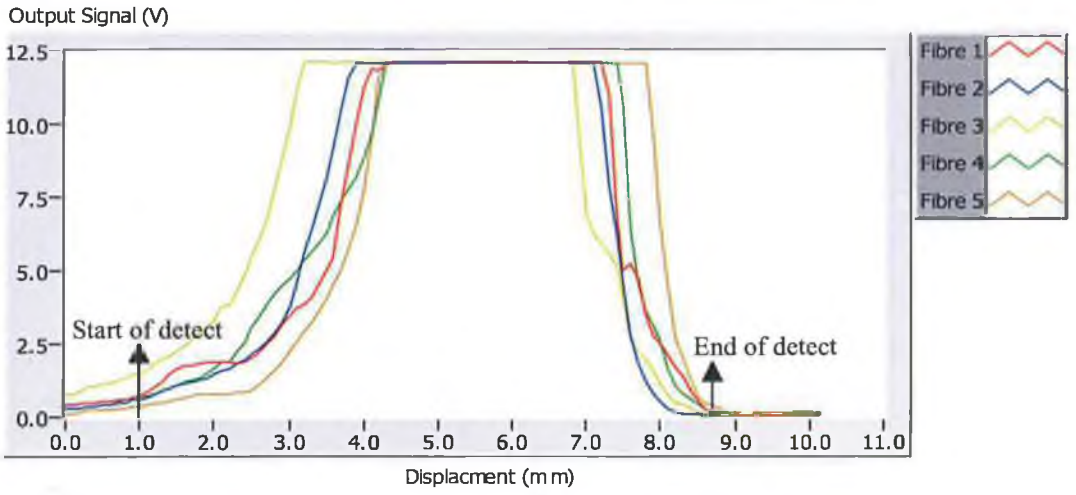

Figure 5.4 Vertical displacement diagram of the reflected signals from the aluminium surface.

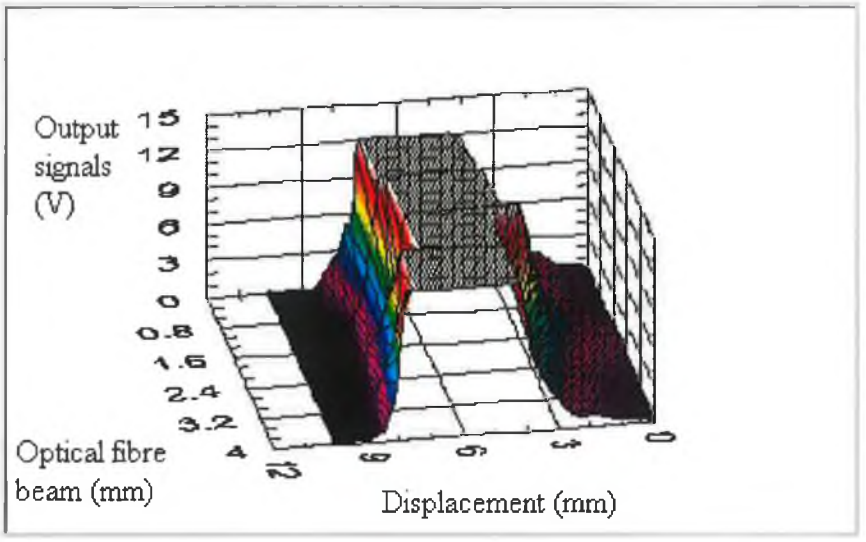

Figure 5.5 Profile of the reflected signals from the aluminium surface.

The transparent polycarbonate surface was quite different from the metal surface. This was a transparent surface which allowed light to pass through it diffusely. These laser spots where reflected off the top and bottom surfaces, so that two sets of signal peaks were detected. Figure 5.6 shows the actual reflected signals from the surface with the two peaks show. This system can therefore be used to measure the thickness of transparent materials. Figure 5.7 shows the profile of the reflected signals for five fibres.

(a)

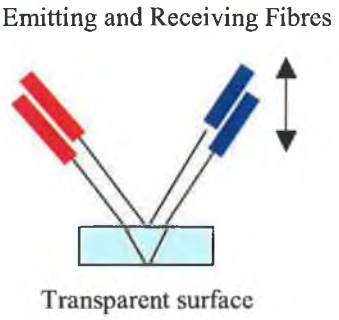

(b)

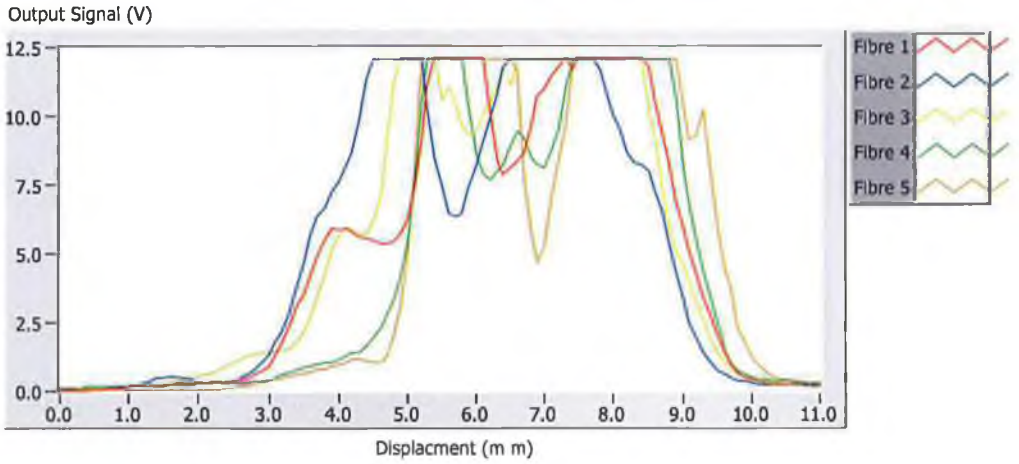

Figure 5.6 (a) Scanning set-up and (b) vertical displacement diagram of the reflected signals from the transparent polycarbonate surface using a laser diode light source.

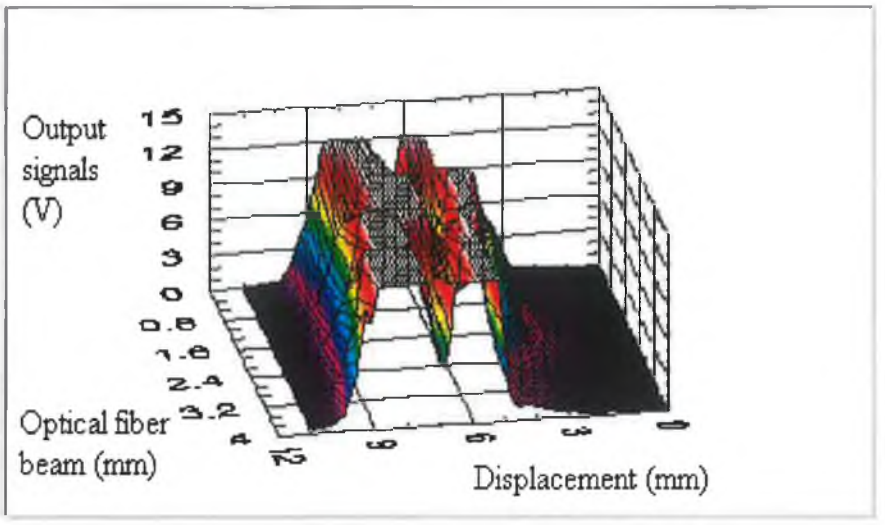

Figure 5.7 Profile of the reflected signals from the transparent polycarbonate surface.

The results for the same test procedure but for the diffuse tufnol material (An epoxy glass laminate with extremely high mechanical and electrical strength) are presented in Figure 5.8. Figure 5.9 shows the five signal profiles. The results show that the incident signals were significantly effected by how far the fibre ends were from the surface for this material surface. This was due to the diffuseness of the surface. Metal materials have a high reflectivity, which allow the system to more easily detect the reflected signals.

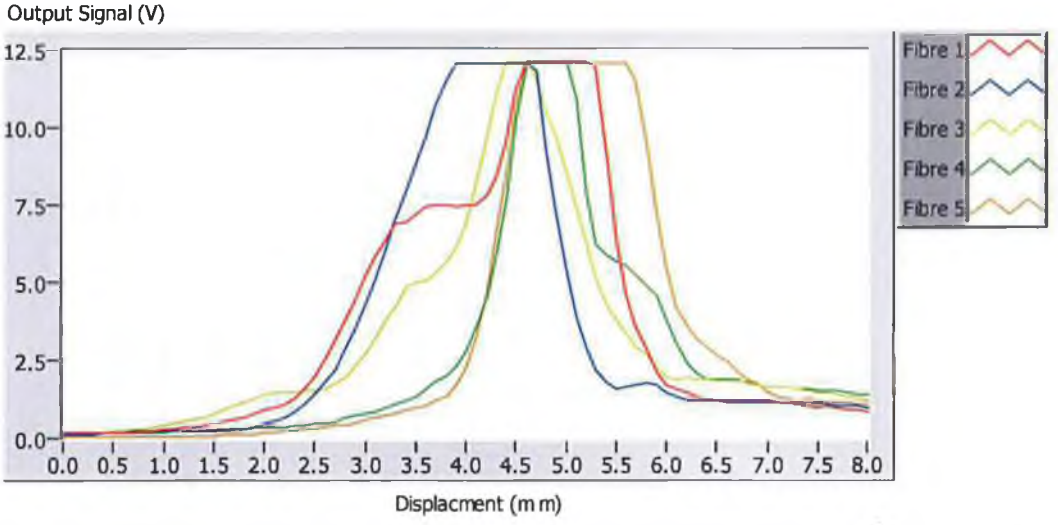

Figure 5.8 Vertical displacement diagram of the reflected signals from the Tufnol surface.

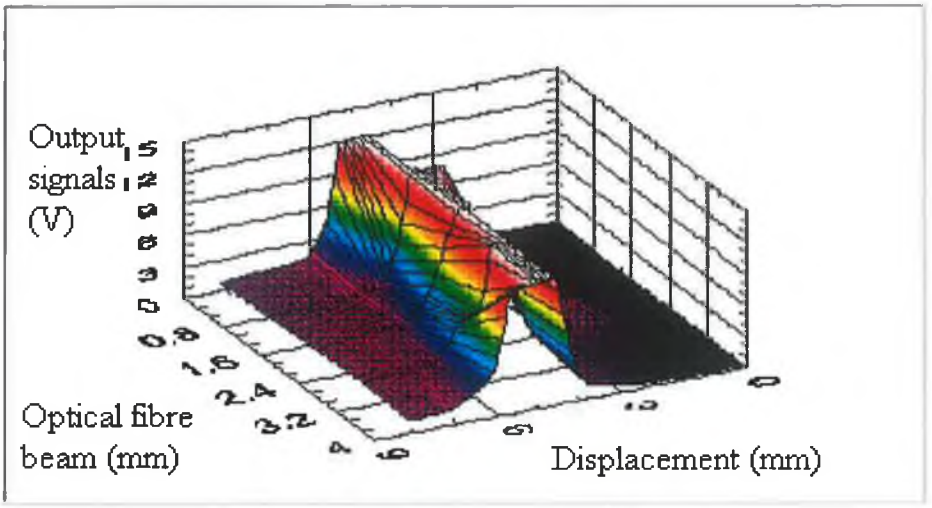

Figure 5.9 Profile of the reflected signals from the Tufnol surface.

5.4 Notched surface measurements

This part of results shows the measurements of surface notch on different materials. The optimum fibre end height was set as per the result of the previous section. Five beams passing over the surface scanned a notch on the aluminium plate. Figure 5.10 (a) shows the materials tested. Signal results are shown in Figure 5.10 (b). A profile of the reflected signals from a notched surface is show representing a shaped irregular defect, in Figure 5.11. The variation of the signals through the notch is due to the irregular shape of the notch (drilling machine).

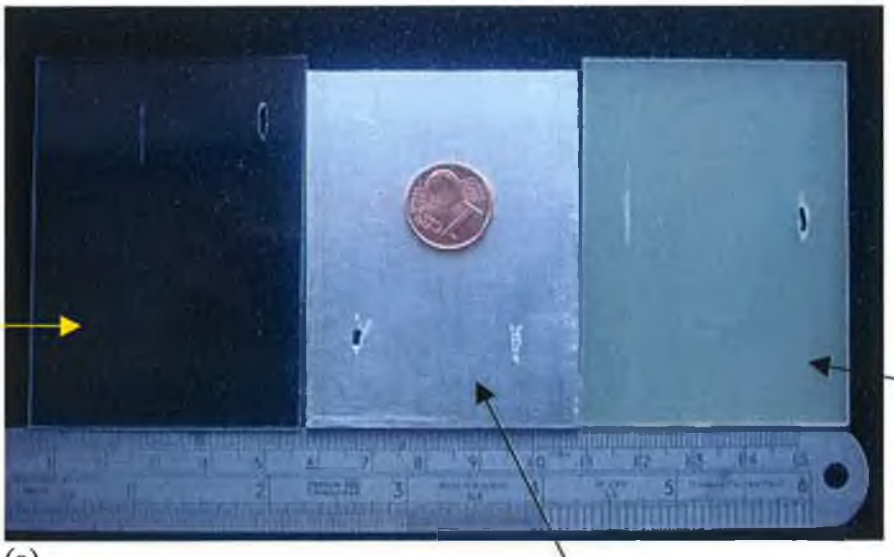

(a)

(b)

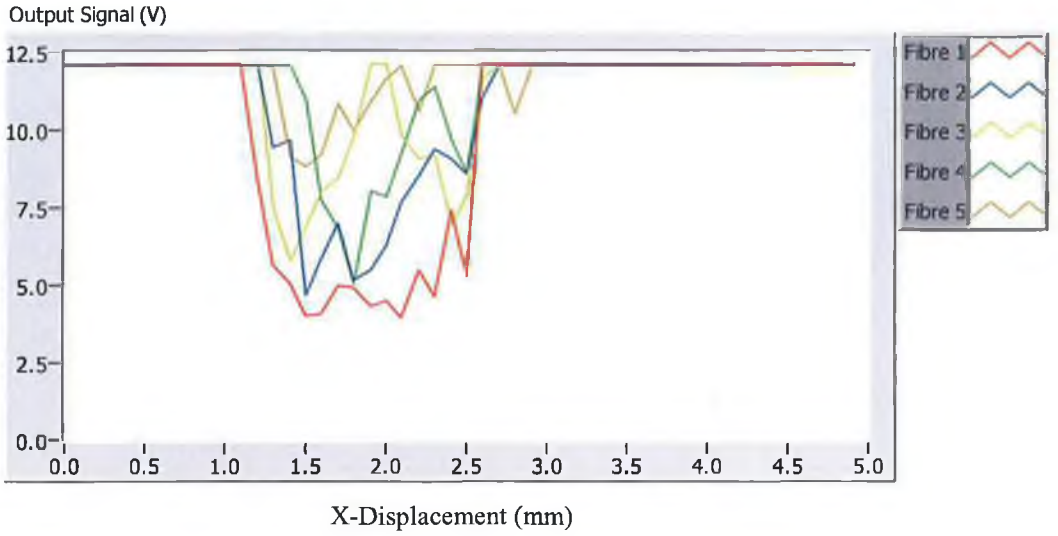

Figure 5.10 (a) Material samples: transparent polycarbonate, aluminium, and tufnol (b) Signals from the notched surface on the aluminium plate.

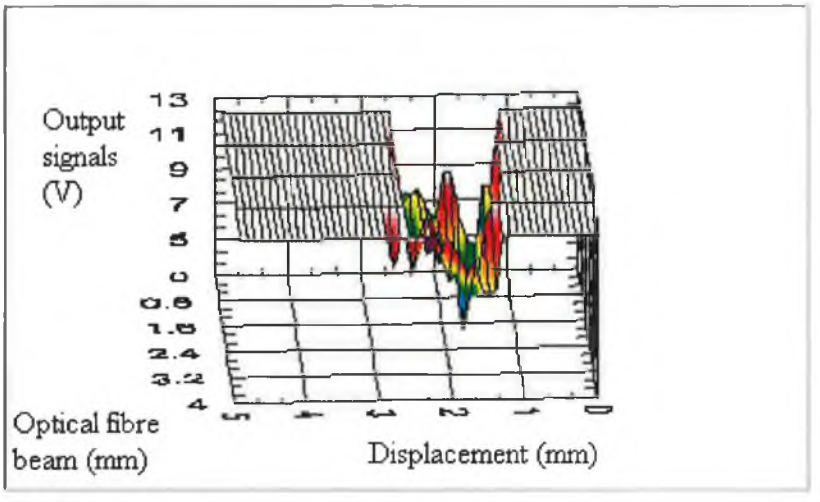

Figure 5.11 Profile of notch surface scan.

Figure 5.12 shows the scan of the transparent polycarbonate notched surface (see Figure 5.10 (a)). Two notches, side by side, were scanned for this measurement. The signals droped down and were reflected again from the island between the notches before

falling as the second notch was passed, see Figure 5.12. A profile of this scan was showed in the figure 5.13.

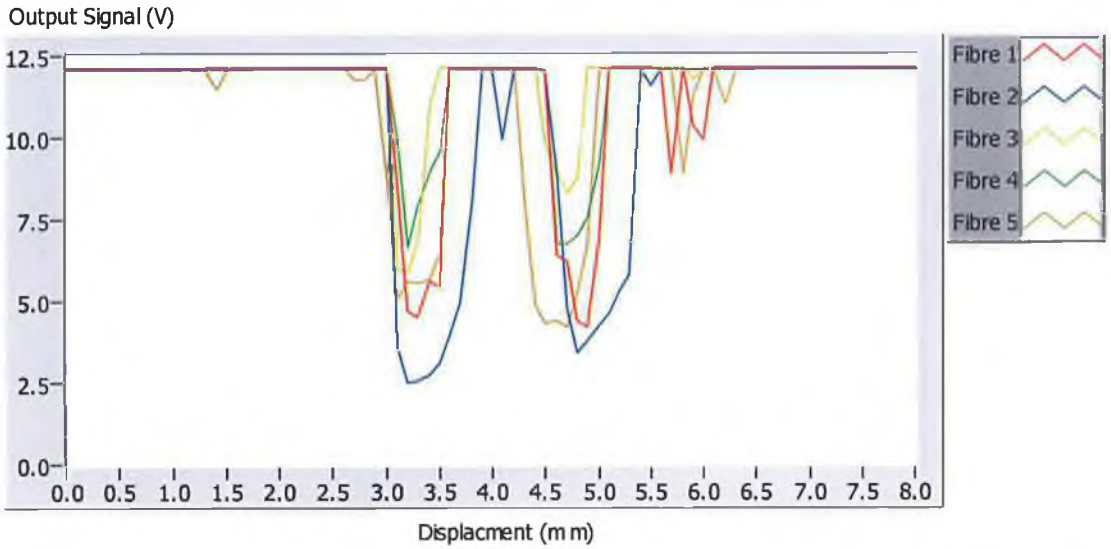

Figure 5.12 Signals from the notched surface on the transparent polycarbonate surface.

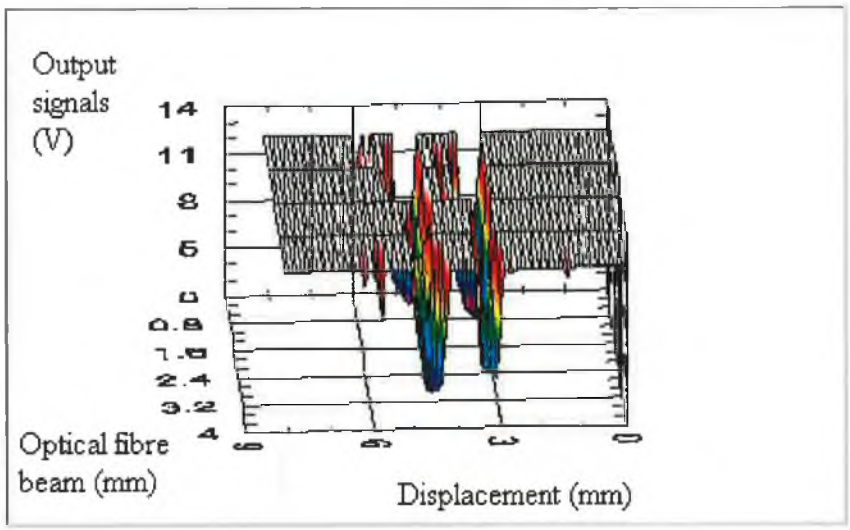

Figure 5.13 Profile of notch surface scan.

The diffuse tufnol surface also produced reasonable results for the surface notch measurement. Much more scatter was however detected with this material due to its diffuseness. Figure 5.14 represents tufnol the notched surface. The signals from the

surface fluctuated greatly. The signal droped down when the system passed the notch and then raised back again with the similar fluctuations. Figure 5.15 shows the profile of the Tufnol notch surface.

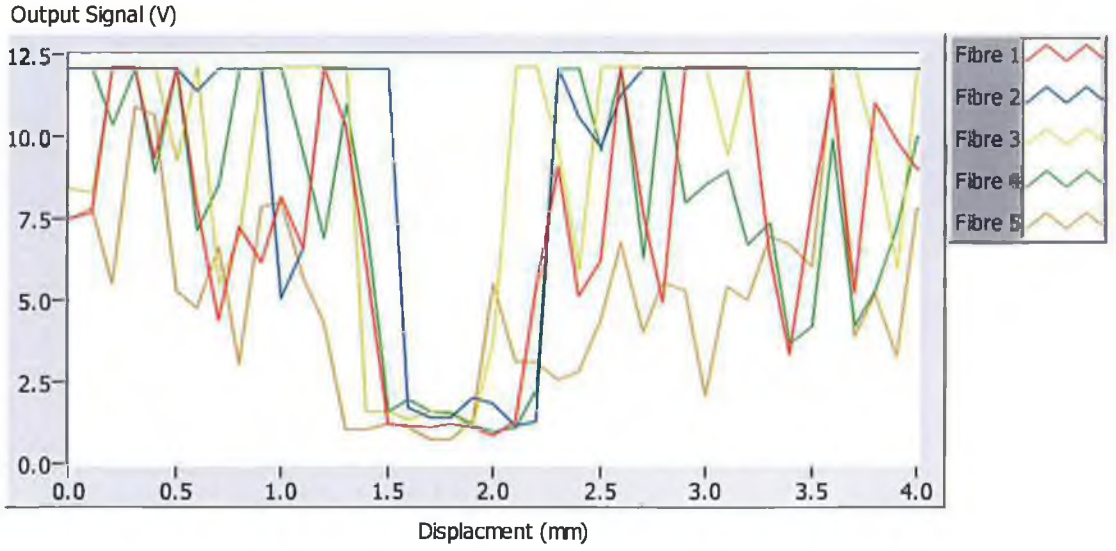

Figure 5.14 Signals from the notched surface on the tufnol.

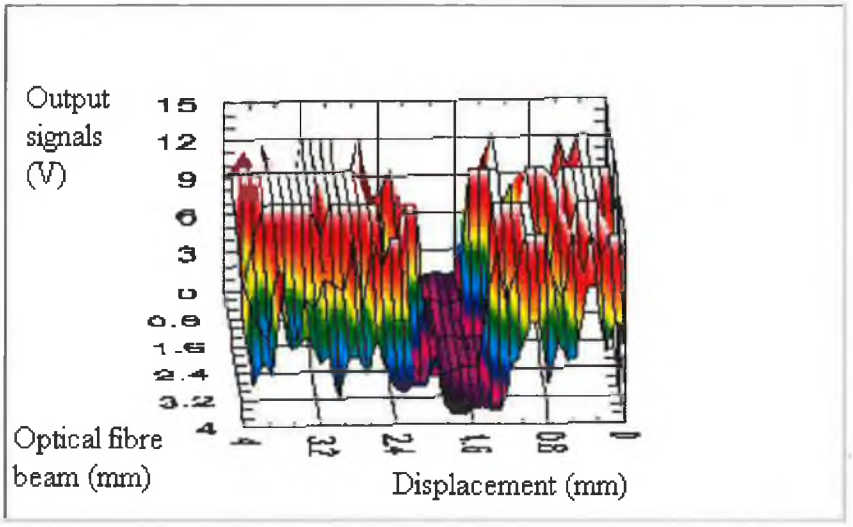

Figure 5.15 Profile of notch surface

5.5 Measurement of aluminium sheet thickness

The five reflected signals from the vertical displacement of the metal sheet surface were considered in order to obtain a calibration curves for sheet thickness measurements. Figure 5.16 was generated from the average vertical displacement results from the first half of Figure 5.5. With each of the five signals, the voltage variation is measured from the first point detected by the system and ending with the highest point detected by the system as shown in the Figure 5.16 below. This curve presents the average voltage against the distance moved by the aluminium sheet. This curve can be used to assess the thickness of sheets placed beneath the stationary sensor head. The sensor head needs to be positioned at the farthest distance from the base plate where signals can still just be detected. This approximately 8.9 mm from the aluminium plate (see Figure 5.5).

In order to determine the scatter associated with using Figure 5.16 for thickness measurements an aluminium sheet was placed at an angle on the base plate and moved laterally. The averages of the five reflected signals from the aluminium sheet are shown in Figure 5.17.

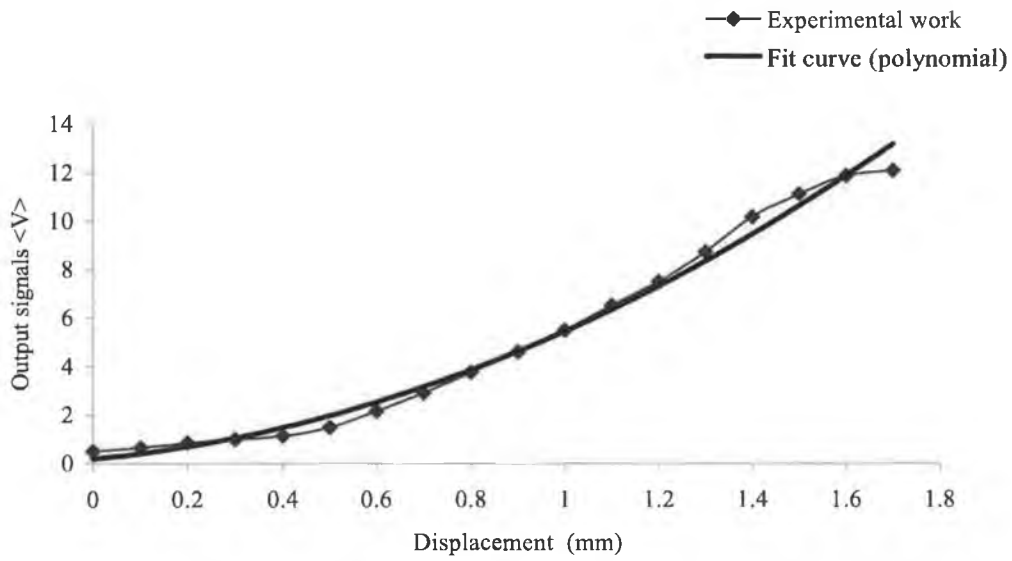

Figure 5.16 Average voltage against the displacement for aluminum sheet surface.

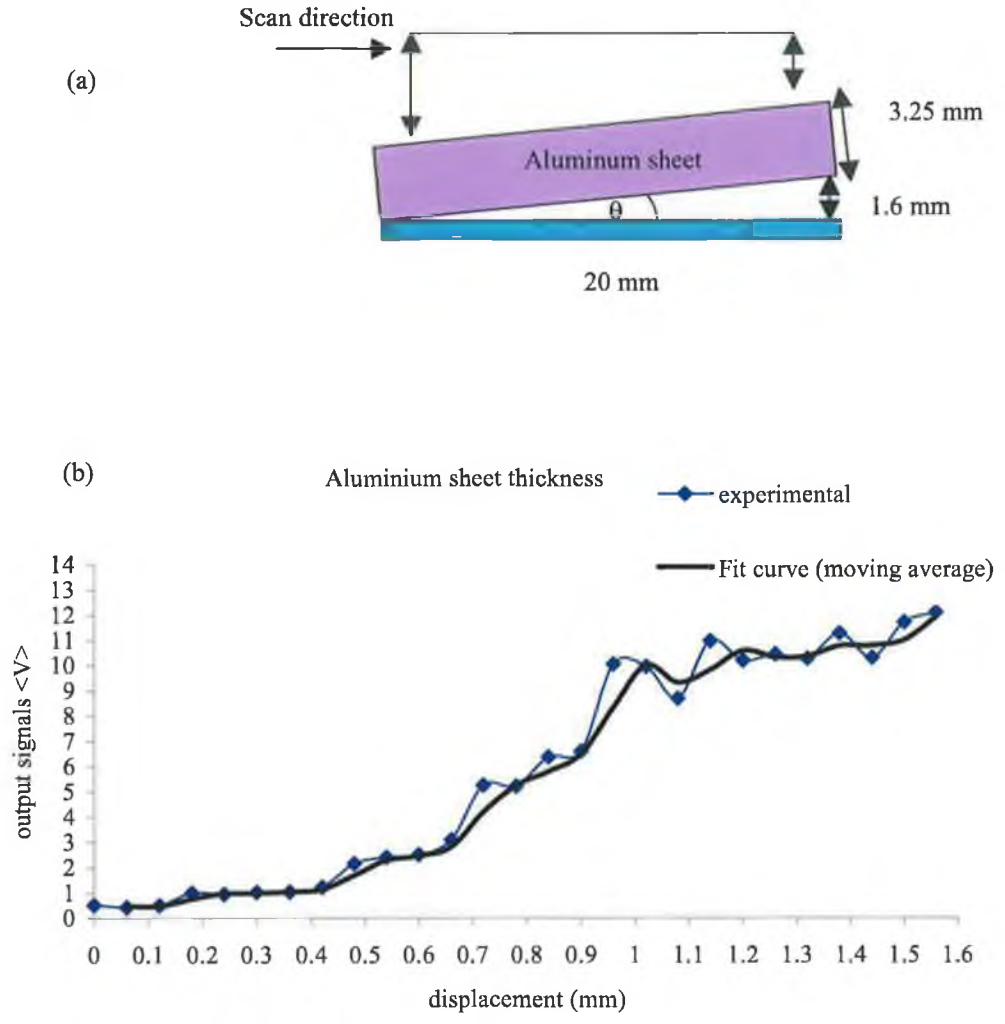

Figure 5.17 (a) Profile of aluminum sheet placed with an angle (b) Average voltage against the displacement from aluminum sheet surface.

5.6 Surface roughness measurement

It is important to note that as the Ra roughness value increases the intensity of the specular component becomes weaker. Moreover it was observed that with increasing values of Ra, the scattered light spreads over a wider angle.

Different surfaces with different values of surface roughness (Ra) were tested with the developed system. Figure 5.18 shows the relation between the surface roughness and the reflected signals. These results were determined from the average of the five signals reflected from the aluminum surface with different roughness Ra (0.1, 0.8, 1.6, and 5.4 μm).

Figure 5.19 shows the scan of the stainless steel plates with different surface roughness and the average of five output signals. The value of the surface roughness used were as Ra = (0.025, 0.05, 0.1, 0.2, 0.4, 0.8. 1.6 and 3.2 μm). For both the stainless steel and aluminum plates, as the value of the surface roughness Ra increased, the reflected signals from the surfaces became weaker. The scattered light spread over a wider angle for the roughness surface.

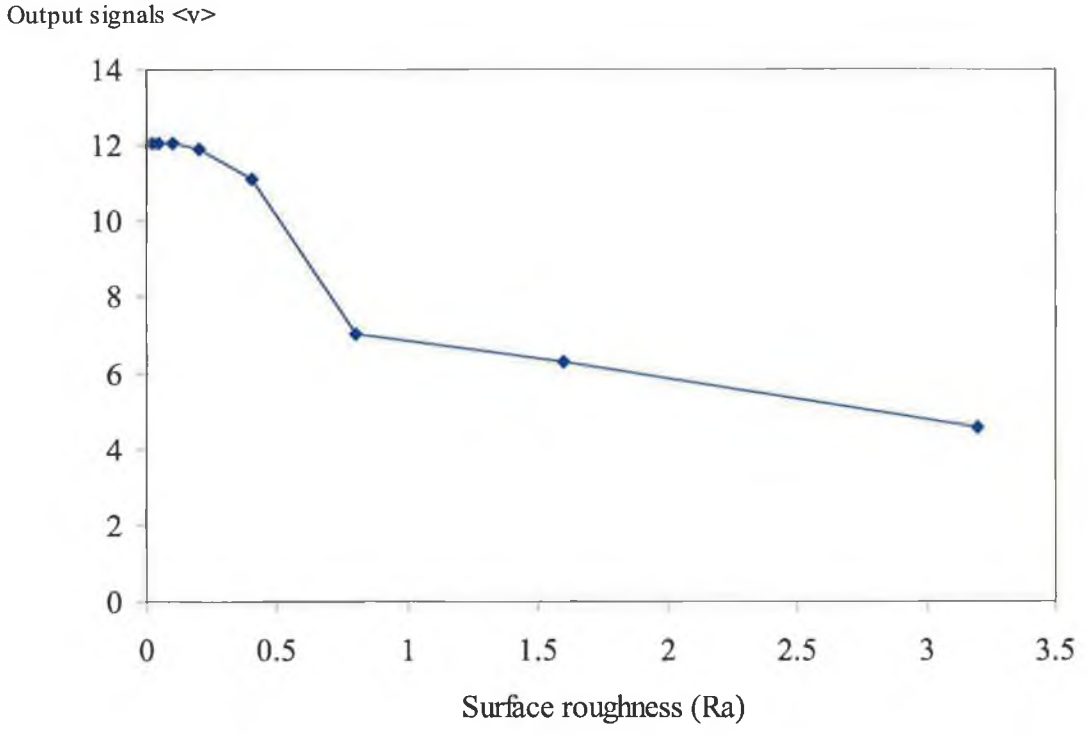

Figure 5.18 Aluminum surface roughness measurements.

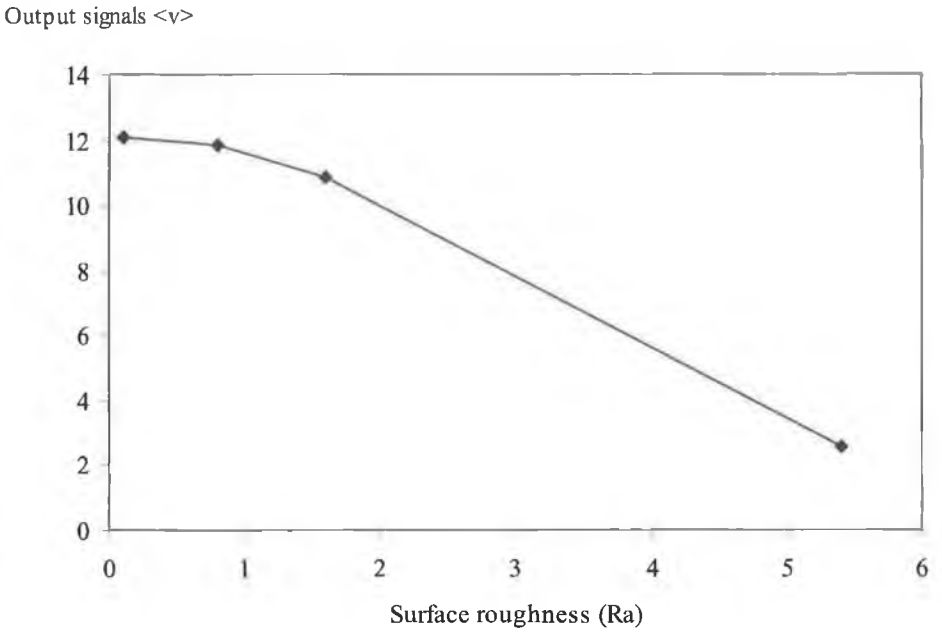

Figure 5.19 Stainless steel surface roughness measurements.

5.7 Semi-automated surface profile measurement

For the results in this section a transducer was used to control the rotation plate (Appendix B_7). Appendix C_5 shows the rotary sensor positioned between the translation stages and the rotation plate. This sensor was connected to the digital and counter input channel in the data acquisition card. A liner-guide motor (Appendix B_8) simulated an on line production environment by moving the sample beneath the newly developed inspection sensor. Results from this system at variable resolution are presented.

The new method of the adjustable resolution was described in the chapter 3. Using the rotary sensor fixed the rotation plate to accurately angle of the fibres to the same direction controlled the scan angle. Stainless steel plate with two holes (2 and 3 mm) was tested from different sides. A series of scans were made to detect the defect on the surface. Figure 5.20 describes the path over the defects.

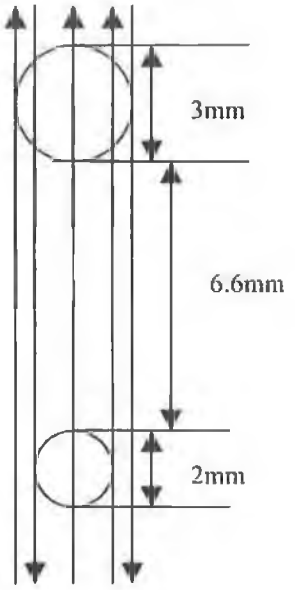

Figure 5.20 Direction of series of semi-automated scans of the stainless steel surface with two holes (2 and 3 mm)

Figures from 5.21 to 5.32 shows a series of automated scans of the two holes on the stainless steel surface. Profiles of the five received signals showed the existence and absence of the surface, which represents part of the holes. The average time between any two signals was 5 m sec. Figures 5.23 to 5.24 represent the five signals passing a surface with a defect represented by a 3 mm hole.

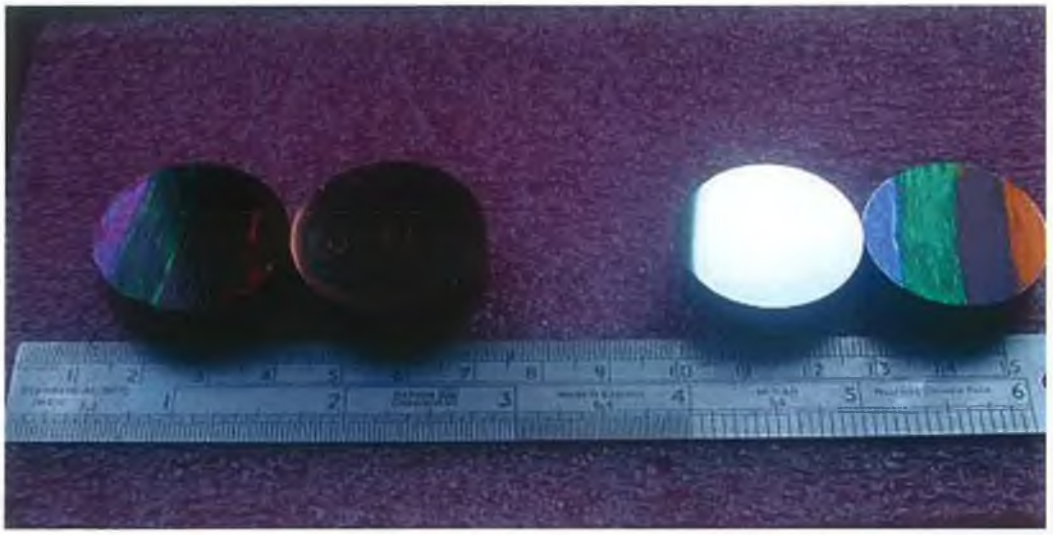

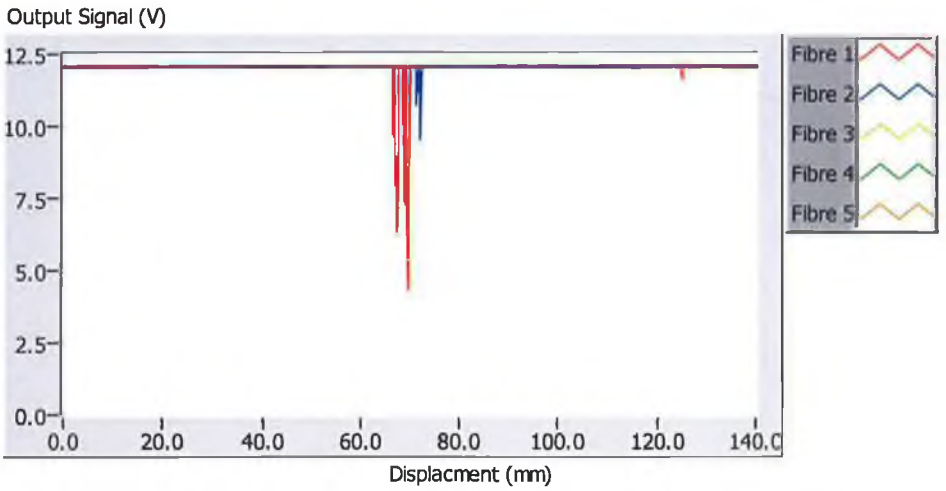

Figure 5.21 (a) Photo of the stainless steel and brass plan and coloured surfaces (b) Signal passing the edge of the 3 mm hole.

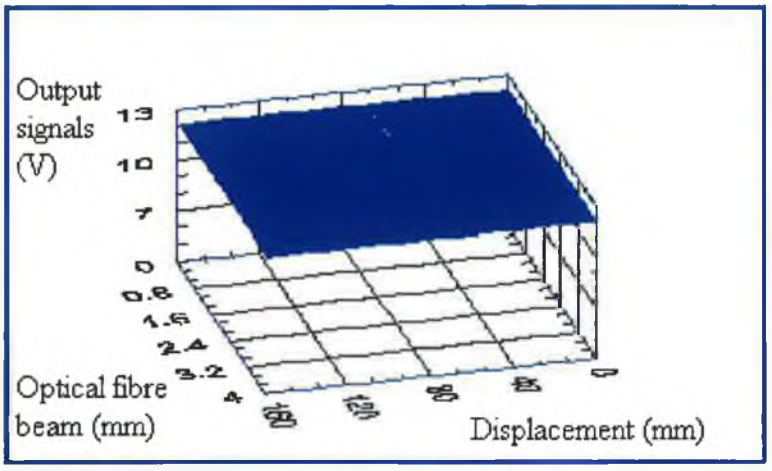

Figure 5.22 Measurement profile the edge of 3 mm hole.

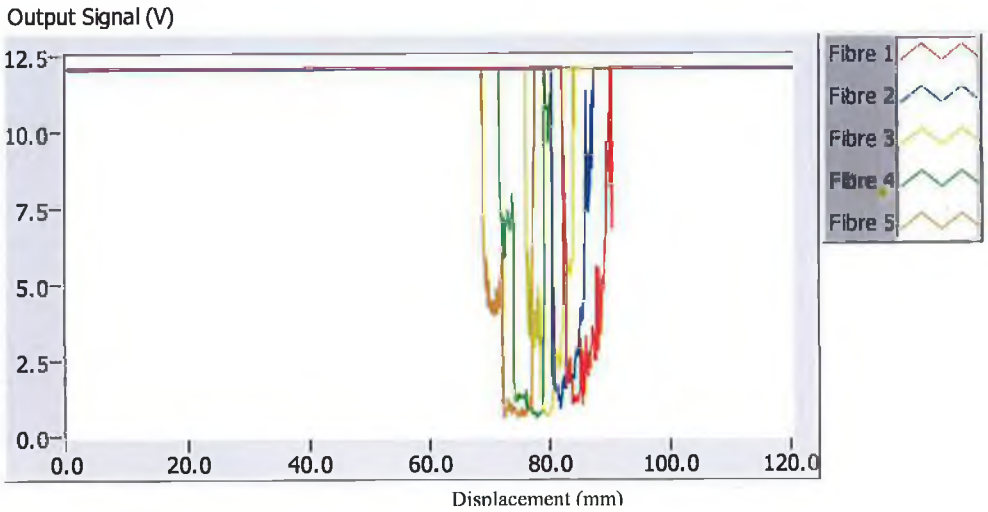

Figure 5.23 Signal passing through a 3 mm hole.

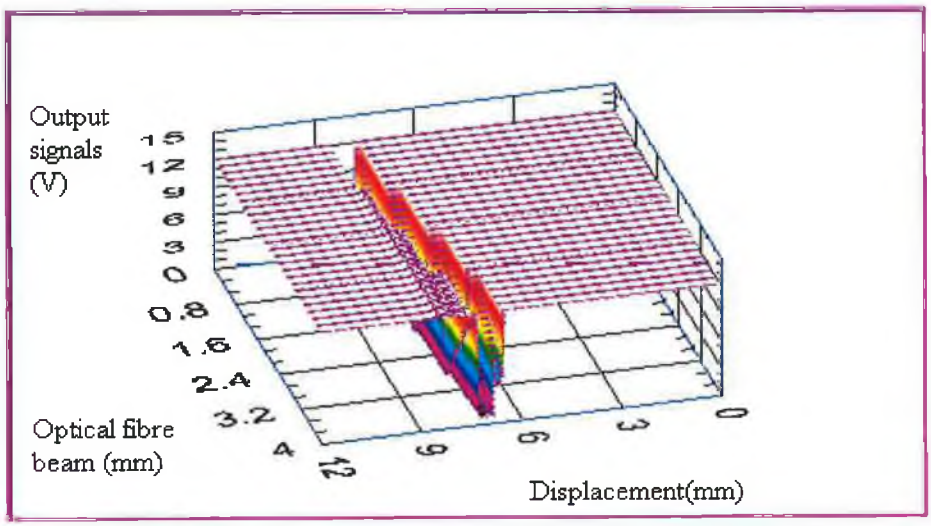

Figure 5.24 Measurement profiles through a 3 mm holes.

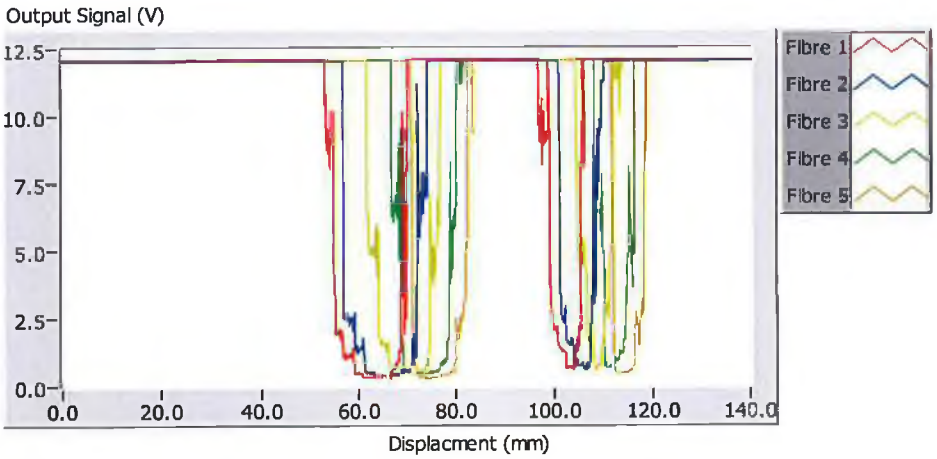

Figure 5.25 Signal through 2 and 3 mm holes

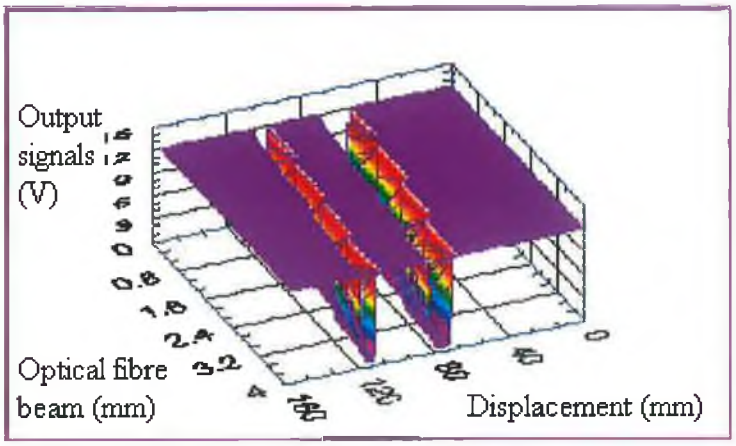

Figure 5.26 Measurement profiles through 2 and 3 mm holes.

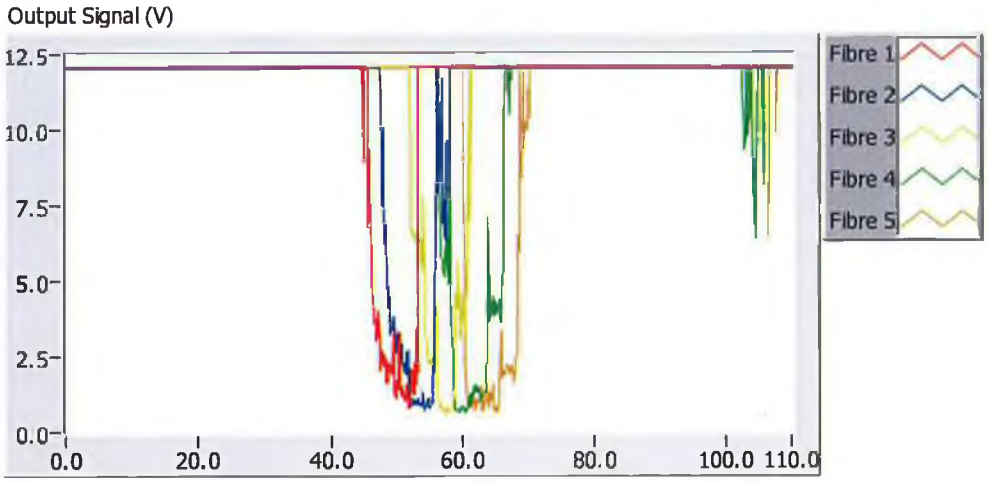

Figure 5.27 Signals passing through a 3 mm hole of and 2 mm edge hole.

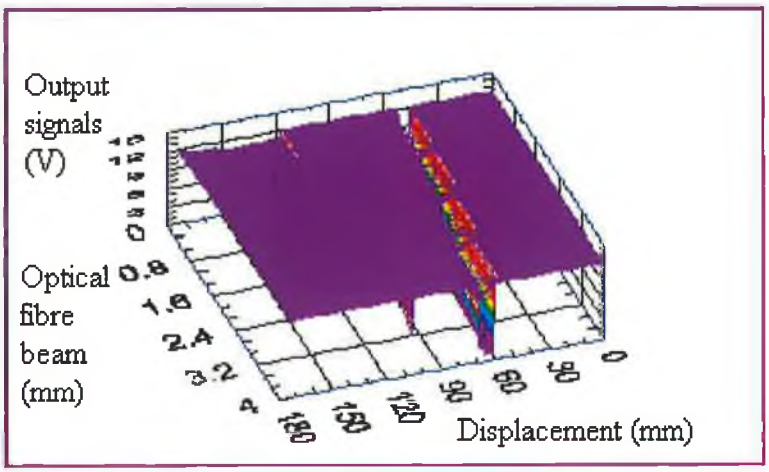

Figure 5.28 Measurement profile through a 3 mm hole and the edge of a 2 mm hole.

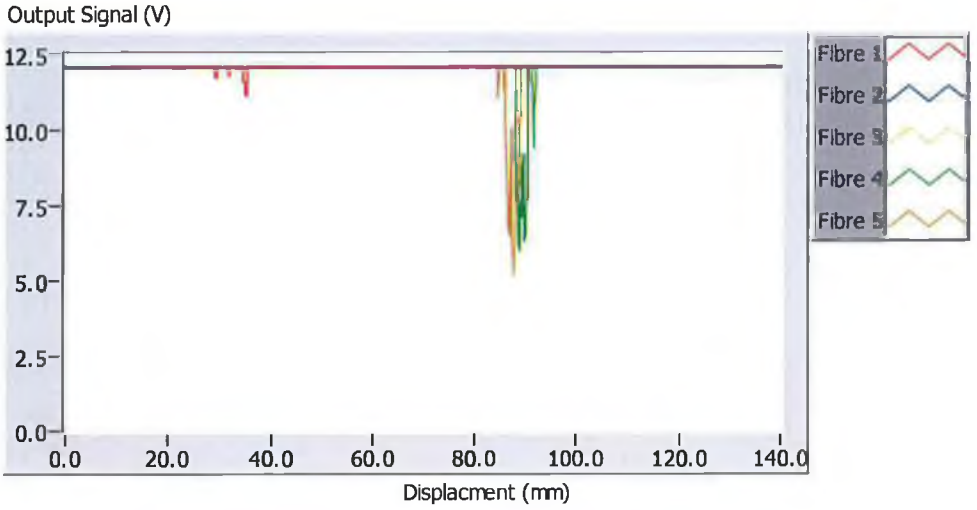

Figure 5.29 Signal passing the edge of 3 mm hole.

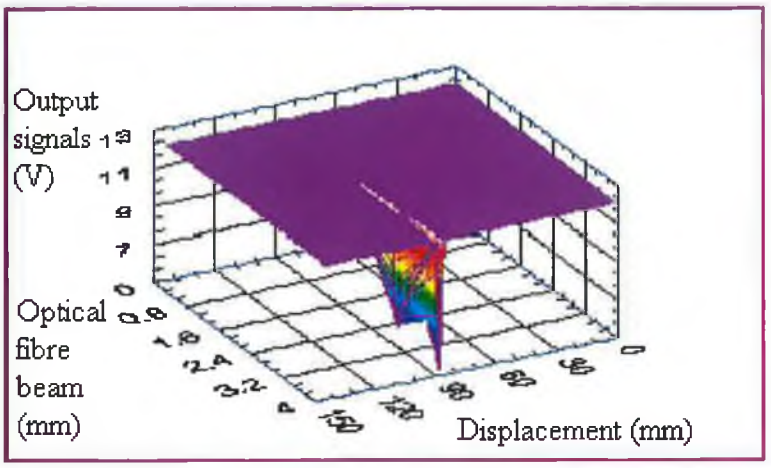

Figure 5.30 Measurement profile of the 3 mm edge hole.

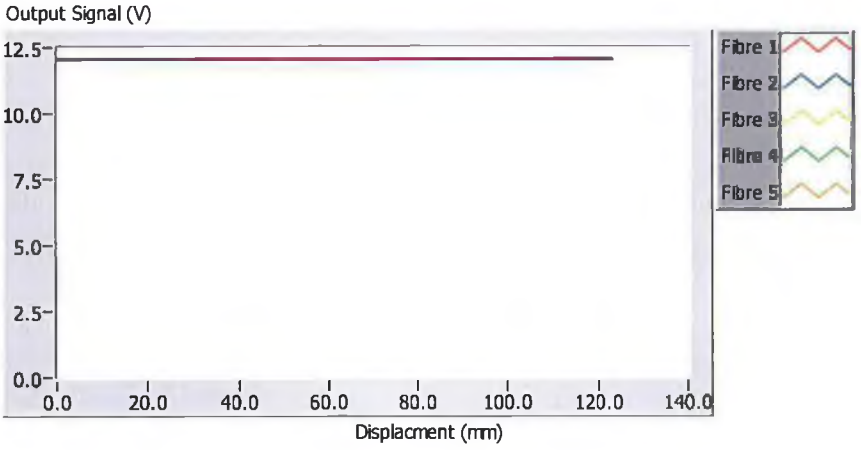

Figure 5.31 Signals passing the stainless steel surface

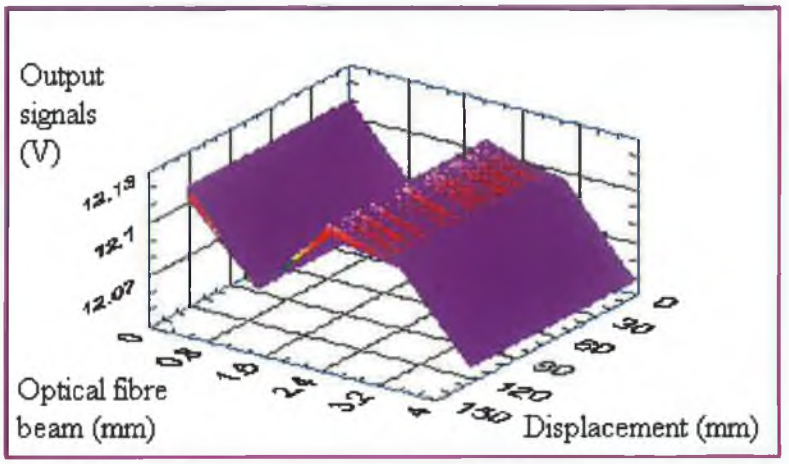

Figure 5.32 Measurement profile of the stainless steel surface.

5.8 Case study for accuracy of scanning system

The accuracy of the system has been measured. The resolution of the distance and time of scan between two points was measured. The number of points measured by the system within a distance of 1 mm was approximately 106 ± 1 points. In this case the dimension of the surface and the defect can be measured by dividing the number of points by 106. The system is capable of recognising the average time between the two scan points, which was 5 m sec. Noting the speed of the system was (1.9 mm/sec) and the time between the two points could determine the distance between two points on the sample plate. The distance between two data points was approximately 9.5 ± 0.01 μm. Figure 5.33 shows the aluminum plate with two slots, which was used in this study.

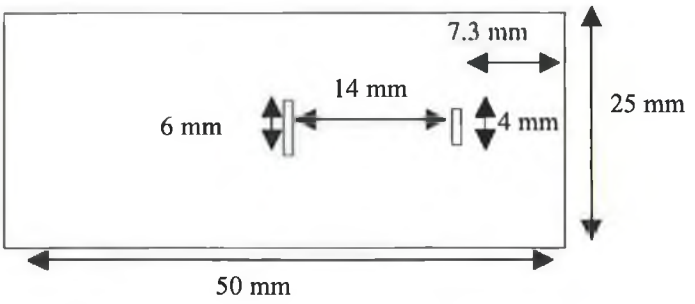

Figure 5.33 Schematic of the aluminum plate used.

Several tests were made on the aluminum plate with the two slots. This scan was carried on from different positions on the plate. Figure 5.34 shows the one set of scans on the aluminum plate. The last figure is divided into three regions to give more details for this scan. Figure 5.35 shows the first region scanned, which consists of the first slot on the surface. The last region of these scans presents the second slot as shown in Figure 5.36.

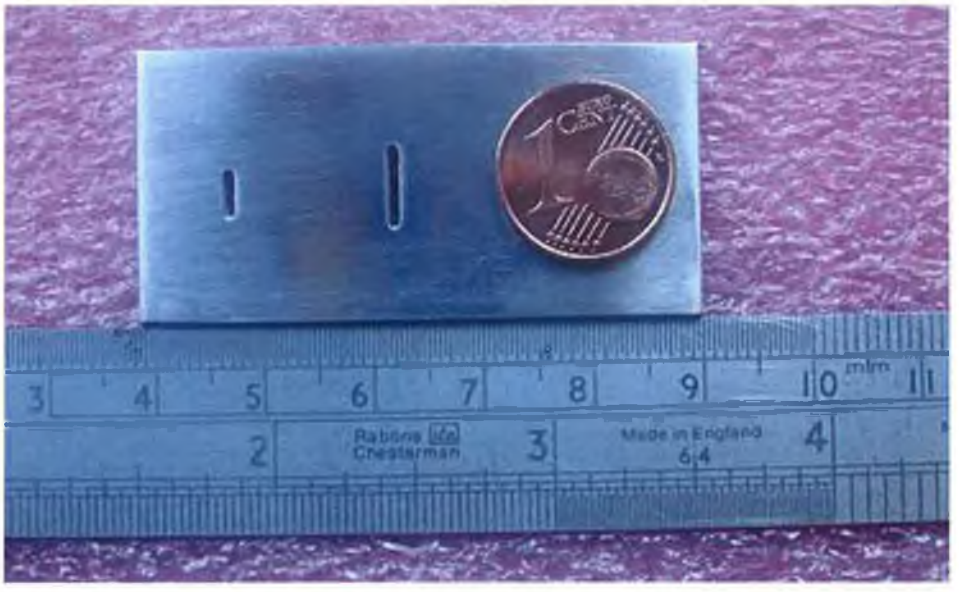

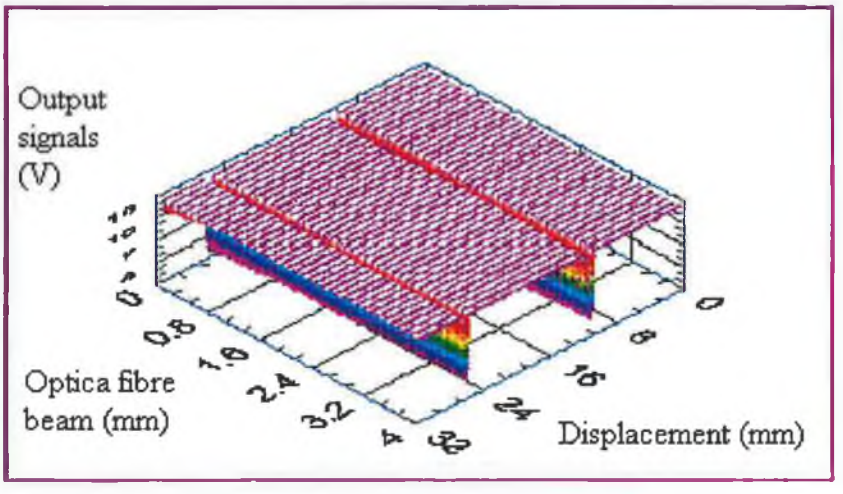

Figure 5.34 (a) Photo of aluminum plate (b) Measurement profile of the two slots on the aluminum plate.

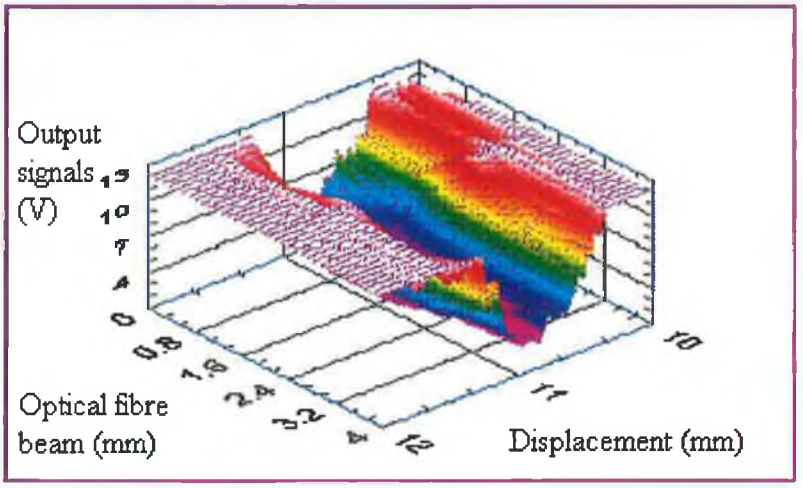

Figure 5.35 Measurement profiles of the first slot.

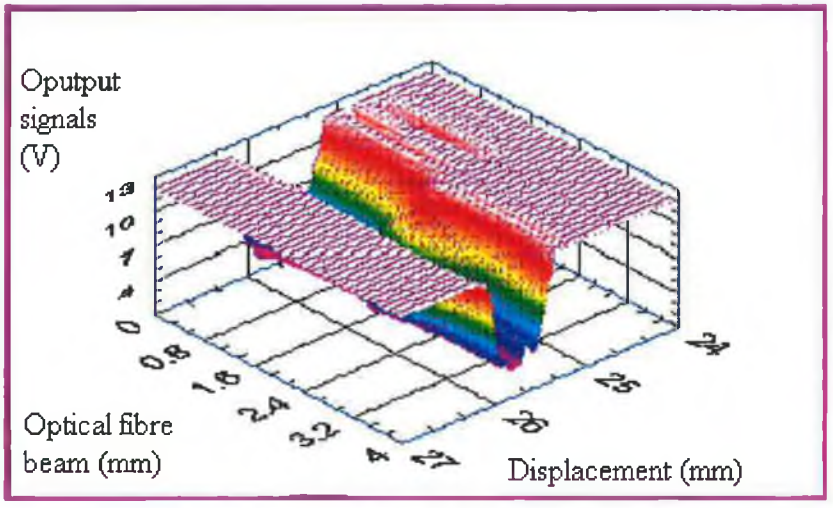

Figure 5.36 Measurement profiles of the second slot.

As shown in Figure 5.37 it is clear that the signals passed through part of the first slot scanned. The rest of these signals passed along the surface at the slot side. Figure 5.38 shows the signals around the slot edge area.

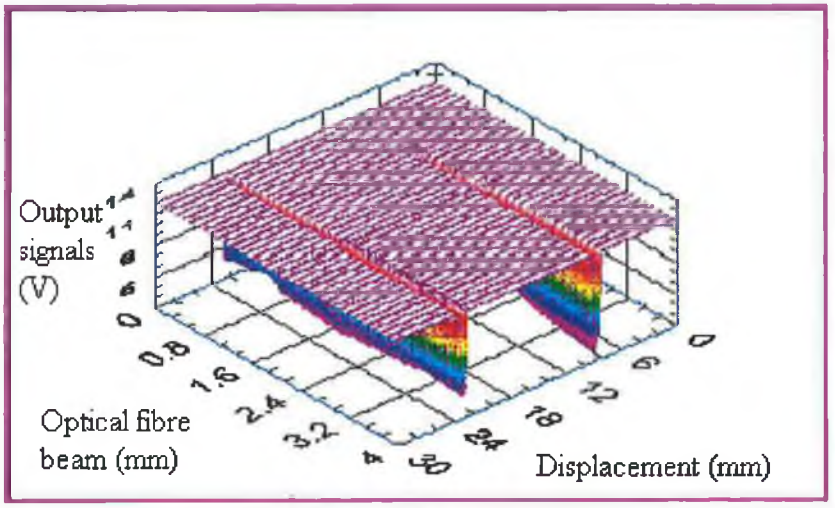

Figure 5.37 Measurement profile of different position of aluminum plate scans.

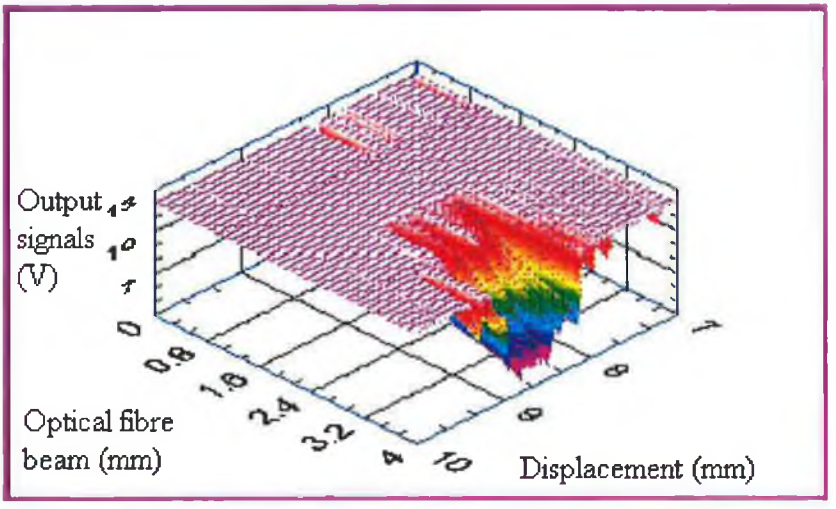

Figure 5.38 Measurement profile of edge slot in the aluminum plate.

Scans shown in Figures 5.39 and Figure 5.40 indicate that the results from the forward and the reverse motions obtained that the slot is not symmetrical due to the engineering drill. This result indicates that the surface is irregular in shape.

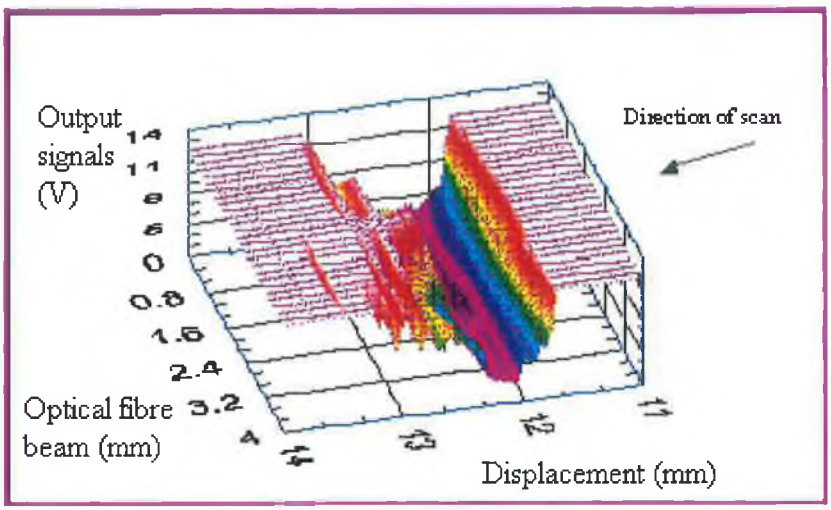

Figure 5.39 Measurement profile the forward way of the slot in aluminum plate.

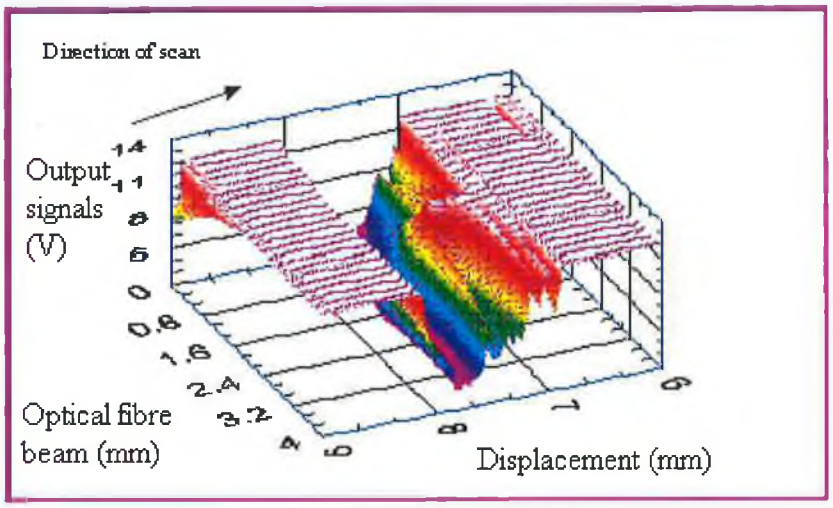

Figure 5.40 Measurement profile of reverse way of the slot in the aluminum plate.

5.9 Scanning of the coloured surfaces

This section describes the results of the coloured surface scans. Two type of the materials were used, stainless steel and brass. Figure 5.41 and 5.42 shows the 3-D profile of the non-coloured surfaces, which were scanned for the stainless steel and brass materials.

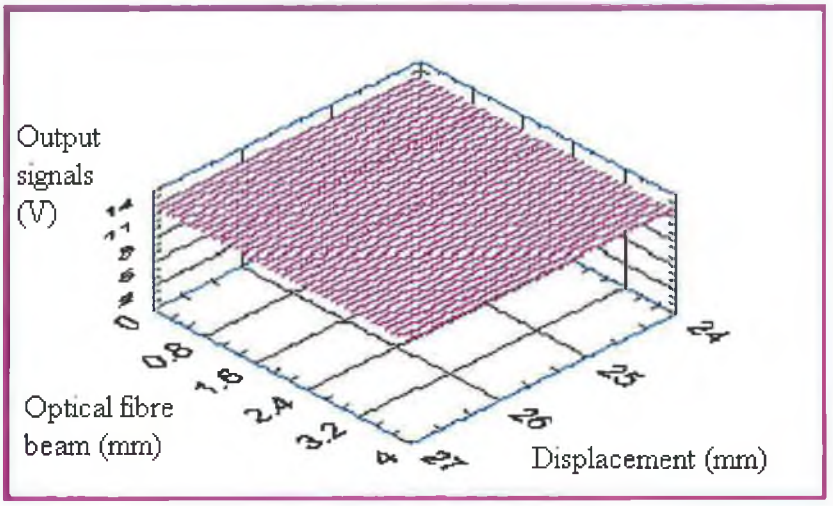

Figure 5.41 Measurement profile of the non-colour surface (stainless steel).

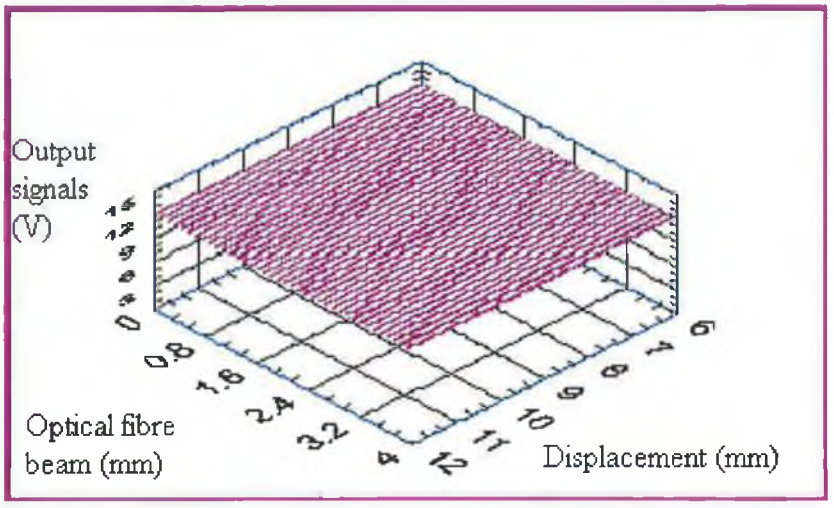

Figure 5.42 Measurement profile of the non-colour surface (stainless steel).

The two surfaces were covered with four colours, which were orange, black, green and blue. A 3-D profile of the collected signals from the coloured surface is shown in Figure 5.43. Even though different colours covered the surface the system still detected the light. This is relates to the electric properties of the material surface (Eq. 5.2).

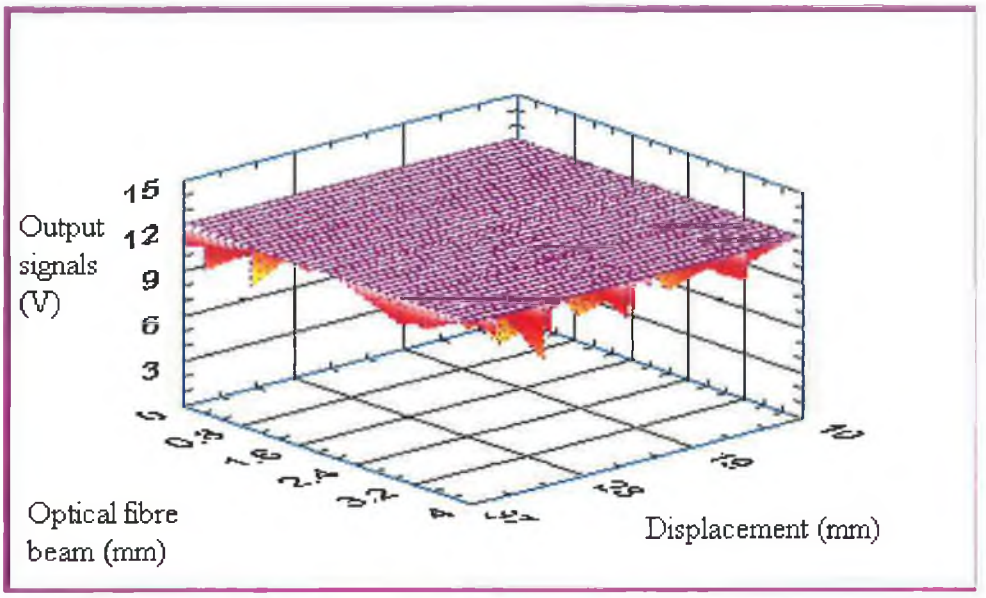

Figure 5.43 3-D profile of brass surface covered with colours.

The first area scanned on the brass surface is covered by orange colour. The system detects perfect signals from the brass surface (7x4.15 mm covered by orange colour). The previous (Figure 5.44) shows the particular area scanned with high reflectivity surface and the different areas scanned by the system (8x4.15 mm, 8x4.15 mm and 5x4.15 mm covered by black, green and blue respectively). Most of the areas scanned obtained that brass surface have high reflectivity surface.

The second sample used in this study was the stainless steel surface. The same procedure of the scan was made on the stainless steel sample as that used on the brass surface. The stainless steel plate was covered by 5x4.15 mm orange, 8x4.15 mm black, 8x4.15 mm green and 4x4.15 mm blue respectively. Figure 5.44 shows recorded signals from all the coloured areas of the surface plate. The coloured have small affect on a surface compared with Figure 5.41 (original stainless steel surface) especially on the

orange colour and blue colour. These results indicate that the stainless steel surface have lower reflectivity than the brass surface.

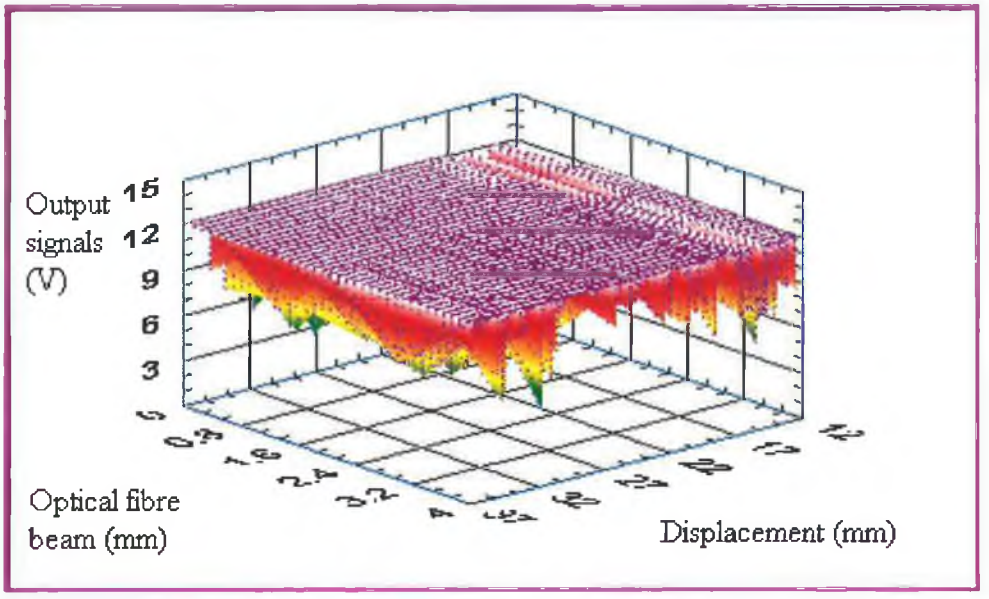

Figure 5.44 Measurement profile of stainless steel surface covered with different colours.

Chapter 6

Discussion, Conclusion and recommendation for future work

6.1 Discussion

Many industrial processes for material machining require continuous monitoring or inspection of the process product in order to detect parameter variations due to process imperfections and tool wear. However, manual measurements are slow and have relatively poor accuracy. These measurements are performed for randomly picked samples and a parameter dispersion histogram is constructed along with the calculation of various statistical quantities. Due to the low speed achieved with manual measurements only a small percentage (a few percent) of the resulting parts can be measured on line. If the number of parts measured is large enough statistical results are accurate. These results would be affected by time loss before the detection of any variation. [101]. The laser detection systems described in this thesis was constructed in order to achieve an on line inspection system for surface defect recognition.

Two types of scan were presented in this thesis vertical displacement and lateral displacement. Vertical displacement scan were used to optimise the system by setting the fibre end-sample distance to that at which the highest signals were detected. Ordinary engineering surfaces generally reflect irregularly. For that reason the vertical displacement characteristics can differ between the same plate for different sets of measurement for example, there was some difference in the signal peaks detected from the five different fibre points.

During the early stages of the experiment four fibre optics were used to emit and receive the signals. The output voltage profile differences from the beams were noted

for all the sample plates tested. These scattered due to rough fibre surfaces as a result of poor mechanical cleaving. Due to the poor initial results, factors that could affect the quality of the sensor were examined. Other factors affecting the operation of the sensor included as fibres alignment, cleaving, cleaning, and polishing the fibres. It is clear from the comparison of between Figures 4.30 to 4.33 (four-fibres) and Figures 4.34 to 4.37 (five-fibres) that carefully alignment, well-cleaved and cleaned fibre ends produced much enhanced sensing result. These parameters were much improved, although precise quantification is difficult.

The results of the optimisation of the fibre optic detection system showed that the output signal of five and even four arrays successfully measured the existence of the size and position of a hole in a plate. All the metal samples showed very good reflector at infrared wavelength, as was also seen by [100].

Scans of the different sizes of polycarbonate plate through holes and blind holes, and the notch on the tufnol surface plate, showed the disadvantages of using this sensor with surfaces that reflects light diffusely (Figure 5.14). The contrast was much less than that obtained from the copper, aluminium, stainless steel and brass surfaces. The depth of the blind hole in the polycarbonate plate (0.6 mm) was also measurable with the sensor. The transparent surface was quite different from the metal surfaces. This surface reflected the laser spots off the top and bottom surfaces, so those two sets of laser spots were detected, allowing potentially for thickness measurements to be made.

The increasingly higher standards of part quality tests necessitate new, fast, flexible sensors which should, as far as possible, be non-interacting (i.e. non-contact), to record the quality characteristics directly in the production environment in non-contact way. Robust, optoelectronic sensor systems provide a good basis for the implementation of quality control circuits in the process environment [102].

Continuous on-line inspection of moving sheet is one of the most active fields of optical inspection [23]. The last results of chapter five simulated an on line production inspection system using a liner guide motor to move the part. This system has potential multiple applications in the industrial or manufactories environment

such as surface defect, thickness, material reflectivity and surface roughness measurement.

6.1.1 Defect simulation

This section presents the tested samples, which are made from materials such as stainless steel, brass, copper, aluminium, Tufnol, polycarbonate and transparent polycarbonate. Holes from 1mm to 7 mm and blind hole from 2 mm to 7 mm were examined. When the system scanned these types of defects the signals had some fluctuations at the edge of the holes due to the rough surface produced by the drilling operation, see Figure 4.68. The depth of the blind hole on sample plates, which was tested by the system, was 0.6 mm. This depth of the blind hole was detected by the system.

Different types of defect were simulated, such as a notch on the surface. Figure 5.10 shows the profile of 3-D graph of the aluminium surface and through the notch. The signals were fluctuating through the notch, which represented to the irregular valley in the notch.

6.1.2 Resolution

The novel method, used to reach high resolution, is dependent on the projection of the spots on the x-axis. Figure 6.1 (a) shows that the spots are elliptical due to incidence angle of light on the surface. It also shows the total distance between the spots, the distance between any two spots projections. Two approximate diameters of the fibre spot, small diameter (d = 62.50 μm) and large diameter (D = 72.12 μm) were used.

The rotation plate was moved by an angle θ with respect to the y-axis. In Figure 6.1 (a) $\theta = 0$, the angle should be about 8^0 to achieve a projection distance of 560 μm as shown in Figure 6.1 (b).

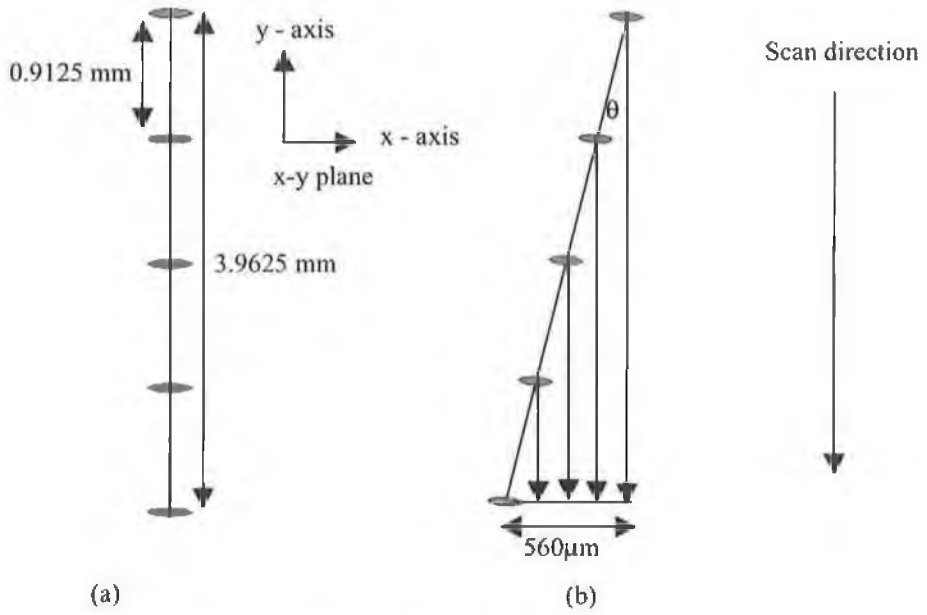

Figure 6.1 Resolution of the system

A rotary sensor (encoder) with an error of $\pm 0.7^0$ was used to control the angle of scan as show in Figure 6.2. This sensor was connected by cable with the data acquisition card in counter.

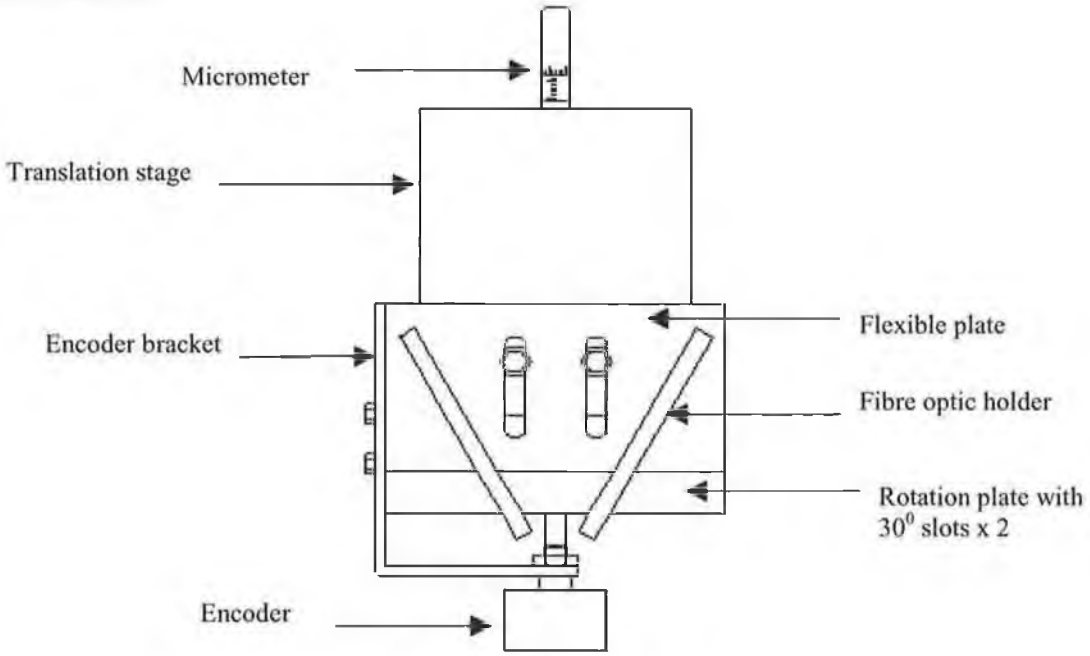

Figure 6.2 Side view of the system

6.1.3 Stand–off distance

The distance between the fibre-cable end and the workpiece surface was varied to obtain a maximum probe response. Once the probe response was maximised it is set at this stand off distance [103]. The intensity of the detected light depends upon how far the reflecting surface is from the fibre optic sensor [32]. The distance between the fibre end face and the material surface was one of the most important parameters to achieve good signal response. All the metal samples tested by this system showed reflected signals from around 2 mm fibre stand off distance from the surface. Signals could be detected over a wide range of stand off distance. This range of the detected signals was dependent on the type of the materials under the test. The dimension of the emitted light area highly dependent on the stand-off distance and the numerical aperture. In order to get high resolution measurement the system should be customised for each type of material, especially for diffuse surfaces.

Figure 6.3 shows the behaviour of the five scan signals of the vertical displacement for the stainless steel surface. The position of the end faces were approximately 0-16 mm off the surface plate. This test was done to optimise the stand off distance. In order to analysis the vertical displacement scan of the material surface this Figure can be divided in to three regions. The first region of the vertical displacement scans is that where the system started to detect signals. When moving the Z-stage up off the surface the signals appear at 5 mm. Then the signals continue rise. Different fluctuations of the output signals are observed in this region of the vertical displacement scan. The reason of this fluctuating is due to the irregularities in the surface and mis-alignment of the end face fibres. The second regions of the scan were the signals reach the top value. In this case the stand off distance reach approximately 7 mm and it is continues until the stand off distance is 10 mm. The right position of the fibre end face can be chosen in this range and then fixed. In the third region of the vertical displacement scans, the signals starts to drop down proportional with the movement of the fibres optic end faces up off the surface plate. The display screen shows that the signals are fluctuating and they continues to drop until the distance between the fibres end faces and the material surface reach about 16 mm.

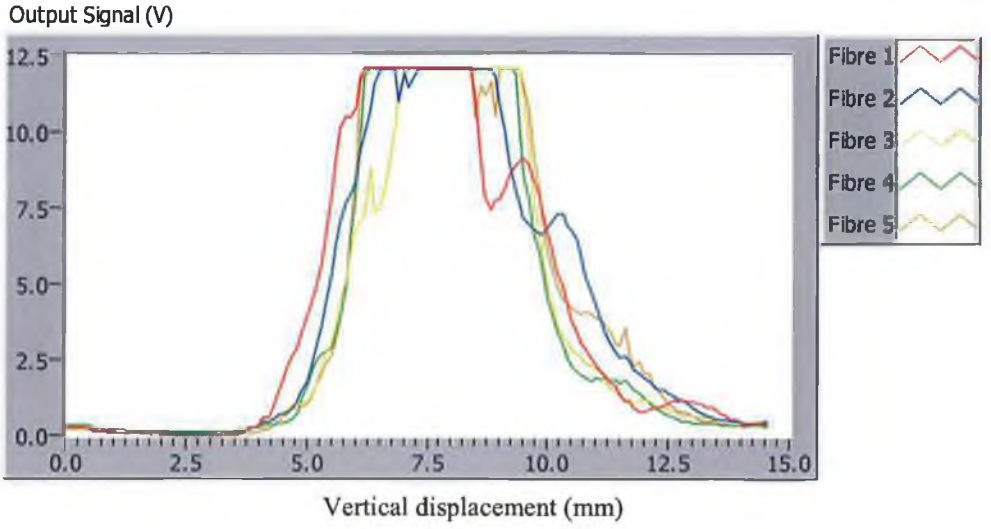

Figure 6.3 Vertical displacement scans of stainless steel.

6.1.4 Speed of the system

In order to achieve a high-speed laser scanning system that would be useful for the on line part inspection the time of the scan must be small. The present system has a speed, which of up to 1.9 mm/sec. This system speed should be increased if it is to be used in the automated industrial. Most of the system speed limitation is due to the data acquisition card, which was used to convert the signals from analog to digital. The speed of the data acquisition card is 100,000 samples/sec. This speed system can not be increase unless an improve the data acquisition card is used. Also a faster part movement is also required.

6.1.5 Resolution of time

Laser range finders and vision systems have found many applications in different areas, including manufacturing and automated control systems. Considerable efforts

have been made to collect real-time, high-resolution image data to provide high quality 3-D information about the object under study [40,104-107].

This system was able to measure the time of scan. Theoretically the dimension of the material surface defect can be measured according to the speed of the scan which was measured. This system allowed the measurement of the number of points per mm of scan of the material surface. The number of points in one-mm scan was approximately 106±1 points. Once the number of points through the defect is identified then the size of the defect can be theoretically measured. The system is measured the average time between the two scan points, as 5 m sec. This time is considered as the resolution of the time of scan. The distance between the two points on the sample plate can be obtained from the speed of the system and the time used to travel between the two points. The distance between two points was approximately 9.5 ±.01μm.

6.2 Conclusions

In this thesis, The design construction and operation of fibre optic laser scanning inspection system for surface defect was presented in detail. The five fibres used covered a distance of up to 4.15 mm. The last results simulate on line inspection using a liner guide motor production line was simulated by moving the samples under the sensor at a speed of 1.91 mm/s. New techniques were used to adjust the resolution of the system to obtain higher accurate results.

The resolution of the system was made adjustable by mounting the fibre holder on an adjustable rotation stage. This system has high response and accuracy. The experimentally obtained results from several materials shows the system's ability to recognise defects. The achieved results show that even though this system is capable of 2-D scanning it may also be operated as a limited 3-D vision inspection system. The fibre optic laser scanning system, which has been discussed in this thesis offers an effective means of highly accurate measurements, high resolution, and flexibility to capture the output signal reliably.

In order to test the development of the fibre-optics laser scanning system for surface defect recognition, a simple laser scanning system was designed, constructed and tested. The results from several materials were tested for the vertical displacement. Most of these results obtained indicate that all the metals are very good reflectors in the infrared wavelength.

Such a sensor would be useful in automated industries due to its simple design high sensitivity and low cost. The system presented has been shown as an effective means of collecting surface profile information. The system successfully scanned a simulated defects, which were a holes and notches on the sample plates. The advantages of using the system are high measuring speed, high resolution, and great flexibility to reliably capture surface profile information.

The signal drift effect of this system over a period of time were considered and shown to have no considerable effect. As this effect was not very significant the system is considered quite stable.

A fibre -optic sensor for on-line production inspection was proposed and developed. Applications with multi-mode fibres are discussed and were tested in the

experiments. The proposed simple fibre optic sensor would be effective in determining surface defect recognition. This system was successfully used to measure the following parameters:

1. Measurement of the notched surfaces from different materials such as aluminium, tufnol, and transparency polycarbonate.
2. Measurements of the material's reflectivity for several materials such as plastic, transparent polycarbonate, aluminium and stainless steel
3. Aluminium sheet thickness measurement.
4. Surface roughness for aluminium and stainless steel materials
5. Automated surface profile measurement with adjustable resolution
6. Scan coloured material

The results explain that the incident signals were affected by how far is the system from the surface and the type of the surface material. The high reflectivity of the metal surfaces allows the system to detect high intensity signals from these surfaces. In the case of transparent polycarbonate reflected signals are generated from the top and bottom surface. This type of surface scanning could be useful in materials thickness measurements.

6.3 Recommendation

This chapter recommends further work for analysing the performance of the design and the components used in the system which may need improvements. This thesis described some properties of the material surface, which was tested by the present system. Automated industries have wider ranges of the applications such as in the medical devices, and semiconductor industries. In order to use the system in further industrial applications adjustments of the system may be required to achieve more accurate results and a high level of efficiency in using and analysing the results acquired.

The fibre optic scanning system has been used with limited speed scanning simulations of on line production. The limitation of the systems peed depends on the data acquisition card and the guideline motor used. The system will be useful for the industrial online production if the system speed is increased.

The present fibre optic holders which were used in this system has some mis-alignment of the fibre along the angle axis for both the fibres end faces and the straight line of the fibre. This mis-alignment causes some variation in the achieved results. More accurate design and construction of the fibre optic holder is required to develop the stability and accuracy of the fibre optic system.

The rotation plate is part of the mechanical design of this system and should be developed and designed accordingly. The rotation plate would be controlling the fibre optic holder and the resolution of the system. Micrometers could be used for adjusting the rotation plate and to move the holder up and down along the angle of the slot. The advantages of a newer design would be to increase the stand off distance and to optimise the system for this position.

This system tested the coloured surface for two types of material surface plate's stainless steel and brass. Four colours used to cover the surface in these results, orange, black, green and blue. More study needed for this section of the results. The last result can be satisfactory if more colour used and more material surface tested.

References

[1] J. Hecht, The laser guidebook – laser & applications, 1986, McGraw-Hill Book Company, New York.

[2] P. Das, Lasers optical engineering, 1990 Springer-Verlag New York Inc.

[3] T. H. Maiman, Stimulated optical radiation in ruby maser, 1960, Nature, 197, 493.

[4] P. Milonni, J. Eberly, Lasers, 1988, John Wiley & Sons, UK.

[5] S. Ungar, Fibre Optics, 1990, John Wiley & Sons, UK.

[6] http://www.bell-labs.com/history/laser/invention/

[7] H.G. Rubahn, Laser applications in surface science and technology, 1999, John Wiley & Sons, UK.

[8] J. Wilson, J.F. Hawles, Optoelectronics, an introduction, 1989, Prentice Hall International, UK.

[9] http://www.gensacn.com.laser_frame/lasers.htm

[10] http://floti.bell.ac.uk/MathsPhysics/

[11] A.W. Snyder, Asymptotic expressions for eignefunctions and eignevalues of a dielectric or optical waveguide, 1969, IEEE Trans in microwave theory tech, MTT, vol. 17, pp.1130 – 1138.

[12] J.T. Luxon, D.E. Parker and P.D. Plotkowski, Laser in manufacturing, 1987, IFS Ltd, U.K.

[13] M. Steman, K. Lindsey, Limits of surface measurement by stylus instruments, 1988, Proc. SPIE, p. 1009.

[14] F. Soliman, Radiation testing of fibre optic system, 1996, Elsevier Science Ltd, Appl. Radiatiat. Isot., vol. 47, no. 2, pp. 175-183.

[15] F. Dezelsky, R. Sprow, and F. Topolski, Lightguide packaging, 1980, The Western Electric Engineer, Winter, pp 81-85.

[16] D. Goff, Fibre optic reference guide, 1996, Butterworth-Heinemann, USA.

[17] T. Okoshi, Optical fibres, 1982, Academic Press, p. 72.

[18] K. Grattan, T. Sun, Fibre optic sensor technology: an overview, 2000, Sensors and Actuators 82, pp 40-61.

[19] J.C. Owiz, Optoelectric: an introduction, 1989, Butterworth-Heinemann

[20] H brueggemann, Loa cost laser scanner, , Inernational levs design conference, 1985, SPIE vol. 554, pp457-462.

[21] S. Sullivan, Acquiring image laser scanning, 1986, Lincoln Laser Company, Phoenix Arizona.

[22] A. Abuazza, M.A. El-Baradie, Laser-scanning inspection system, an overview, AMPT, 99 and IMC 16 Conf., 1999, Dublin City University, Ireland, pp 1939-1945.

[23] P. Cielo, On line optical sensor for industrial inspection, 1990, In- process optical measurement and industrial methods, vol. 1266, pp. 22-38.

[24] P. Cielo, Optical techniques for industrial inspection, 1988, Academic Press, Boston.

[25] R. Pirlet, R. Franessen, V. Laforge, and F. Surleau, Slab thickness identification with the 'Optimac', 1976, CRM 46, no. 3, pp 29-34.

[26] J. Kerr, A laser thickness monitor, 1969, J. of IEEE, no. 5, part 6, pp 338-339.

[27] V. Bodlaj, E. Klement, Remote measurement of distance and thickness using a deflected laser beam, 1976, Appl. Opt., no. 15N, part6, pp. 1432-1436.

[28] D. Rosenberger, Laser sensors for industry, 1972, Alta Frequenza, no. 41, pp. 771-779.

[29] D. Whitton, A laser technique for precise measurement, 1972, Elect. & Power 2, pp 46-48.

[30] W. Rowley, Interferometer measurement of light and distance, 1972, Alta Freqenza 41, pp. 887-896.

[31] V. Bodlaj, Industrial application of laser, 1984, John Wiley & Sons Ltd.

[32] G. Butler, G. Gregoriou, A novel noncontact sensor for surface topography measurement using a fibre optic principle, 1992, Sensors Actuators, vol. 31, pp 68-74.

[33] J. Stover, Optical scattering measurement and analysis, 1990, McGraw-Hill, New-York.

[34] C. Quan, S.H. Wang, Inspection of micro-crack on solderball surface using laser scattering method, 2000, Optical Communication, no. 183, pp 19-27.

[35] F. His-Yung, L. Yixin, X. Fengfeng, Analysis of digitizing errors of a laser scanning system, 2001, Precision Engineering, no. 25, pp 185-191.

[36] A. Anon, Laser inspection system, 1988, Optical Information Systems, vol. 8, no. 5, pp. 226-229.

[37] J. Luxon, and D.E. Parker, Industrial lasers and their applications, 1985, Prentice Hall Inc., New Jersey.

[38] E. Udd, Fibre optic smart structures, 1995, John Wiley and Sons, New York.

[39] A. Timothy and A. Hojjat, Monitoring the behaviour of steel structures using distribute optical fibre sensors, 2000, Elsevier, vol. 53. pp. 267-281.

[40] A. Pugh, Vision In: robot sensors, 1986, vol. 1, IFS publication Ltd, UK.

[41] D. Cromwell, Sensor and processor enable robot to see and understand, Laser Focus World, March 1993, pp 67-78.

[42] http://www.qualitymag.com/articles_1998.html

[43] Z. Fuzessy and N. Abramson, Measurements of 3-D displacement: sandwich holography and regulated path length interferometry, 1982, Applied Optics, no. 21, p 260.

[44] R. Sirohi, M. Kothiyal, Optical components system and measurement techniques, 1991, New York: Marcel Dekker, pp 399-408.

[45] D. Himmel, A laser measuring system for automatic industrial inspection, In: Proceedings of the 4th International Joint Conference on Pattern Recognition, New York, 1978, IEEE, pp.925-54.

[46] J. Taboada, Coherent optical methods for applications in robot visual sensing, 1981, Proc. Soc. Photo-Opt. Instrum. Eng., no. 283, p 25.

[47] N. Nimrod, A. Margalith, H. Mergler, A laser based scanning range-finder for robotic applications. In: A. Pugh, Ed. Vision. Robot Sensors, vol. 1, 1986, IFS Publication Ltd, pp. 159-73, UK.

[48] B. Paul, Advances in machine vision - Active optical range imaging sensors, 1989, Springer-Verlag, pp 1–63.

[49] G. Hausler and W. Heckel. Light sectioning with large depth and high resolution, Dec. 1988, Applied Optics, no. 27, part 24, pp. 5165–5169.

[50] R. Jarvis, A perspective on range-finding techniques for computer vision, March 1983, IEEE Trans. Pattern Analysis Mach. Intell., no. 5, pp. 122–139.

[51] J. Mundy and G. Porter. Three-dimensional machine vision - a three-dimensional sensor based on structured light, 1987, Kluver Academic Publishers, pp 3–61.

[52] M. Rioux, G. Bechthold, D. Taylor, and M. Duggan. Design of a large depth of view three-dimensional camera for robot vision, Dec 1987, Optical Engineering, no. 26, part 12, pp 1245–1250.

[53] T. Strand. Optical three dimensional sensing. Jan-Feb 1983, Optical Engineering, no. 24, part 1, pp 33–40.

[54] M. Buzinski, A. Levine, and W. Stevenson. Performance characteristics of range sensors utilizing optical triangulation. In proceedings of the IEEE May1992, National Aerospace and Electronics Conference, NAECON 1992, pp 1230–1236.

[55] M. Soucy, D. Laurendeau, D. Poussart, and F. Auclair. Behaviour of the centre of gravity of a reflected gaussian laser spot near a surface reflectance discontinuity, Sept 1990, Industrial Metrology, no.1, part 3, pp 261–274.

[56] R. Dorsch, G. Hausler, and J.M. Herrmann. Laser triangulation: fundamental uncertainty in distance measurement, March 1994, Ap-plied Optics, no. 33, part, 7 pp 1306–1314.

[57] T Kanade, A Gruss, and L Carley. A very fast vlsi rangefinder. April 1991, IEEE International Conference on Robotics and Automation, volume 39, pp 1322–1329.

[58] B. Cahill & M. El-Baradie. Industrial applications of optical fibre sensor, IMC14, Conference, Trinity College Dublin, September 1997, pp 577-586.

[59] A. Jackson, Monomode optical fibre interferometers for precision measurement, J. Phys. E: Sci. Instrum., 1985, pp 981-1001.

[60] P Weir, and V. Grattan, Accurate measurement of small displacement using optical techniques, Int. J. optoelectronic, 1994, no. 9, part 6, pp 449-455.

[61] J. Rao, A. Jackson, Recent progress in fibre optic low-choherent interferometry, Meas. Sci. Technol., 1996, 7, pp 981-999.

[62] V Grattan, and T Meggitt, Optical fibre sensor technology, 1995, Chaman & Hall.

[63] A. Shimamoto, and K. Tanaka, Geometrical analysis of an optical fibre bundle displacement sensor, Applied Optics, 1996, no. 35, part 34, pp 6767-6774.

[64] L. Hoognboom, G. Hull-Allen, and S. Wangg, Theoretical and experimental analysis of a fibre optic proximity probe, Proc. SPIE, 1984, no. 478, pp 46-57.

[65] B. Hok, L. Tenerz, K. Gustafsson, Fibre-optic sensor: a micro-mechanical approach, Sensors and actuators, 1989, no. 17, pp 157-166.

[66] B. Culshaw, Fibre optic sensor: integration with micromachined devices, Sensors and actuator, 1995, vol. 46-47, pp463-469.

[67] A. domanski and T. Wolinski, Surface roughness measurement with optical fibres, 1992, IEEE Trans. Instrument measurement, Vol. 419, part 6, pp 1057-1061.

[68] Y. Yang and K. Yamazaki, Fibre optic surface topography measurement sensor and its design study, 2000, Precision engineering no. 24, pp 32-40.

[69] D. Spurgeon and R. Slater, In-process indication of surface roughness using a fibre-optics transducer, Proceedings of the 15th International machine tool design and research conference, 1974, vol. 15, pp 339-347.

[70] F. Lin, T. Shea, and K. Hoang, Measurement of surface roughness with a laser beam, Pre-print papers organised by national committee on manufacturing engineering of the institution of engineers, Australia, Barton, ACT: Institution of Engineers, Australia, Series title: National Conference Publication; no. 7717, 1977, Australia conference manufacturing. engineering, pp 132-133 1977.

[71] W. North, and A. Agarwal, Surface roughness measurement with fibre-optic, ASME J. Dynamic system. measurement control; 1983, Vol. 105 pp 295-297.

[72] J. Stou, Optical assessment of surface roughness, 1984, Precision engineering no. 6, part 1, pp 35-39.

[73] J. wyant, O. Kwon and C. Hayslett, Rough surface interferometer at 10.6 μm, 1980, Applied Optics 19, p. 1862.

[74] H. Wang, Theoretical analysis and measurement on near specular scattering, 1997, Optics Laser Engineering, no.27 part 3, pp285-296.

[75] Y. Zahide, and M. S. J. Hasmi, Surface roughness measurement using an optical system, 1999, Journal of material processing technology, no.88, pp10-22.

[76] M. Bennett and L. Mattson, Introduction to surface roughness and scattering, 1963, Optical Society of America.

[77] P. Beakmann , A. Spizzichino, The scattering of electromagnetic waves from rough surface, 1963, Pperogamon Press.

[78] C. Manuel, and A. Jose, System optical noncontact microtopography 1993, Appl. Opt, vol. 32, no. 25, pp 4860-4863.

[79] W. Welford, Optical estimation of statistical of surface roughness from light scattering measurements, Optics Quantum Electronic, 1977, no. 9, pp 269-287.

[80] C. Manuel, Surface inspection by an optical triangulation method, September 1996, Optical Engineering, vol. 35, part 9, pp 2743-2747.

[81] H. Hensler, Light scattering from fused polycrystalline aluminium oxide surface, Applied. optics, 1972, no. 11, part 11, pp2522-2528.

[82] C. Burrus and R. Dawson, Small-Area High-Current Density GaAs Electro-luminescent Diodes and a method of operation for Improved Degradation Characteristics, 1970, Applied Physics letters. vol. 17, pp. 97-98.

[83] B. Bruce, In introduction to fibre optics system design, Elsevier Science Publishers B. V., 1988, Netherlands.

[84] S. Ungar, Fibre optics theory and applications, 1990, John Wiley and Sons Ltd, UK.

[85] A. Chaimowicz, Optoelectronic-an introduction, 1989, Butterworth-Heinemann Ltd, Oxford.

[86] B. Cahill, M. El-Baradie, LED-based fiber-optic sensor for measurement of surface roughness, Journal of materials processing technology, no. 119, 2001, pp299-306.

[87] E. Uiga, Optoelectronic, 1995, Prentice Hall, Inc., New Jersey.

[88] Hoeywell, Fibre optic products, 1998, The Honeywell catalog 27.

[99] Fujikura Ltd, data unknow, Instruction Manual for the Optical Fibre Cleaver, Fujikura Ltd, Tokyo, Japan.

[90] C. Yeh, Handbook of fibre optics-theory and applications, 1990, Academic Press, Inc., San Diega, California.

[91] D. Sell, Laser control circuit, Feb. 22, 1977, U.S. Patent, no. 4, pp 009.385.

[92] National Instruments Corporation, AT-MIO/AI E Series Manual, National Instruments Corporation, 1997, Austin, Texas.

[93] National Instruments Corporation, Labview User Manual, National Instruments Corporation, 1997, Austin, Texas.

[94] http://www.natinst.com

[95] A Krau, U. Weimar and W. Gopel, Labview for sensor data acquisition, 1999, Trends in Analytical Chemistry, vol. 18, no. 5.

[96] http://www.cord.org/lev3.cfm/48

[97] J. Tompkins, G. Webster, Interfacing sensors to the IBM PC, 1988, Prentice Hall, Inc., New Jersey

[98] http://www.advancedphotonix.com/pinstory.htm

[99] M. Poterasu, M. Morales, J. Azpeitia, A laser system for high accuracy measurement of small apertures in mechanical parts, 2001, Optics and Lasers in Engineering, no.36, pp 545 –550.

[100] P. Das, Laser and optical engineering, 1991, springer-Verlag New York

[101] Z. Yong, L. Pengsheng, P. Zhaobang, Internal thread used for aerospace and its noncontact test method with fiber-optic sensor, 1999; SPIE no. 3740, pp 501-04.

[102] Z. Yilbas and M. S. J. Hashmi, An optical method and neural network. 1998, Optics and lasers in Engineering, no.29, pp 1-15

[103] W. Chen, B. Jiang, Pattern recognition 1991; no. 24, part 1 pp 57-67.

[104] D. Lowe. Artif Intell 1987; no. 20 pp 355-95.

[105] R. Davies. Machine vision theory algorithms practicalities, 1990, Academic Press, New York.

[106] C. Bastuchech, Proceedings on computer vision and pattern recognition, San Diego, 1989, pp 262-68.

[107] M. Rioux, A. Pugh,. Robot sensors, vol. 1-vision. IFS Publication Ltd., 1986. pp. 175-90, UK.

Appendix A

Fibre optic and electronic boxes design

A_1

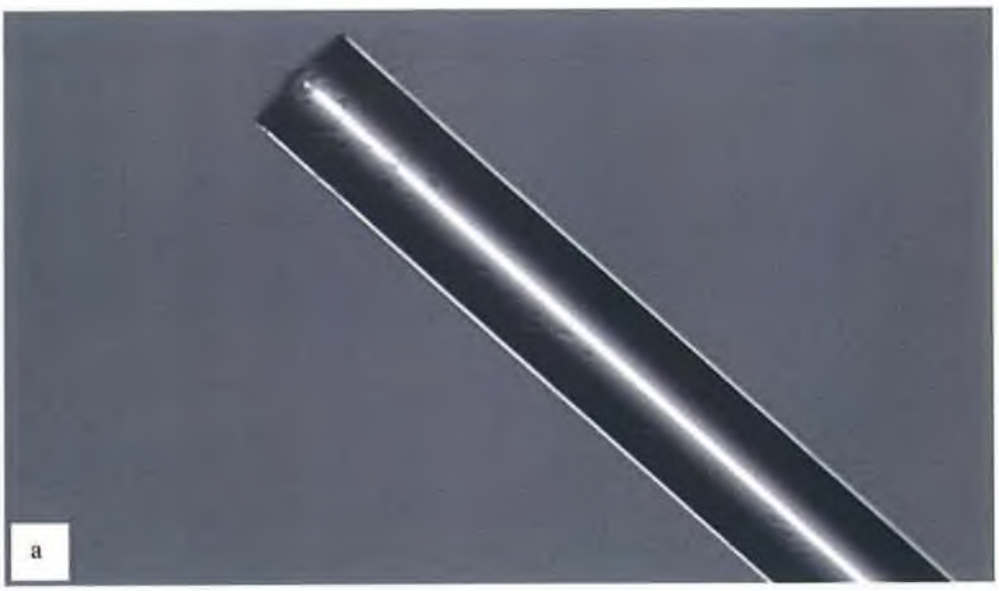

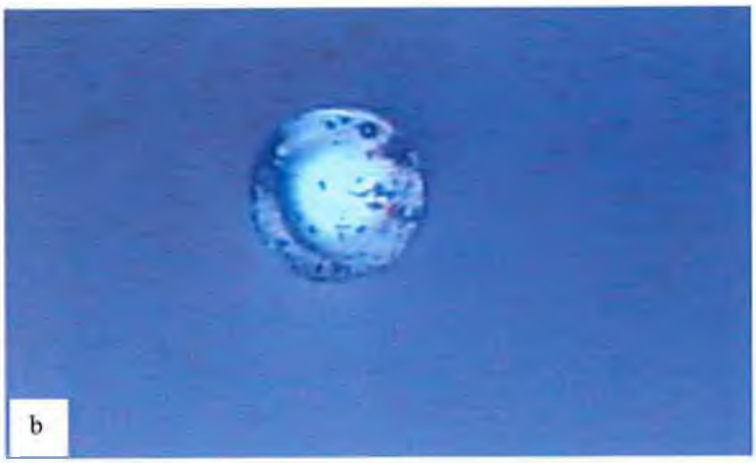

(a) Fibre Optic (b) Fibre optic end face core and cladding (E. microscope 40 M)

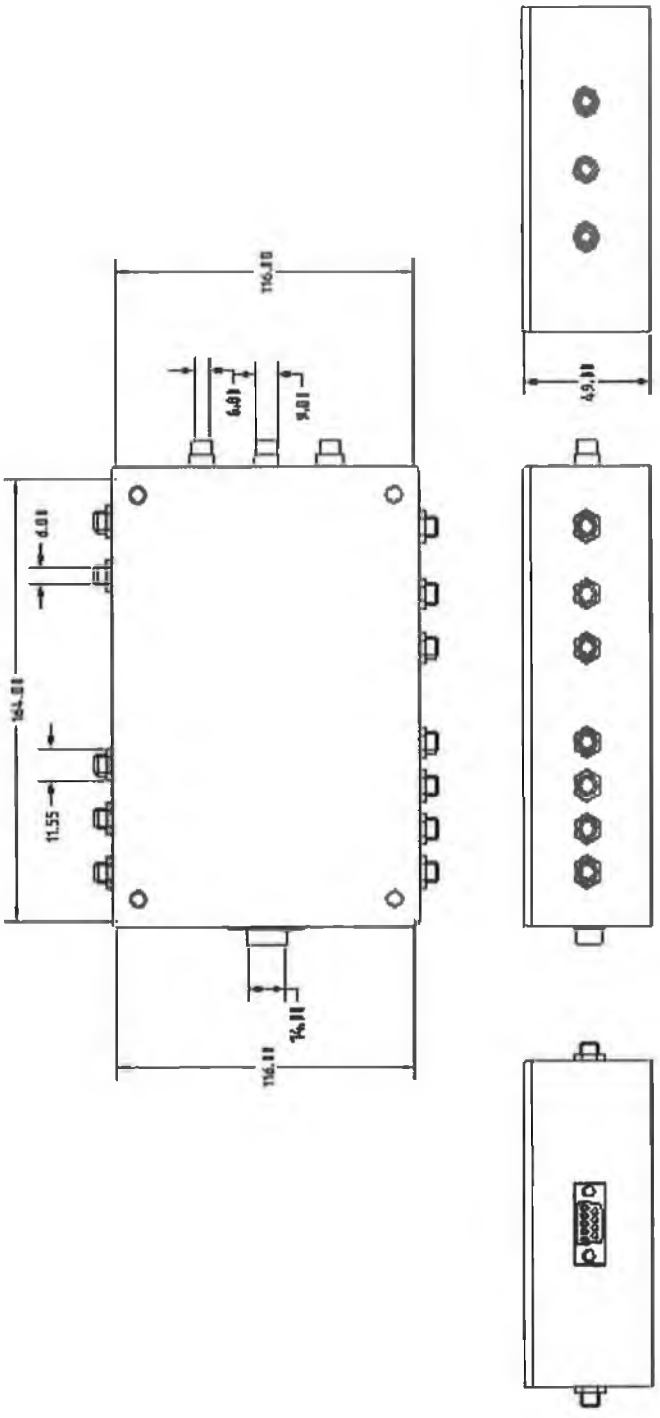

Dimensions of the main circuit box.

A_3

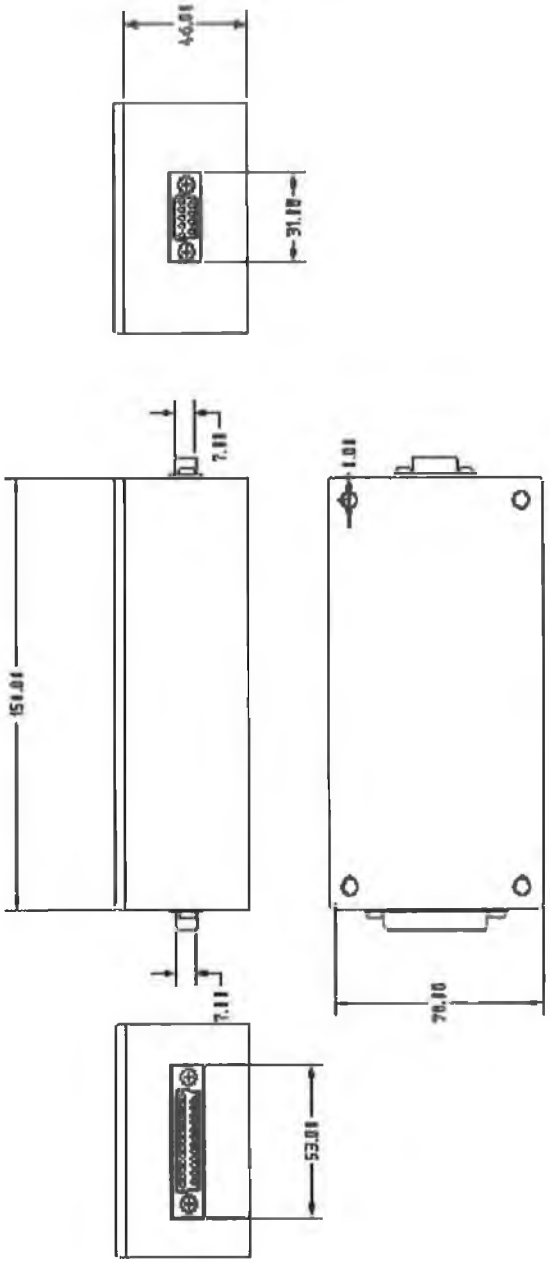

Dimensions of the divided circuit box.

Appendix B

Mechanical, electronic devices data sheet and material data sheet

B_1

Precision, Double-Row Ball Bearing Linear Stages

Key Features

- 0.16–3.15 in. (4–80 mm) of travel
- Low-profile design
- Steel construction for high stability and rigidity
- Double-row ball bearings for higher load capacity (except UMR12)
- Angular deviation better than 100-200 µrad
- Threaded micrometer mounting

Shown with optional M-PBN Base Plate. *Order actuators and base plates separately.*

UMR Series Linear Stages feature steel construction for high stability and rigidity. The ball bearings and precision-ground bearing surfaces provide exceptional linear travel, with angular deviation better than 100-200 µrad. UMR3, UMR5, and URM8 Series stages have double-row ball bearings making them an excellent choice for carrying high loads. UMR12 Series stages contain a single row of ball bearings. In all UMR stages, the moving carriage is preloaded by two springs to ensure constant micrometer contact for smooth, backlash-free motion.

Four stage sizes, each available in several travel ranges, allow you to closely match both your physical and performance requirements. UMR5, UMR8, and UMR12 have aperture versions available with a clear hole through the carrier and stage body. Apertures are very useful for positioning of optics, fiber optics, or cabled devices.

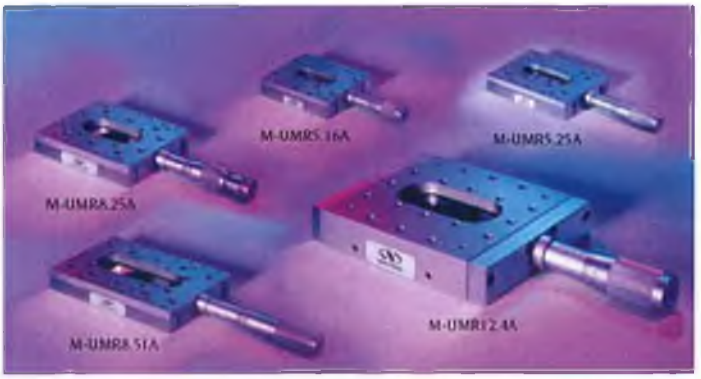

UMR stages are available with clear apertures for demanding applications. Actuators sold separately.

Phone: 1-800-222-6440 • Fax: 1-949-253-1680

UMR linear stage

Multi-axis stage configurations are easily assembled using UMR *stages and* EQ *Series angle brackets.*

Load Characteristics

Model	Cz (N)	+Cx (N)	-Cx (BM) (N)	-Cx (DM) (N)	a (mm)	ω (Nm)	Kαx (mrad/Nm)	Kαy (mrad/Nm)	Kαz (mrad/Nm)
UMR3.5	600	10	40	30	20	0.04	0.7	0.3	0.5
UMR5.5	600	12	40	30	22	0.05	0.1	0.2	0.2
UMR5.16	600	15	40	30	22	0.05	0.1	0.2	0.2
UMR5.25	600	11	40	30	22	0.05	0.1	0.2	0.2
UMR8.4	900	18	100	50	40	0.07	0.05	0.05	0.05
UMR8.25	900	17	100	50	40	0.07	0.05	0.05	0.05
UMR8.51	900	11	100		40	0.07	0.05	0.05	0.05
UMR12.40	400	35	450		70	0.08	0.02	0.02	0.02
UMR12.63	400	25	450		70	0.08	0.02	0.02	0.02
UMR12.80	400	20	450		70	0.08	0.02	0.02	0.02

Q	Off-center load must be ≤Cz/(1 + D/a)
Cz	Centered load capacity normal to bearing axis
D	Cantilever distance in mm
a	Bearing constant
-Cx	Load capacity parallel to bearing axis in the direction toward the micrometer (BM) or differential micrometer (DM)
+Cx	Load capacity parallel to bearing axis in the direction away from the actuator
ω	Drive torque for + Cx = 10 N
kαx	Angular stiffness (roll)
kαy	Longitudinal stiffness (pitch)
kαz	Transverse stiffness (yaw)

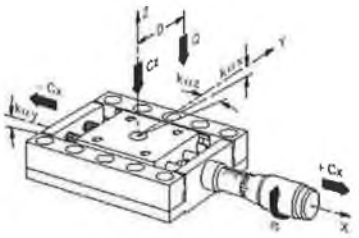

Related Products

- M-PBN *Base Plates*
- UTR *Rotation Stages*
- EQ *Series Angle Brackets*

Mounting Bridles aid in constructing complex systems (see the Accessories Section).

Continues

Model ADAPT-BM25-375

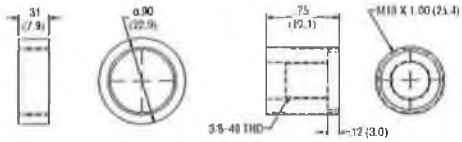

MODEL	THREAD A	THREAD B	DIMENSION C
	ENGLISH		
UMR3.5	4-40	8-32	0.500
	METRIC		MILLIMETERS
M-UMR3.5	M3	M4	12.5

Model UMR3.5

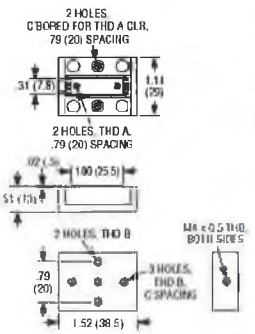

Model UMR8.4/8.25

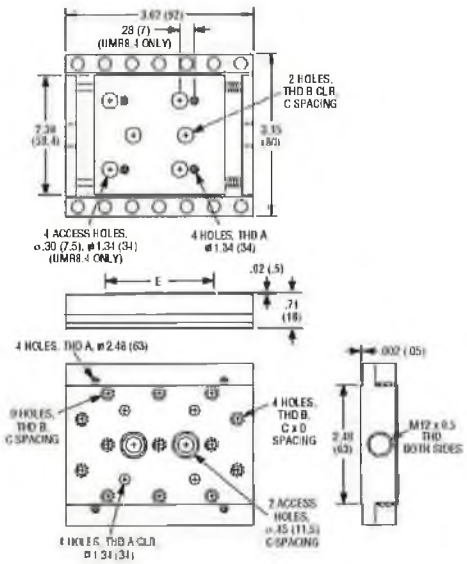

Model UMR8.51

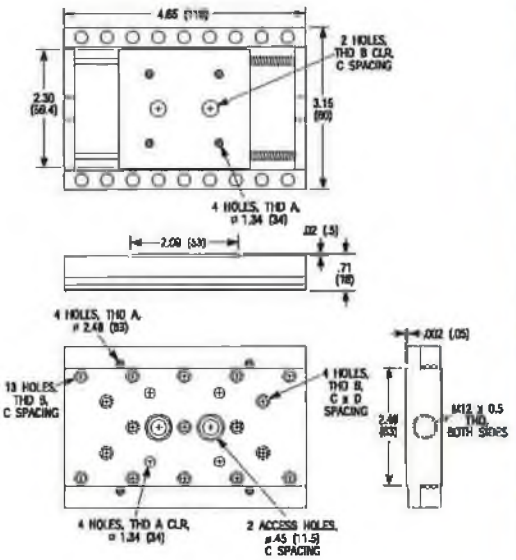

MODEL	THREAD A	THREAD B	DIMENSION C	DIMENSION D	DIMENSION E
	ENGLISH			INCHES	
UMR8.4	8-32	1/4-20	1.000	3.000	2.62
UMR8.25	8-32	1/4-20	1.000	3.000	2.09
UMR8.51	8-32	1/4-20	1.000	3.000	
	METRIC			MILLIMETERS	
M-UMR8.4	M4	M6	25.0	75.0	64
M-UMR8.25	M4	M6	25.0	75.0	53
M-UMR8.51	M4	M6	25.0	75.0	

Continues

B_2

BM Series

Micrometers

BM Series Micrometers feature micron-scale resolution and very smooth motion for precision positioning applications. Depending on the model, they are available in travel ranges from 4–80 mm and with axial load capacities from 40–450 N. Model designations correspond to the diameter of the control knob and the travel range. Turning the control knob one division represents a linear travel of 10 µm. **BM Series Micrometers are the standard choice of actuator on UMR and MVN Series Stages and on SL and SK Series Mirror Mounts.**

Specifications

Graduations	
BM11	20 µm
BM17, 25, 30, 32	10 µm
Sensitivity	1 µm

Ordering Information

Model	Travel (mm)	Load Capacity lb (N)
BM11.5	5	9 (40)
BM11.10	10	9 (40)
BM11.16	16	9 (40)
BM11.25	25	9 (40)
BM17.04N	4	23 (100)
BM17.25	25	23 (100)
BM17.51	51	23 (100)
BM25.40	40	100 (450)
BM25.63	63	100 (450)
BM30.10	10	90 (400)
BM32.80	80	100 (450)

Key Features

- *1 µm sensitivity*
- *4–80 mm travel*
- *Threaded mounting*
- *Steel construction*

Compatible with these stages:*

- UMR3 Series
- UMR5 Series
- UMR8 Series
- UMR12 Series
- MVN Series
- TGN Series

**in addition to our SL, SLA and SK Series optical mounts.*

BM Micrometer

Model BM30.10

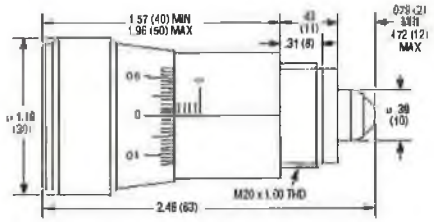

Model BM17.04N

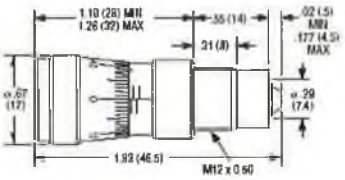

Model BM11, BM17.25, BM17.51, BM25, BM32.80

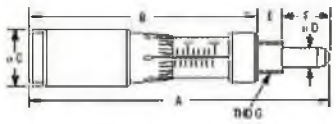

		DIMENSION (in. (mm))							
		B					F		
MODEL	A	MIN	MAX	C	D	E	MIN	MAX	G
BM11.5	1.35 (34.5)	1.00 (25.5)	1.20 (30.5)	0.43 (11)	0.16 (4)	0.13 (3.2)	0.03 (0.8)	0.23 (5.8)	M6 x 0.50
BM11.10	2.01 (51)	1.40 (35.5)	1.79 (45.5)	0.43 (11)	0.16 (4)	0.19 (4.7)	0.03 (0.8)	0.43 (10.8)	M6 x 0.50
BM11.16	2.24 (57)	1.40 (35.5)	2.03 (51.5)	0.43 (11)	0.16 (4)	0.19 (4.7)	0.03 (0.8)	0.66 (16.8)	M6 x 0.50
BM11.25	3.00 (76.2)	1.81 (46)	2.80 (71)	0.43 (11)	0.16 (4)	0.19 (4.7)	0.02 (0.5)	0.98 (25)	M6 x 0.50
BM17.25	3.25 (82.5)	1.95 (49.5)	2.93 (74.5)	0.67 (17)	0.28 (7)	0.28 (6.7)	0.05 (1.3)	1.04 (26.3)	M12 x 0.50
BM17.51	5.43 (138)	3.04 (77.1)	5.04 (128.1)	0.67 (17)	0.28 (7)	0.35 (9)	0.09 (2.4)	2.10 (53.4)	M12 x 0.50
BM25.40	5.04 (128)	2.78 (70.5)	4.35 (110.5)	0.98 (25)	0.31 (8)	0.67 (16.5)	0.12 (3)	1.69 (43)	M16 x 1.00
BM25.63	6.79 (172.5)	3.70 (94)	6.18 (157)	0.98 (25)	0.31 (8)	0.57 (14.5)	0.04 (1)	2.52 (64)	M16 x 1.00
BM32.80	8.25 (212)	4.17 (106)	7.32 (186)	1.26 (32)	0.47 (12)	0.94 (24)	0.08 (2)	3.23 (82)	M22 x 1.00

Continues

HFE4050

High Power Fiber Optic LED, Metal Package

FEATURES

- High power LED sends 410 µW into 100/140 micron fiber
- High speed: 85 MHz
- Rated to 100 mA forward current operation
- Metal can TO-46 type package
- Designed to operate with Honeywell fiber optic receivers
- Metal can, TO-18 package also available (HFE4070)

FIBER01.TIF

OUTLINE DIMENSIONS in inches (mm)

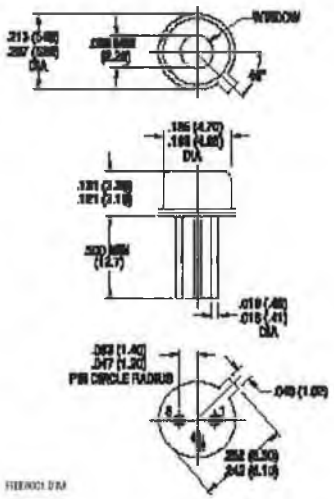

FIBER001.DWG

DESCRIPTION

The HFE4050 is a high radiance AlGaAs 850 nanometer LED optimized for coupling into small fiber core diameters at a forward current of 10 to$100 mA. The patented "Caprock"™ LED chip is designed to combine high power coupling with wide bandwidth. The peak wavelength is matched for use with Honeywell silicon fiber optic detectors and receivers.

APPLICATION

The HFE4050 is a high radiance LED packaged on a TO-46 header with a metal can. Data rates can vary from DC to above 85 MHz depending upon component application. The LED is designed for use in fiber optic communications. As the current varies (typically from 10 to 100 mA), the light intensity increases proportionally. Heat sinking is recommended to maintain the expected long life. If the HFE4050 is heat sinked, the package has a typical thermal resistance of 150°C per watt. If not heat sinked, typical thermal resistance is 300°C per watt.

The HFE4050 LED provides the maximum amount of radiance for the amount of forward current in the industry. A 0.25 mm diameter glass microlens over the "Caprock"™ junction collimates the light, increasing the intensity. Thus, greater power is directed toward standard fiber optic cables.

Pinout

1. Anode
2. Cathode
3. Case (ground)

Honeywell

High power fibre optic LED

HFE4050

High Power Fiber Optic LED, Metal Package

ELECTRO-OPTICAL CHARACTERISTICS(T_C = -40°C to +100°C unless otherwise stated)

PARAMETER	SYMBOL	MIN	TYP	MAX	UNITS	TEST CONDITIONS
Fiber Coupled Power [1]	P_{OC}					I_F = 100 mA, 50/125 micron, [2] 0.20 NA fiber, T = 25°C [3]
HFE4050-013		30	40		uW	
		-15.2	-14.0		dBm	
Over Temp. Range		20			µW	
		-17.0			dBm	
HFE4050-014		50	70		µW	
		-13.0	-11.5		dBm	
Over Temp. Range		33			uW	
		-14.8			dBm	
Forward Voltage	V_F	1.50	1.85	2.25	V	I_F = 100 mA
Reverse Voltage	B_{VR}	1.0	5.0		V	I_R = 10 µA
Peak Wavelength	λ_P	810	850	885	nm	I_F = 50 mA DC
Spectral Bandwidth (FWHM)	$\Delta\lambda$		50		nm	I_F = 50 mA DC
Response Time					ns	1 V Prebias, 100 mA peak [3]
T = 25°C, 10-90%	t_R		6	10		
T = 25°C, 90-10%	t_F		6	10		
Analog Bandwidth	BWE		85		MHz	I_F = 100 mA DC, sinusoidal modulation [3]
Po Temperature Coefficient	$\Delta P_O/\Delta T$		-0.02		dB/°C	I_F = 100 mA (over 25 to 125°C)
Series Resistance	rs		4.0		Ω	DC
Capacitance	C		70		pF	V_R = 0 V, f = 1 MHz
Thermal Resistance			150		°C/W	Heat sinked [3]
			300		°C/W	Not heat sinked

Notes

1. Dash numbers indicate power output. See ORDER GUIDE.
2. HFE4050 is tested using a 10 meter length of 50/125 µm dia. fiber cable, terminated in a precision ST ferrule. Actual coupled power values may vary due to alignment procedures and/or receptacle and fiber tolerances.
3. HFE4050 must be heat sinked for continuous I_F > 100 mA operation for maximum reliability (i.e. mounted in a metal connector with thermally conductive epoxy).

ABSOLUTE MAXIMUM RATINGS

(25°C Free-Air Temperature unless otherwise noted)

Storage temperature	-65 to +150°C
Case operating temperature	-55 to +125°C
Lead solder temperature	260°C, 10 s
Continuous forward current (heat sinked)	100 mA
Reverse voltage	1 V @ 10 µA
Case/cathode (anode) voltage	125 V

Stresses greater than those listed under "Absolute Maximum Ratings" may cause permanent damage to the device. This is a stress rating only and functional operation of the device at these or any other conditions above those indicated in the operational section of this specification is not implied. Exposure to absolute maximum rating conditions for extended periods of time may affect reliability.

FIBER INTERFACE

Honeywell LEDs are designed to interface with multimode fiber with sizes ranging from 50/125 to 200/230 microns. Honeywell performs final tests using 50/125 micron core fiber. All multimode fiber optic cables between 50/125 and 200/230 should operate with similar excellent performance. See table for typical powers.

TYPICAL COUPLED POWER (µW/dBm) ● I_F=100 mA

Dia.	Index	N.A.	-013	-014
8/125	Step	---	1.0/-30.0	1.8/-27.5
50/125	Graded	0.20	40/-14.0	70/-11.5
62.5/125	Graded	0.28	88/-10.6	153/-8.1
100/140	Graded	0.29	232/-6.4	406/-3.9

Honeywell

Continues

HFE4050

High Power Fiber Optic LED, Metal Package

ORDER GUIDE

Description	Catalog Listing
Standard screening, metal package, typical power out 40 µW	HFE4050-013
Standard screening, metal package, typical power out 70 µW	HFE4050-014

This package is also available in special interface receptacles for interfacing to standard fiber optic cables.

WARNING

Under certain application conditions, the infrared optical output of this device may exceed Class 1 eye safety limits, as defined by IEC 825-1 (1993-11). Do not use magnification (such as a microscope or other focusing equipment) when viewing the device's output.

CAUTION

The inherent design of this component causes it to be sensitive to electrostatic discharge (ESD). To prevent ESD-induced damage and/or degradation to equipment, take normal ESD precautions when handling this product.

Fig. 1 Typical Optical Power Output vs Forward Current

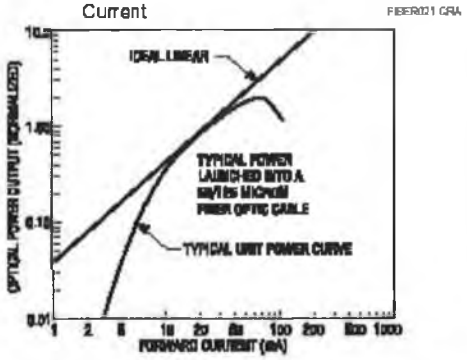

Fig. 2 Typical Spectral Output vs Wavelength

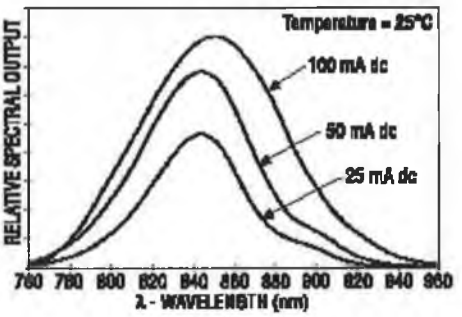

Fig. 3 Typical Optical Power Output vs Case Temperature

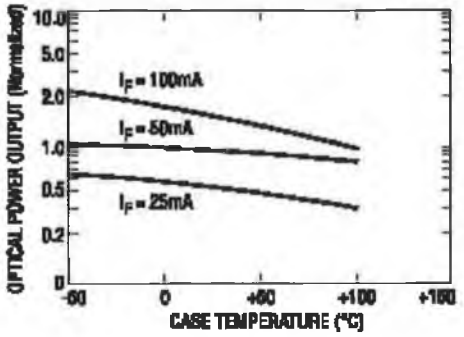

All Performance Curves Show Typical Values

Honeywell

Continues

HFD3002-002/XXX

Silicon PIN Photodiode

FEATURES

- Low capacitance
- High speed: t_r = 30 ns max. at V_R = 5 V; 10 ns max. at V_R = 15 V
- High responsivity
- Housing electrically isolated
- Wave solderable
- Mounting options
  - SMA single hole
  - ST single hole
  - SMA PCB
  - ST PCB
  - SMA 4 hole

DESCRIPTION

The HFD3002-002/XXX PIN Photodiode is designed for high speed use in fiber optic receivers. It has a large area detector, providing efficient response to 50 - 1000 mm diameter fibers at wavelengths of 650 to 950 nanometers.The HFD3002-002/XXX is comprised of an HFD3002 PIN photodiode which is mounted in a fiber optic connector which aligns the component's optical axis with the axis of the optical fiber.

The HFD3002-002/XXXs case is electrically isolated from the anode and cathode terminals to enhance the EMI/RFI shielding which increases the sensitivity and speed. The housing acts as a shield for the PIN photodiode component.

Honeywell

HFD3002-002/XXX

Silicon PIN Photodiode

ELECTRO-OPTICAL CHARACTERISTICS (T_C = 25°C unless otherwise stated)

PARAMETER	SYMBOL	MIN	TYP	MAX	UNITS	TEST CONDITIONS
Peak Response Wavelength	λ_P		850		nm	
Flux Responsivity [1]	R				A/W	λ = 850 nm
			0.6			50 µm core fiber, 0.20 µA
		0.45	0.6			100 µm core fiber, 0.28 µA
			0.55			200 µm core fiber, 0.40 µA
			0.30			1000 µm core fiber, 0.53 µA
Dark Leakage Current	I_D		0.05	2	nA	V_R = 5 V
Reverse Breakdown Voltage	B_{VR}	110	250		V	I_R = 10 mA
Package Capacitance	C		1.4		pF	V_R = 5 V, f = 1 MHz
Rise Time	t_R				ns	
10-90%			17	30		V_R = 5 V
			5	10		V_R = 15 V
			1			V_R = 90 V
Field of View	FoV		85		Degrees	

Notes

1. Responsivity is measured with a fiber optic cable centered on the mechanical axis, using an 850 nm LED as the optical source to the fiber.

ABSOLUTE MAXIMUM RATINGS

(Tcase = 25°C unless otherwise noted)

Storage temperature	-65 to +150°C
Operating temperature	-55 to +125°C
Lead solder temperature	260°C for 10 s
Case/cathode (anode) voltage	110 V
Power dissipation	200 mW
Reverse voltage	110 V

Stresses greater than those listed under "Absolute Maximum Ratings" may cause permanent damage to the device. This is a stress rating only and functional operation of the device at these or any other conditions above those indicated in the operational section of this specification is not implied. Exposure to absolute maximum rating conditions for extended periods of time may affect reliability.

Honeywell

Continues

HFD3002-002/XXX

Silicon PIN Photodiode

ORDER GUIDE

Description	Catalog Listing
Standard silicon PIN photodiode	HFD3002-002/XXX

MOUNTING OPTIONS

Substitute XXX with one of the following 3 letter combinations

SMA single hole	- AAA
ST single hole	- BAA
SMA PCB	- ABA
ST PCB	- BBA
SMA 4 hole	- ADA

Dimensions on page 441

CAUTION

The inherent design of this component causes it to be sensitive to electrostatic discharge (ESD). To prevent ESD-induced damage and/or degradation to equipment, take normal ESD precautions when handling this product.

FIBER INTERFACE

Honeywell detectors are designed to interface with multimode fibers with sizes (core/cladding diameters) ranging from 50/125 to 200/230 microns. Honeywell performs final tests using 100/140 micron core fiber. The fiber chosen by the end user will depend upon a number of application issues (distance, link budget, cable attenuation, splice attenuation, and safety margin). The 50/125 and 62.5/125 micron fibers have the advantages of high bandwidth and low cost, making them ideal for higher bandwidth installations. The use of 100/140 and 200/230 micron core fibers results in greater power being coupled by the transmitter, making it easier to splice or connect in bulkhead areas. Optical cables can be purchased from a number of sources.

Fig. 1 Rise/Fall Time vs Reverse Bias Voltage

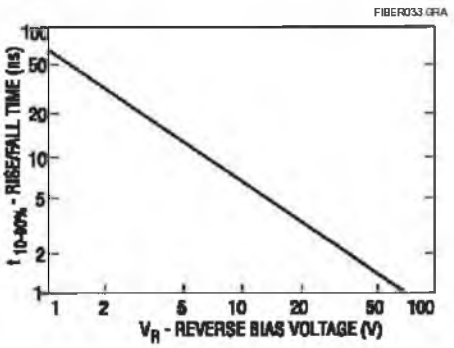

Fig 2 Package Capacitance vs Reverse Bias Voltage

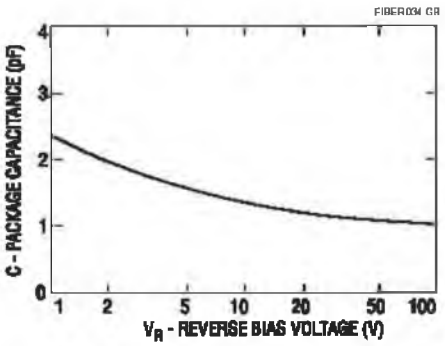

Honeywell

Continues

HFD3002-002/XXX

Silicon PIN Photodiode

Fig. 3 Spectral Responsivity

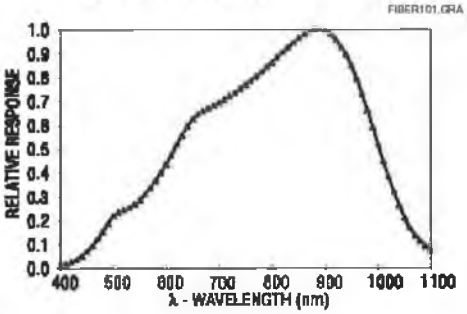

Fig. 4 Dark Leakage Current vs Temperature

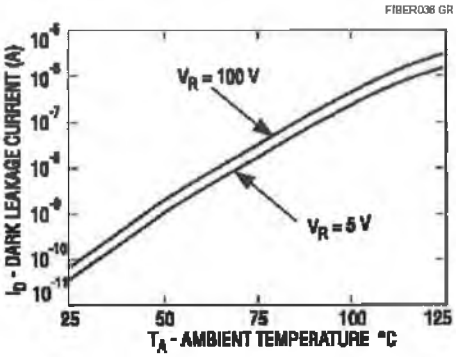

Fig. 5 Angular Response

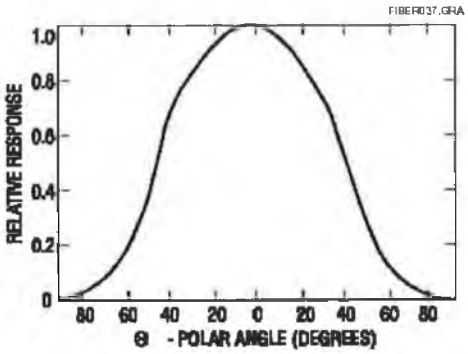

Honeywell

Continues

MITSUBISHI (OPTICAL DEVICES)

FU-17SLD-F1

FC-CONNECTORIZED MODULE

DESCRIPTION

FU-17SLD-F1 is FC-connectorized devices designed to be used with singlemode optical fiber.
This module is the optimum light source for medium haul digital optical communication systems.

FEATURES

- FC connectorized package
- High optical output
- Low threshold current
- Built-in photodiode for output monitoring
- Wide operating temperature range (-40°C to +85°C)
- MQW* active layer
- FSBH** structure fabricated by all MOCVD process

*Multiple quantum well
**Facet selective-growth buried heterostructure

APPLICATION

FitL,LAN

ABSOLUTE MAXIMUM RATINGS (Tc=25°C)

Parameter		Symbol	Conditions	Rating	Unit
Laser diode	Optical output power from fiber end (Note1)	Pf	CW	2.5	mW
	Reverse voltage	Vrl	-	2	V
Photodiode for monitoring	Reverse voltage	Vrd	-	15	V
	Forward current	Ifd	-	2	mA
Operating case temperature		Tc	-	-40~+85	°C
Storage temperature		Tstg	-	-40~+85	°C

Note 1. Singlemode fiber master plug with mode field diameter 9.5μm

Laser diode (1300 nm)

ELECTRICAL/OPTICAL CHARACTERISTICS (Tc=25°C, unless otherwise noted)

Parameter	Symbol	Test Conditions	Limits			Unit
			Min.	Typ.	Max.	
Threshold current	Ith	CW	3	7	15	mA
Operating current	Imod	CW	8	-	28	mA
Operating Voltage	Vop	CW ,If=Ith+Imod (Note 2)	-	1.2	1.6	V
Optical output power from fiber end (Note 3	Pf	CW, If=Ith+Imod	1	-	-	mW
Center wavelength	λ_C	CW, If=th+Imod	1285	1300	1330	nm
Rise and fall time(LD)	tr, tf	Ib=Ith, 10~90% (Note4)	-	0.3	0.5	ns
Tracking error (Note 5)	Er	Tc=-40~85°C, CW.APC	-	0.5	-	dB
Differential efficiency (Note 3)	η	-	-	0.07	-	mW/mA
Monitor current	Imon	CW, If=ith+Imod, Vrd=5V	0.2	0.9	1.5	mA
Dark current (Photodiode)	Id	Vrd=5V	-	0.1	0.5	μA
Capacitance (Photodiode)	Ct	Vrd=5V, f=1MHz	-	-	20	pF

Note 2. If : Forward current (LD)

3. Singlemode fiber master plug with mode field diameter 9.5μm
4. Ib : Bias current (LD)
5. Er=MAX|10×log(Pf(Tc)/Pf(25°C))|

Continues

OUTLINE DIAGRAM

(Unit : mm)

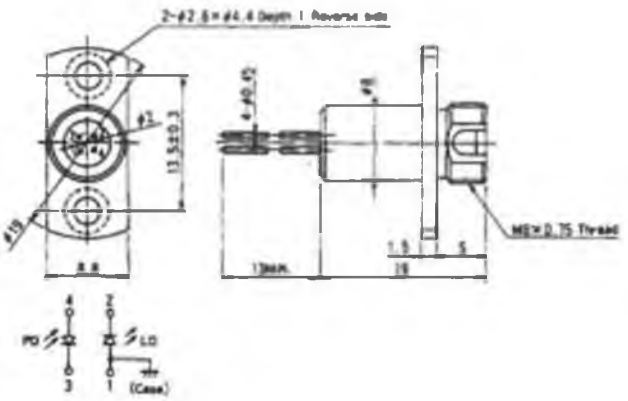

FU-17SLD-F1

Continues

EG&G OPTOELECTRONICS Canada

C30616, C30637, C30617, C30618
High-Speed InGaAs Photodiodes

DATASHEET

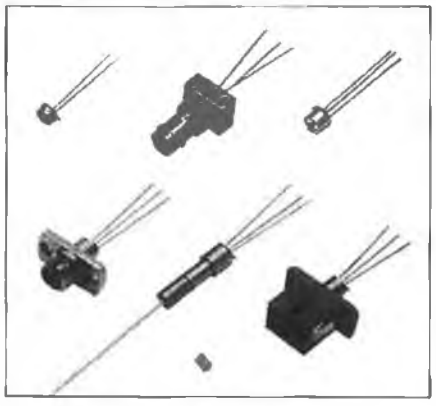

Features:

- 50, 75, 100, 350 µm diameters
- High responsivity at 1300 and 1550nm
- Low capacitance for high bandwidths (to 3.5 GHz)
- Available in various package options

Applications:

- High-speed communications
- SONET/ATM, FDDI
- Datalinks & LANs
- Fiber optic sensors

Product Information

High-speed InGaAs photodiodes from EG&G are designed for use in OEM fiber optic communications systems and high-speed receiver applications including trunk line, LAN, fiber-in-the loop and data communications. Ceramic submount packages are available for easy integration into high-speed SONET, FDDI, or datalink receiver modules, or as back-facet power monitors in laser diode modules.

Photodiodes are available in hermetic TO-18 packages, or in connectorized receptacle packages with industry standard ST, FC or SC connectors. These are designed for mating to either single or multimode fibers. Photodiodes are also available in a fibered package with either single or multimode fiber pigtail, which can be terminated with either an ST, FC or SC connector. Connectorized and fibered packages use a ball-lens TO-18 package to maximize coupling efficiency. All devices are planar passivated and feature proven high reliability mounting and contacting. An MTTF of $>10^9$ hours ($\sim 10^5$ years) at 50°C has been demonstrated to date from standard production samples.

Quality and Reliability

EG&G is committed to supplying the highest quality product to our customers, and we are certified to meet ISO-9001 and operate to MIL-Q-9858A and AQAP-1 quality standards. Process control is maintained through annual re-qualification of production units and includes extensive electrical, thermal and mechanical stress as well as an extended lifetest. In addition every wafer lot is individually qualified to meet responsivity, capacitance and dark current specifications, and reliability is demonstrated with an extended high temperature burn-in at 200°C for 168 hours (V_R=10V), ensuring an MTTF$>10^7$ hours at 50°C (E_A=0.7eV). Finally all production devices are screened with a 16 hour, 200°C burn-in (V_R=10V) and tested to meet responsivity, spectral noise and dark current specifications.

High speed InGaAs photodiode

Specifications *(at $V_R = V_{OP}$ (typical), 22 °C)*

Parameter	C30616 Min	C30616 Typ	C30616 Max	C30637 Min	C30637 Typ	C30637 Max	UNITS
Active Diameter		50			75		µm
Responsivity @ 1300nm ceramic TO-18	0.80	0.90		0.80	0.90		A/W
fiber/FC/ST/SC[1]		-			-		
Responsivity @ 1550nm ceramic/TO-18	0.85	0.95		0.85	0.95		A/W
fiber/FC/ST/SC[1]		-			-		
Dark Current		<1.0	2.0		<1.0	2.0	nA
Spectral Noise Current (10kHz, 1.0Hz)		<0.02	0.15		<0.02	0.15	pA/√Hz
Capacitance @ $V_R = V_{OP}$ (typ) ceramic		0.35	0.55		0.40	0.60	pF
TO-18		-			-		
Rise/Fall Time (10% to 90%)		0.07	0.5		0.07	0.5	ns
Bandwidth (-3dB, $R_L = 50\Omega$)		3.5			3.5		GHz
Available package types		D1			D1		-

Operating Ratings

Parameter	C30616 Min	C30616 Typ	C30616 Max	C30637 Min	C30637 Typ	C30637 Max	UNITS
Operating Voltage	1	5	10	1	5	10	V
Breakdown Voltage	25	100		25	100		V
Maximum Forward Current			10			10	mA
Power Dissipation			100			100	mW
Storage Temperature	-60		125	-60		125	°C
Operating Temperature	-40		125	-40		125	°C

[1] Coupled from 62.5 µm, 0.28 NA, graded index multi-mode fiber using 1300 nm SLED source.

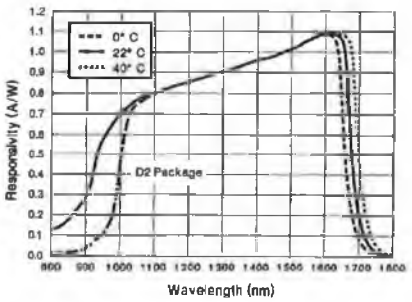

Figure 1: Typical spectral responsivity vs. wavelength. Dotted line shows response in D2 package (with silicon window).

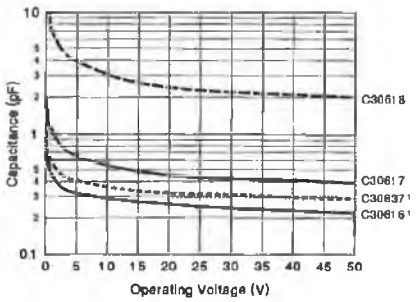

Figure 2: Typical capacitance vs. operating voltage.
Note 1: Ceramic submount.

Continues

Specifications *(at $V_R = V_{OP}$ (typical), 22 °C)*

Parameter	C30617 Min	C30617 Typ	C30617 Max	C30618 Min	C30618 Typ	C30618 Max	UNITS
Active Diameter		100			350		µm
Responsivity @ 1300nm ceramic TO-18	0.80	0.90		0.80	0.90		A/W
fiber/FC/ST/SC[1]	0.65	0.75		0.65	0.75		
Responsivity @ 1550nm ceramic/TO-18	0.85	0.95		0.85	0.95		A/W
fiber/FC/ST/SC[1]	0.70	0.80		0.70	0.80		
Dark Current		<1.0	2.0		2.0	5.0	nA
Spectral Noise Current (10kHz, 1.0Hz)		<0.02	0.15		0.02	0.20	pA/√Hz
Capacitance @ $V_R = V_{OP}$ (typ) ceramic		0.6	0.8		4.0	6.0	pF
TO-18		0.8	1.0		4.0	6.0	
Rise/Fall Time (10% to 90%)		0.07	0.5		0.5	1.0	ns
Bandwidth (-3dB, $R_L = 50\Omega$)		3.5			0.75		GHz
Available package types		D1, D2, D3, D4, D5 D6, D8, D9, D10, D21			D1, D2, D3, D4, D21		-

Operating Ratings

Parameter	C30617 Min	C30617 Typ	C30617 Max	C30618 Min	C30618 Typ	C30618 Max	UNITS
Operating Voltage	1	5	10	0	5	10	V
Breakdown Voltage	25	100		25	80		V
Maximum Forward Current			10			10	mA
Power Dissipation			100			100	mW
Storage Temperature[2]	-60		125	-60		125	°C
Operating Temperature[2]	-40		125	-40		125	°C

[2] Maximum storage and operating temperature for connectorized and fibered devices is +85°C

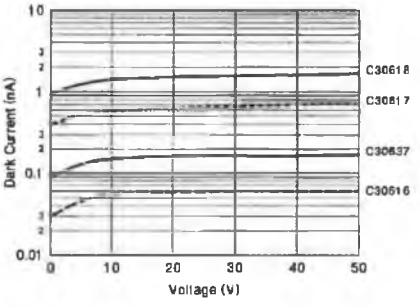

Figure 3: Typical dark current vs. voltage.

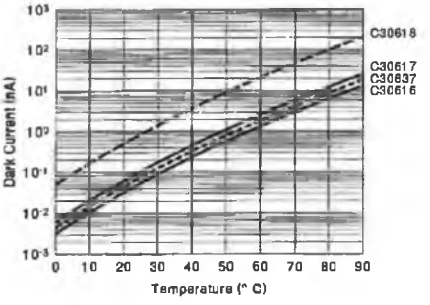

Figure 4: Typical dark current vs. temperature at V_{op} = -5V.

Continues

Ordering Guide

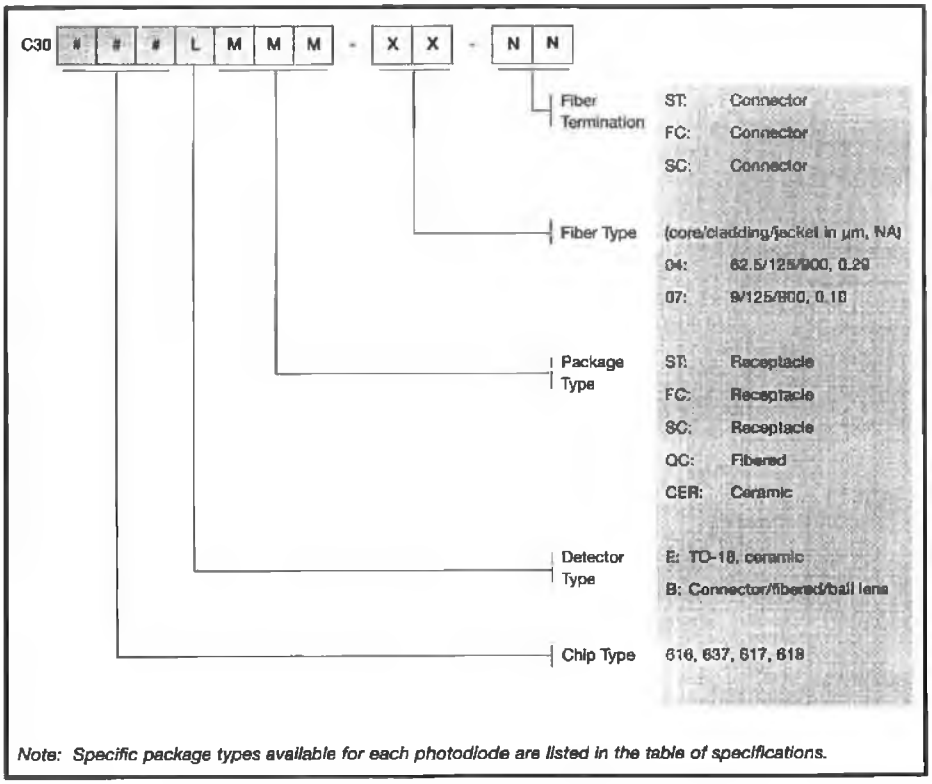

Note: Specific package types available for each photodiode are listed in the table of specifications.

For further information please contact your local EG&G Optoelectronics Canada representative or EG&G Optoelectronics Canada, 22001 Dumberry Road, Vaudreuil, Quebec J7V 8P7 Canada
Tel: (514) 424-3300 **Fax:** (514) 424-3411

East Coast Sales Office
221 Commerce Drive
Montgomeryville, PA, 18936
Tel: (215) 368-4003 **Fax:** (215) 362-6107

West Coast Sales Office
23832 Rockfield Blvd, Suite 235
Lake Forest, CA, 92630
Tel: (714) 583-2250 **Fax:** (714) 583-2277

EG&G OPTOELECTRONICS CANADA

Printed in Canada ED-0019/07/94

Continues

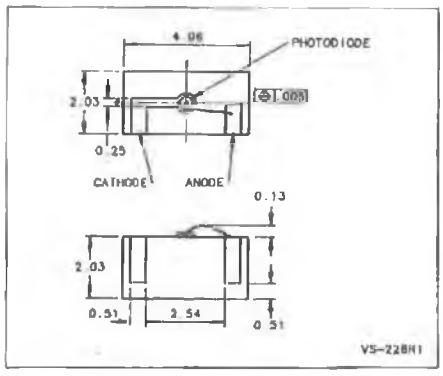

Figure 5: Package D1: Ceramic Submount.

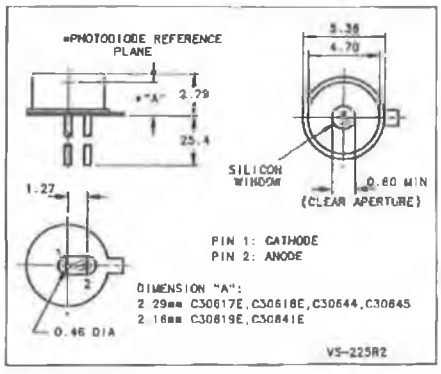

Figure 6: Package D2: TO-18 low profile with silicon window.

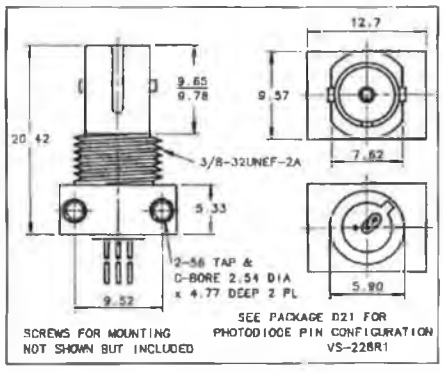

Figure 7: Package D3: ST detector module.

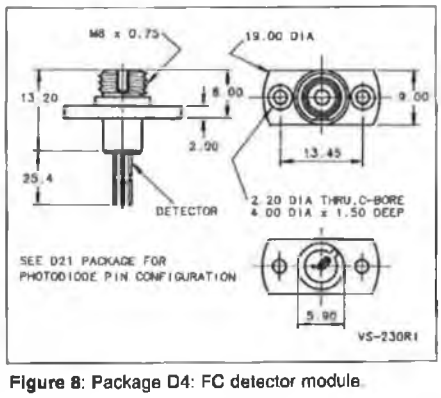

Figure 8: Package D4: FC detector module.

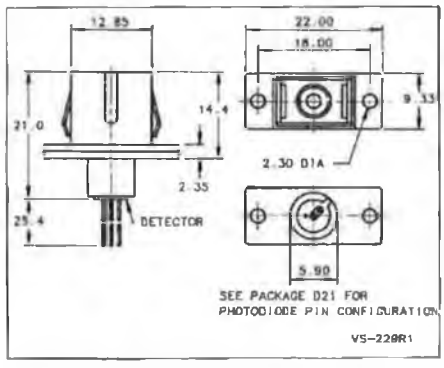

Figure 9: Package D5: SC detector module.

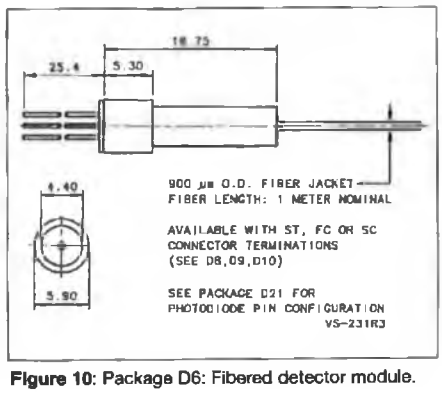

Figure 10: Package D6: Fibered detector module.

Continues

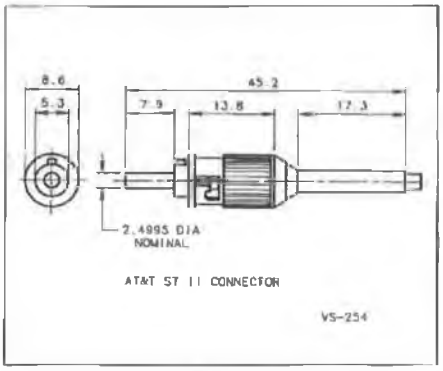

Figure 11: Termination D8: ST connector.

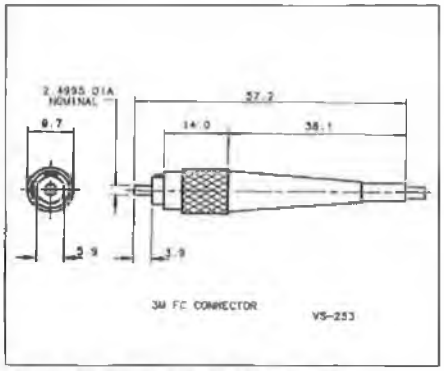

Figure 12: Termination D9: FC connector.

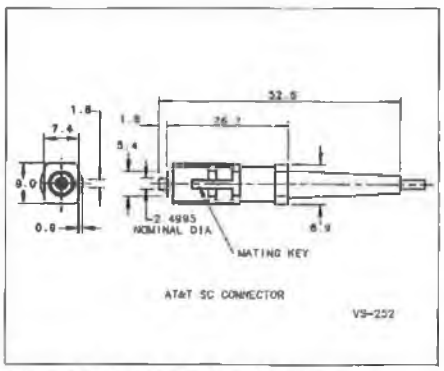

Figure 13: Termination D10: SC connector.

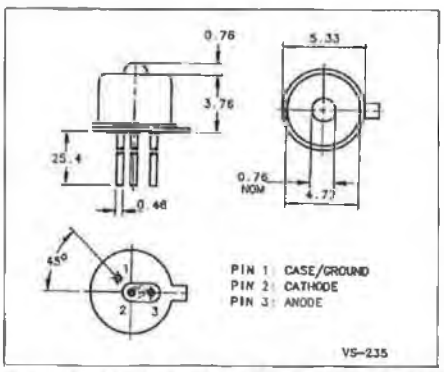

Figure 14: Termination D21: TO-18 ball-lens package.

See back page for ordering information and guide.

Continues

B_7

Package Dimensions

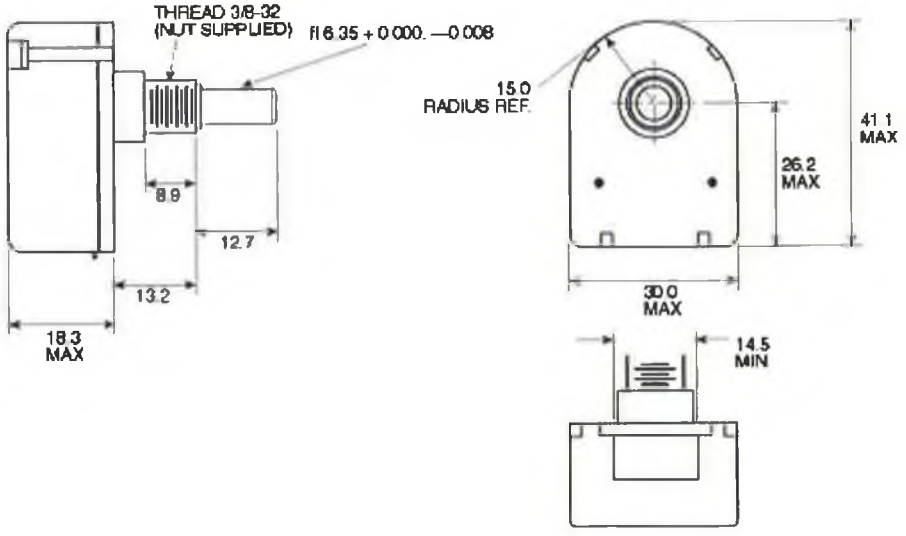

Rotary sensor

B_8

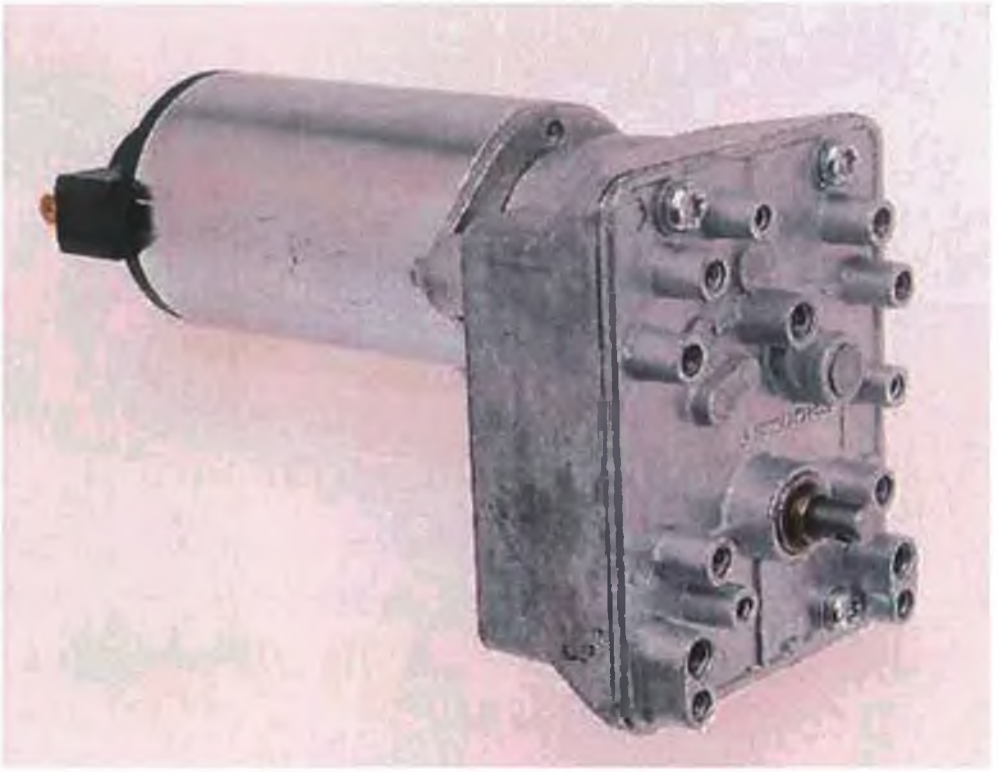

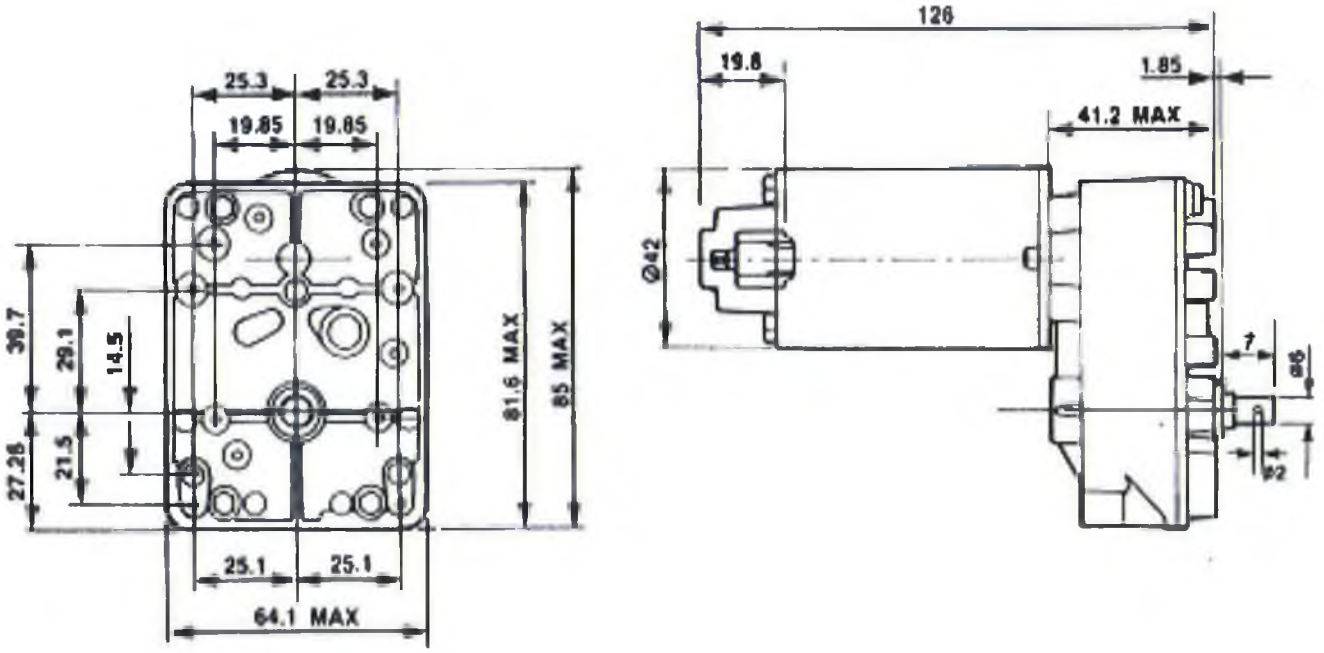

Motor guide

Data Pack G *Issued March 1997* **232-3614**

Data Sheet

Engineering materials

This data sheet is intended as a guide for users of engineering materials and will be useful for selection of the correct material for various applications.

Plastic Stock

	Nylon 66	Nylatron™ GS	Acetal (Copolymer)	PTFE	Polyethylene (UHMW)	PVC
Tensile strength (kgf/cm^2)	630/840	700/980	620	120/240	220/250	422-528
Elongation (%)	20/200	5/150	60	100/300	450	20
Modulus of elasticity (kgf/cm^2)	17,500/28,000	31,600/42,000	28,800	3,500/8,500	5,000	2,500
Hardness (Rockwell R)	112-120	110-125	120			
(Shore D)	80-85	86-90		60-65	64-67	65-80
Flexural strength (kgf/cm^2)	880-940	1,100-1,300	915		270	714
Deformation under load 140 kgf/cm^2 at 50°C after 24hrs (%)	1.0-3.0	0.5-2.5	1.0			—
Impact strength – IZOD 23°C (kgf cm/cm notch	5.4	3.4	6.5	18	No break	4-10
Linear thermal expansion coefficient 30-100°C/C	100 5×10^{-6}	63 5×10^{-6}	95 5×10^{-6}	100-120 5×10^{-5}	200 5×10^{-4}	5-10 5×10^{-5}
Melting point °C	260	260	165	327	135/138	—
Flammability	Self extinguishing	Self extinguishing	Slow burning	Non flammable	Slow burning	Self extinguishing
Thermal conductivity (Kcal/m hr °C)	0.21	0.21	0.2	0.22	0.36	0.18
Deflection temp °C at 4.6 kgf/cm^2 / 18.6 kgf/cm^2	204 / 93	204 / 93	158 / 110	132 / 49	95	60-82 / 60-77
Permitivity 50-10^6 Hz	3.4/4.1	3.5/4.2	3.7	2.0/2.1	2.3	2.8-4.0
Dielectric strength (kV/mm)	>12	>12	>16	>24	>28	>20
Volume resistivity (ohm.cm)	$>10^{13}$	$>10^{13}$	$>10^{14}$	$>10^{18}$	$>10^{17}$	$>10^{16}$
Chemical resistance	Resists common solvents and hydrocarbons, esters ketones aqueous solutions of acids and alkalis between ph5 and ph11 Not resistant to phenols, cresols, formic acid, conc mineral acid and alkalis, strong oxidising agents including halogens		As Nylon 66 but slightly more prone to attack	Only attacked by molten or dissolved alkali, metals and some fluorine compounds at high temperature	All commonly used chemicals Not resistant to strong oxidising acids Aromatic or halogenated hydrocarbons may cause slight swelling	Good resistance to dilute acids and alkalis Fair resistance to alcohols, greases and oils, concentrated acids and halogens Poor resistance to ketones and aromatic hydrocarbons
Specific gravity (g/cm^3)	1.14-1.15	1.14-1.16	1.4-1.42	2.1-2.3	0.94	1.30-1.60
Water absorption (%) 24hr	0.6-1.5	0.5-1.3	0.22	0.01	Non-absorbent	<0.4
(%) Saturation	7-9	6-8	0.80	<0.02		N/A
Applications	Gears, seals, bearings, valve seats, bushes, washers, wheels, spacers, rollers, gaskets, cams, insulators, nuts, screws	Bearings, rollers, bushes, sleeves, gears, cams, valve seats, wheels, thrust washers	Bearings, impellers, bushes, gears, meter components, pump housing, valve and valve seating, tap washers and parts, lawn sprinkler parts, windscreen washer parts, cistern valves and bushes, carburettor components	Co-axial parts, bearing bushes, repetition turned parts, insulators, gaskets and rollers, components for food, manufacturing and chemical industries	Chemical tanks and vessels, electronic components, hospital equipment, valves, pumps and fans, photographic equipment, ducting	Chemical plant, tanks, ducting electrical components, aircraft fitments, valves and pumps, photographic equipment

The data are typical values and are not intended to represent specifications. Nylatron™ is a registered trade mark of Polypenco Ltd.

232-3614

Plastic Stock (cont'd)

Acrylic

Density (DIN 53 479)	g/cm³	1.18
Tensile strength (DIN 53 455)	N/mm²	70
Crushing stress (DIN 53 454)	N/mm²	103
Flexural strength (DIN 53 452)	N/mm²	120
Impact strength (DIN 53 453)	kJ/m²	11
Notched impact strength (DIN 53 453)	kJ/m²	2
Creep rupture strength (DIN 53 444)	N/mm²	28
Ball indentation hardness (DIN 53 456) H 961/30	N/mm²	190
Module of elasticity (DIN 53 457)	N/mm²	3300
Thermal conductivity	W/m°C	0.19
Spec heat	Ws/g°C	1.5
Lin. coeff. of therm. expan	1/°C	70×10^{-6}
Heat distortion temperature Vicat method (DIN 53 460)	°C	100
Heat distortion temperature Martens method	°C	72
Refractive index 20°C (DIN 53 491)	°D	1.491
Water vapour permeability	g.cm/gm²hPg	$4.5\ 10^{-13}$
Dielectric constand E 50Hz (DIN 53 483)	—	3.7
Dielectric Hz loss factor 1MHz	—	0.06 0.03
Dielectric strength (DIN 53 481)	kV/mm	30
Spec. resistance (DIN 53 482)	Ω cm	10^{15}
Surface resist after 24 hours water immersion	Ω cm	-10^{13}
Light transmission	%	92
Flammability DIN 4102 Teil 1	—	B2
Flammability UL94	mm/min	94 HB
Applications		Illumination signs, sanitary ware, machine guards, models/ prototypes, screens/ windows, catering equipment, name plates, covers

Tufnol™ Carp brand

Sheet: Cross breaking strength		kgf/cm²	1530
Impact strength, notched, Charpy		kJ/m²	8.6
Compressive strength, flatwise		kgf/cm²	3570
Compressive strength, edgewise		kgf/cm²	2040
Resistance to flatwise compression		%	1.4
Shear strength, flatwise		kgf/cm²	1070
Water absorption 50mm² sections oven dried then left in water for 24 hours	1.6mm	mg	55
	3mm	mg	70
	6mm	mg	90
	12mm	mg	125
Electric strength, flatwise in oil at 90°C	1.6mm	MV/m	7.2
	3mm	MV/m	4.9
	6mm	MV/m	4.0
Electric strength, edgewise in oil at 90°C		kV	23
Insulation resistance after immersion in water		ohms	7×10^{6}
Relative density		—	1.36
Maximum working temperature	continuous	°C	120
	intermittent	°C	130
Thermal classification		—	E
Thermal conductivity through laminae		W/(mK)	0.37
Thermal expansion in plane of laminae		$\times 10^{-6}$/K	1.9
Specific heat		kJ/(kgK)	1.5
Round rods: Flexural strength		kgf/cm²	1734
Water absorption		mg/cm³	2.5
Insulation resistance after immersion in water		ohms	5×10^{8}
Axial electric strength in oil at 90°C		kV	15
Relative density		—	1.35
Applications			Fine pitched gears, precision components, electrical test jigs

Test methods for Tufnol as BS 2572, BS 5102 or BS 3953
Tufnol™ is a registered trade mark of Tufnol Ltd

Continues

Plastic Stock (cont'd)

ABS (acrylonitrile butadiene styrene)

Properties	Test condition DIN	ISO IEC	ASTM		Unit	Values	Applications
Mechanical							
1 Tensile strength	53455	R 527	D 638	N/mm²	45		Easily vacuum formed it is an ideal material for making trays, covers, housings, cases, etc
2 Yield strength	53455	R 527	D 638	N/mm²	45		
3 Tensile strength at break	53455	R 527	D 638	N/mm²	34		
4 Elongation at yield	53455	R 524	D 638	%	3		
5 Elongation at maximum load	53455	R 524	D 638	%	3.5		
6 Elongation at break	53455	R 527	D 638	%	14		
7 Youngs-modulus	53457	R 524	D 638	N/mm²	2350		
8 Shear modulus	53445	R 537	D 2236	N/mm²			
9 Flexural stress	53452	R 178	D 790	N/mm²	70		
10 Impact strength at 23°C	53453	R 179		kJ/m²	without break		
11 Impact strength at –40°C					70-80		
12 Impact strength notched 23°C	53453	R 179		kJ/m²	12		
13 Impact strength notched –40°C							
14 Izod impact strength notched at 23°C		R 180	D 256	J/m			
15 Indentation hardness	53456	–	–	N/mm²	80	H_{30}	
16 Rockwell hardness	–	–	D 785/A	–			
Thermal							
17 Vicat softening point – VST	53460	R 306		°C	93	Process B	
18 ISO/R 75 process A	53461	R 75	D 648	°C			
19 ISO/R 75 process B	53461	R 75	D 648	°C			
20 Continuous working temperature				°C	90		
21 Thermal coefficient of linear expansion				10^{-4}/K	9		
22 Thermal conductivity between –40° and +80°C	52612			W/Km	0.087		
23 Spec/Heat				kJ/kgK	2.4		
Electrical							
24 Dielectric constant at 1MHz	53483	IEC 250	D 150	–	2.9	dry	
25 Dissipation factor	53483	IEC 250	D 150	–	0.011	dry	
26 Spec. volume resistivity	53482	IEC 167	D 257	Ωcm	2×10^{15}	dry	
27 Surface resistivity	53482	IEC 167	D 257	Ω	6×10^{12}	dry	
28 Dielectric strength	53481	IEC 243	–	kV/mm	31	dry	
29 Resistance of tracking	53480		–	level			
Physical							
30 Water absorption proc. A	53495	R 62	D 570	%	0.3		
31 Density	53479	R 1183	D 792	g/cm³	1.04-1.06		

Polycarbonate

Properties	Test method	Units	Values	Applications
Mechanical				Suitable for general glazing applications which are vulnerable to vandalism or accidents. Other applications include machine guards/shields, safety visors and light fittings.
Tensile stress at yield	DIN 53455	N/mm²	60	
Elongation at break	DIN 53455	%	>100	
Tensile modulus of elasticity	DIN 53457	N/mm²	2300	
Unnotched impact strength (Charpy)	DIN53453	kJ/m²	no break	
Notched impact strength: Charpy	DIN 53453	kJ/m²	>30	
Izod	ASTMD 256	J/m	600-800	
Thermal				
Glass transition temperature		°C	140	
Thermal conductivity	DIN 52612	W/km	0.21	
Coeff. of linear thermal expansion, average value between 0 and 60°C		K^{-1}	65×10^{6}	
Heat deflection temperature under load acc. to ISO/R75 method A: 1.81N/mm²	DIN53461	°C	135-140	
Max. service temperature in air:				
for short periods		°C	145	
continuously		°C	120	
Min. service temperature		°C	–100	
Flammability				
acc. to ASTM (oxygen-index)	ASTM D 2863	%	25	
acc. to UL 94: 1.5mm thick sheet	UL94	rating	V-2	
6mm thick sheet	UL94	rating	V-0	
acc. to French standard: 3mm thick sheet		rating	M3	
acc. to British standard: surface spread of flame test 4mm thick sheet	BS476 Part 1	rating	Class O	
Electrical				
Dielectric strength	DIN 53481	kV/mm	>30	
Volume resistivity	DIN 53482	Ohm.cm	$>10^{16}$	
Surface resistivity	DIN 53482	Ohm	$>10^{15}$	
Dielectric constant at 10^3 Hz	DIN 53483	–	3	
Dissipation factor tg δ at 10^3 Hz	DIN 53483	–	0.001	
Tracking resistance	DIN 53480	rating	KC 250-300	
Physical				
Density	DIN 53479	g/cm³	1.2	
Moisture absorption: saturated at 23°C/50% RH		%	0.15	
Index of refraction n_D at 20°C	DIN 53491		1.585	

continues

232-3614

Non-ferrous metals

	Brass	Copper	Aluminium	Phosphor Bronze
Chemical analysis	BS2874/CZ121M Copper 56.5/58.5 Lead 2.5/4.5	BS2870/C101 BS2874/C101 Copper 99.90 Lead 0.005 Bismuth 0.0010	BS1474/1987 HE30 Si 0.7-1.3 Ni - Fe 0.5 Zn 0.20 Cu 0.1 Bi - Mn 0.40-1.0 Pb - Mg 0.8-1.2 Ti 0.10 Cr 0.25 Al remainder BS1470 SIC (1987) Si 0.05 Ni 0.10 Fe 0.05 Zn 0.10 Cu 0.05 Bi - Mn - Pb - Mg - Ti 0.05 Cr - Al remainder	BS1400:1985:PBI-C Sn 10.0-11.5% Zn 0.05 max % Pb 0.25 max. % P 0.50-1.00% Ni 0.10 max % Fe 0.10 max % Si 0.02 max % S 0.05 max. % Cu * *The percentage of copper present shall be the remainder of the analysis. Apart from the main elements (copper, tin and phosphorus) the total of residual elements shall not exceed 0.80%
Mechanical properties	Tensile strength 400 N/mm²	Rod/Bar: Tensile strength 240 N/mm² Sheet Tensile strength soft 210 h-hard 240	0.2% proof stress N/mm² 270 (TF) Tensile strength N/mm² 310 (TF)	0.2% proof stress N/mm² 170-280 Tensile strength N/mm² 360-800 Elongation on 5.65/S. 6-26% Hardness HB 100-150
Description and application	Machining quality Free turning brass - limited cold working properties	Rod and bar: high conductivity, corrosion resistant, malleable. Silver increases the softening temperature and has negligible effect on conductivity. Used for electrical conductors and also cold heading applications. Sheet: high conductivity copper. General purpose electrical applications. Also used for presswork.	Rod and bar: good resistance to atmospheric attack. Good formability. Very good machinability. Very suitable for inert gas welding, fair for oxy gas and resistance welding. Offers good suitability for protection anodising. Sheet: very good resistance to atmospheric attack. Very good formability. Fair machinability. Very suitable for inert gas, oxy gas and resistance welding. Very suitable for anodising.	Tube: Produced by continuous casting, the material possesses high mechanical strength, is of consistent quality with freedom from porosity. Machining qualities are excellent. Typical applications include bearings, bushes, thrust washers, gears, worm wheels. For bearing applications involving high work loads, high speeds and impact loading, hardened shafts or journals are advised.

TF = Material which has been solution treated and precipitation treated. The information contained in this data sheet should be treated as a guide only. Data compiled with assistance from Polypenco Ltd, Macreadys, Tufnol Ltd and Righton Ltd.

continues

Ferrous metals

	Ground flat stock	Silver steel	Key steel	Stainless steel
Chemical analysis	% min. % Max Carbon 0 85 1 00 Silicon — 0 40 Manganese 1 10 1 35 Chromium 0 40 0 60 Tungsten 0 40 0 60 Vanadium — 0 25	% min. % Max Carbon 0 95 1 25 Manganese 0 25 0 45 Silicon — 0 40 Chromium — 0 50 Sulphur — 0 045 Phosphorus — 0 045	% max. % Max *Permitted variation Carbon 0 26 0.34 ±0.03 Manganese 0 60 1 00 ±0.04 †Silicon — — — Sulphur — 0 050 +0 008 Phosphorus — 0 050 +0 008 †Silicon content depends on whether the steel is rimming, balanced or killed. *Variations in analysis permissible within the specification	BS970 – Part 1 1983 303 S31 – rod BS970 – Part 1 1983 316 S31 – bar/sheet % max. unless range stated Carbon 0.12 0.07 Manganese 2 0 2 0 Silicon 1 0 1 0 Sulphur 0 15/0 35 0 030 Chromium 17 0/19 0 16 5/18 5 Phosphorus 0.060 0.045 Molybdenum 1 00 2 00/2 50 Nickel 8.0/10.0 10 5/13 5
Characteristics	A high quality electrically melted alloy tool steel, ground to close tolerances. It can be easily hardened by oil quenching and possesses excellent dimensional stability. The high carbon content, in conjunction with chromium, gives good wear resistance. Material removal during grinding ensures that the ground flat stock is free of decarburisation	Silver steel is a high carbon tool steel ground to very close tolerances. It is so called because of the highly polished appearance created by the extremely fine surface finish. The high carbon content of this steel means that it can be hardened to give considerable wear resistance and the chromium content increases strength and hardenability. It is readily machinable as supplied in the annealed condition	A medium carbon bright drawn steel possessing tensile strengths in the range 35/45tsi. This key steel complies with BS40: Part 1: 1958 'Keys and Keyways'	303 S31 – An austenitic free cutting steel. Contains additional sulphur to induce free machine properties and has a high corrosion resistance. Non-magnetic 316 S31 – A very high corrosion resistant steel due to additional molybdenum. Non-magnetic
Typical applications	Widely used in tool rooms for applications where a close tolerance ground steel is required. Suitable for gauges, dies, punches, jigs, templates, cams and machine parts	Punches, dowels, mandrels, spindles, shafts, gauges, collets, knurls, lathe centres, engraving tools, etc	Square parallel keys. Square taper, gib-head and plain keys	303 S31 – Used for automatic turning, boring, cutting, etc 316 S31 – Used for photography, food, chemical, marine equipment etc
Tolerances	Imperial sizes: Width –0 000in +0 005in Thickness ±0 001in Length Nominal	Rounds Imperial sizes Below .005in ±0 00025in .005in and over ±0 0005in	Imperial sizes of key steel are drawn to plus tolerances (BS46) Squares <1in –0 000in +0 002in Metric sizes of key steel are drawn to minus tolerances (BS4235): Squares +0.0mm –0 030mm	
Heat treatment	Annealing 760-780°C Hardening 780-820°C Tempering 150-300°C Ground flat stock is supplied annealed. Figures below show hardness values at selected tempering degrees Temp (°C) . Hardness (Rc) 150 62 200 60-61 250 58-59 300 56-58	Hardening: heat to 770-790°C and when thoroughly soaked through, quench in water. (Sizes up to ¾in dia. May be oil hardened from 800-810°C.) Tempering: tempering should be carried out immediately after hardening in the range 150-300°C according to the hardness required. The figures below show what can be achieved. Temp. (°C) Hardness (Rc) 120 65-63 150 64-62 200 62-61 250 59-58 300 58-55 350 54-53 400 50-48	—	—
Mechanical properties	—	—	Size Tensile Elongation (mm) Strength N/mm² % min <19 540-695 8	—

continues

continues

232-3614

Shim stock

	Shim steel: (cold rolled steel strip)	Brass shim: (cold rolled brass strip)	Plastic shim:
Chemical analysis	% min. % Max. Carbon — 0.12 Manganese — 0.60 Silicon — 0.050 Phosphorus — 0.050	Copper 62.0-65.0% Lead 0.30% (max) Iron 0.20% (max) Zinc* Remainder *The percentage of zinc present shall be the remainder of the analysis except that the total impurities (excluding lead) shall not exceed 0.50%	0.002in to 0.010in polyester 0.015in and 0.020 in polypropylene
Characteristics	Complies with the requirements of BS1449: Part 1 Specification for carbon and carbon-manganese plate, sheet and strip. It is cold rolled and the surface finish falls within the BR category ie. bright finish	Complies with BS2870: CZ 108 common brass. It is produced by the cold rolling process and the edges are rotary sheared. The surface finish is of a high quality, free from blemishes and with tolerances controlled to close limits.	Polyester has a high tensile strength of up to 276MPa and has an excellent resistance to moisture and most chemicals. Polypropylene has a tensile strength of 25MPa and is resistant to aqueous solutions of non-oxidising or inorganic compounds, most alcohols, ketones and mineral oils.
Typical applications	Shims for tolerance compensation, alignment, end play adjustment, washers, small pressing and a wide range of uses in tool rooms, maintenance, shops, etc.	Shim stock is used in toolrooms, maintenance workshops, prototype shops and production departments for a range of applications such as alignment, end play adjustment, tolerance and wear compensation.	Coloured coded plastic shims are an effective replacement for metal shims of various descriptions.
Tolerances	Thickness Tolerance ± Up to and including 0.006in 0.006in Over 0.006in up to and including 0.015in 0.010in	Thickness Tolerance ± Up to and including 0.006in 10% Over 0.006in up to and including 0.010in 0.0006in 0.015in 0.0008in	Thickness Tolerance ± Up to and including 0.004in ±10% Over 0.005in up to and including 0.010in ±5% 0.015in and 0.020in ±10%
Physical properties	Tensile strength N/mm² 540 Hardness VPN min 165	Tempers and VPN hardness: Temper Hardness VPN Soft 80 max Quarter hard 75-110 Half Hard 110-135 Hard 135-165 Extra hard 165min	Polyester: Impact strength 2350N-cm/mm Density 1.377 Moisture absorption <0.8% (Immersion for 24 hrs at 23°C) Polypropylene: Impact strength 240psi Specific gravity 1.395-1.405 Moisture absorption 0.6% (prolonged immersion)

Continues

Appendix C

Electronic circuits design, Photographs (System and materials samples) and Mechanical main parts design

C_1

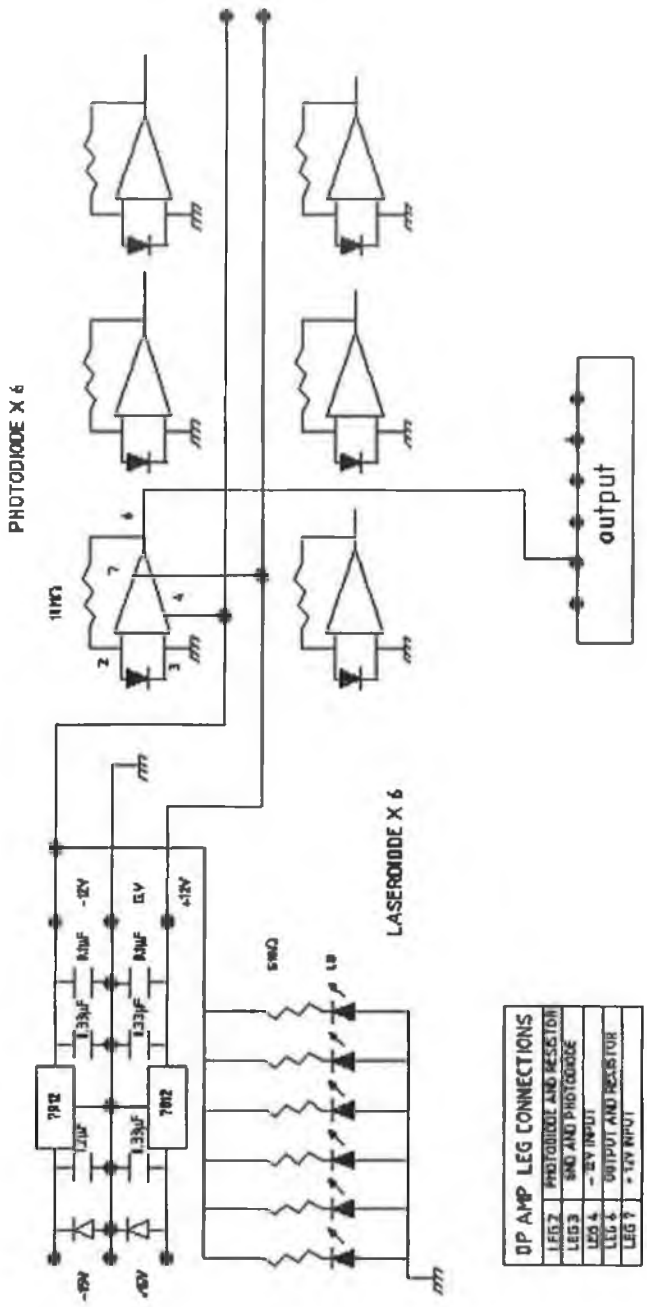

Electronic main circuit

C_2

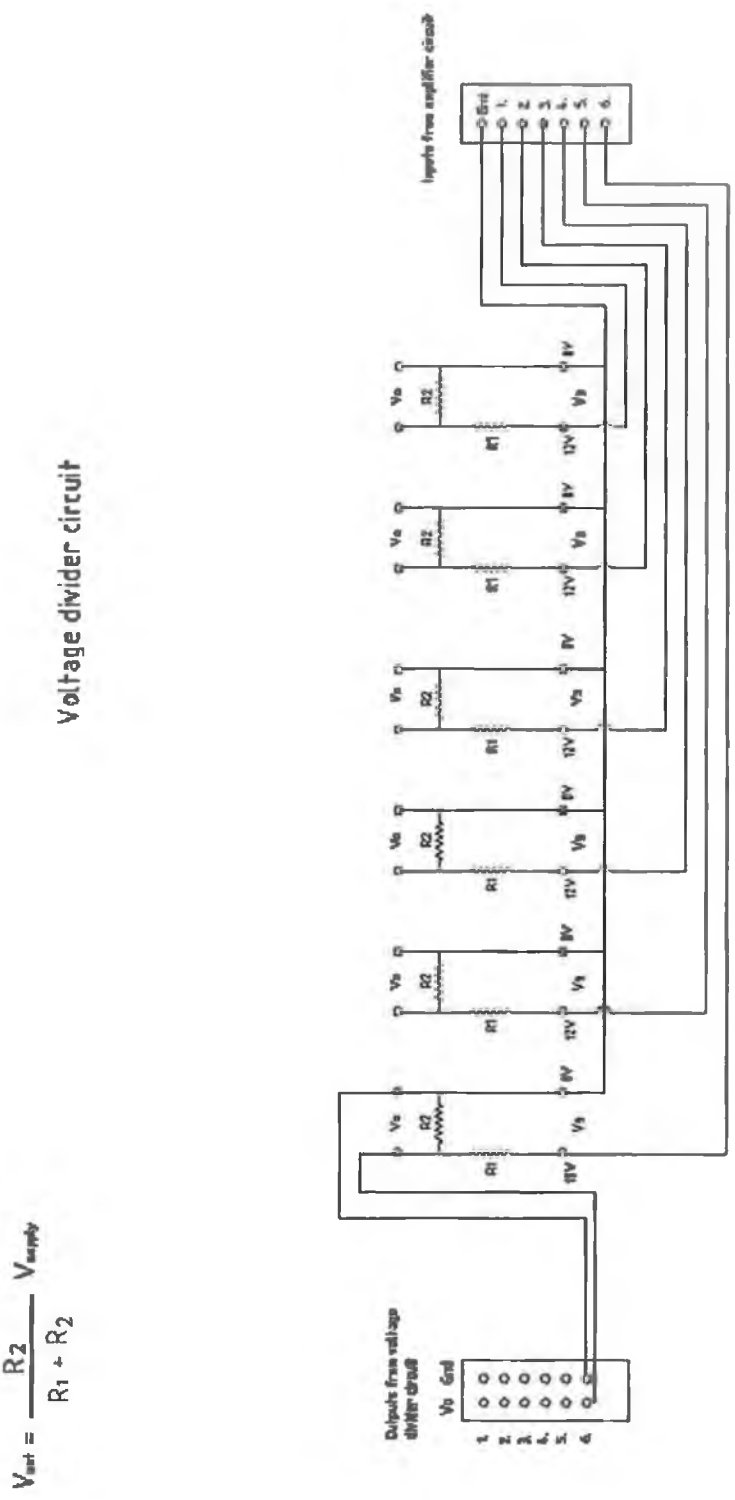

Electronic divided circuit

C_3

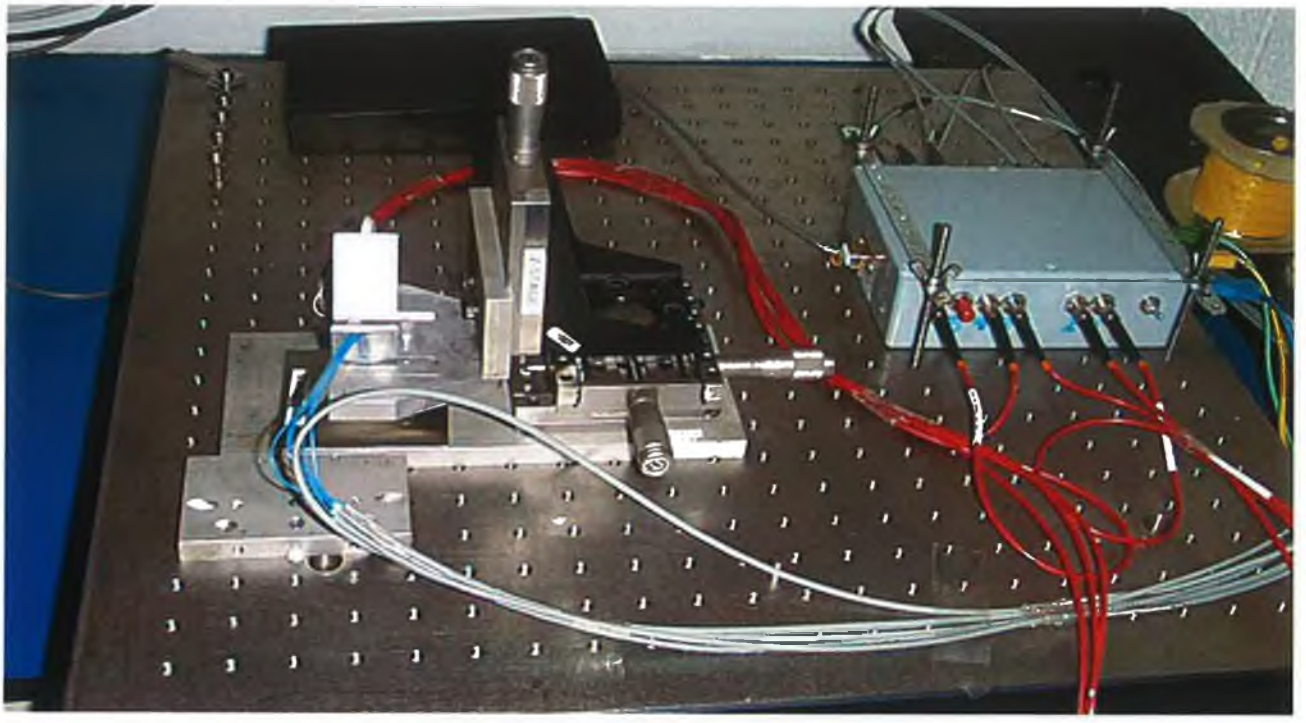

The experimental rig (two side views)

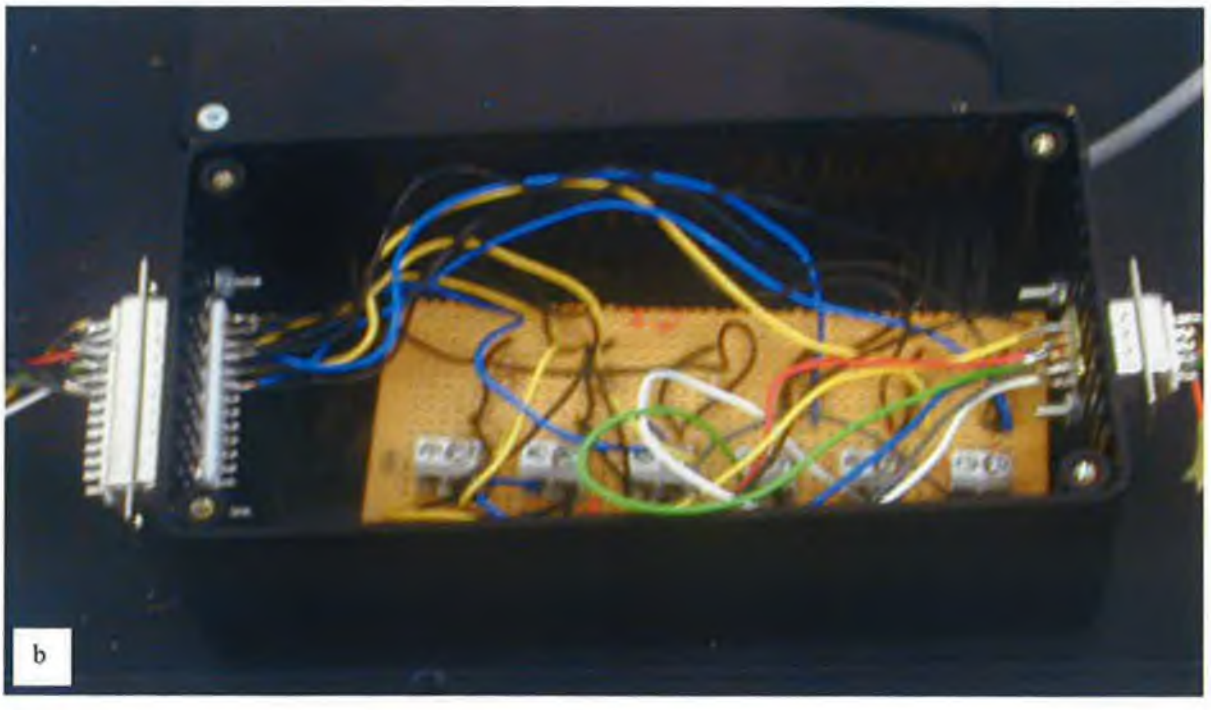

Continues

(a) data acquisition card, (b) the electronic divided circuit.

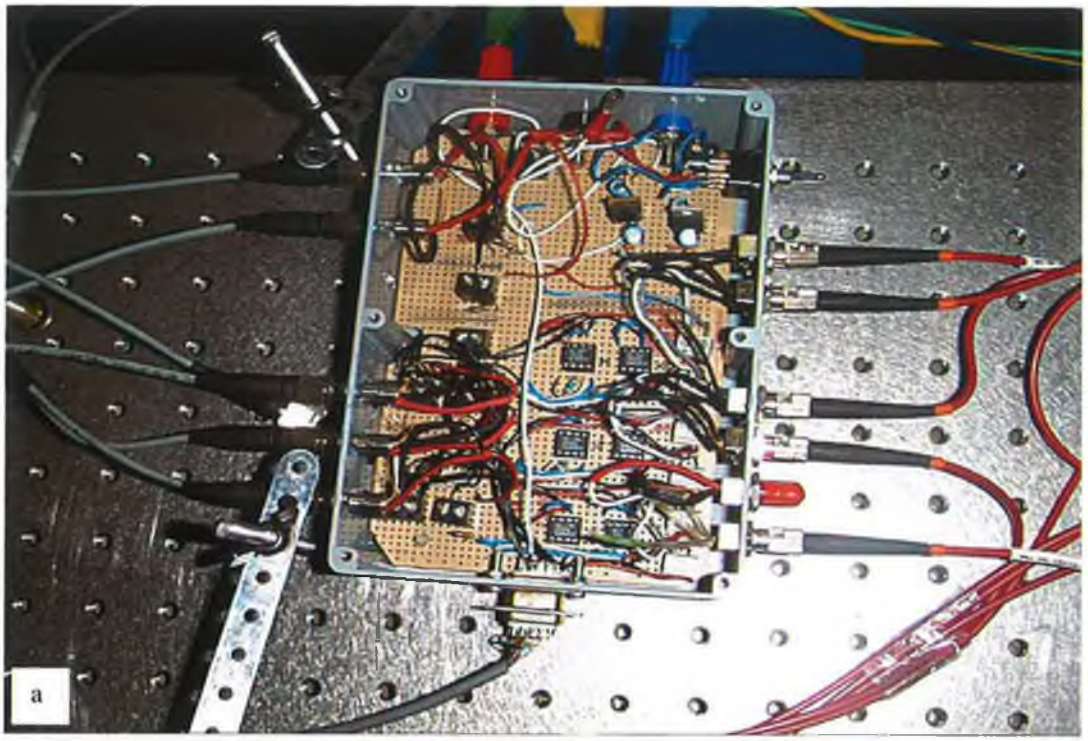

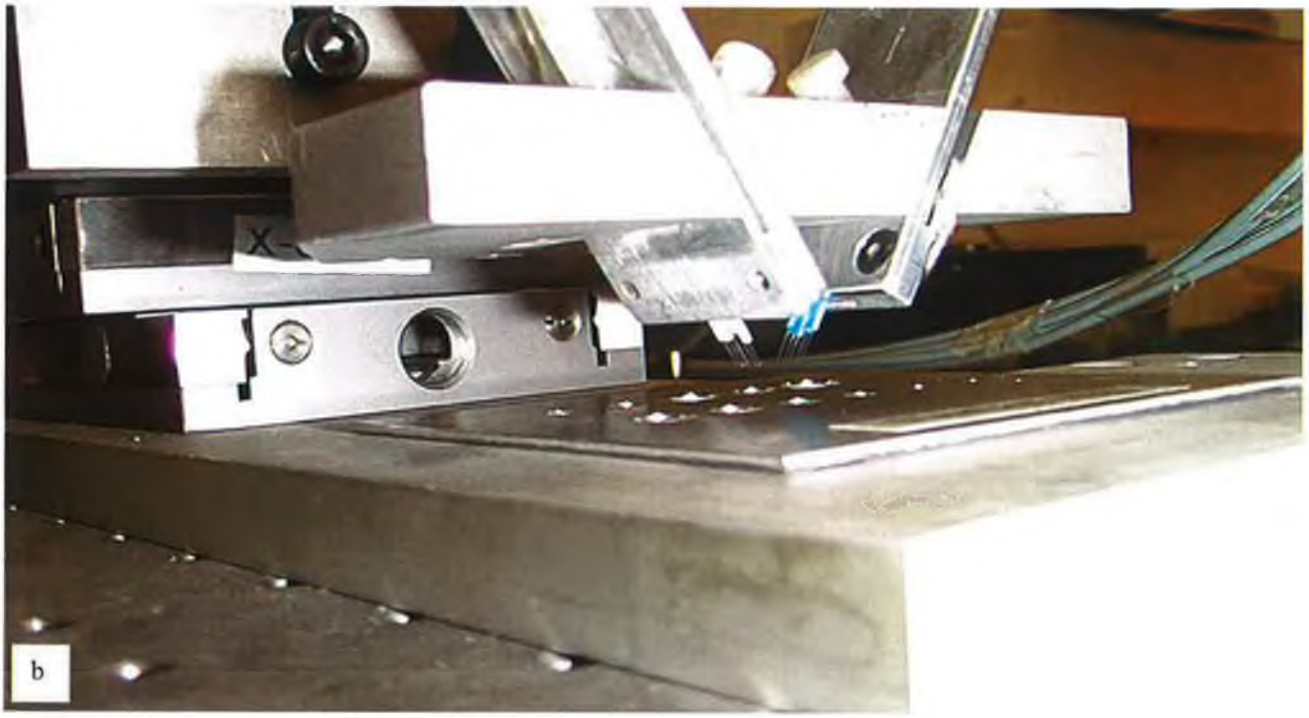

Continues

(a) electronic main circuit and (b) side view of the holders

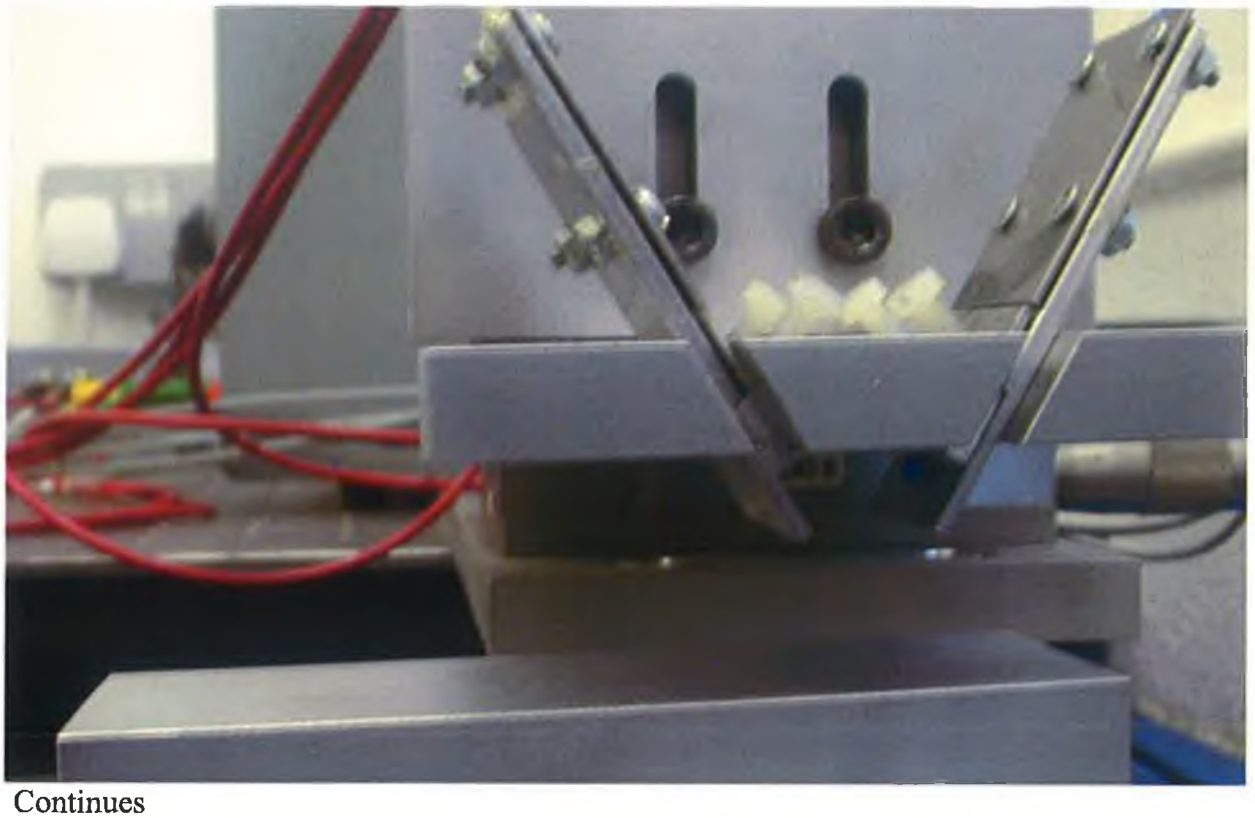

Continues

Two side views of the holders with protect edge and the rotation plate.

C_4

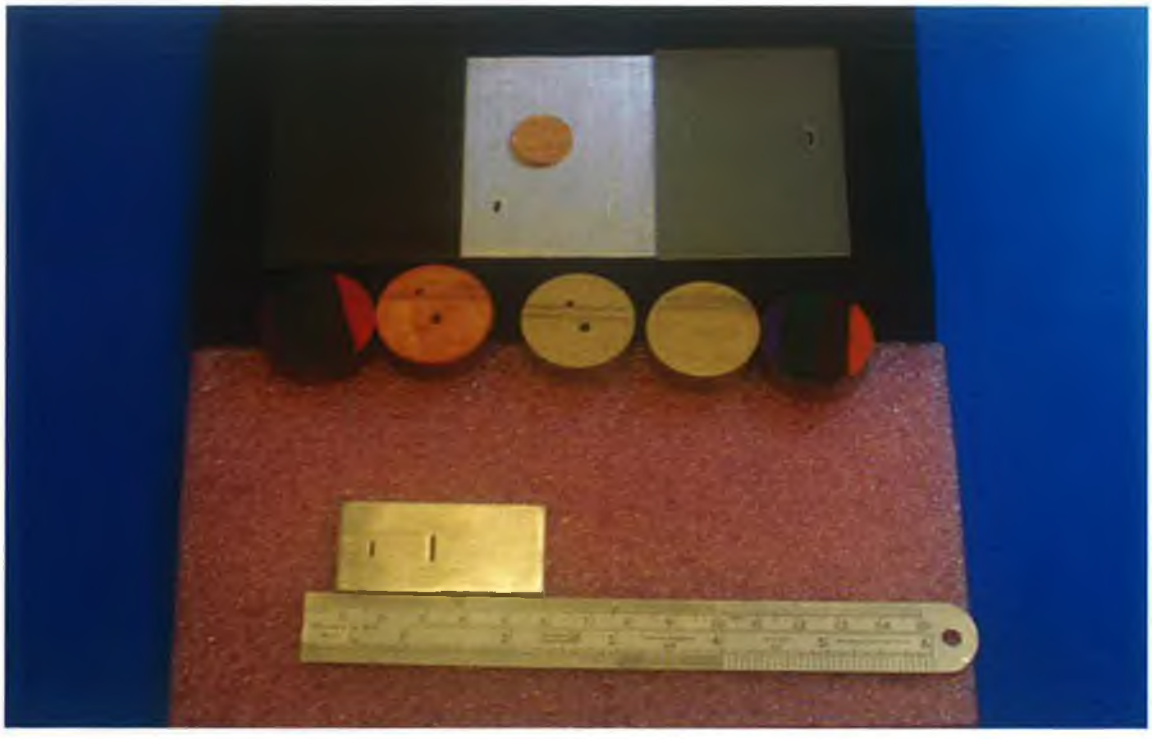

Material samples: polycarbonate, aluminium, tufnol, brass and stainless steel

C_5

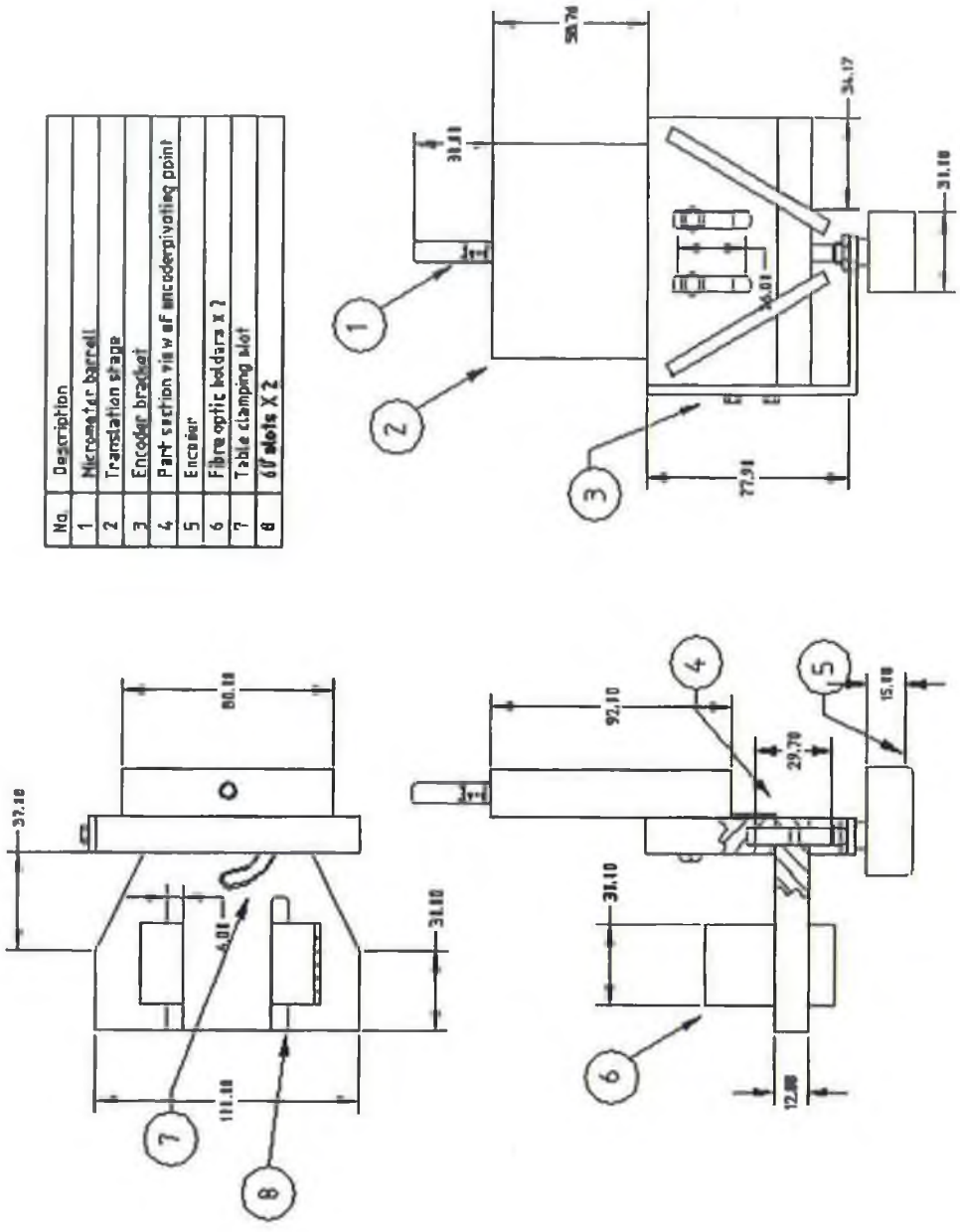

Side views of the main parts of the system (dimension in mm)